ÉCOLE DE TECHNOLOGIE SUPÉRIEURE
UNIVERSITÉ DU QUÉBEC

THESIS PRESENTED TO
ÉCOLE DE TECHNOLOGIE SUPÉRIEURE

IN PARTIAL FULFILLEMENT OF THE REQUIREMENTS FOR
THE DEGREE OF DOCTOR OF PHILOSOPHY
Ph. D.

BY
Mohammad Habibur RAHMAN

# DEVELOPMENT OF AN EXOSKELETON ROBOT FOR UPPER-LIMB REHABILITATION

MONTRÉAL, JULY 11, 2012

**BOARD OF EXAMINERS**

THIS THESIS HAS BEEN EVALUATED

BY THE FOLLOWING BOARD OF EXAMINERS


Mr. Maarouf Saad, Thesis Supervisor
Département de génie électrique at École de technologie supérieure

Mr. Jean-Pierre Kenné, Thesis Co-supervisor
Département de génie mécanique at École de technologie supérieure

Mr. Rachid Aissaoui, President of the Board of Examiners
Département de génie de la production automatisée at École de technologie supérieure

Mr. Guy Gauthier, Member of the Jury Board
Département de génie de la production automatisée at École de technologie supérieure

Mr. Philippe S. Archambault, External Member
School of physical and occupational therapy, McGill University

Mr. Robert E. Kearney, External Independent
Department of biomedical engineering, McGill University



THIS THESIS WAS PRENSENTED AND DEFENDED

BEFORE A BOARD OF EXAMINERS AND PUBLIC

JUNE 27, 2012

AT ÉCOLE DE TECHNOLOGIE SUPÉRIEURE

## ACKNOWLEDGMENT

First and foremost, I would like to pay my gratitude to almighty ALLAH (SWT), who gives me the strength, courage and patience for completing this thesis work at last. Most projects involve the collaboration of people, and composing this thesis has been no exception.

My heartiest thanks to Professor Maarouf Saad, who recommend me for the Doctoral program at École de technologie supérieure and gave me the opportunity to carry out my research work under his kind supervision. He is not only scientifically my mentor, but also socially my teacher and philosopher. I appreciate the lively discussions we had in which he supplied me with academic arguments that have aided the understanding of my research. I value very highly the fact that he was always available to answer questions. His strengths lie in his intelligence and consistency, straight-forwardness and compassion. These traits make him both a great advisor and, most importantly, a wonderful person. The suggestions and comments of Dr. Saad have been a source of constant reference and inspiration. For the guidance he provided whenever I tended to lose the path I owe him more than I can express in words. I hope the bond that we established will continue for many years to come. This thesis has benefited a great deal from his advice.

I would like to thank Professor Jean-Pierre Kenné for being my co-supervisor, and providing me the CAD/CAM Lab facilities to develop the exoskeleton robot, a major part of this research.

I must also express my gratitude Dr. Philippe S. Archambault for his invaluable comments and suggestions in writing papers those were used to compose this thesis.

My committee members have been truly wonderful in their comments and creative ideas. I would like to thank Professor Rachid Aissaoui, Dr. Philippe Archambault, Professor Jean-Pierre Kenné, Professor Robert E. Kearney, Professor Guy Gauthier and Professor Maarouf Saad for taking time to help me progress as a researcher and for having kindly agreed to participate in my thesis research and final PhD committees.

I am grateful to Thierry K-Ouimet who patiently listened to many of my half-developed ideas and provided useful support in developing control architecture.

I wish to thank my father and mother, who although far away, gave me courage and strength through their understanding and endless moral encouragement. My brothers and sister shared with me more than I could possibly express here and were always there when I needed them.

I would like to thank the former and current members who work with me in the Robotics Lab (ETS). In all the years we have shared an office, I’ve learned so much from them, and I have enjoyed working with them including Hasan, Raouf, Amel, Jawhar, Hugo, Katia, Samuele, Mario, Samuel, AbdelKrim, Antonio, Cristobal, Ramon, Bruce and Mustapha.

I owe my deepest gratitude to Mr. M. A. Jahangir and Ms. D. Veadra who showed great interest in reading the thesis and edited the thesis to improve its readability.

Special thanks go to Sylvain, Andre and Jorge, who supported me in developing the electronic components so my experiments could be completed in time.

The list of acknowledgements would be incomplete, if I did not mention my gratitude to R.I Chowdhury, F.R Chowdhury, Siddika Alam, A.Z.M. Happy, M.M.A Hayder, A. Khan, L. Rahman, M.S. Alam, M.J. Alam, Junaid and the many colleagues in the department of mechanical engineering at Khulna University of Engineering & Technology, Bangladesh.

I also gratefully acknowledge the support provided for this research through the FQRNT-V1 scholarship.

Last but not least, I would like to thank my wife S.T. Shefa, who did not only help immensely through this long journey but also bravely endured my mood swings during this stressful time, and made me the proud father of a wonderful boy, Muhammad Taanish-ur Rahman, Tahsin. Without her continuous support and assistance this work would never have been possible.

**DEVELOPMENT OF AN EXOSKELETON ROBOT FOR UPPER-LIMB REHABILITATION**

Mohammad Habibur RAHMAN

## RESUME

Pour assister ou réadapter les personnes présentant une altération du fonctionnement d'un membre supérieur, nous avons développé un exosquelette robotique représentant un membre supérieur nommé, *ETS-MARSE (motion assistive robotic-exoskeleton for superior extremity)*. *MARSE* est composé d'un support déplaçable pour l'épaule, d'un support déplaçable pour le coude et l'avant-bras et d'un support déplaçable pour le poignet. Il est conçu pour être porté sur le côté latéral du membre supérieur afin de fournir des mouvements naturels de l'épaule (flexion/extension verticale et horizontale et rotation interne/externe), du coude (flexion/extension), de l'avant-bras (pronation/supination) et de l'articulation du poignet (déviation radiale/ulnaire et flexion/extension). Cette thèse se concentre sur la modélisation, la conception (composants mécaniques et électriques), le développement et le contrôle de *MARSE*.

Le robot *MARSE* proposée a été modélisé à partir de la biomécanique d'un membre supérieur, il a un poids relativement faible, un excellent rapport puissance/poids, facilement mis ou enlevé, et il est capable de compenser efficacement la gravité. De plus, afin d'éviter l'acheminement complexe des câbles qui pourraient se trouver dans plusieurs types d'exosquelettes, un nouveau mécanisme de transmission de puissance a été introduit pour aider la rotation interne/externe de l'articulation de l'épaule ainsi que la pronation/supination de l'avant-bras. L'exosquelette est conçu pour être utilisé par des adultes typiques. Cependant, des dispositions pour ajuster la longueur des membres ont été effectuées afin d'accommoder un grand éventail d'utilisateurs. La totalité du bras robotique est fabriquée principalement en aluminium, excepté pour les sections sous forte pression qui ont été fabriquées en acier pour donner à l'exosquelette une structure relativement légère. Des moteurs synchrones (incorporés avec des systèmes d'entraînement harmonique direct) ont été utilisés pour actionner *MARSE*.

La cinématique de *MARSE* a été développée en se basant sur les notations de Denavit-Hartenberg modifiées. Dans le modèle dynamique et le contrôle, les paramètres du robot tels que les longueurs, la masse de ses membres et l'inertie sont estimés en fonction des propriétés d'un bras d'un adulte typique. Bien que l'exosquelette ait été développé avec l'objectif d'offrir différentes formes de thérapie de réadaptation (nommé *mouvements passifs du bras*, *thérapie active-assistée,* et *thérapie résistive*), cette recherche s'est concentrée uniquement sur la forme passive de la réadaptation.

Les mouvements et les exercices passifs d'un bras sont généralement effectués à une vitesse plus lente que la vitesse naturelle du bras. Par conséquent, un PID simple et un PID avec

souplesse ‘compliance’ ont été initialement utilisés pour contrôler le robot MARSE. Par la suite, la réalisation de la modélisation de la dynamique du mouvement du bras humain, qui est non linéaire par sa nature, ainsi qu’une méthode de commande par couple précalculé (CTC) et une méthode de commande par mode de glissement avec une loi de convergence exponentielle (mSMERL) ont été employées pour contrôler *MARSE*. Notez que pour améliorer les performances transitoires de poursuite et pour réduire les vibrations, cette thèse a proposé le *mSMERL*, une nouvelle approche de contrôle non linéaire qui combine le concept de la technique de mode glissant avec une loi de convergence exponentielle. L'architecture de contrôle a été mise en œuvre sur un FPGA (field-programmable gate array) conjointement avec un ordinateur incluant un système d’exploitation en temps réel.

Pour les expériences, des exercices typiques de réadaptation pour le déplacement d’une ou plusieurs articulations ont été exécutés. Ces expériences ont été réalisées avec des sujets humains sains où les poursuites (trajectoires préprogrammées recommandées par un thérapeute ou un clinicien) de trajectoires sous la forme d'exercices de réadaptation passive ont été effectuées.

Cette thèse se concentre aussi sur le développement d’un prototype (modèle réduit) d’un membre supérieur à 7 DDL nommé « master exoskeleton arm » (*mExoArm*). De plus, des expériences ont été réalisées avec le *mExoArm* où les sujets (utilisateurs de robots) ont opéré *mExoArm* pour manœuvrer *MARSE* dans le but de fournir une réadaptation passive. Les résultats expérimentaux montrent que *MARSE* peut accomplir efficacement des exercices de réadaptation passive pour des mouvements de l'épaule, coude et poignet. Utiliser *mExoArm* offre aux utilisateurs une certaine souplesse sur les trajectoires préprogrammées sélectionnées, en particulier dans le choix de l'amplitude des mouvements et la vitesse du mouvement. Par ailleurs, le *mExoArm* pourrait potentiellement être utilisé pour la réadaptation à distance.

**Mots Clés :** Bras déficient, Thérapie de réadaptation passive, Exosquelette robotique; réhabilitation; Contrôle non linéaire, PID, Commande par mode précalculé, Loi de convergence exponentielle modifiée, Poursuite de trajectoire.

**DEVELOPMENT OF AN EXOSKELETON ROBOT FOR UPPER-LIMB REHABILITATION**

Mohammad Habibur RAHMAN


## ABSTRACT

To assist or rehabilitate individuals with impaired upper-limb function, we have developed an upper-limb exoskeleton robot, the *ETS-MARSE (motion assistive robotic-exoskeleton for superior extremity)*. The *MARSE* is comprised of a shoulder motion support part, an elbow and forearm motion support part, and a wrist motion support part. It is designed to be worn on the lateral side of the upper limb in order to provide naturalistic movements of the shoulder (i.e., vertical and horizontal flexion/extension, and internal/external rotation), elbow (i.e., flexion/extension), forearm (i.e., pronation/supination), and wrist joint (i.e., radial/ulnar deviation, and flexion/extension). This thesis focuses on the modeling, design (mechanical and electrical components), development, and control of the developed *MARSE*.

The proposed *MARSE* was modeled based on the upper-limb biomechanics; it has a relatively low weight, an excellent power/weight ratio, can be easily fitted or removed, and is able to effectively compensate for gravity. Moreover, to avoid complex cable routing that could be found in many exoskeleton systems, a novel power transmission mechanism was introduced for assisting shoulder joint internal/external rotation and for forearm pronation/supination. The exoskeleton was designed for use by typical adults. However, provisions are included for link length adjustments to accommodate a wide range of users. The entire exoskeleton arm was fabricated primarily in aluminum except the high stress joint sections which were fabricated in mild steel to give the exoskeleton structure a relatively light weight. Brushless DC motors (incorporated with Harmonic Drives) were used to actuate the developed *MARSE*.

The kinematic model of the *MARSE* was developed based on modified Denavit-Hartenberg notations. In dynamic modeling and control, robot parameters such as robot arm link lengths, upper-limb masses, and inertia, are estimated according to the upper limb properties of a typical adult. Though the exoskeleton was developed with the goal of providing different forms of rehab therapy (namely *passive arm movements, active-assisted therapy,* and *resistive therapy*), this research concentrated only on passive form of rehabilitation.

Passive arm movements and exercises are usually performed slowly compared to the natural speed of arm movement. Therefore, to control the developed *MARSE,* a computationally inexpensive a PID controller and a PID-based compliance controller were primarily employed. Further, realizing the dynamic modeling of human arm movement which is nonlinear in nature, a nonlinear computed torque control (CTC) and a modified sliding mode exponential reaching law (*mSMERL*) techniques were employed to control the *MARSE*. Note that to improve transient tracking performance and to reduce chattering, this thesis proposed the *mSMERL,* a novel nonlinear control strategy that combined the concept of boundary layer

technique and the exponential reaching law. The control architecture was implemented on a field-programmable gate array (FPGA) in conjunction with a RT-PC.

In experiments, typical rehabilitation exercises for single and multi joint movements (e.g., reaching) were performed. Experiments were carried out with healthy human subjects where trajectories (i.e., pre-programmed trajectories recommended by therapist/clinician) tracking the form of passive rehabilitation exercises were carried out.

This thesis also focused on the development of a 7DoFs upper-limb prototype (lower scaled) 'master exoskeleton arm' (*mExoArm*). Furthermore, experiments were carried out with the *mExoArm* where subjects (robot users) operate the *mExoArm* (like a joystick) to maneuver the *MARSE* to provide passive rehabilitation.

Experimental results show that the developed *MARSE* can effectively perform passive rehabilitation exercises for shoulder, elbow and wrist joint movements. Using *mExoArm* offers users some flexibility over pre-programmed trajectories selection approach, especially in choosing range of movement and speed of motion. Moreover, the *mExoArm* could potentially be used to tele-operate the *MARSE* in providing rehabilitation exercises.

**Key words:** Arm impairment, Passive rehabilitation therapy, Robotic exoskeleton; Rehabilitation; Nonlinear control, PID control, Computed torque control, Modified exponential reaching law, Trajectory tracking

## TABLE OF CONTENTS

Page

## LIST OF TABLES

## LIST OF FIGURES

Page

## LIST OF ABREVIATIONS

| | |
|---|---|
| CTC | Computed Torque Control |
| DALYs | Disability-Adjusted Life years |
| DoF | Degree of Freedom |
| EMG | Eletromyogram |
| ERL | Exponential Reaching Law |
| FPGA | Field-Programmable Gate Array |
| GHJ | Glenohumeral Joint |
| HD | Harmonic Drive |
| MARSE | Motion Assistive Robotic-Exoskeleton for Superior Extremity |
| mExoArm | Master Exoskeleton Arm |
| mSMERL | Modified Sliding Mode Exponential Reaching Law |
| PD | Proportional Derivative Controller |
| PID | Proportional Integral Derivative Controller |
| SMC | Sliding Mode Control |
| SMERL | Sliding Mode Exponential Reaching Law |

## LIST OF SYMBOLS

| | |
|---|---|
| $a_{i-1}$ | Link length, $m$ |
| $d_i$ | Link offset, $m$ |
| $\alpha_{i-1}$ | Link twist, $rad$ |
| $F(\theta, \dot{\theta}) \in \mathbb{R}^7$ | Friction vector, $N.m$ |
| $G(\theta) \in \mathbb{R}^7$ | Gravity vector, $N.m$ |
| $I$ | Moment of inertia , $kg/m^2$ |
| $V(\theta, \dot{\theta}) \in \mathbb{R}^7$ | Coriolis/centrifugal vector, $N.m$ |
| $M(\theta) \in \mathbb{R}^{7\times7}$ | Inertia matrix |
| $K_p$ | Diagonal positive definite position gain matrix |
| $K_v$ | Diagonal positive definite velocity gain matrix |
| $K_i$ | Diagonal positive definite integral gain matrix |
| $\theta \in \mathbb{R}^7$ | Joint variables vector, $rad$ |
| $\theta_d \in \mathbb{R}^7$ | Desired joint variables vector, $rad$ |
| $\dot{\theta} \in \mathbb{R}^7$ | Measured velocity vector, $rad/s$ |
| $\dot{\theta_d} \in \mathbb{R}^7$ | Desired velocity vector, $rad/s$ |
| $(\Delta\theta)$ | Joint space displacement, $rad$ |
| $(\Delta x)$ | Cartesian space displacement, $m$ |
| $K_s$ | Joint space stiffness matrix |
| $F \in \mathbb{R}^{6\times1}$ | Force and torque vector |
| $K_{px} \in \mathbb{R}^{6\times6}$ | Diagonal positive definite spring constant matrix |
| $J(\theta) \in \mathbb{R}^{6\times n}$ | Jacobian matrix |
| $\Delta x \in \mathbb{R}^{6\times1}$ | Generalized displacement vector |
| $\Sigma$ | Switching/ sliding surface |
| $\tau \in \mathbb{R}^7$ | Generalized torques vector, $N.m$ |

# INTRODUCTION

Physical disabilities such as full or partial loss of function in the shoulder, elbow or wrist are a common impairment in the elderly, but can also be a secondary effect due to strokes, sports injuries, trauma, occupational injuries, and spinal cord injuries. Through the last decades the number of disabled people has increased at an alarming rate. Further, studies have shown that a majority of disabled people are senior citizens. Recent statistics among G8 nations reveal that 15.9% of the total population in Canada is aged 65 and over compared with 22.9% in Japan, 20.3% in Italy, 20.6% in Germany, 16.8% in France, 16.5% in the United Kingdom, 13.0% in Russia and 13.1% in the United States (CIA, 2011).

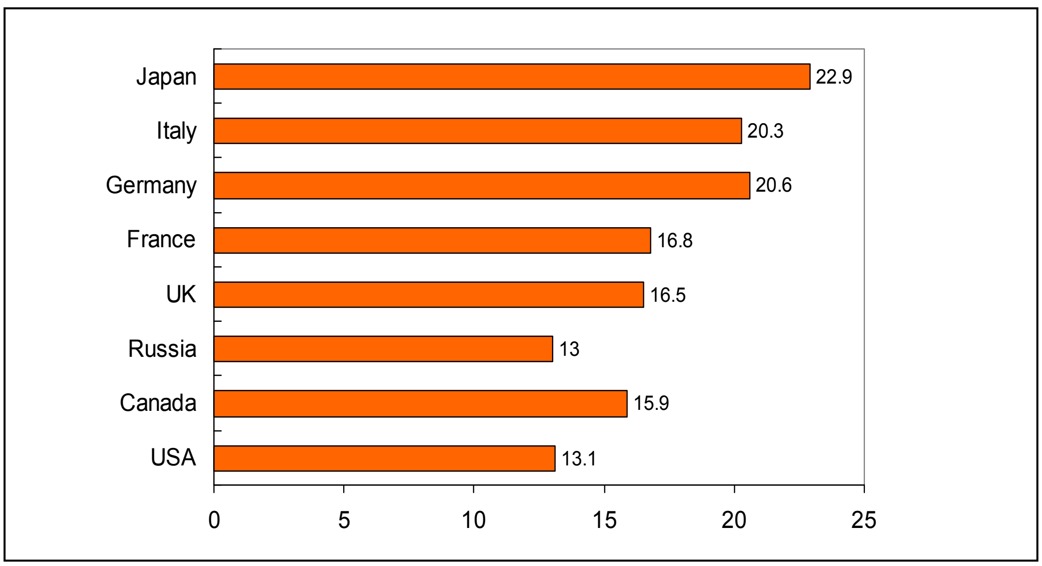


Figure 0.1 Percentage of people aged 65 years and over in G8 countries, 2011

In Canada, the number of seniors has reached a record 4.5 million, accounting for 13.5 % of the total population (Turcotte and Schellenberg, 2007). The number is 0.2 % higher than one year earlier. It can be seen from the Figure 0.2 that this number has progressively increased since 1920, where seniors accounted for about 5 % of the total population. It is projected that in 2026 this number will be increased to 21.2%, i.e., more than four times more than in 1920 (Turcotte and Schellenberg, 2007). In 2036, one of four people in the population may be estimated to be aged. This statistic is quite alarming as aging is one of leading causes of disabilities.

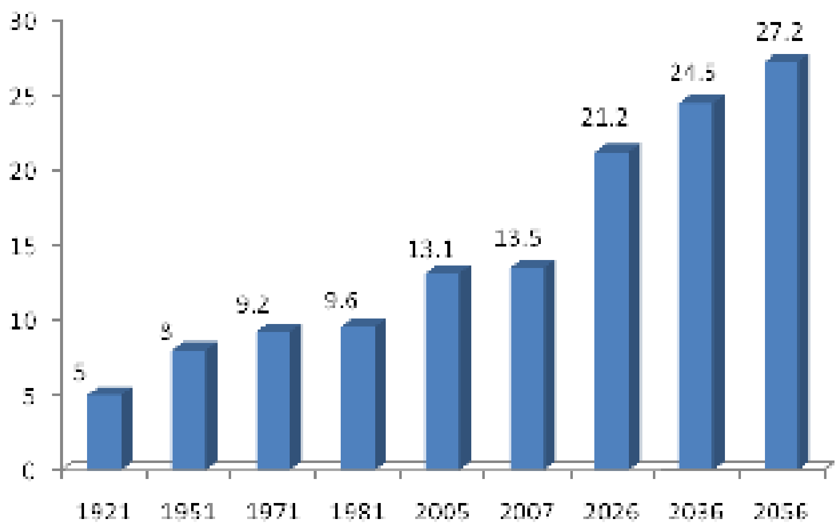


Figure 0.2 Statistics of Canadian population aged 65 or older
Adapted from Turcotte and Schellenberg (2007)

In addition to geriatric disorders, the other major cause of disabilities is stroke. Stroke remains an important cause for morbidity and mortality, and the most common cause of disability. According to the World Health Organization, strokes affects more than 15 million people worldwide each year (Mackay and Mensah, 2004). Among these, 85% of stroke survivors will incur acute arm impairment, and 40% will be chronically impaired or permanently disabled (Parker, Wade and Langton, 1986). This results in a burden on their families, communities and to the country as well. According to the statistics found in '*Atlas of Heart Disease and Stroke*' (Mackay and Mensah, 2004) "stroke burden is projected to rise from around 38 million disability-adjusted life years (DALYs) globally in 1990 to 61 million DALYs in 2020". The Canadian Stroke Network reports that fifty thousand Canadians suffer from strokes each year, and over 300,000 Canadians are currently living with the effects of a stroke (*Tracking Heart Disease and Stroke in Canada*, 2009). Moreover, arm impairment, especially dislocation of the shoulder, elbow, and/or wrist joint, is very common in children and adults alike due to sports, falls, and traumatic injuries such as car crashes (Arciero and Taylor, 1998; Mehta and Bain, 2004; Reid, 1992; Sheps, Hildebrand and Boorman, 2004; Westin *et al.*, 1995). Rehabilitation programs are the main method to promote functional recovery in these individuals (Gresham *et al.*, 1997), which implies a long commitment by a therapist/clinician or an instructed family member. Since the number of such cases is constantly growing and that duration of treatment is long, exoskeleton robots could significantly contribute to the success of these programs. Recent studies also revealed that stroke-affected patients who received robot-assisted therapy showed considerable reduction in motor impairments and regained significant functional abilities (Colombo *et al.*, 2005; Lo *et al.*, 2010). For example, researchers at MIT have conducted clinical trials with more than 300 stroke patients since 1991, where the MIT-MANUS, a planar robotic device, was used to provide therapy for shoulder and elbow joint movement (Masia *et al.*, 2007). This approach could significantly reduce arm impairment (Kwakkel, Kollen and Krebs, 2008).

To assist physically disabled individuals with impaired upper limb function, extensive research has been carried out in many branches of robotics, particularly on wearable robots e.g., exoskeletons (Garrec *et al.*, 2008; Nef *et al.*, 2009; Rahman *et al.*, 2006). Although much progress has been made, we are still far from the desired achievement, as existing robots have not yet been able to restore body mobility or function.

Therefore, to take part in this venture, this research focuses on the development of a 7DoFs exoskeleton type robot named *ETS-MARSE* (*motion assistive robotic-exoskeleton for superior extremity*) to ease daily upper-limb movements as well as to provide effective rehabilitation therapy to the superior extremity of physically weak persons (such as elderly people and/or physically disabled individuals who are no longer possess a full range of motion), so that they would be able to take care of themselves with the help of *MARSE*. In society, it is important that physically handicapped people be able to take care of themselves without the help of others. The *ETS-MARSE* is comprised of a shoulder motion support part, an elbow and forearm motion support part, and a wrist motion support part. It is designed to be worn on the lateral side of the upper limb in order to provide naturalistic movements of shoulder (i.e., vertical and horizontal flexion/extension, and internal/external rotation), elbow (i.e., flexion/extension), forearm (i.e., pronation/supination), and wrist joint (i.e., radial/ulnar deviation, and flexion/extension).

This thesis focuses on the modeling, design, development, and control of the *ETS-MARSE* (Rahman *et al.*, 2011c; 2011e; 2012c). A kinematic model of the *MARSE* was developed based on modified Denavit-Hartenberg (DH) notations (Denavit and Hartenberg, 1955). In dynamic modeling and control, robot parameters such as robot arm link lengths, masses of different link segments, upper-limb masses, and inertia, were estimated according to the upper limb properties of a typical adult (Winter, 1990; Zatsiorsky and Seluyanov, 1983).

It is to be noted that, though the *ETS-MARSE* was developed with the goal of providing different forms of rehab therapy (namely *passive rehabilitation therapy; active rehabilitation therapy, active-assisted therapy, and resistive therapy*), this research concentrated only on the passive form of rehabilitation. Passive arm movements and exercises are usually performed slowly (Gordon *et al.*, 2004; Mary and Mark, 2004; Physical Therapy Standards, 2011; *Stroke Rehab Exercises*, 2010; Tsao and Mirbagheri, 2007) compared to the natural speed of arm movement. Therefore, as a first step, we implemented a computationally inexpensive PID controller, rather than complex model-based control algorithms. Most industrial robots nowadays use this control technique because of problems with estimation of dynamic parameters (Craig, 2005). Later on, to introduce some compliance in the system, we have applied a ‘compliance control with gravity compensation’ technique as an alternative approach to perform similar ‘passive rehabilitation therapy’ (Rahman *et al.*, 2012d). Furthermore, to realize better tracking performance of the *MARSE,* the dynamic models of human upper-limb (ANNEX I and ANNEX II) and *ETS-MARSE* were considered in the nonlinear control techniques (Rahman *et al.*, 2011d; 2011f). Note that the dynamic modeling of human arm movement is nonlinear in nature, therefore nonlinear computed torque control (CTC) and modified sliding mode exponential reaching law (*mSMERL*) techniques were employed to control the *ETS-MARSE,* where trajectory tracking (i.e., pre-programmed trajectory tracking approach) that corresponds to typical rehabilitation (passive) exercises of the shoulder, elbow, forearm and wrist joint movements were carried out to evaluate performances of the *ETS-MARSE* and the controllers. Note that the exponential reaching law (ERL) (Fallaha *et al.*, 2011) shows high control activity during the transient even though it was able to reduce chattering in steady state. To solve this problem, this research introduced a *mSMERL* (Rahman *et al.*, 2012c) that combined the concept of the boundary layer function with a ERL (Fallaha *et al.*, 2011) to implement trajectory tracking in the developed *MARSE.*

In experiments, typical rehabilitation exercises for single and multi joint movements (e.g., reaching) were performed. Experiments were carried out with healthy human subjects where trajectories (i.e., pre-programmed trajectories recommended by a therapist/clinician) tracking the form of passive rehabilitation exercises were carried out. Furthermore, experiments were carried out with the *mExoArm,* an upper-limb prototype 7DoFs (lower scaled) motion indicator) where subjects (robot users) operate the *mExoArm* (like a joystick) to maneuver the *MARSE* to provide passive rehabilitation. Experimental results show that the *ETS-MARSE* can efficiently perform the passive rehabilitation therapy. This thesis is organized as follows:

**Chapter 1: Literature Review**

This chapter is a critical overview of research work conducted in the fields of development of orthoses and/or robotic exoskeletons, methods adopted to control such robots and their real world applications are presented.

**Chapter 2: Motion Assistive Robotic-Exoskeleton for Superior Extremity (*MARSE*)**

This chapter outlines the overall design of the proposed *ETS-MARSE*. It describes the motivation for the major design choices and gives the reader an overall sense of the complete hardware package and the components that comprise it.

**Chapter 3: Kinematics and Dynamics**

Chapter 3 describes the kinematics and the dynamics of the *ETS-MARSE.* The modified DH notations were used to develop the kinematic modeling, whereas in dynamic modeling the iterative Newton-Euler formulation was used.

**Chapter 4: Control and Simulation**

This chapter presents the theoretical structure of the different control techniques (such as PID, Computed Torque Control, Sliding Mode Control with Exponential Reaching Law, and Compliance Control with Gravity Compensation) that were applied to maneuver the *MARSE* to follow a reference trajectory. This chapter also presents simulation results to validate the *ETS-MARSE* model developed in Chapter-3, and also to evaluate the performance of the different control techniques with regard to trajectory tracking.

**Chapter 5: Experiments and Results**

To evaluate the performance of the *ETS-MARSE* and the control techniques, this chapter describes experimental set-up and the procedure carried out during the experiments. The chapter presents all the test results, discusses the test results in great detail, and gives some specific comments on the test results.

**Conclusions and Recommendations**

Finally, the Conclusions section of the paper summarizes the research outcomes and suggests directions for further research in section Recommendations.

# CHAPTER 1

# LITERATURE REVIEW

To assist physically disabled individuals with impaired upper limb function, extensive research has been carried out in many branches of robotics, particularly on wearable robots (e.g., exoskeletons, powered orthosis devices etc.) and/or end-effector based robotic devices (i.e., devices which do not actively support or hold the subject's upper-limb but connect with the subject's hand or forearm (Brose *et al.*, 2010; Burgar *et al.*, 2000; Culmer *et al.*, 2010; Krebs *et al.*, 2000; Loureiro *et al.*, 2003; Takahashi *et al.*, 2008). Note that exoskeleton type robotic devices are either wheelchair mounted (Alexander, Nelson and Shah, 1992; Gopura, Kiguchi and Yang, 2009; Homma and Arai, 1995; Johnson and Buckley, 1997; Kiguchi *et al.*, 2003; Rahman *et al.*, 2000; Sanchez *et al.*, 2005; Tsagarakis and Caldwell, 2003) or floor mounted (Carignan, Tang and Roderick, 2009; Frisoli *et al.*, 2009; Garrec *et al.*, 2008; Gupta and O'Malley, 2006; Nef *et al.*, 2009; Noritsugu and Tanaka, 1997; Perry, Rosen and Burns, 2007; Rahman *et al.*, 2010c) but the end-effector devices are commonly floor/desk mounted.

## 1.1 End-effector based Rehabilitative Devices (State of the Arts)

Some potential end-effector based rehabilitative devices are: MIT-MANUS (a 3DoFs planar robot developed at MIT (Krebs *et al.*, 2000), a later version of which includes a hand module for whole arm rehabilitation (Masia *et al.*, 2007); GENTLE/s system (Loureiro *et al.*, 2003) (which utilized an active 3DoFs haptic master robot that connects the subject's arm through a wrist orthosis and uses virtual reality (VR) technologies to deliver therapy); iPAM system (Culmer *et al.*, 2010) (developed at the University of Leeds that uses dual robotic arms (each having 3 active DoFs) to deliver therapy via two orthoses located on the upper arm and wrist of the subjects); MIME system (Burgar *et al.*, 2000) (developed under the joint collaboration of VA Palo Alto and Stanford University, the system incorporated a PUMA-260 robot and two commercial mobile arm supports modified to limit arm movement to the horizontal plane (2D), a later version of which uses PUMA-560 to provide therapy in 3D workspace); and HWARD (Takahashi *et al.*, 2008) (a 3 DoFs desk mounted pneumatically actuated device that was developed at University of California to assist the subject's hand in grasp and in release movements). Another upper limb motion assist system was developed by Homma and Arai (1995) around the mid 90s. The system used parallel strings/cords (one end of which was attached to a plate mounted over the subject's head and other end to the subject's arm) to suspend the arm at the level of the elbow and wrist (Homma and Arai, 1995). Motion of the subject's arm was generated by changing each string's length according to the subject's voice command or head motion. Researchers of Okayama University have developed an active support splint (ASSIST) driven by pneumatic soft actuators to assist wrist joint

Table 1.2 State of the arts: end-effector based rehabilitative devices

| **Project / Institute/ Researcher / Year** | **Arm Support** | **Control / Method** | **Actuation/Operating Mechanism / Brief Description** |
|---|---|---|---|
| MIT-MANUS, MIT (Masia *et al.*, 2007) | Forearm, Wrist | IMC | The 1st version of this device used a 3DoFs planer robot to provide physical therapy to stroke victims. A later version includes a hand module for whole arm rehabilitation. |
| iPAM system, University of Leeds | Upper arm, Wrist | ADC | This system uses a dual robotic arm (each having 3 active DoFs) to deliver therapy via two orthoses located on the upper arm and wrist of the subjects. |
| HWARD, (Takahashi *et al.*, 2008) | Wrist | PneC | This system is a 3DoFs desk-mounted pneumatically actuated device that was developed to assist the subject's hand in grasp and in release movements. Joint angle sensors in the robot are used to measure the movement of the robot's joints. |
| MIME system, VA Palo Alto and Stanford University, 2000 | Forearm | - | The system incorporated a PUMA-260 robot and two commercial mobile arm supports modified to limit arm movement to the horizontal plane (2D); a later version uses PUMA-560 to provide therapy in 3D workspace. |
| Homma and Arai, AIST, (Homma and Arai, 1995) | Forearm, wrist | - | The system used a parallel mechanism to suspend the upper arm at the elbow and wrist level. Motion of the upper limb was generated by changing the length of each string according to the command given by the user using voice, head motion and so on. |
| GENTLE/s system (Loureiro *et al.*, 2003) | Through Wrist Orthosis | BP | The system utilizes an active 3DoFs haptic master robot that connects the subject's arm through a wrist orthosis and uses virtual reality (VR) technologies to deliver therapy. |

ADC = Admittance Control; IMC = Impedance Control; PneC = Pneumatic Control, BP = Bead Pathway flexion/extension motion for elderly or physically handicapped individuals in need of care and therefore to relieve a burden for caregivers (Sasaki, Noritsugu and Takaiwa, 2005). Experiments have shown that with ASSIST the amplitude of EMG signals decreases compared to without the use of ASSIST. Therefore, it was evident that the burden for the muscle can be decreased considerably using the ASSIST.

## 1.2 Exoskeleton type Rehabilitative Devices (State of the Arts)

One of the earliest wheelchair mounted robotic orthoses was the Balanced Forearm Orthosis (BFO), developed in the mid-sixties, designed to move subjects' arms in the horizontal plane (Alexander, Nelson and Shah, 1992). A later version of the BFO includes an additional joint to allow movement assistance in the vertical direction but the device was rarely used due to its poor gravity compensation techniques. The motorised upper-limb orthosis system (MULOS) was also a wheelchair mounted device having 5 DoFs developed at the University of Newcastle in 1997 (Johnson and Buckley, 1997). Apart from some limitations in safety and control issues, the project seemed promising but was ended in 1997 (Tsagarakis and Caldwell, 2003). Some other wheelchair or chair mounted exoskeleton or orthosis devices developed for upper limb rehabilitation are: the 'Functional upper limb orthosis' (Rahman *et al.*, 2000) (a 4 DoFs orthosis developed under the joint project between Drexel University and A.I. duPont Hospital for children, informally tested on 10 subjects); the Pneu-WREX (Sanchez *et al.*, 2005) (a 5 DoFs pneumatically actuated robot developed at University of California); the Saga University's 'exoskeleton robot for shoulder and elbow joint motion assist' (Kiguchi *et al.*, 2003; Rahman *et al.*, 2006), a later version of which was named as SUEFUL-7, having 7 DoFs and controlled by skin surface electromyogram (EMG) signals (Gopura, Kiguchi and Yang, 2009). Another chair mounted orthosis is the Hybrid Arm Orthosis (HAO) developed by Benjuya and Kenney in 1990 to assist upper limb motion at the level of shoulder abduction, elbow flexion and wrist supination (Benjuya and Kenney, 1990).

Table 1.3 State of the arts: exoskeleton type rehabilitative devices

| **Project / Institute / Researcher / Year / Ref.** | **DoFs** | **Sensors** | **Actuators** | **Actuator Placement** | **Actuation Mechanism** | **Control** | **Therapeutic Regime** |
|---|---|---|---|---|---|---|---|
| **Floor-Mounted** | | | | | | | |
| *ETS-MARSE,* (Rahman *et al.*, 2011c; 2012b) | 7 | Force sensor | Brushless DC motors | Joint | Gear Drive | PID, CTC, CC, SMC, SMERL | E, F, W |
| ABLE, (Garrec *et al.*, 2008) | 4 | Force sensor | DC faulhaber | Remote | Ball-screw and cable | Force Feedback | S, E |
| CADEN-7, University of Washington, (Perry, Rosen and Burns, 2007) | 7 | Force, EMG | Rare earth brushed motors | Joint and Remote | Gear Drive, Cable | PID, EMG | S, E, F, W |
| L-EXOS, PERCRO, (Frisoli *et al.*, 2009) | 5 | Force sensor | DC servo | Joint and Remote | Gear Drive, Cable | IMC | S, E, F |
| Soft-actuated exoskeleton, (Tsagarakis and Caldwell, 2003) | 7 | Strain gauge | Pneumatic muscle actuators | Remote | Linkage, Cable | IMC | S, E, F, W |
| MGA exoskeleton, (Carignan, Tang and Roderick, 2009) | 6 | Force sensor | Brushless DC motors | Joint | Gear Drive | ADC, IMC | S, E, W |
| Ritsumeikan Univ., (Nagai *et al.*, 1998) | 8 | Force sensor | DC servo | Joint and Remote | Linkage, Direct Drive | Power Assist Control, IMC | S, E, F, W |
| ARMin-III, (Nef, Guidali and Riener, 2009) | 4 | Force sensor | Brushed motors | Joint and Remote | Gear Drive, Belt Drive, Cable | PD, CTC, IMC | S, E |
| MAHI exoskeleton, (Gupta and O'Malley, 2006) | 5 | Force sensor | Frameless electrical motors | Joint | Direct Drive, Parallel mechanism | - | E, F, W |
| Noritsugu and Tanaka, (Noritsugu and Tanaka, 1997) | 2 | Force sensor | Pneumatic rubber muscle | Remote | Linkage, Cable | IMC | S,E |
| **Chair-Mounted** | | | | | | | |
| SUEFUL-7 (Gopura, Kiguchi and Yang, 2009) | 7 | Force, EMG | DC servo motors | Joint and Remote | Gear Drive, Cable | Force , EMG | S, E, F, W |
| Pneu-WREX , Univ. of California, 2005 | 5 | - | Pneumatic | Remote | Linkage | Force Control | S, E, W |
| MULOS, University of Newcastle, 1997 | 5 | Pressure, Force | Electric motors, hydraulic actuator | Joint and Remote | Gear drive, Hydraulic transmission, Linkage | - | S, E, |

PID = Proportional Integral Derivative; CTC = Computed Torque Control; SMC = Sliding Mode Control; SMERL = Sliding Mode Exponential Reaching Law; EMG = Electromyogram based Control; IMC = Impedance Control; ADC = Admittance Control;
S = Shoulder; E =Elbow; Forearm = F; Wrist = W.

Some potential floor mounted (or grounded type) exoskeletons found in recent years are: ABLE (Garrec *et al.*, 2008) (a 4 DoFs exoskeleton developed at CEA-LIST, Interactive Robotics Unit, France); CADEN-7 (Perry, Rosen and Burns, 2007) (a 7 DoFs cable driven exoskeleton developed at the University of Washington); L-EXOS (Frisoli *et al.*, 2009) (a 5 DoFs force-feedback exoskeleton developed by PERCRO, Italy to provide neuro-rehabilitation in VR environments); 'Soft-actuated exoskeleton' (Tsagarakis and Caldwell, 2003) (a 7 DoFs exoskeleton actuated by pneumatic muscle actuators developed at the University of Salford, UK to provide physiotherapy under isotonic, isokinetic, and training modes of operation); MGA exoskeleton (Carignan, Tang and Roderick, 2009) (a 6 DoFs exoskeleton designed primarily for shoulder rehabilitation where as a control approach impedance and admittance control schemes were used); ARMin (Nef *et al.*, 2009) (a 6 DoFs robot developed at the Swiss Federal Institute of Technology, currently under clinical evaluation in hospitals in Switzerland and in the United States); 'Rehabilitation Robot' developed at Okayama University (Noritsugu and Tanaka, 1997) (a 2 DoFs robot actuated by pneumatic rubber artificial muscles); and MAHI exoskeleton (Gupta and O'Malley, 2006) (a 5 DoFs haptic arm exoskeleton developed at Rice University). The detailed background of exoskeleton robot research is explained in Refs. (Kiguchi *et al.*, 2003; Rahman, 2005; Rahman *et al.*, 2011h; Tsagarakis and Caldwell, 2003). Tables 1.1 and 1.2 highlight and compare some features (e.g., DoFs, sensors and actuators used, placement of actuators, actuation mechanism, therapeutic regime, control approach) of these devices.

## 1.3 Limitations of Existing Rehabilitative Devices and Robotic Exoskeletons

Although much progress has been made in the field of rehabilitation robotics to develop an upper-limb motion assistive robotic device/exoskeleton, we are still far from the desired goal, as existing robots have not yet been able to restore body mobility or function. This is due to limitations in the area of proper *hardware design* and also of *control algorithms* to develop intelligent and autonomous robots to perform intelligent tasks.

Limitations in design of hardware:

Our survey of the recent literature revealed some of the limitations of existing exoskeleton systems, which encouraged and motivated us to go through this research. In particular, exoskeleton systems have been designed with limited degrees of freedom and range of motion compared to that of human upper extremities (Frisoli *et al.*, 2009; Garrec *et al.*, 2008; Homma and Arai, 1995; Takahashi *et al.*, 2008). Others have employed a robust and complex structure (Yupeng, Hyung-Soon and Li-Qun, 2009), are relatively heavy, with bulky joints (Carignan, Tang and Roderick, 2009), or have relatively weak joint mechanisms (Homma and Arai, 1995; Kiguchi *et al.*, 2003). Some show a lack of proper safety measures and compensation for gravity forces (Culmer *et al.*, 2010; Homma and Arai, 1995; Takahashi *et al.*, 2008). Some have been designed using a closed circular structure as an arm holder (Gopura, Kiguchi and Yang, 2009; Gupta and O'Malley, 2006), making it unrealistic and inconvenient to insert and remove the arm. The use of wire ropes or complex cable routing as a transmission mechanism has been an approach in other types of robots (Frisoli *et al.*, 2009; Kiguchi *et al.*, 2003; Perry, Rosen and Burns, 2007), which can produce undesirable vibration and excessive compliance in the system. Problems can become severe when transmission wires, ropes and/or cables slide away from the guide pulleys.

The *ETS-MARSE* developed in this research has considered the above limitations and is designed based on the upper-limb joint movements; it has a relatively low weight, a higher power to weight ratio, can be easily fitted or removed, and is able to effectively compensate for gravity. Moreover, to avoid complex cable routing that could be found in many exoskeleton systems (Frisoli *et al.*, 2009; Kiguchi *et al.*, 2003; Perry, Rosen and Burns, 2007), a novel power transmission mechanism has been introduced for assisting shoulder joint internal/external rotation (Rahman *et al.*, 2010a; 2012b; 2012d), and for forearm pronation/supination (Rahman *et al.*, 2011b; Rahman *et al.*, 2010c). Cable transmissions always add some undesirable vibration and can loosen up during operation, therefore they should be avoided. On the other hand, it is practically impossible to use conventional gear mechanisms (for shoulder joint internal/external rotation and for forearm pronation/supination), since in such a case, meshing gears are supposed to rotate around a physical axis of rotation (e.g., shaft), but we are unable to fit such a mechanical shaft along the line of axis of human arm motion (e.g., with the humerus/radius) especially in case of shoulder joint internal/external rotation and for forearm pronation/supination. To solve these issues, this research introduced an innovative concept of power transmission, a combination of custom made open type bearing and open type meshing gear assembly, where motion is transmitted from an anti-backlash gear (mounted on a motor shaft) to an open-type custom-made meshing ring gear. A detail of this mechanism is discussed in Chapter 2.

Limitations in control approaches:

Like limitations in the design of exoskeleton hardware, developing smart control algorithms is another major issue that needs to be properly addressed. Unlike most industrial robots which can be modeled easily and controlled by linear control techniques, the control strategy for this type of exoskeleton robots is quite complex and difficult. This is mainly due to the nonlinear characteristics of their dynamic model and to the limitation of estimating proper dynamic parameters. In the literature, robotic devices have been used to provide a passive form of rehabilitation, which involves moving the person's limb through a pre-determined trajectory (i.e., trajectory tracking). This has been performed using various linear approaches, such as PD (Nef, Mihelj and Riener, 2007), PID (Tsagarakis and Caldwell, 2003; Yu and Rosen, 2010); as well as other nonlinear control techniques, e.g., computed torque control (Nagai *et al.*, 1998; Nef, Mihelj and Riener, 2007) and impedance control (Noritsugu and Tanaka, 1997). Note that as a key requirement to provide passive rehabilitation and/or passive arm movement assistance, a consistent high dynamic tracking performance is required to maneuver the exoskeleton in an efficient, smooth and continuous manner. The use of linear control approaches seems limited in its ability to solve the issues associated with nonlinearity in modeling. On the other hand, for other examples where the computed torque control approach was used, the dynamic model was simplified ignoring mass/inertia terms, and/or centrifugal terms (Bergamasco *et al.*, 1994; Nef, Mihelj and Riener, 2007). In such cases, tracking performance of the controller was significantly reduced. Moreover, these controllers may lack the robustness necessary to cope with uncertainties, for instance the mass of the human upper-limb which varies from person to person.

Several other nonlinear control strategies have been proposed for the trajectory tracking of exoskeleton robots, such as the work of Kyoungchul and Tomizuka (Kyoungchul and Tomizuka, 2009); their approach is based on an fictitious gain, which is postulated to be in the motion control system of a human body. Yang *et al.* (Yang *et al.*, 2009) proposed a model based on a fuzzy-adaptation technique for control of the lower extremity. Gomes *et al.* (Gomes, Silveira and Siqueira, 2009) proposed an adaptation algorithm based on neural networks. However, neural network and fuzzy logic controls suffer from a slow response time as these control techniques require heavy computation.

The sliding mode control (SMC) approach has previously been used for many motion control systems (Sabanovic, 2011) such as control of mobile robots (Defoort *et al.*, 2008), actuator control (Foo and Rahman, 2010), control of robotic manipulators (Islam and Liu, 2011; Xu *et al.*, 2007) etc. However, its application to exoskeleton robots is relatively new and a few researchers are using this approach (Beyl *et al.*, 2008; Ming-Kun and Tsan-Hsiu, 2009). The robustness of the SMC can theoretically ensure perfect tracking performance despite parameters or model uncertainties (Slotine and Li, 1991; Xinghuo and Kaynak, 2009). Moreover, the SMC is simple in structure, has good transient performance and is fast in response. We therefore consider the SMC as a good solution to deliver a consistently high dynamic tracking performance. One major drawback of using SMC in practical application is chattering, defined as a high frequency finite amplitude control signal originating from the discontinuous *sign* function. Various methods were proposed to minimize and/or eliminate this chattering, e.g., replacing the *sign* function with a boundary layer function (Slotine and Li, 1991), using fuzzy logic to adjust the boundary layer function (Bartolini *et al.*, 2000), using a continuous smooth approximation, using a disturbance observer (Kawamura, Ito and Sakamoto, 1992), using an adaptive fuzzy system (Erbatur and Kaynak, 2001), and/or using power rate reaching strategy (Gao and Hung, 1993). Although chattering can be controlled with these modifications, it comes at a cost as tracking performance of the system is negatively affected and steady-state errors increase. The reaching law proposed by Fallah *et al.* (Fallaha *et al.*, 2011) considers the above limitations and is designed based upon the choice of an exponential term that adapts with the variations of the switching function, which is able to deal with the chattering/tracking performances dilemma. However, the control effort using the ERL (Fallaha *et al.*, 2011) is still higher during the transient even the chattering is reduced. To solve this issue, this research introduced a *mSMERL* that combined the concept of the boundary layer function (Slotine and Li, 1991) with a ERL (Fallaha *et al.*, 2011) to implement trajectory tracking in the developed *MARSE.* Note that to evaluate the performance of *mSMERL,* similar passive rehabilitation exercises were carried out using PID, CTC, conventional SMC and *mSMERL* techniques. Details of these control technique are given in Chapter 4.

Research on robotic exoskeletons and/or orthoses as discussed above implies that there are still significant problems in the development of upper limb rehabilitative and motion assistive exoskeleton. To fulfill the aspirations of the exoskeleton robot users, those problems should be solved.

## 1.4 Research Objectives and Hypothesis

The *specific aims* of this research project, based on the limitations outlined above, are:

- to develop an *exoskeleton robot* that includes its modeling (kinematic and dynamic), design (mechanical and electrical components), development and control;
- to develop a control strategy to provide passive rehabilitation therapy to the upper extremities.

It is expected that the developed controller will be able to maneuver the *ETS-MARSE* effectively to provide passive rehabilitation therapy. In next section a brief description on passive arm therapy is presented.

## 1.5 Passive Rehabilitation Therapy

Upper extremity impairment is very common due to geriatric disorders and/or following a stroke or other conditions such as sports, falls, and traumatic injuries. Its treatment relies on rehabilitation programs, especially on passive arm movement therapy at the early stages of impairment. The complete rehabilitation protocol is comprised of several therapeutic approaches, namely *passive rehabilitation therapy, active rehabilitation therapy, active-assisted therapy,* and *resistive therapy*. Depending on the patient's arm impairment, their physiotherapist or clinician selects the appropriate therapeutic approach and exercises. In this research, however, we have focused only on *passive rehabilitation therapy.*

Passive arm movement therapy is the very first type of physiotherapy treatment given to patients, mainly to improve their passive range of movement. In this therapeutic approach, patients remain relaxed (i.e., the therapy does not require subject's participation) while physical therapies in the form of different (joint based) exercises (Physical Therapy Standards, 2011) are employed by physiotherapists, skilled caregivers, and/or trained family members to restore or regain the upper-limb mobility and function (*Post-Stroke Rehabilitation Fact Sheet*, 2011; *Stroke Rehab Exercises*, 2010; Wang, 2011). To be noted, this therapy is the key treatment for the patients who are unable to actively move their arm throughout their complete range of motion following a surgery (Physical Therapy Standards, 2011) at the shoulder joint, elbow joint or wrist joint due to the dislocation of the joints; or as the result of a stroke mostly due to spasticity and increased muscle tone (*Nonoperative Treatment: Physical Therapy*, 2011; *Post-Stroke Rehabilitation Fact Sheet*, 2011).

Several hypotheses exist as to how upper extremity rehabilitation may be improved. Studies reveal that intensive and repetitive therapies significantly improve motor skill (Huang et al., 2009). Note that the passive rehabilitation therapy does not contribute in building muscle but does help to prevent contractures, increases range of motion and thus maintains and promotes mobility of the patients (Wang, 2011). Therefore, once resistance to passive arm movements in individuals has diminished it is essential that they practice active movements. For example, the subjects perform any specific task under the guidance of a physiotherapist or a caregiver. This therapeutic approach is known as 'assist as need'. To provide such therapy with a robotic rehabilitation protocol, the robotic devices will guide the subject's movement to complete the specified task. Further studies reveal that enhanced motor learning occurs in the 'active rehabilitation therapy' mode, when patients (independently) practice a variety of functional tasks (Winstein, Merians and Sullivan, 1999) such as grasping and reaching movements and receive feedback (e.g., visual and haptic feedback) intermittently (Lum, Burgar and Shor, 2004; Winstein *et al.*, 2003). However, this research concentrates on *passive rehabilitation therapy,* therefore the key factors of this therapy (i.e., the *intensive and repetitive movements* of the affected extremity) need to be integrated in rehabilitation paradigms and this can be done through rehabilitation robotics.

It has already been shown in several studies that robotic devices are able to provide consistent training (Colombo *et al.*, 2005; Fazekas, Horvath and Toth, 2006) and to measure performance with high reliability and accuracy (Dobkin, 2004; Nef, Mihelj and Riener, 2007; Rahman *et al.*, 2012d). Moreover, experimental studies reveal that patients who receive robot assisted therapy show considerable improvement of motor skills compared to conventional therapy techniques (Lum *et al.*, 2002; Masiero *et al.*, 2007). The *ETS-MARSE* was therefore developed to take part in rehabilitation programs. Experiments were carried out to evaluate its performance in providing passive arm movement therapy (Rahman *et al.*, 2011a). Details of these experiments are given in Chapter 5.

## 1.6 Contribution

This research focused on the modeling design, development and control of a 7 DoFs robotic exoskeleton, *ETS-MARSE*. Contributions of this research are as follows:

- *ETS-MARSRE,* a prototype of human upper-limb corresponding to the natural range of motion of superior extremities, was developed (Rahman *et al.*, 2010a; 2011c; 2011d; 2012b; 2012d; Rahman *et al.*, 2009) with the goal of providing different forms of rehabilitation therapy. The *ETS-MARSE* should be worn on the lateral sides of subject's upper limb and will assist upper-limb movements for the:
    - horizontal flexion/extension motion of the shoulder joint;
    - vertical flexion/extension motion of the shoulder joint;
    - internal/external rotation of the shoulder joint;
    - flexion/extension motion of the elbow joint;

- pronation/supination of forearm motion;
- flexion/extension of the wrist joint; and
- radial/ulnar deviation of the wrist joint.

- introduction of an innovative concept of power transmission, a combination of custom made open type bearing and open type meshing gear assembly (Rahman *et al.*, 2010a; Rahman *et al.*, 2010c);

- introduction of a *mSMERL* (Rahman *et al.*, 2012c) that combines the concept of the boundary layer function (Slotine and Li, 1991) with a ERL (Fallaha *et al.*, 2011) to implement the dynamic trajectory tracking of the *ETS-MARSE.* Compared to conventional SMC, the proposed *mSMERL* significantly reduces chattering and gives smother trajectory tracking both in transient and in steady state position; and

- design and development of a *mExoArm* (Rahman *et al.*, 2009)*,* an upper-limb prototype 7DoFs (lower scaled manipulator) exoskeleton arm to maneuver or tele-operate (like a joystick) the *ETS-MARSE* (or any other exoskeletons) to follow a desired trajectory.

.

# CHAPTER 2

# MOTION ASSISTIVE ROBOTIC EXOSKELETON FOR SUPERIOR EXTREMITY (ETS-MARSE)

This chapter outlines the overall design of the *ETS-MARSE.* Based on the concept of human upper limb articulations and joint movements, the robotic exoskeleton for this study was designed to provide movement assistance for:

- shoulder abduction/adduction (2DoFs);
- upper arm rotation (1DoF);
- elbow flexion/extension ( 1DoF);
- forearm pronation/supination (1DoF); and
- wrist joint movements (2DoFs).

In the next section of this chapter, the general design considerations for a motion assistive rehabilitative device and/or exoskeleton system are highlighted for the motivation of major design choices of the *ETS-MASRE.* The midsection of the chapter focuses on some key design aspects of the *ETS-MARSE.* The last section of this chapter gives the reader an overall sense of the complete hardware package and the components that comprise it.

## 2.1 General Design Considerations

The fundamental design criteria (Meng and Lee, 2006; Tsagarakis and Caldwell, 2003) for an upper extremity motion assistive device or a robotic exoskeleton system are as follows:

1) Degrees of freedom and range of motion:

   To assist humans' daily activities properly, the degrees of freedom (DoFs) and the range of motion of the exoskeleton robot must correspond to the natural range of a human. Humans upper extremities are composed of 7DoFs (shoulder joint: 3DoFs, elbow joint: 1DoF, forearm: 1DoF, wrist joint: 2DoFs). The shoulder joint having 3DoFs is considered a ball-and-socket joint (Gray and Clemente, 1985; Hallaceli, Manisali and

Gunal, 2004; Holzbaur, Murray and Delp, 2005), whereas the elbow joint is a simple hinge joint (Gray and Clemente, 1985), therefore, it has only 1DoF. The movements associated with shoulder, elbow, forearm and wrist joints are as follows:

Movements associated with the shoulder joint:

- horizontal flexion/extension motion (Figure 2.1);
- vertical flexion/extension motion (Figure 2.2);
- internal/external rotation (Figure 2.3).

Movements associated with the elbow joint and forearm:

- flexion/extension (Figure 2.5);
- pronation/supination (Figure 2.6).

Movements associated with the wrist joint:

- flexion/extension (Figure 2.7);
- radial/ulnar deviation (Figure 2.7).

A combination of the shoulder joint's horizontal and vertical flexion/extension motion is depicted in Figure 2.4. This motion is also known as abduction/adduction motion of the shoulder joint. Note that Figures 2.1-2.5, and Figure 2.7 were drawn using '*Interactive Functional Anatomy'* software (Hillman, 2003). The anatomical ranges of human upper limbs (shoulder, elbow, forearm and wrist joints' movements) are presented in Table 2.1 to Table 2.3.

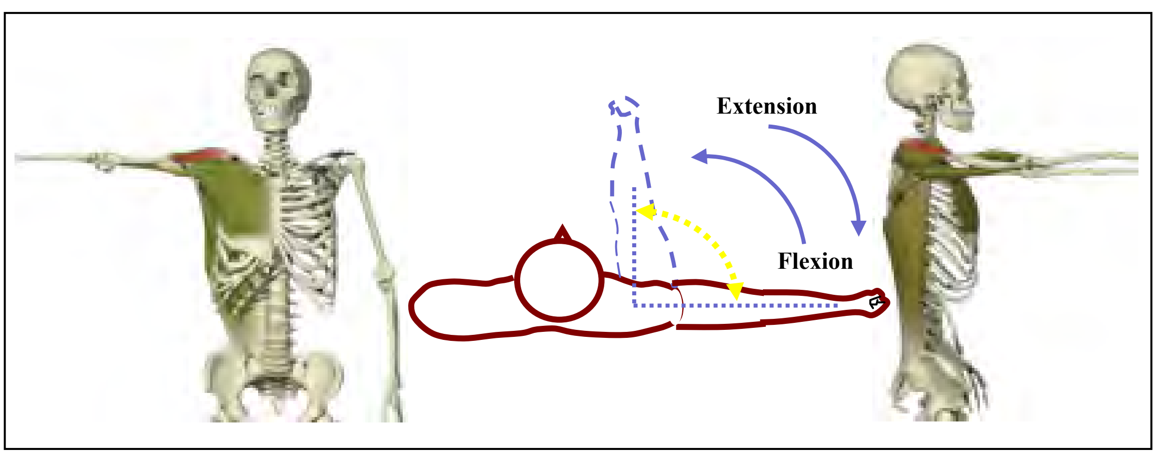


Figure 2.1 Shoulder joint, horizontal flexion/extension

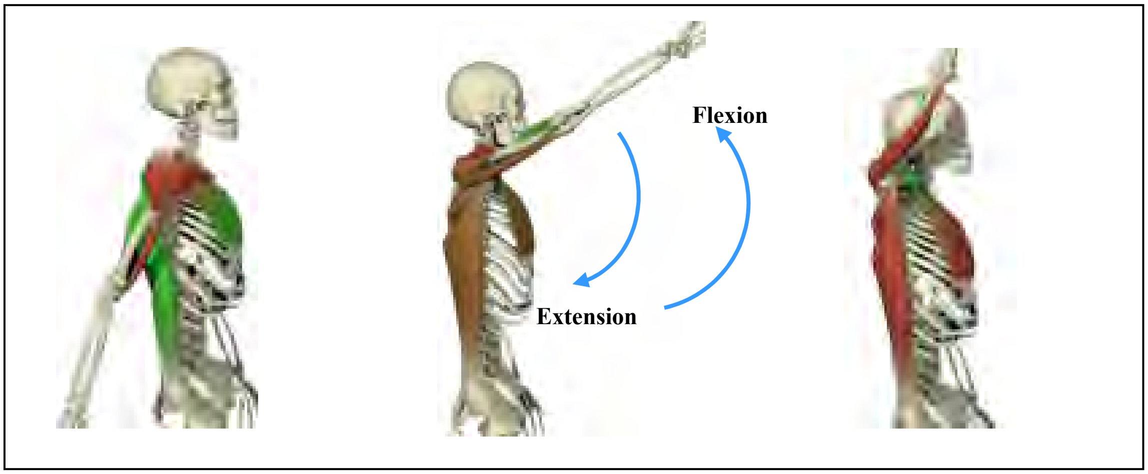


Figure 2.2 Shoulder joint, vertical flexion/extension

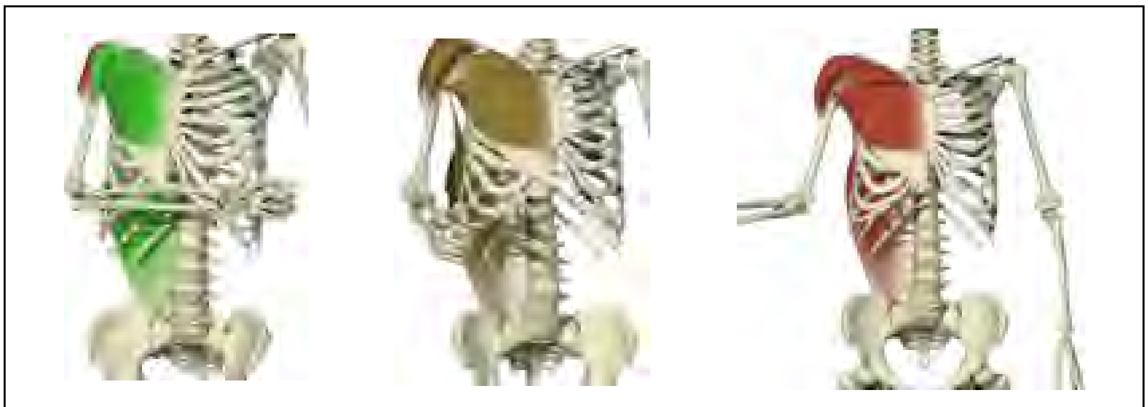


Figure 2.3 Shoulder joint, internal/external rotation

Table 2.1 Shoulder joint's range of movements

| Types of motion | Anatomical Range (Hamilton, Weimar and Luttgens, 2008) | | |
|---|---|---|---|
| | Source1 | Source2 | Source3 |
| Vertical Flexion | 180° | 170° | 180° |
| Vertical Extension | 50° | 30° | 60° |
| Abduction | 180° | 170° | 180° |
| Adduction | 50° | - | - |
| Internal rotation | 90° | 90° | 90° |
| External rotation | 90° | 90° | 60°-90° |

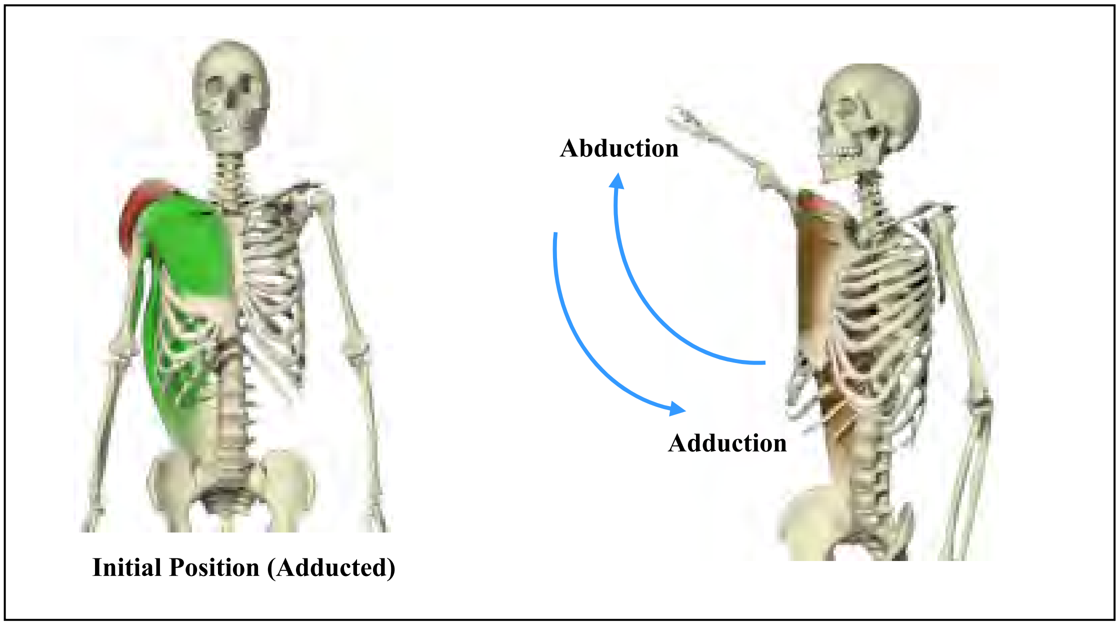


Figure 2.4 Shoulder joint, abduction/adduction

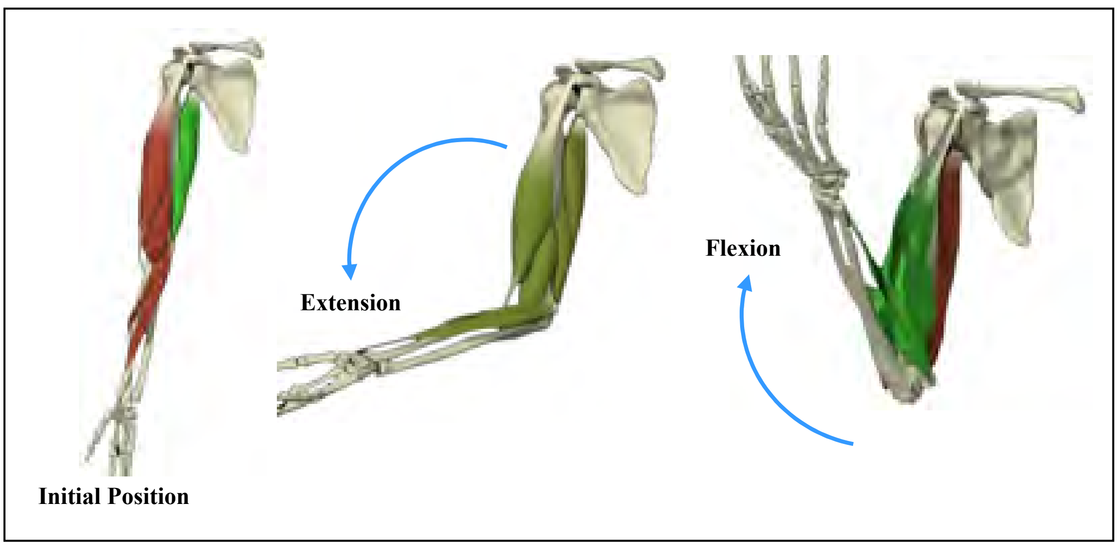


Figure 2.5 Elbow joint, flexion/extension

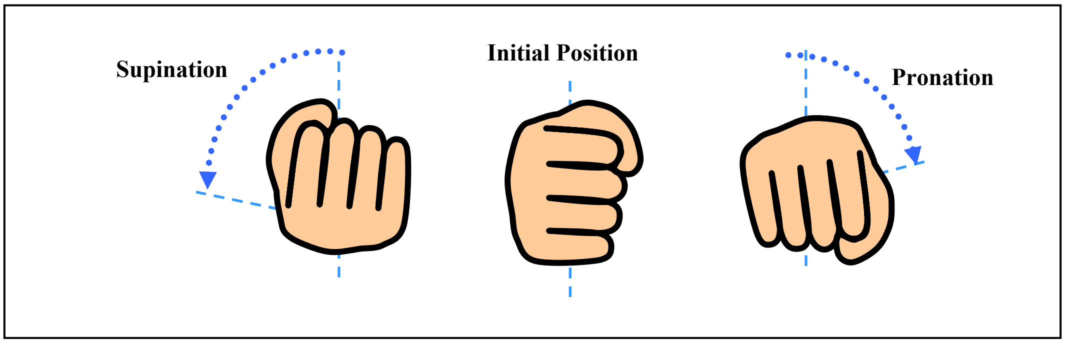


Figure 2.6 Forearm pronation/supination

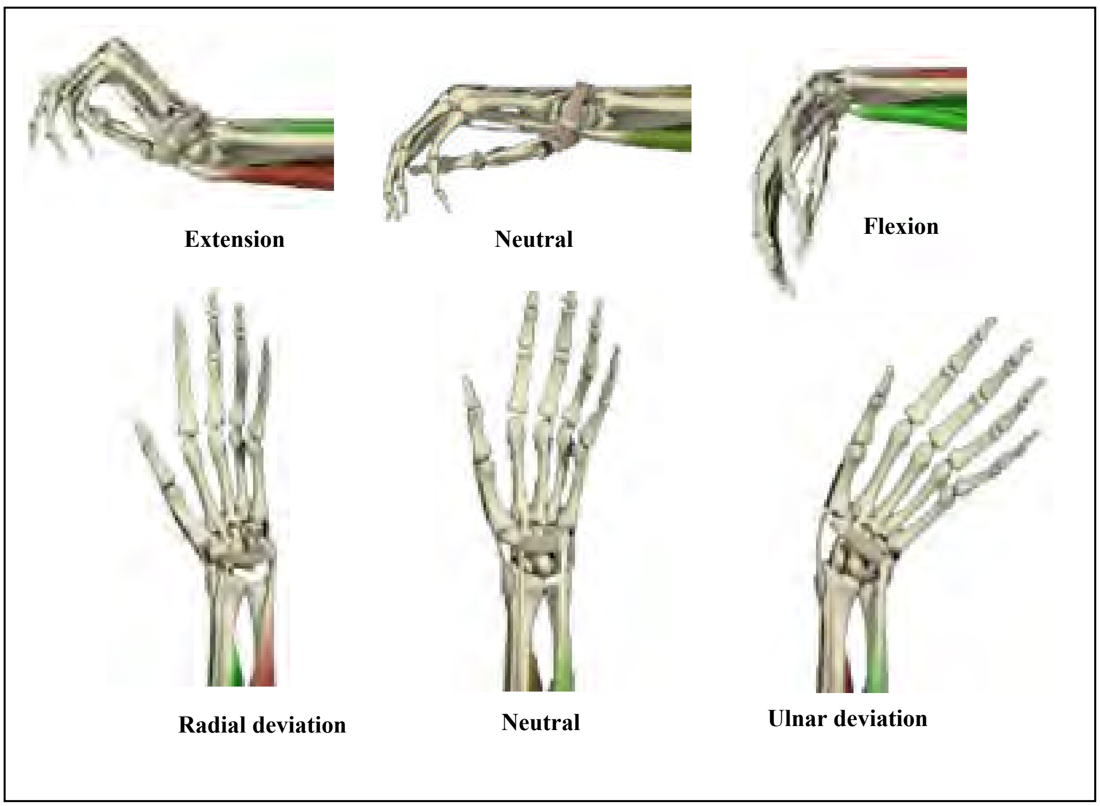


Figure 2.7 Wrist joint movements

Table 2.2 Elbow and forearm range of movements

| Types of motion | Anatomical Range (Hamilton, Weimar and Luttgens, 2008) | | |
|---|---|---|---|
| | Source1 | Source2 | Source3 |
| Flexion | 140° | 140° | 145° |
| Extension | 0° | 0° | 5°-15° |
| Pronation | 80° | 90° | 80° |
| Supination | 80° | 85° | 90° |

Table 2.3 Wrist joint range of movements

| °Types of motion | Anatomical Range (Hamilton, Weimar and Luttgens, 2008) | | |
|---|---|---|---|
| | Source1 | Source2 | Source3 |
| Flexion | 60° | 90° | 60° |
| Extension | 60° | 70° | 50° |
| Radial Deviation | 20° | 20° | 20° |
| Ulnar Deviation | 30° | 30° | 30° |

Therefore, an upper extremity robotic exoskeleton should have 7DoFs and must correspond to the natural range of a human to be able to provide every variety of movement to the upper extremities.

2) Light weight with low mass/inertia:

The structure of the exoskeleton arm should be light in weight to minimize the gravity load and the inertia effects. Therefore, a proper selection of materials is necessary so that the structure possesses sufficient strength and is light in weight. Reasonable material choices could include duralumin, aluminum, or carbon fiber. Besides, a proper selection of actuators is necessary as it is the actuators which are usually heavier in weight and contribute significantly to gravity/inertia effects.

3) Safety:
   A motion assistive device such as an exoskeleton type robot usually works in close contact with the patient, therefore proper and adequate safety features (in hardware and in software) must be included in the design of such devices.

4) Wearing comfort:
   Such devices are supposed to be used by patients for longer periods of time, e.g., for rehabilitation therapy which may take 30-90 minutes per session. Therefore, the device must be comfortable (e.g, ease of fitting, adjustment and removal) and should cause no pain or fatigue to the patient.

5) Accurate force feedback:
   Accurate force feedback is essential for proper control of the motion of the exoskeleton, as well as to relieve robot users from fatigue. Inaccurate or delayed force feedback tends to restrict motion rather than assist it.

6) Complexity:
   In general, a device with a simple structure will be easier to fabricate, be less costly, be more reliable, and thus gain more user acceptance than an unnecessarily complex device. Therefore, in design steps complexity should be kept to a minimum level.

7) Gravity force compensation:
   It is very important that an assistive device can actively support or compensate the subject's arm gravity load as well as the device's own weight while in motion. Poor gravity compensation may add extra load to the subject's arm which is problematic.

## 2.2 Design Consideration for *ETS-MARSE*

Based on the aforementioned requirements; the steps towards meeting the design criteria for the *ETS-MARSE* are presented under the same sub headings:

1) Degrees of freedom and range of motion:

   To ease daily upper-limb movements as well as to provide effective rehab therapy to the upper extremities, the *ETS-MARSE* developed in this research is composed of 7DoFs, therefore it is able to provide every variety of movement to the shoulder, elbow, forearm and wrist joint. Considering the safety of the robot users and the range of movements required to perform essential daily activities e.g., eating, grasping, washing the body etc.(Rosen *et al.*, 2005), preliminary studies on the anatomical range of upper limb motion were conducted (Hamilton, Weimar and Luttgens, 2008; Rahman *et al.*, 2011e; Rosen *et al.*, 2005) to choose the suitable range for the *ETS-MARSE (Rahman et al., 2011c)*. Details on the selected range of motion of the *ETS-MARSE* are summarized in Table 2.4.

Table 2.4 *ETS-MARSE's* Workspace

| | **Types of Motion** | ***ETS-MARSE*'s Workspace** |
|---|---|---|
| | Shoulder Joint | |
| Joint 1 } | Flexion | 140° |
| | Extension | 0° |
| Joint 2 } | Abduction | 140° |
| | Adduction | 0° |
| Joint 3 } | Internal rotation | - 85° |
| | External rotation | +75° |
| | Elbow & Forearm | |
| Joint 4 } | Flexion | 120° |
| | Extension | 0° |
| Joint 5 } | Pronation | - 85° |
| | Supination | +85° |
| | Wrist Joint | |
| Joint 6 } | Flexion | + 60° |
| | Extension | - 50° |
| Joint 7 } | Radial Deviation | + 20° |
| | Ulnar Deviation | - 25° |

2) Light weight with low mass/inertia:

   The entire *ETS-MARSE* arm was fabricated in aluminum to give the exoskeleton structure a relatively light weight. Note that aluminum is a low density metal having reasonable strength characteristics and is very suitable for this kind of application. The high stress joint sections of the exoskeleton system were fabricated in mild steel. This resulted in a stable and light structure to the exoskeleton. It is to be noted that, in the design of *ETS-MARSE,* power to weight ratio was maximized by selecting appropriate actuators for each joint mechanism. Simulation was carried out to investigate the maximum torque required or developed for each joint movement. Results of these simulations are presented in Chapter-4. Note that the actuators were then selected based on the simulated results, to optimize the power/weight ratio

   In this research we have used brushless DC motors, Maxon EC90, Maxon EC45. Detailed specifications of these motors can be found in ANNEX IX and ANNEX X. It should be mentioned that brushless DC motors have many advantages compared to brushed DC motors, including high torque to weight ratio, long life span (as there is no brush and commutator erosion), more torque per watt, increased reliability, reduced noise, and little or no maintenance (Glinka and Polak, 2001; Kothari and Nagrath, 2004). Moreover these motors are able to develop maximum torque when stationary (Gopal, 2002).

3) Safety:

   To satisfy this requirement, mechanical stoppers were added at each joint to limit the joints' rotation within the range of *ETS-MARSE's* workspace (Table 2.4). An emergency switch is also installed to cut off the power should the need arise. On top of these *hardware safety features*, *software safety features* were added in the control algorithm which include limiting the joints' ranges of movements depending on patient requirements, limiting the joints' speed, limiting the joints' torques and limiting the voltage values, which are the final output of the controller and the command values to the motor drivers.

4) Wearing comfort:

   Soft flexible straps were used to hold the upper arm, forearm and wrist in proper position. The *ETS-MARSE* arm was designed for use by a 'typical adult'. However, provisions are included to adjust the link length to accommodate a wide range of users (5ft ~6.2ft), which is one of the key aspects of the design. To facilitate ease of fitting adjustment and removal, an open-type forearm and upper arm cup is used to hold the subject's arm instead of closed structure (Gopura, Kiguchi and Yang, 2009).

5) Accurate force feedback:

   To satisfy this requirement, a high linearity 6 axis force sensor (NANO17-R-1.8-M2-M1PCI, ATI) was instrumented underneath the wrist handle to obtain accurate real time force measurements. The detailed specifications of the force sensor can be found in ANNEX VIII. Note that the force sensor signals are intended to input information to the controller while developing a control strategy to provide active rehabilitation therapy.

6) Gravity force compensation:

   The controllers were designed so that they update the gravity terms in real time to compensate for gravity effects. Note that the *compliance control with gravity force compensation technique* and other nonlinear control techniques such as *computed torque control*, *sliding mode control* and *modified sliding mode exponential reaching law control* used in this research include the human arm dynamics (i.e., mass/inertia properties) as well as the dynamics of the *ETS-MARSE* arm.

7) Complexity:

   The key design consideration of the *ETS-MARSE* was to make it compact in shape while keeping the complexity to a minimum. For example, to avoid the complex cable routing that can be found in many exoskeleton systems (Frisoli *et al.*, 2009; Kiguchi *et al.*, 2003), a novel power transmission mechanism was introduced for assisting shoulder joint internal/external rotation (Rahman *et al.*, 2010a) and for forearm pronation/supination (Rahman *et al.*, 2011b).

Details of the development of the *ETS-MARSE* are described in the next sections.

## 2.3 Development of *ETS- MARSE*

The general layout of the development of the *ETS-MARSE* system is outlined in Figure 2.8. As seen from the layout, the entire process is divided into two major phases; the *hardware phase* that includes CAD modeling, simulation, design, and fabrication; and the *control phase* which includes kinematic and dynamic modeling, control, simulations, and experiments. This chapter describes only the hardware implementation steps.

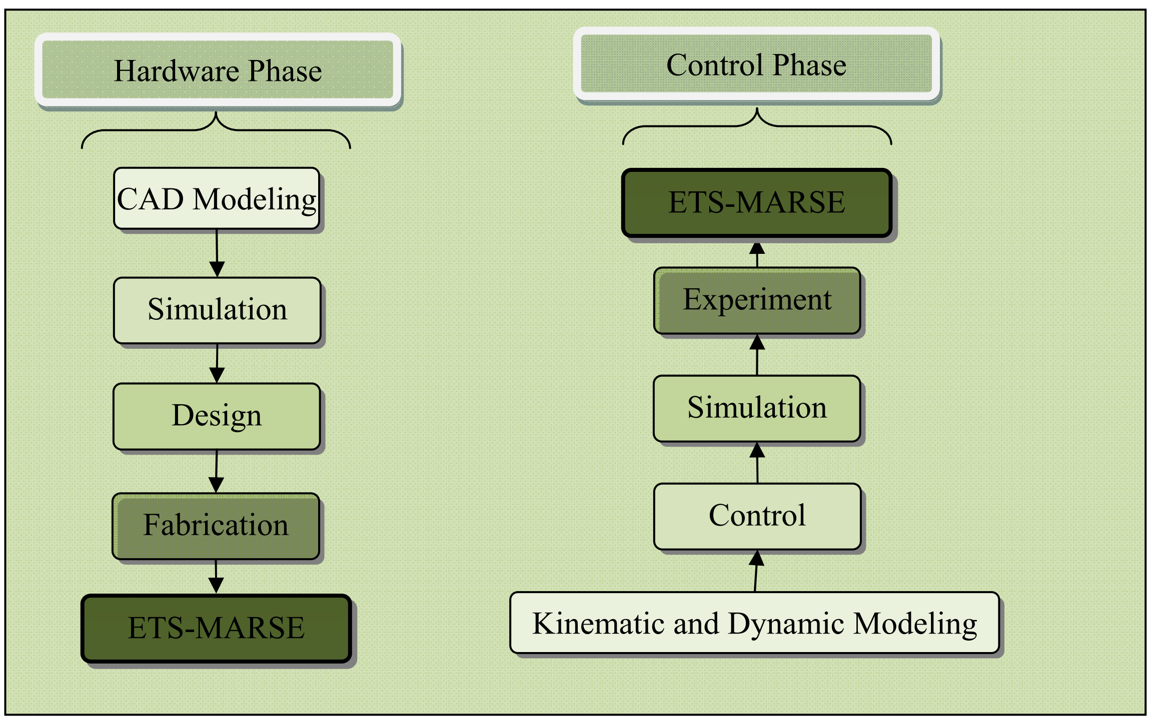


Figure 2.8 General layout of the development of *ETS-MARSE*

## 2.4 Hardware implementation of *ETS-MARSE*

### 2.4.1 CAD Modeling

In this step, a detailed study of the biomechanics of human upper extremities was performed (Rahman *et al.*, 2011e) to estimate the upper limb parameters such as arm length, mass of different limb segments (ANNEX I), joint articulations and range of movements. (Holzbaur, Murray and Delp, 2005; Rosen *et al.*, 2005; Winter, 1990) to model the *ETS-MARSE.* Later, taking into account the aforementioned design considerations, CAD modeling of the proposed exoskeleton system was carried out using Pro-Engineer software. Note that the mass and inertial characteristics of the *ETS-MARSE* were estimated in CAD environment (ANNEX III to ANNEX VII).

### 2.4.2 Simulation

In the *hardware implementation phase,* simulation was carried out in two stages. In the first stage, a simulation was carried out to determine the maximum torque for each joint movement (Rahman *et al.*, 2011e). The mass and inertia characteristics of human upper extremities used in the simulation are given in ANNEX I and ANNEX II and those for the *ETS-MARSE* arm are given in ANNEX III to ANNEX VII. Note that the simulation was carried out in Simulink (MathWorks, USA) environment. Details of the simulation results are presented in CHAPTER 4 (Rahman *et al.*, 2011e). Based on the simulated results, actuators were selected to optimize the power/weight ratio. The second stage of the simulation was performed just before beginning the fabrication process, where the CAD model of the *ETS-MARSE* was double checked and validated in regards to achieving the targeted joints' range of motion. Moreover, in this stage, the compatibility of the system was verified for necessary instrumentation of electrical and electronic parts. It should be noted that the second stage of simulation was carried out in CAD (Pro-Engineer software) environment.

### 2.4.3 Design

1) Mechanical Design

   The exoskeleton-robot *ETS-MARSE* developed in this research (Figure 2.9) is comprised of three major parts: the shoulder motion support part, the elbow and forearm motion support part, and the wrist motion support part.

Shoulder motion support part (horizontal and vertical flexion/extension):

The shoulder joint motion support part has 3DoFs (Rahman *et al.*, 2010a) and is able to assist with horizontal and vertical flexion/extension motion, and internal/external rotation of shoulder joint. To assist with horizontal and vertical flexion/extension motions, it

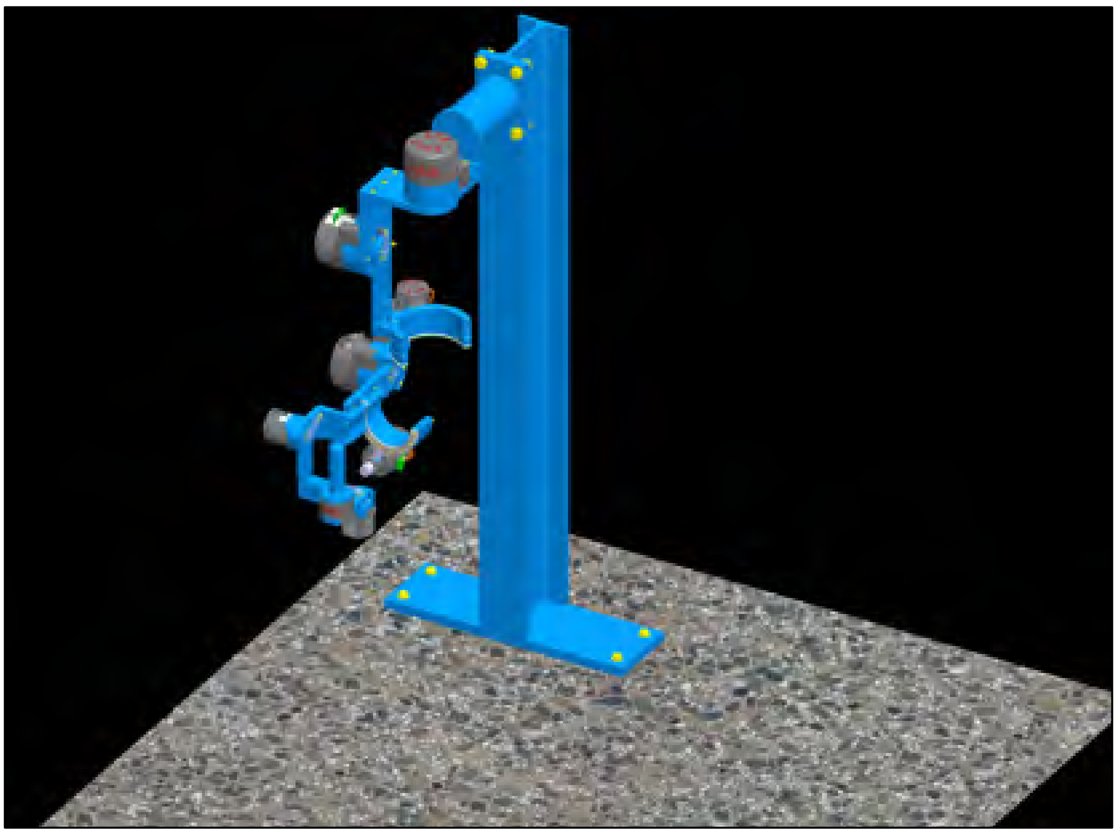

Figure 2.9 ETS-MARSE (CAD, view)

consists of two motors (Maxon EC-90), two links (link-A, and link-B), and two potentiometers. Link-A holds motor-1 at one end (Figure 2.11) and is rigidly fixed to the base structure of the robot (Figure 2.10) at its other end. As shown in Figure 2.11, link-B, which is hinged with motor-1 and carries motor-2 on its other end, is 'L' shaped in order to accommodate the subject's shoulder joint. Therefore, the axes of rotation of motors 1 and 2 intersect at the centre of rotation of the subject's shoulder joint (point-B, Figure 2.10). Moreover, by adjusting the seating height (e.g., using a height adjustable chair) it would be easy to align the centre of rotation of the shoulder joint of the subject to that of the *ETS-MARSE*. It is worth mentioning here that there is no scapular elevation (rather than pure rotation) during the abduction of the glenohumeral joint (GHJ) (Hallaceli, Manisali and Gunal, 2004). However, the scapular elevation of subjects, which is common due to GHJ flexion, will be allowed normally during the vertical flexion motion of the *ETS-MARSE* and there should be no discomfort to the subject if the centre of rotation of their shoulder joint is aligned with that of *ETS-MARSE*. Note that motor-1 is responsible for the shoulder joint's horizontal flexion/extension motion and motor-2 is for the vertical flexion/extension motion.

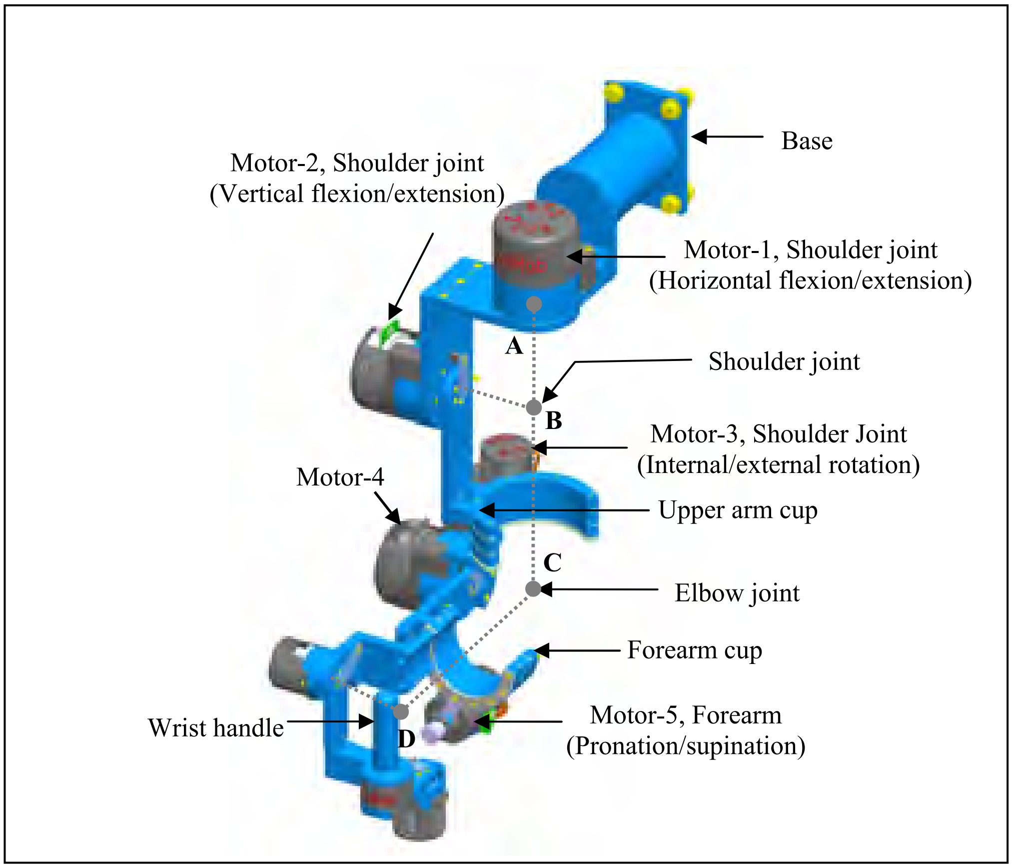


Figure 2.10 A 7 DoFs *ETS-MARSE* arm, (right hand side view)

The actuation mechanisms developed for the shoulder joint internal/external rotation (1DoF) support part and the forearm motion support part (1DoF) are somewhat complex, as it is impossible to place any actuator along the axis of rotation of the upper arm (e.g., with the humerus/radius), due to the anatomical configuration of the human arm. Some devices use gear mechanisms with a closed circular structure of forearm/upper arm cup

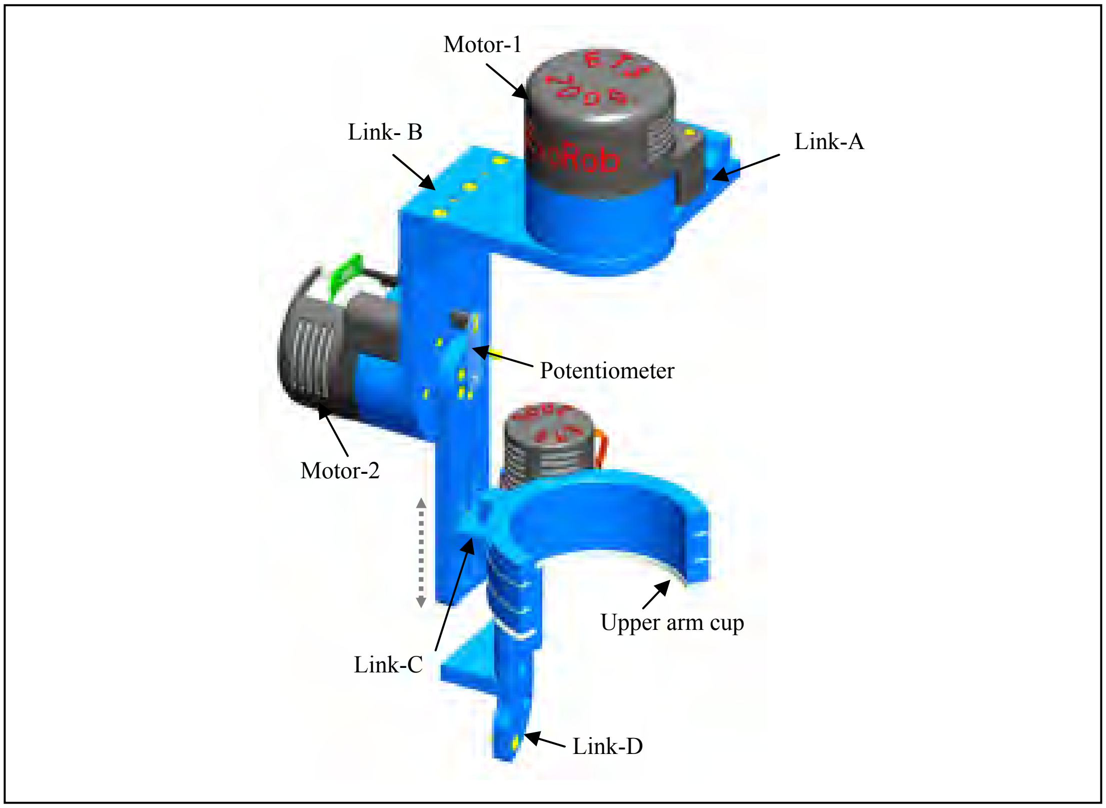


Figure 2.11 Shoulder motion support part
(horizontal and vertical flexion/extension motion)

(Gopura, Kiguchi and Yang, 2009; Gupta and O'Malley, 2006). However, it is unrealistic and inconvenient to insert and remove the arm through a closed circular structure. Other devices make use of a complex cable transmission mechanism to assist with forearm motion (Frisoli *et al.*, 2009; Perry, Rosen and Burns, 2007). One of the major limitations of such cable driven systems is that it delivers undesirable vibration and excessive compliance to the system. To deal with this problem, this research introduced an innovative concept of power transmission, a combination of a custom-made open-type bearing and open type meshing gear assembly (Rahman *et al.*, 2010c), where motion is transmitted from an anti-backlash gear (mounted on a motor shaft) to an open type, custom-made meshing ring gear that is rigidly attached to the open type upper/forearm cup. Details of this transmission mechanism are discussed below.

A new power transmission mechanism (alternate gear mechanism):

The transmission mechanism as proposed in this research introduced the concept and the development of an open type bearing. Unlike conventional bearings as depicted in Figure 2.12, this open type bearing makes use of two layers of bearing balls (Figure 2.13), therefore it requires two specially designed bearing ball cages. Moreover, it has three bearing races (upper race, intermediate race, and lower race, Figure 2.13 and Figure 2.14) instead of two as often found in the conventional type of bearing. Figure 2.13 shows the intermediate race which is designed to hold stainless steel balls (4mm diameter) on its both sides by using the bearing ball cages. The upper and lower race assembly is shown in Figure 2.14, where it can be seen that the bearing races were assembled with the upper arm or forearm cup. As also depicted in Figure 2.14, the ring gear which is used in transmitting power from the actuator is assembled underneath the arm cup. The entire bearing assembly is shown in Figure 2.15. Note that the ball bearings are positioned between the groove of the intermediate race and the upper/lower races, and act as a frictionless rotating mechanism.

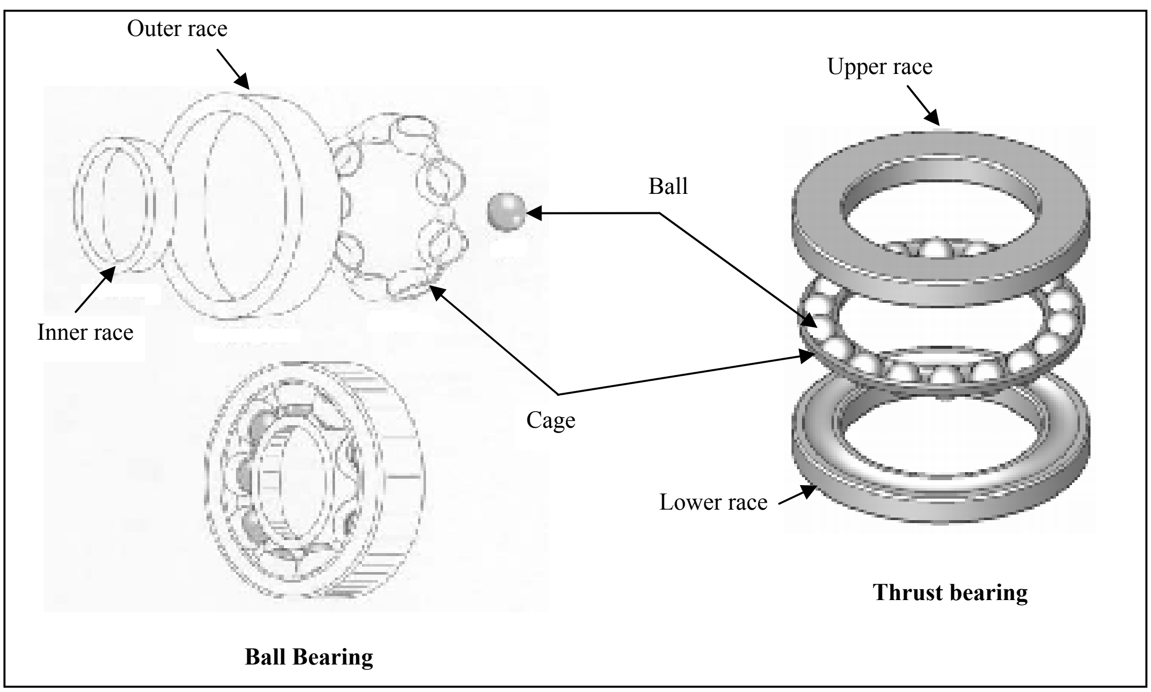


Figure 2.12 Conventional bearing
Adapted from Silberwolf (2006)

The developed actuation mechanism, which is a combination of an open type gear and bearing, is depicted in Figure 2.16, where it can be seen that the actuator (motor) is rigidly mounted on the back of the intermediate race. It is the anti-backlash gear which is clamped along the motor shaft and transmits the actuator (rotary) motion to the ring gear. Since the ring gear is firmly fixed to the arm cup, it rotates the arm cup as well over the custom-designed open type bearing.

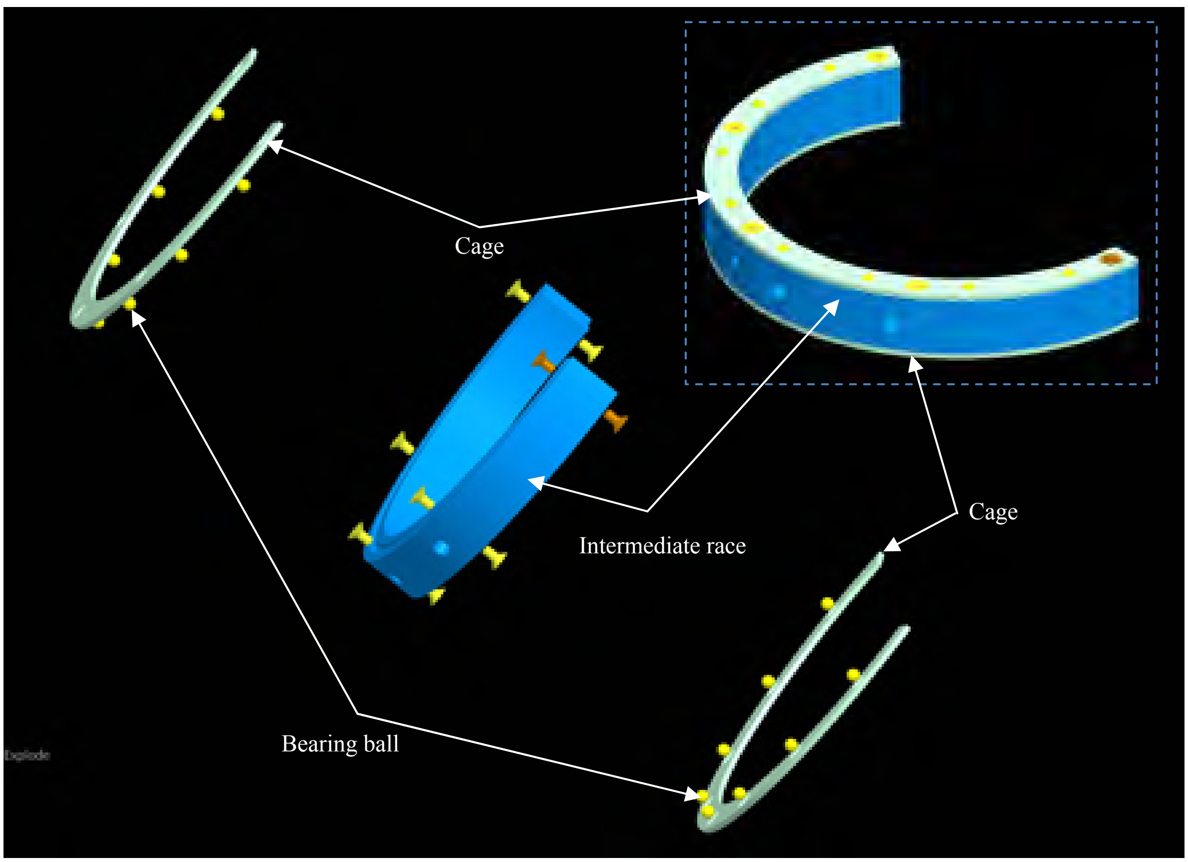


Figure 2.13 Intermediate race assembly

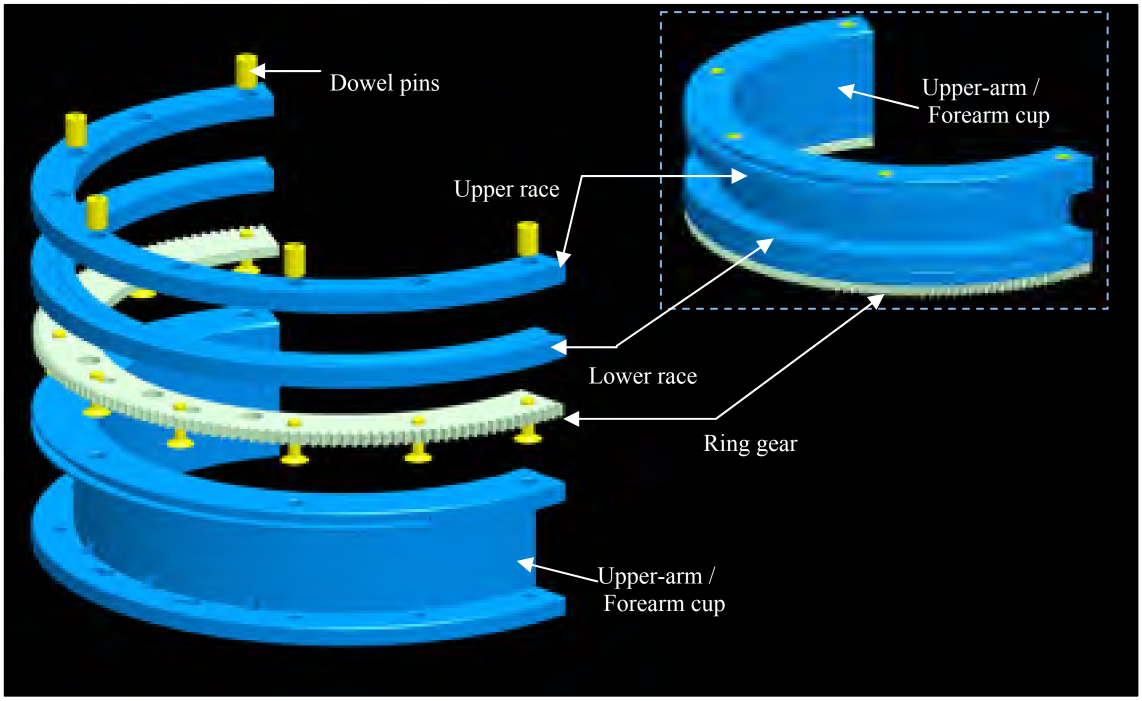


Figure 2.14 Upper and lower race assembly

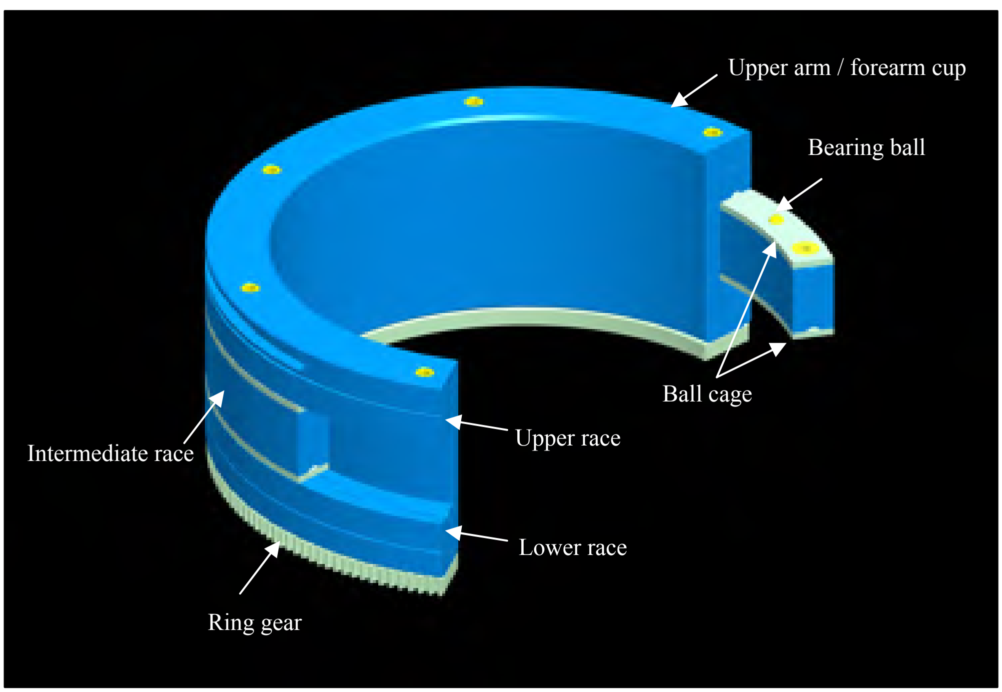


Figure 2.15 An open type bearing assembly

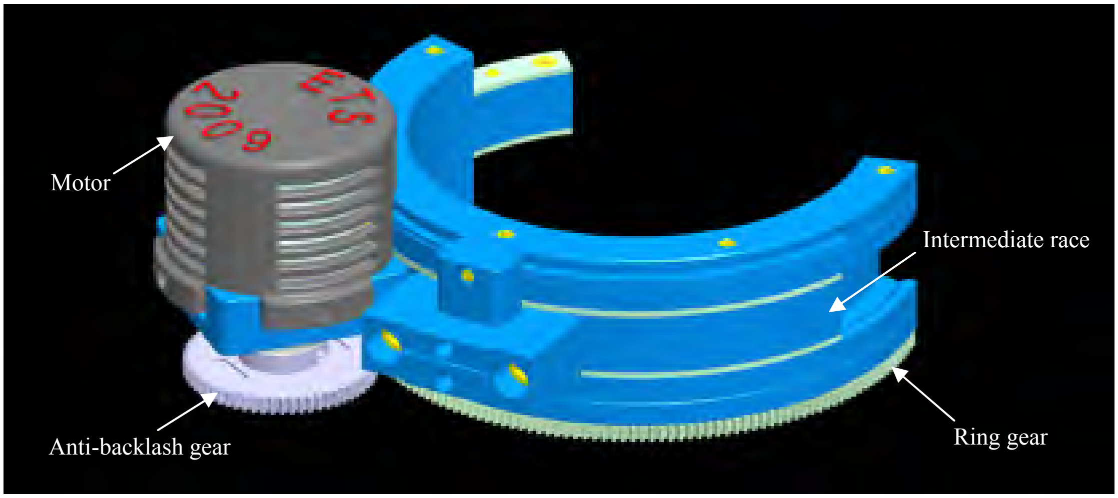


Figure 2.16 Actuation mechanism with an open type bearing and a ring gear

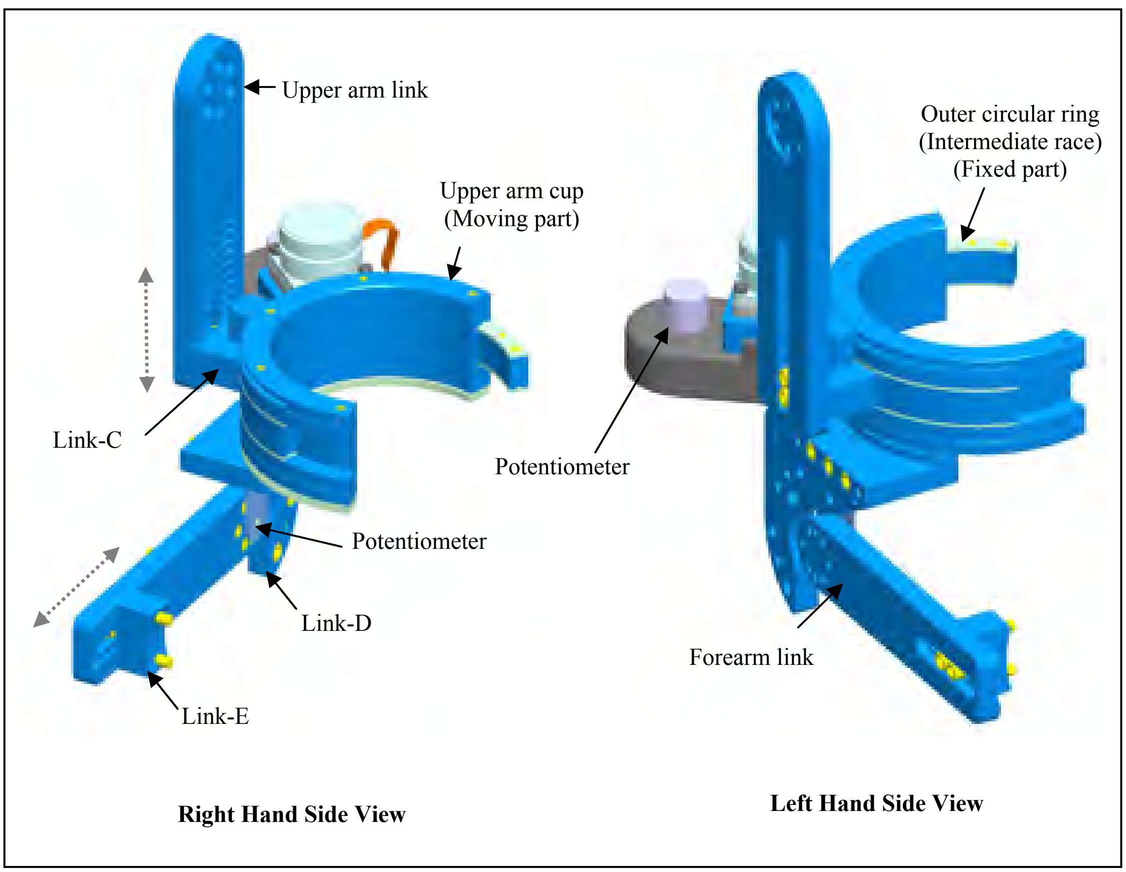


Figure 2.17 Shoulder joint internal/external rotation support part
(when elbow motor is unplugged from elbow joint)

Shoulder motion support part (internal/external rotation) (Rahman *et al.*, 2012d):
To assist with shoulder joint internal/external rotation, the *ETS-MARSE* is comprised of an upper arm link, a sliding link (link-C), a motor (Maxon EC-45), a potentiometer, and an alternate gear mechanism as discussed above (i.e., a custom-made open type bearing, a ring gear, and an anti-backlash gear assembly). The upper-arm link, as shown in Figure 2.17, is hinged with the motor-2 (Figure 2.11) and holds the entire *MARSE* arm. The link-C (Figure 2.18) is rigidly fixed with the outer circular ring (i.e., with the intermediate race of the bearing) and is able to slide along the upper arm link (Figure 2.18, dotted arrow) so that the distance between the upper arm cup and shoulder joint (as well as the distance between elbow joint and shoulder joint) may be adjusted to accommodate a wide range of users. The open half-circular structure of the upper arm cup allows users to position the arm easily, without having to insert the arm through a closed circular structure. As depicted in Figure 2.18, the motor-3 (Maxon EC-45) is rigidly mounted on the back of

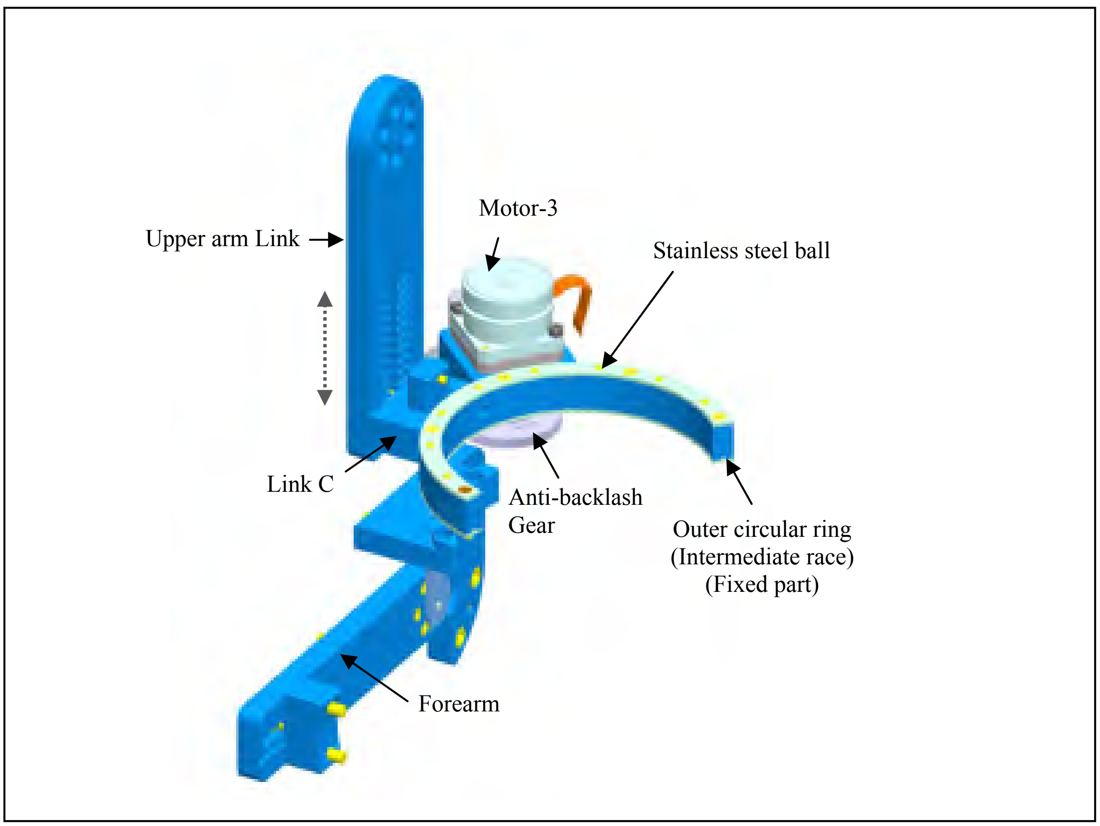


Figure 2.18 Intermediate race assembly with the upper arm link

the intermediate race (i.e., with the fixed outer ring). Figure 2.19 shows the anti-backlash gear which is clamped along the motor shaft to transmit the rotary motion to the ring gear. As discussed previously, in the development of '*alternate gear mechanism'*, since the ring gear is firmly fixed underneath the upper arm cup (Figure 2.19), it is therefore responsible for rotation of the upper arm cup over the custom-designed open type bearing.

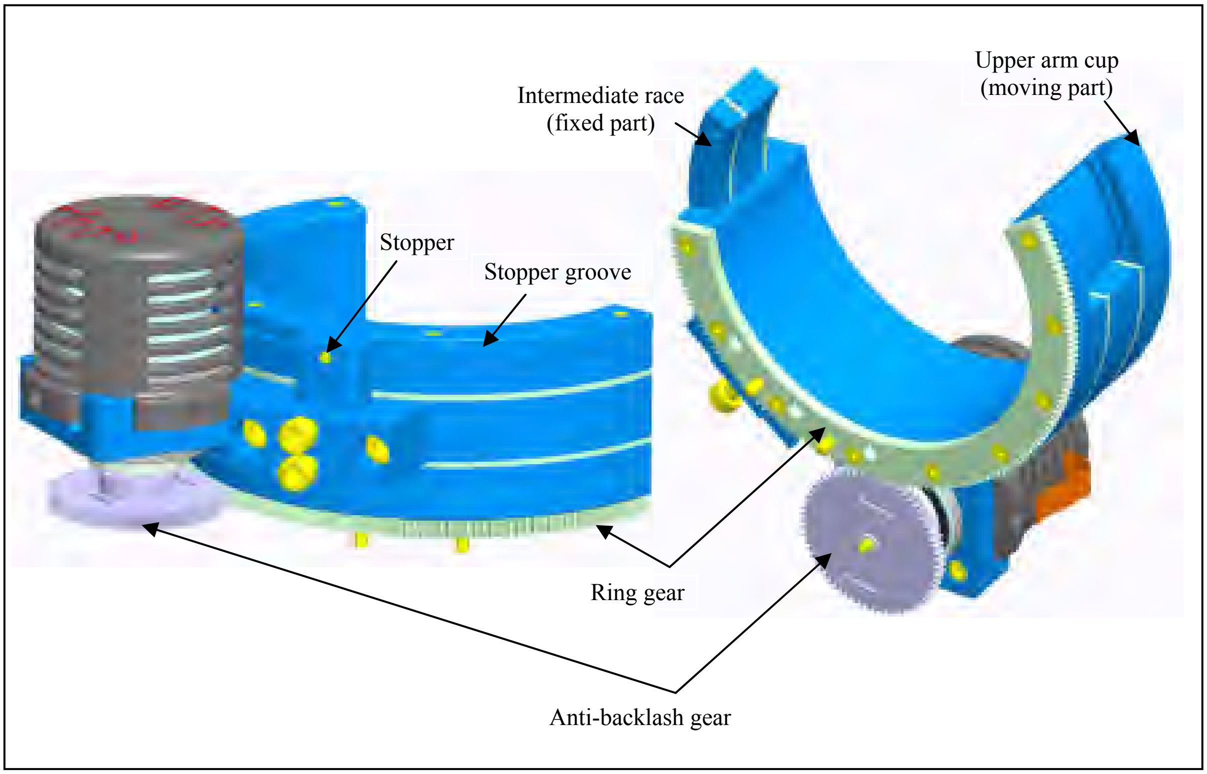


Figure 2.19 Actuation mechanism for shoulder joint internal/external rotation

Elbow and forearm motion support part (Rahman *et al.*, 2011b; Rahman *et al.*, 2010c): The elbow motion support part is comprised of a forearm link, a fixed link (Link-D), a motor (Maxon EC-90) and a potentiometer. As shown in Figure 2.20, link-D acts as a bridge between the shoulder joint internal/external rotation support part and the elbow motion support part. One end is assembled with the upper-arm cup and the other end holds the elbow motor as well as the elbow motion support part. The forearm link as depicted in Figure 2.20 is hinged with the elbow motor at the elbow joint (Figure 2.20) and carries the entire forearm motion support part.

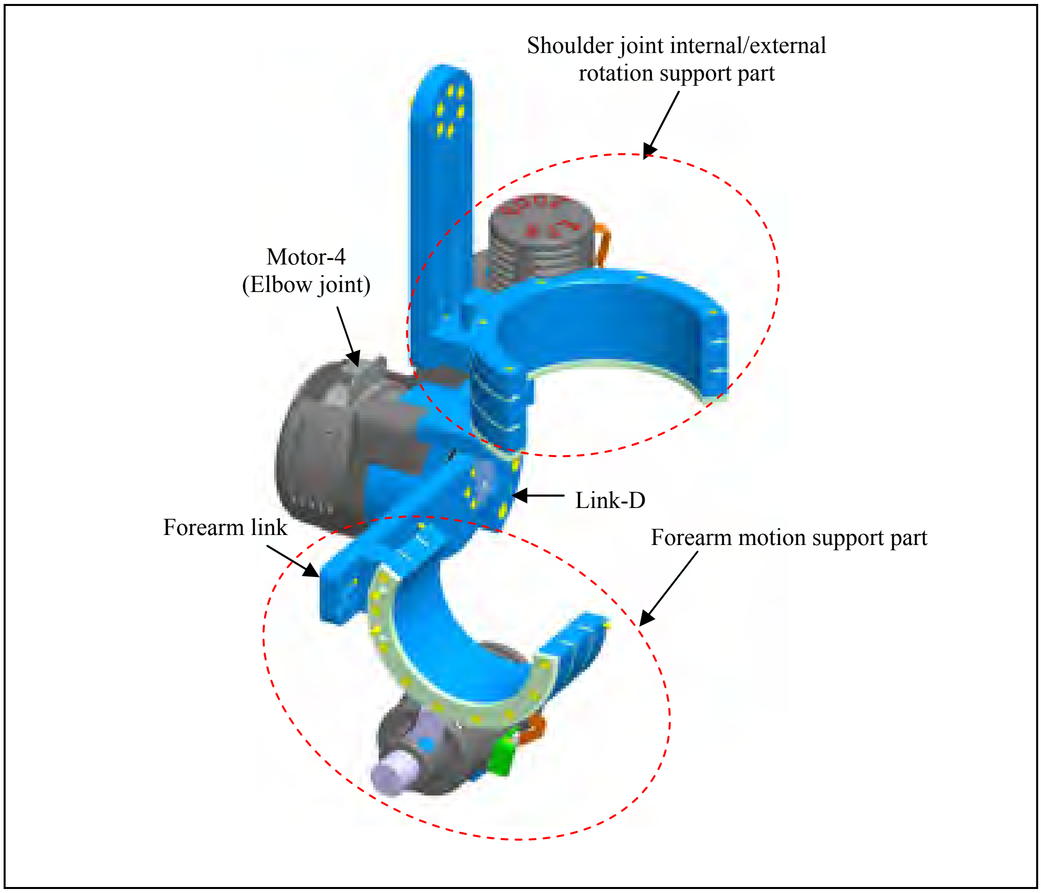


Figure 2.20 Elbow motion support part

The forearm motion support part consists of a sliding link (link-E), a motor (Maxon EC-45), a potentiometer, and an alternate gear mechanism (i.e., a custom made open type bearing, a ring gear, and an anti-backlash gear assembly). The sliding link (link-E) is rigidly fixed with the intermediate race (i.e., outer circular ring as depicted in Figure 2.22) and is able to slide along the forearm link (Figure 2.22 dotted arrow) to adjust the distance between the forearm strap and the elbow joint (as well as to adjust the distance between elbow and wrist joints). The design principle of the forearm motion support part is quite similar to that of the shoulder joint internal/external support part. As for the upper-arm cup, the open half-circular structure of the forearm cup allows users to place and position their forearm easily, without having to insert the forearm through a closed circular structure. The motor (Maxon-EC45) is rigidly mounted on the back of the fixed outer circular ring. Figure 2.22 shows the anti-backlash gear, which is clamped along the motor shaft to transmit the rotary motion to the ring gear. As also shown in Figure 2.22, the ring gear (open type) is firmly fixed to the forearm arm cup and is responsible for rotating the forearm arm cup over the custom-designed open type bearing. Note that to hold the upper arm/forearm in a proper position, soft arm straps (Figure 2.23) are attached to the upper-arm and forearm cups.

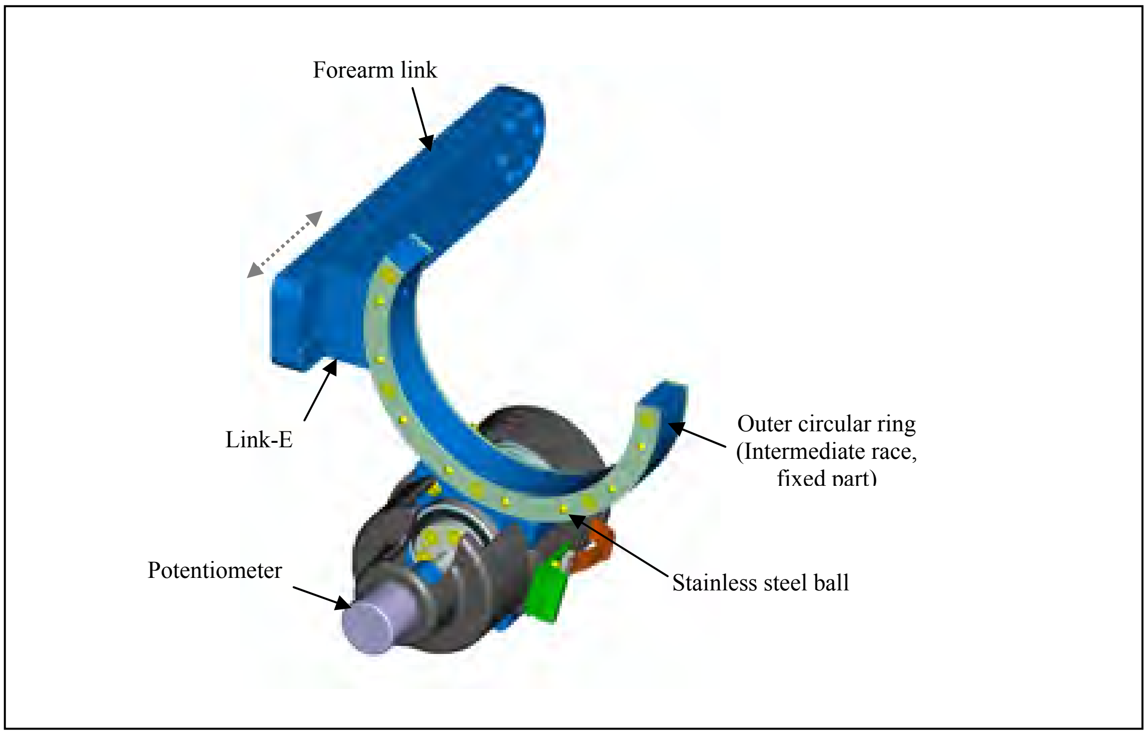


Figure 2.21 Forearm motion support part (when forearm cup is not assembled)

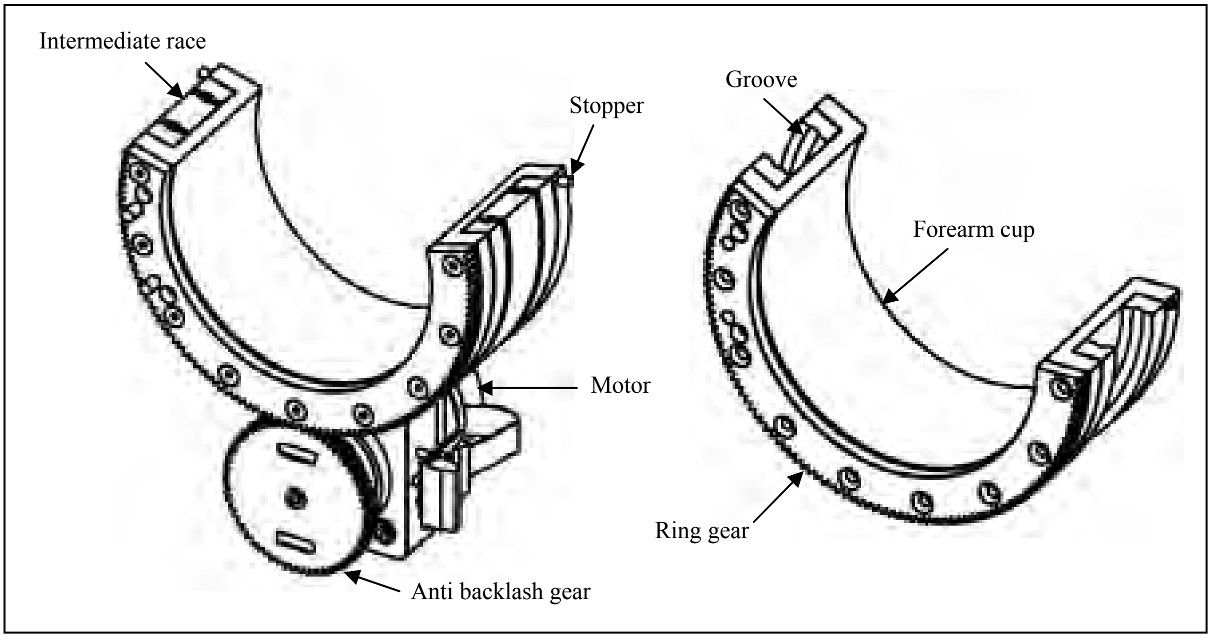


Figure 2.22 Forearm motion support part, showing the gear arrangement and forearm cup assembly to the fixed outer ring

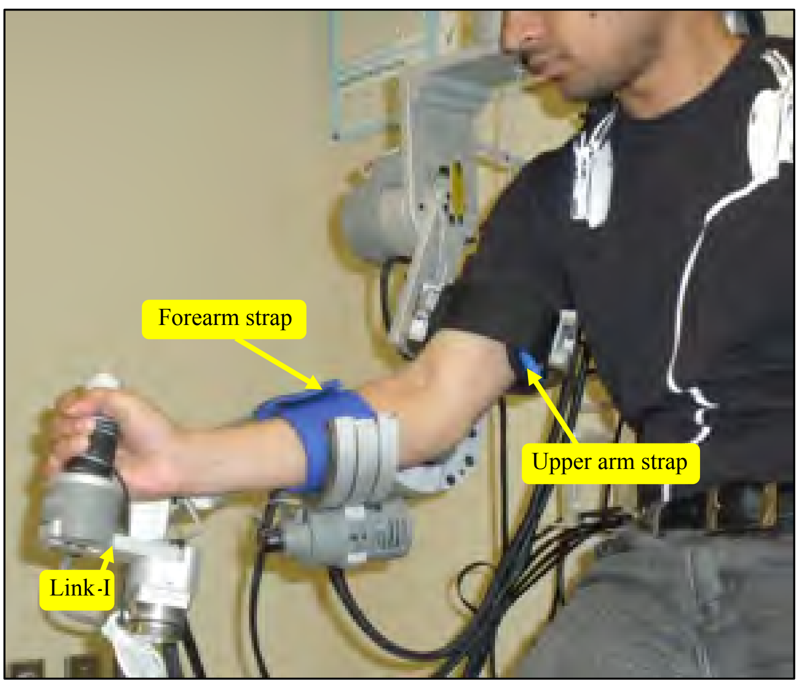


Figure 2.23 *ETS-MARSE* with its user

Wrist motion support part (Rahman *et al.,* 2010b):

The wrist motion support part (as shown in Figure 2.24) has 2DoFs: one for assisting *'radial/ulnar deviation,'* the other for assisting *'flexion/extension'* motion. To assist in the movement of radial/ulnar deviation (at wrist joint), the *ETS-MARSE* is comprised of a fixed link (link-F), a motor (Maxon EC-45), and a potentiometer. Link-F (as shown in Figure 2.24) is rigidly fixed with the forearm cup and holds motor-6 (Maxon EC-45) at its other end, which corresponds to joint 6 (radial/ulnar deviation) of the *ETS-MARSE*.

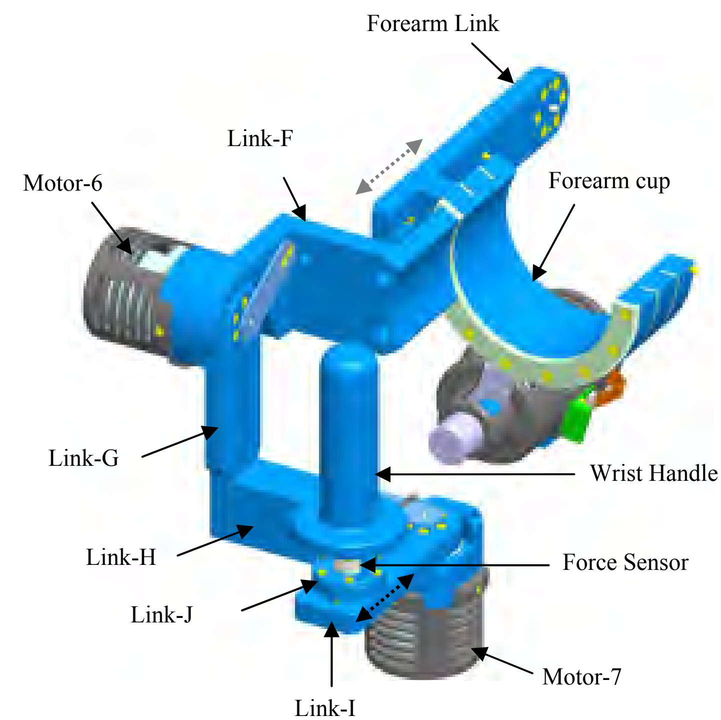


Figure 2.24 Wrist motion support part (2DoFs)

The flexion/extension motion support part of the wrist joint consists of three fixed links (G, H and I), one sliding link (link-K), a motor (Maxon EC-45), a potentiometer, and a wrist handle. As shown in Figure 2.24, link-G is hinged with joint-6 and holds the flexion/extension motion support part of the wrist joint. Link-H at its one end is fixed with link-G and rigidly holds motor-7 to its other end. It can be seen also from Figure

2.24 that link-I is hinged to motor-7 and carries the wrist handle on its other end. A sliding link (link-J) is positioned in between link-I and the wrist handle, which allows to adjust the distance between the wrist joint and the wrist grip.

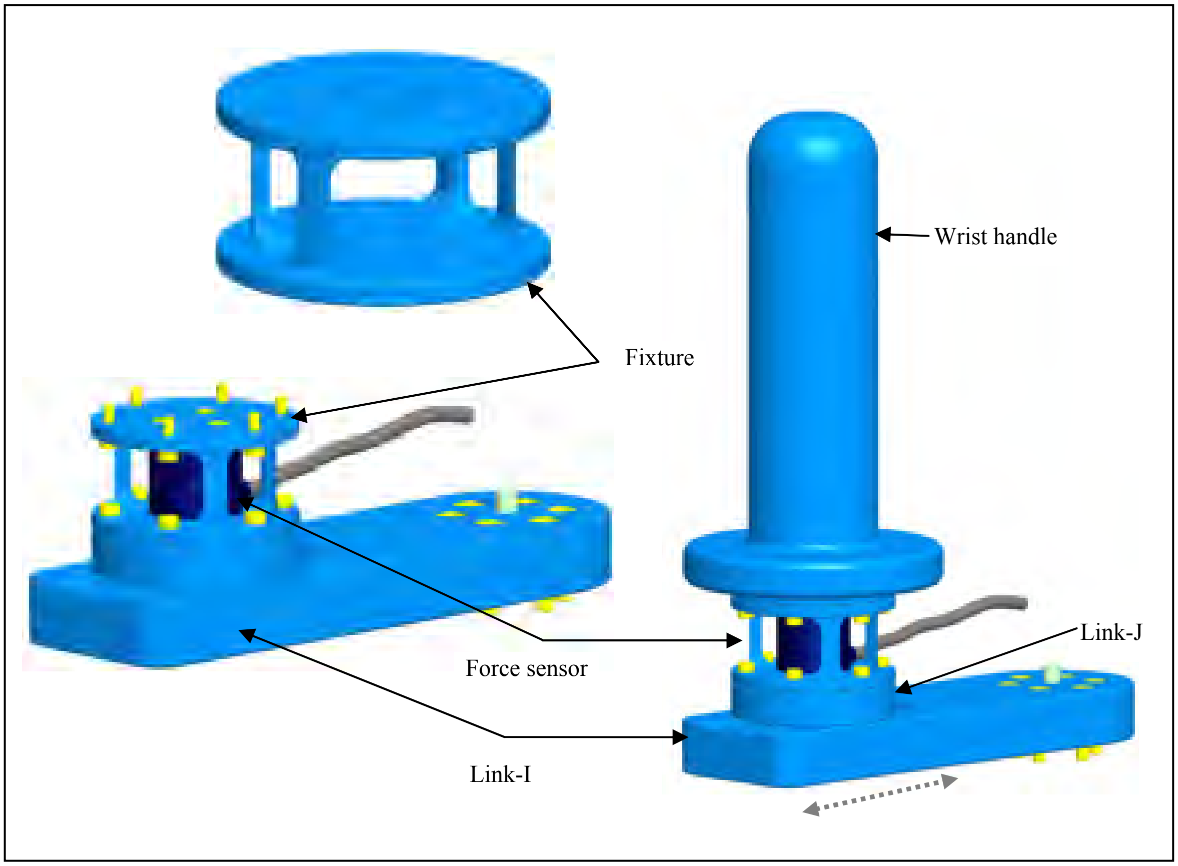


Figure 2.25 Force sensor assembly

As shown in Figure 2.25, a high linearity 6-axis force sensor (Nano 17, ATI) is instrumented underneath the wrist handle to measure the instantaneous reaction force. Note that the force sensor is installed within a fixture which is designed in such a way so that it can protect the sensor from overloading and/or torque. This signal will be used to actuate *ETS-MARSE* in order to provide active assistance.

The detailed specifications of the *ETS-MARSE* are summarized in Table 2.5.

Table 2.5 *ETS-MARSE* at a Glance

| **Mass and Inertia* (*diagonal terms*) Characteristics** | | | | | |
|---|---|---|---|---|---|
| *ETS-MARSE* Arm Segment | Segment length (cm) | Segment weight (kg) | Moment of Inertia *I* (kg.m²) | | |
| | | | *Ixx* | *Iyy* | *Izz* |
| Shoulder Joint[A] | 14.0 | 3.47 | 0.0232 | 0.0148 | 0.013 |
| Upper arm[B] | 25 ± 8.85 | 3.737 | 0.0233 | 0.0128 | 0.020 |
| Forearm[C] | 26 ± 4.75 | 2.066 | 0.0166 | 0.0100 | 0.0126 |
| Wrist | - | 0.779 | 0.0029 | 0.0019 | 0.0012 |
| Hand [D] | 9.8 ± 3.55 | 0.49 | 0.0010 | 0.0012 | 0.0003 |

| Actuators, Maxon (Brushless) | | |
|---|---|---|
| Spec | EC-90, Flat 90W (Joint-1,2,4) | EC-45, 30W (Joint-3,5-7) |
| Nominal Voltage (V) | 24 | 12 |
| Nominal Speed (rpm) | 2650 | 2860 |
| Nominal Torque (mNm) | 387 | 59 |
| Max. Perm. Speed (rpm) | 5000 | 10000 |
| Torque Const. (mNm/A) | 70.5 | 25.5 |
| Stall Torque (mNm) | 4670 | 255 |
| Weight (g) | 648 | 88 |

| Harmonic Drives | | | |
|---|---|---|---|
| Spec: CSF-2XH- | 2UH-17-120-F (Joint 1,2) | 2XH-14-100-F (Joint 4) | 2XH-11-100-F (Joint 3,5-7) |
| Torque at 2000 rpm (Nm) | 24 | 7.8 | 5 |
| Repeated Peak Torque (Nm) | 54 | 28 | 11 |
| Average Torque (Nm) | 39 | 11 | 8.9 |
| Gear Ratio | 120 | 100 | 100 |

| Force Sensors, ATI, Nano 17 | | | | |
|---|---|---|---|---|
| Axes: | Fx, Fy (±N) | Fz (±N) | Tx, Ty (±Nmm) | Tz (±Nmm) |
| | 50 | 70 | 500 | 500 |

[A]Point-A to point-B (shoulder joint, Figure 2.10); [B]Shoulder joint to Elbow (point-C, Figure 2.10);

[C]Elbow to Wrist (point-D, Figure 2.10); [D] Wrist / Knuckle II middle

*The mass and inertia properties of the *MARSE* were estimated from the CAD modelling using Pro/Engineer software.

It can be seen from Table 2.5 that the weight of the ETS-MARSE arm from shoulder joint to wrist handle is 7.072 kg (and from point-A (Figure 2.10) to wrist handle is 10.542 kg). Compared to the existing exoskeleton devices having at least shoulder and elbow motion support parts the developed ETS-MARSE is found to be light in weight. For example, weight of the ARMin-III exoskeleton (4DoFs) is 18.775 kg (Nef, Guidali and Riener, 2009), and weight of MGA exoskeleton (6DoFs) is 12 kg (Carignan, Tang and Roderick, 2009).

2) Electrical and Electronic Design (Rahman *et al.*, 2011c):

The electrical and electronic configuration for the *ETS-MARSE* system is depicted in Figure 2.26. It consists of a CompactRIO (NI cRIO-9074), a main board, motor driver cards, a real-time PC, a host PC, and actuators.

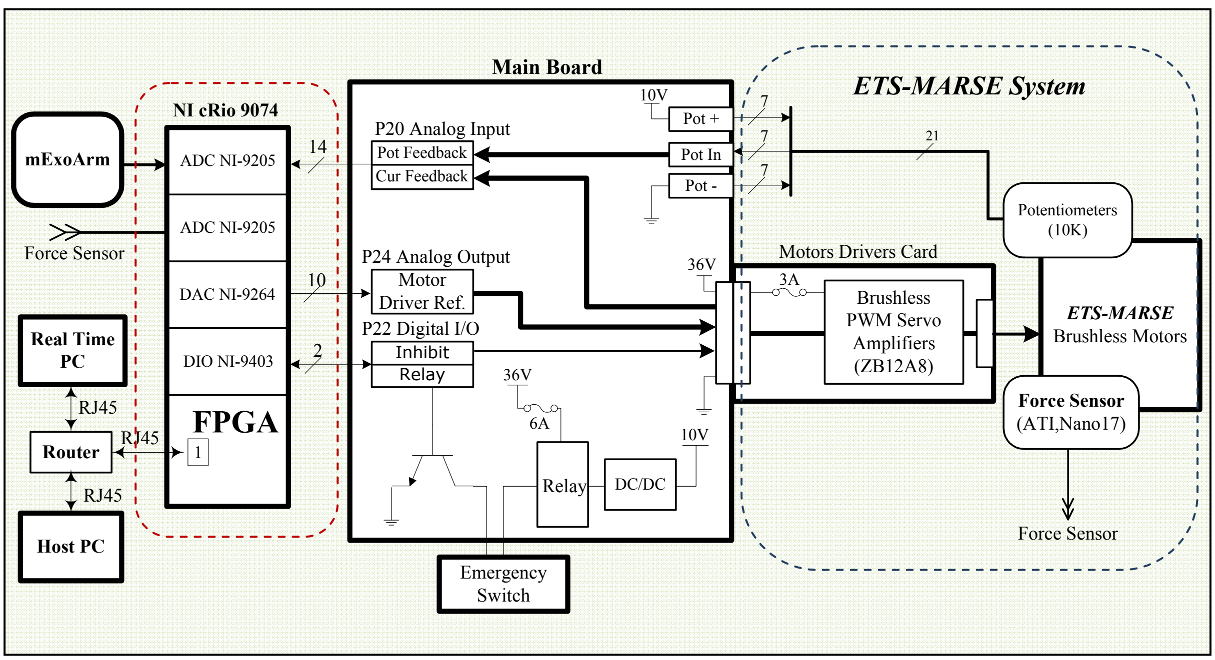


Figure 2.26 Electrical and electronic configuration

CompactRIO:

The cRIO-9074 by National Instruments is an integrated system that combines a real-time 400 MHz processor, 128 MB of DRAM, 256 MB of non-volatile memory, and a reconfigurable field-programmable gate array (FPGA) for embedded machine control and data logging. The unit has two Ethernet ports (10/100 Mb/s) and a RS232 port, which is used for communication with the host PC and real-time PC via TCP/IP. The input/output modules used with cRIO-9074 unit were NI 9205 - analog input module (*spec*: 16-bit, 32 channels, ± 10 V); NI 9264 -analog output module, (*spec:* 16-bit, 16 channels, ± 10 V); and NI 9403 -digital I/O module (32 channels).

Main board:

The main board as shown in Figure 2.26 acts as a motherboard, and is powered by an AC 120V (60Hz) power supply. A voltage regulator was used to convert the AC supply to DC 36V and 10V, as required by its various components. The motherboard routes various analog and digital signals from/to the cRIO-9074 from/to the *ETS-MARSE* system. For instance, it routes analog inputs (from the potentiometer and current feedback) to the NI-9205 module; analog outputs (e.g., motor driver reference voltage) from the NI-9264 module; and digital outputs (e.g., to activate the motors, relay switch control etc.) from the NI-9403 module to the *ETS-MARSE* system. The board as shown was designed to have slots for motor driver cards, only one of which is depicted in Figure 2.26. Note that as a safety feature, an emergency stop switch was installed with the board to cut off the power in case of emergency. In addition, a 6A safety fuse was also used to protect different electrical /electronic components.

Motor driver cards:

Motor driver cards which carry the motor drivers (ZB12A8) were custom-designed to fit in the slots of the main board. The drivers used are type PWM servo amplifiers, specially designed to drive brushless DC motors at high switching frequency (33 kHz) (*spec:* reference voltage: ± 15 VDC; analog output: ± 10 VDC; maximum continuous current: ± 6 A). Note that to double the safety features, 3A safety fuses were installed in each of the motor driver cards.

Real-Time (RT) PC and host PC:

In the early stages of our research, the NI cRIO-9074 as shown in Figure 2.26 was used for data logging and also to execute the control algorithm (at a maximum of 2.5ms) for a 4DoFs exoskeleton robot. Because the controller now deals with the dynamics of the 7DoFs *ETS-MARSE*, to speed up the execution time an RT-PC (spec: Intel i5 dual core, 3.66 GHz, 2 GB of RAM, OS: LabView Real-Time 10.02f, Ethernet Chipset Intel 5550) was employed to deal with the control algorithm, leaving the tasks of data acquisition and internal current loop control to the FPGA, cRIO-9074. Note that the control architecture of the control techniques as well as all program codes (I/O communication) were built in the LabVIEW environment (National Instruments, USA). The host PC as depicted in the schematic (Figure 2.26) is for display purposes (e.g., joint's position, velocity, torque, etc.) only.

Actuators:

The motors used for the *ETS-MARSE* are brushless DC motors (ANNEX IX and ANNEX X). Harmonic drives are incorporated into the motors in order to increase the torque and to reduce the speed of rotation. Detailed specifications of the HD can be found in ANNEX XI.

### 2.4.4 Fabrication

The entire *ETS-MARSE* arm was fabricated with aluminum to give the exoskeleton structure a relatively light weight. The high stress joint sections such as motor shafts (for joint 3, and joint 5) and the bearing cages of the exoskeleton were fabricated in mild steel.

# CHAPTER 3

# KINEMATICS AND DYNAMICS

In this chapter, we present the kinematic and dynamic modeling of the *ETS-MARSE.* The first section of this chapter describes the details of the kinematic modeling. Modified Denavit-Hartenberg (DH) notations were used to develop the kinematic model. The mid section of the chapter briefly explains the iterative Newton-Euler method which was used to develop the dynamic model of the *ETS-MARSE.* The chapter ends with a brief discussion on Jacobians, which map the joint space velocity with the Cartesian velocity.

## 3.1 Kinematics

To rehabilitate and ease human upper limb movement, the *ETS-MARSE* was modeled based on the anatomy and biomechanics of the human upper limb. Modified DH conventions were used in developing the kinematic model. The procedure of coordinate frame assignment (link frame attachment) and the definition of DH parameters are briefly summarized in the next subsection.

### 3.1.1 Coordinate Frame Assignment Procedure

There are different ways to assign coordinate frames to the manipulator links. For the *ETS-MARSE* we have followed the Denavit-Hartenberg method. (Craig, 2005; Denavit and Hartenberg, 1955). The steps are as follows (Hartenberg and Denavit, 1964):

- assume each joint is 1DoF revolute joint;
- identify and locate the axes of rotation;
- label the joint axes $Z_0, \ldots \ldots, Z_n$;
- locate the origin of each link-frame ($O_i$) where the common perpendicular line between the successive joint axes (i.e., $Z_{i-1}$ and $Z_i$) intersects. If the joint axes are not parallel, locate the link-frame origin at the point of intersection between the axes;

- locate the $X_i$ axis (at link frame origin $O_i$) as pointing along the common normal line between the axes $Z_{i-1}$ and $Z_i$. If the joint axes intersect, establish $X_i$ in a direction normal to the plane containing both axes ($Z_{i-1}$ and $Z_i$);
- establish the $Y_i$ axis through the origin $O_i$ to complete a right-hand coordinate system.

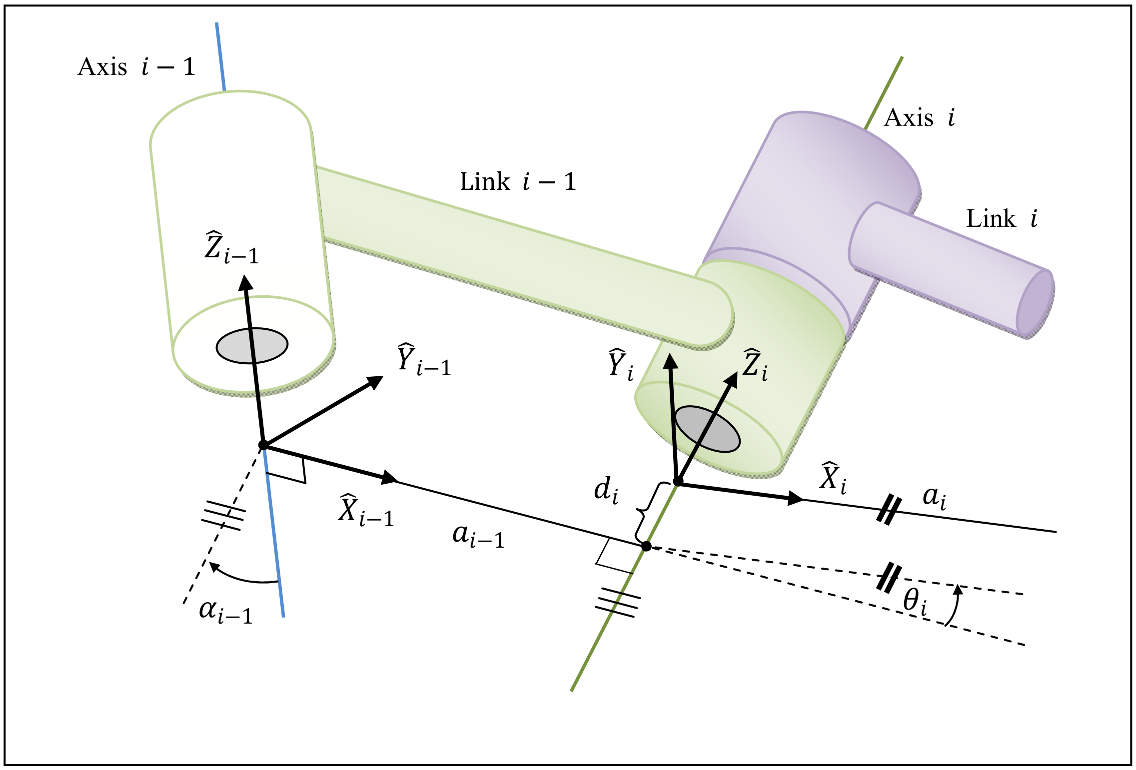


Figure 3.1 Coordinate frame assignment
Adapted from Craig (2005)

### 3.1.2 Definition of D-H Parameters

A link of a robot can be described by four parameters (two parameters for describing the link itself and other two for describing the link's relation to a neighboring link) if we assign the co-ordinate frames as described above (Denavit and Hartenberg, 1955). These parameters are known as Denavit-Hartenberg (DH) parameters. The definitions of the DH parameters are given below (Hartenberg and Denavit, 1964):

Link Length ($a_i$) : the length measured along $X_i$, from axis $Z_i$ to axis $Z_{i+1;}$

Link Twist ($\alpha_i$) : the angle measured about $X_i$, from axis $Z_i$ to axis $Z_{i+1;}$

Link Offset ($d_i$) : the distance measured along the axis $Z_{i;}$ from $X_{i\text{-}1}$ *to* $X_i$, and

Joint Angle ($\theta_i$) : the angle measured about $Z_i$, from $X_{i\text{-}1}$ *to* $X_i$

To obtain the DH parameters, we assume that the co-ordinate frames (i.e., the link-frames which map between the successive axes of rotation) coincide with the joint axes of rotation and have the same order, i.e., frame {1} coincides with joint 1, frame {2} with joint 2, and so on.

As shown in Figure 3.2, the joint axes of rotation of the *ETS-MARSE* corresponding to that of the human upper limb are indicated by dark black arrow heads (i.e., $Z_i$). In this model, joints

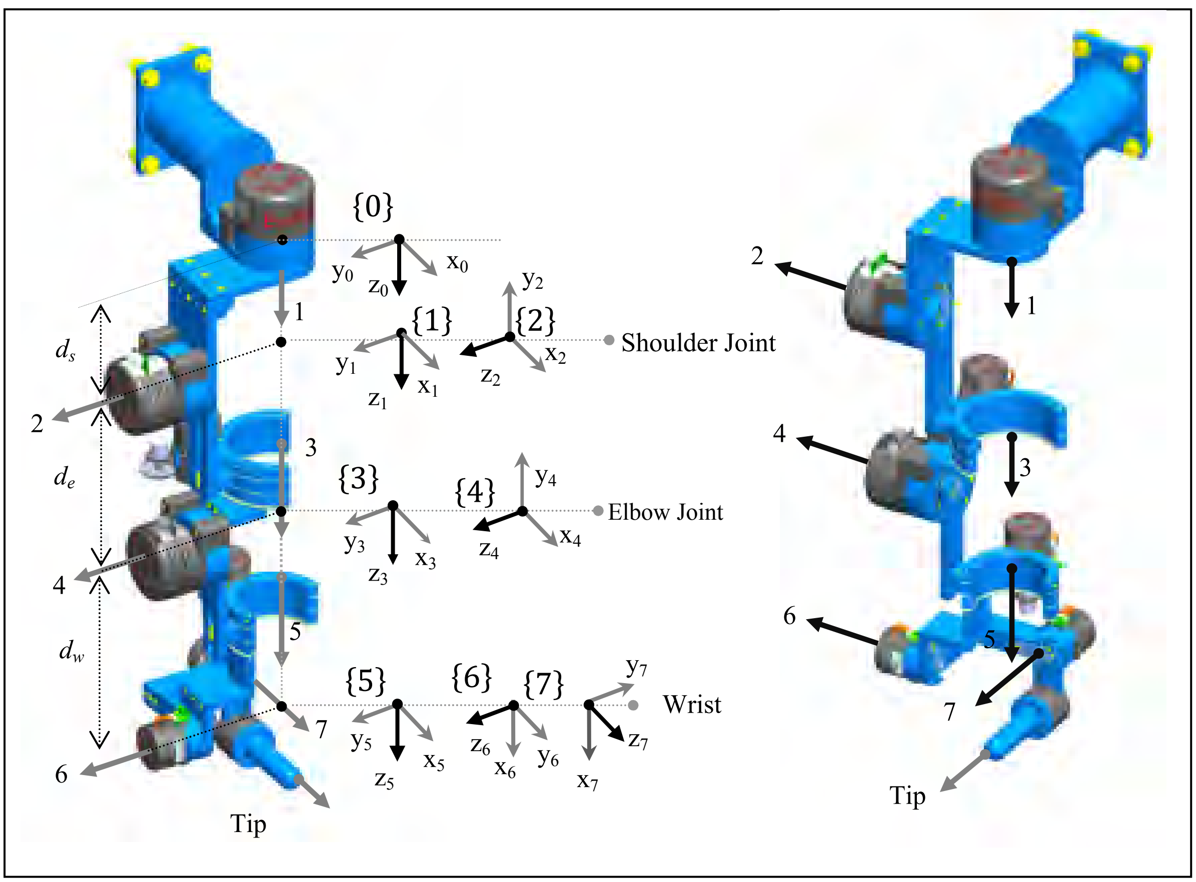


Figure 3.2 Link frame attachments to the *ETS-MARSE*

1, 2, and 3 together constitute the shoulder joint, where joint 1 corresponds to horizontal flexion/extension, joint 2 represents vertical flexion/extension, and joint 3 corresponds to internal/external rotation of the shoulder joint. The elbow joint is located at a distance $d_e$ (length of humerus) apart from the shoulder joint. Note that joint 4 represents the flexion/extension of the elbow joint and joint 5 corresponds to pronation/supination of the forearm. As depicted in Figure 3.2, joints 6 and 7 intersect at the wrist joint, at a distance $d_w$ (length of radius) from the elbow joint, where joint 6 corresponds to radial/ulnar deviation, and joint 7 to flexion/extension.

The modified DH parameters corresponding to the placement of the link frames (in Figure 3.2) are summarized in Table 3.1. These DH parameters are used to get the homogeneous transfer matrix, which represents the positions and orientations of the reference frame with respect to the fixed reference frame. It is assumed that the fixed reference frame {0} is located at distance $d_s$ apart from the first reference frame {1}.

Table 3.1 Modified Denavit-Hartenberg parameters

| **Joint *(i)*** | $\alpha_{i-1}$ | $d_i$ | $a_{i-1}$ | $\theta_i$ |
|---|---|---|---|---|
| 1 | 0 | $d_s$ | 0 | $\theta_1$ |
| 2 | $-\pi/2$ | 0 | 0 | $\theta_2$ |
| 3 | $\pi/2$ | $d_e$ | 0 | $\theta_3$ |
| 4 | $-\pi/2$ | 0 | 0 | $\theta_4$ |
| 5 | $\pi/2$ | $d_w$ | 0 | $\theta_5$ |
| 6 | $-\pi/2$ | 0 | 0 | $\theta_6 - \pi/2$ |
| 7 | $-\pi/2$ | 0 | 0 | $\theta_7$ |

where, $\alpha_{i-1}$ is the link twist, $a_{i-1}$ corresponds to link length, $d_i$ stands for link offset, and $\theta_i$ is the joint angle of the *ETS-MARSE*.

We know that the general form of a link transformation that relates frame $\{i\}$ relative to the frame $\{i-1\}$ (Craig, 2005) is:

$$ {}^{i-1}_{i}T = \begin{bmatrix} {}^{i-1}_{i}R^{3\times3} & {}^{i-1}_{i}P^{3\times1} \\ 0^{1\times3} & 1 \end{bmatrix} \tag{3.1} $$

where, ${}^{i-1}_{i}R$ is the rotation matrix that describes frame $\{i\}$ relative to frame $\{i-1\}$ and can be expressed as:

$$ {}^{i-1}_{i}R = \begin{bmatrix} \cos\theta_i & -\sin\theta_i & 0 \\ \sin\theta_i \cos\alpha_{i-1} & \cos\theta_i \cos\alpha_{i-1} & -\sin\alpha_{i-1} \\ \sin\theta_i \sin\alpha_{i-1} & \cos\theta_i \sin\alpha_{i-1} & \cos\alpha_{i-1} \end{bmatrix} \tag{3.2} $$

and, ${}^{i-1}_{i}P$ is the vector that locates the origin of frame $\{i\}$ relative to frame $\{i-1\}$ and can be expressed as:

$$ {}^{i-1}_{i}P = [a_{i-1} \quad -s\,\alpha_{i-1}\,d_i \quad c\,\alpha_{i-1}\,d_i]^T \tag{3.3} $$

Using Equations (3.1) to (3.3) the individual homogeneous transfer matrix that relates two successive frame (of Figure 3.2) can be found as:

$$ {}^{0}_{1}T = \begin{bmatrix} \cos\theta_1 & -\sin\theta_1 & 0 & 0 \\ \sin\theta_1 & \cos\theta_1 & 0 & 0 \\ 0 & 0 & 1 & d_s \\ 0 & 0 & 0 & 1 \end{bmatrix}, {}^{1}_{2}T = \begin{bmatrix} \cos\theta_2 & -\sin\theta_2 & 0 & 0 \\ 0 & 0 & 1 & 0 \\ -\sin\theta_2 & -\cos\theta_2 & 0 & 0 \\ 0 & 0 & 0 & 1 \end{bmatrix} $$

$$ {}^{2}_{3}T = \begin{bmatrix} \cos\theta_3 & -\sin\theta_3 & 0 & 0 \\ 0 & 0 & -1 & -d_e \\ \sin\theta_3 & \cos\theta_3 & 0 & 0 \\ 0 & 0 & 0 & 1 \end{bmatrix}, {}^{3}_{4}T = \begin{bmatrix} \cos\theta_4 & -\sin\theta_4 & 0 & 0 \\ 0 & 0 & 1 & 0 \\ -\sin\theta_4 & -\cos\theta_4 & 0 & 0 \\ 0 & 0 & 0 & 1 \end{bmatrix} $$

$$
{}^{4}_{5}T = \begin{bmatrix} cos\,\theta_5 & -sin\,\theta_5 & 0 & 0 \\ 0 & 0 & -1 & -d_w \\ sin\,\theta_5 & cos\,\theta_5 & 0 & 0 \\ 0 & 0 & 0 & 1 \end{bmatrix}, {}^{5}_{6}T = \begin{bmatrix} cos\,\theta_6 & -sin\,\theta_6 & 0 & 0 \\ 0 & 0 & 1 & 0 \\ -sin\,\theta_6 & -cos\,\theta_6 & 0 & 0 \\ 0 & 0 & 0 & 1 \end{bmatrix},
$$

(3.4)

$$
{}^{6}_{7}T = \begin{bmatrix} cos\,\theta_7 & -sin\,\theta_7 & 0 & 0 \\ 0 & 0 & 1 & 0 \\ -sin\,\theta_7 & -cos\,\theta_7 & 0 & 0 \\ 0 & 0 & 0 & 1 \end{bmatrix}.
$$

The homogenous transformation matrix that relates frame {7} to frame {0} can be obtained by multiplying individual transformation matrices.

$$
{}^{0}_{7}T = [{}^{0}_{1}T . {}^{1}_{2}T {}^{3}_{4}T . {}^{4}_{5}T . {}^{5}_{6}T . {}^{6}_{7}T] \tag{3.5}
$$

The single transformation matrix thus found from Equation (3.5) represents the positions and orientations of the reference frame attached to the wrist joint (axis 7) with respect to the fixed reference frame {0}.

## 3.2 Inverse Kinematics

The inverse kinematics solution for a manipulator is computationally costly compared to direct kinematics. Due to the nonlinear nature of the equations to solve, it is often hard to find a closed form solution; sometimes multiple solutions may also exist (Siciliano, Sciavicco and Villani, 2009). Moreover, an inverse kinematics problem for a redundant manipulator is much more complex since it gives infinite solutions. We know that, for a manipulator having a square Jacobian, joint velocities can be found from the following relation (Craig, 2005):

$$
\dot{\theta} = J^{-1}(\theta)\, \dot{v} \tag{3.6}
$$

where $J(\theta)$ is $n \times n$ Jacobian matrix, $\dot{\theta}$ is $n \times 1$ joint space velocity vector, and $\dot{v}$ is $6 \times 1$ Cartesian velocity vector. Therefore, inverse kinematic solutions can be obtained easily by simply integrating the joint velocities.

The *ETS-MARSE* is a redundant manipulator; therefore it is not possible to find closed form solutions. Moreover, its Jacobian is not square, therefore we are not able to directly use Equation (3.6) to find joint positions. As an alternative approach, the inverse kinematic solution of the *ETS-MARSE* was obtained by using the pseudo inverse of Jacobian matrix $J(\theta)$ (Siciliano, Sciavicco and Villani, 2009). For a redundant manipulator, the Equation (3.6) can be reformulated as (Siciliano, Sciavicco and Villani, 2009):

$$\dot{\theta} = J^{\dagger}(\theta)\dot{v} \tag{3.7}$$

where $J^{\dagger}(\theta)$ is the pseudo inverse generalized, and can be expressed as:

$$J^{\dagger}(\theta) = J^{T}(\theta)\big(J(\theta)J^{T}(\theta)\big)^{-1} \tag{3.8}$$

## 3.3 Singularity Analysis

The *ETS-MARSE* arm will be in a singular configuration when it is straight down ($\theta_2 = 0^{\circ}$, and/or $\theta_4 = 0^{\circ}$, and/or $\theta_6 = -90^{\circ}$) by the side (i.e., a singularity will occur when the axes of rotation of joint-1 ($Z_1$), and joint-3 ($Z_3$) , and/or joint-5 ($Z_5$), and/or joint-7 ($Z_7$) are aligned with each other). Note that the joint-space based control algorithms (that includes both linear and nonlinear control techniques e.g., PID control, computed torque control, sliding mode control) do not require a Jacobian matrix or inversion of a Jacobian matrix, therefore singularity is not a big issue in this case. On the other hand, Cartesian based control approaches, which are often used to maneuver the manipulator in a straight line motion, require Jacobian or inverse Jacobian matrices; therefore for this type of control the singularity must be properly dealt with. Interestingly to replicate these type of trajectories as a rehabilitative exercises e.g., to follow a square trajectory over the surface of a table, joints 2, 4 and 6 are usually far away from the singular configuration of the *ETS-MARSE* model.

Note that anatomically rotation of joint-6 is limited to +20° to -25°. Moreover, as a safety measure when using Cartesian based control, a singularity could be easily avoided by limiting the position of joint-2, and joint-4 to more than 10° (i.e., $\theta_2$, and $\theta_4 \geq\ 10^{\circ}$).

### 3.4 Dynamics

The studies of dynamics discuss the manipulator motions and the forces and torque that cause them. Among the various methods found in literature the iterative Newton-Euler formulation and the Lagrangian formulation are widely used to develop the dynamic model of a manipulator. Note that for a 6DoFs manipulator the Newton-Euler approach is 100 times (computationally) more efficient compared to the Lagrangian approach (Craig, 2005). Therefore, we have used the iterative Newton-Euler method (Luh, Walker and Paul, 1980) to develop the dynamic model of the *ETS-MARSE.* A brief overview of this method is given below.

Iterative Newton-Euler Formulation:
In this approach, the manipulator's joint torque is computed iteratively using Newton's and Euler's equations. For a rigid body manipulator, Newton's and Euler's equations can be expressed as follows:

Newton's Equation:

$$F = m\dot{v}_C \tag{3.9}$$

where $F$ is the force acting at the centre of mass, $m$, of a rigid body, therefore moving the mass at acceleration $\dot{v}_C$.

Euler's Equation:

$$N = {}^{C}I\dot{\omega} + \omega \times {}^{C}I\omega \tag{3.10}$$

where $N$ is the moment acting on a rigid body having inertia tensor ${}^{C}I$ at its centre of mass; and therefore causing the motion of the rigid body with angular velocity and acceleration, $\omega$, $\dot{\omega}$ respectively.

The algorithm to compute joint torques ($\tau_i$) as well as to derive the dynamic model of a manipulator includes the following steps:

- Outward iterations:
  Step 1: compute the link velocities (angular) and accelerations (linear and angular) iteratively from link 1 out to link *n*.
  Step 2: compute inertial force and torque (acting at the centre of mass) of each link using Newton-Euler equations.

- Inward iterations:
  Step 3: compute forces and torques of interaction and joint recursively from link *n* back to link 1. Complete derivation of Newton-Euler formulation can be found in (Craig, 2005; Luh, Walker and Paul, 1980).

The dynamic equation of a rigid body manipulator derived from the Newton-Euler formulation can be written in the following form:

$$\tau = M(\theta)\ddot{\theta} + V(\theta, \dot{\theta}) + G(\theta) \tag{3.11}$$

where $M(\theta)$ is the $n \times n$ mass matrix of the manipulator, $V(\theta, \dot{\theta})$ is an $n \times 1$ vector of centrifugal and coriolis terms, and $G(\theta)$ is an $n \times 1$ vector of gravity terms. Adding friction to the model, the dynamic equation becomes:

$$\tau = M(\theta)\ddot{\theta} + V(\theta, \dot{\theta}) + G(\theta) + F(\theta, \dot{\theta}) \tag{3.12}$$

where $F(\theta, \dot{\theta}) \in \mathbb{R}^7$ is the vector of nonlinear coulomb friction and can be expressed by the following relation.

$$F(\theta, \dot{\theta}) = c.sgn(\dot{\theta}). \tag{3.13}$$

Identification of *ETS-MARSE* Parameters:

The mass, centrifugal & coriolis terms, and gravity terms ($M(\theta), V(\theta, \dot{\theta})$, and $G(\theta)$) in Equation (3.11) were computed (symbolically) in MATLAB (The Mathworks, USA). To verify and validate the MATLAB outputs the same computation was performed using the HEMERO robotic toolbox (Maza and Ollero, 2001), a toolbox for MATLAB/Simulink. Note that both approaches gave exactly the same results. For the *ETS-MARSE* as depicted in Figure 3.2, the location of centre of mass can be identified as:

$${}^{1}P_{C_1} = [0 \quad 0 \quad -z_1]^T,\ {}^{2}P_{C_2} = [0 \quad -y_2 \quad 0]^T,\ {}^{3}P_{C_3} = [0 \quad 0 \quad 0]^T$$

$${}^{4}P_{C_4} = [0 \quad -y_4 \quad 0]^T,\ {}^{5}P_{C_5} = [0 \quad 0 \quad 0]^T,\ {}^{6}P_{C_6} = [0 \quad -y_6 \quad 0]^T, \text{ and}$$

$${}^{7}P_{C_7} = [x_7 \quad 0 \quad 0]^T$$

## 3.5 Jacobians

In robotics, we generally use Jacobians $J(\theta)$ to relate joints' velocities to the Cartesian velocities of the end-effector (Craig, 2005). For instance,

$${}^{0}v = {}^{0}J(\theta)\dot{\theta} \tag{3.14}$$

For a $n$ DoFs robot, the Jacobian is $6 \times n$ matrix, $\dot{\theta}$ is $n \times 1$ vector, and ${}^{0}v$ is $6 \times 1$ vector. This $6 \times 1$ Cartesian velocity vector is comprised of a $3 \times 1$ linear velocity vector ($v$) and $3 \times 1$ rotational velocity vector ($\omega$).

$$ {}^{0}\mathcal{V} = \begin{bmatrix} {}^{0}v \\ {}^{0}\omega \end{bmatrix}. \tag{3.15} $$

The Jacobian of *ETS-MARSE* was computed in MATLAB/Simulink (The Mathworks, USA). Note that Jacobians of any dimension can be defined. The number of rows equals the number of DoFs in the Cartesian space being considered. The number of columns in a Jacobian is equal to the number of joints for the manipulator.

# CHAPTER 4

# CONTROL AND SIMULATION

This chapter focuses on the different control techniques (such as *PID, Computed Torque Control, Sliding Mode Control with Exponential Reaching Law, and Compliance Control with Gravity Compensation*) which were employed to maneuver the *ETS-MARSE* to follow a reference trajectory.

## 4.1 PID Control

The PID control[1] technique is the most widely used control technique for industrial applications (Craig, 2005). It is simple in design and efficient in computation. Moreover, it is considered a robust control technique. The general layout of the PID control approach is depicted in Figure 4.1. The joint torque commands of the *ETS-MARSE* can be expressed by the following equation:

$$\tau = K_P(\theta_d - \theta) + K_V(\dot{\theta}_d - \dot{\theta}) + K_I \int (\theta_d - \theta)\, dt \tag{4.1}$$

where $\theta_d, \theta \in \mathbb{R}^7$ are the vectors of desired and measured joint angles respectively, $\dot{\theta}_d, \dot{\theta} \in \mathbb{R}^7$ are the vectors of desired and measured joint velocities respectively, $K_P$, $K_V$, $K_I$ are the diagonal positive definite gain matrices, and $\tau \in \mathbb{R}^7$ is the generalized torque vector. Let the error vector $E$ and its derivative be:

$$E = \theta_d - \theta;\ \dot{E} = \dot{\theta}_d - \dot{\theta} \tag{4.2}$$

Therefore, this equation (4.1) can be re-formulated as an error equation:

[1] Passive arm movements and exercises are usually performed very slowly compared to the natural speed of arm movement. As first step, therefore, we implemented PID control techniques.

$$\tau = K_P E + K_V \dot{E} + K_I \int E\, dt \tag{4.3}$$

The relation (4.3) is decoupled, therefore individual torque command for each joint would be as follows.

$$\tau_i = K_{P_i} e_i + K_{V_i} \dot{e_i} + K_{I_i} \int e_i\, dt \tag{4.4}$$

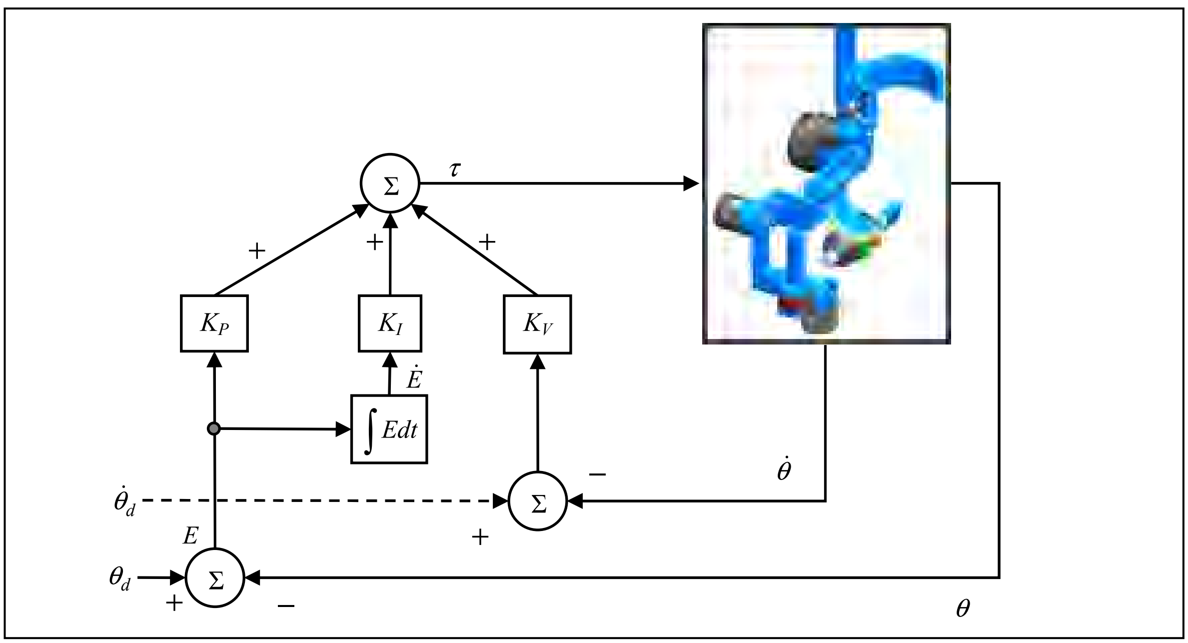


Figure 4.1 Schematic diagram of PID control

where $e_i = \theta_{d_i} - \theta_i \cdots (i = 1, 2, \cdots 7)$; $\theta_i$, $\theta_{d_i}$ are the measured and desired trajectory for joint *i* respectively, and

$\dot{E} = [\dot{e_1} \quad \dot{e_2} \quad \cdots \quad \dot{e_7}]^T$,

$\theta_d = [\theta_{d_1} \quad \theta_{d_2} \quad \cdots \quad \theta_{d_7}]^T$, $\theta = [\theta_1 \quad \theta_2 \quad \cdots \quad \theta_7]^T$;

$K_P = diag[K_{P_1} \quad K_{P_2} \quad \cdots \quad K_{P_7}]^T$, $K_V = diag[K_{V_1} \quad K_{V_2} \quad \cdots \quad K_{V_7}]^T$, and

$K_I = diag[K_{I_1} \quad K_{I_2} \quad \cdots \quad K_{I_7}]^T$.

Simulation with PID:

Simulations were carried out in the SIMULINK environment (The Mathworks, USA). Figure 4.2 shows the results of the simulation that was performed to highlight the tracking performance of the controller for each joint movement (of the *MARSE*). As depicted in Figure 4.2, the trajectory began with shoulder joint vertical flexion (joint-2) up to 90°. Then, maintaining that position, shoulder joint horizontal flexion/extension (joint-1) movements were performed followed by shoulder joint extension to 0°. The exercise again initiates with elbow joint (joint-4) flexion up to 120° followed by elbow extension to 90°, and then while maintaining that position, shoulder joint internal/external rotation (joint-3), forearm pronation/supination (joint-5), wrist joint radial/ulnar deviation (joint-6), and wrist joint flexion/extension (joint-7) movements were performed. The top-most plots of Figure 4.2 compare the desired joint angles, also known as desired trajectories (dotted lines) to measured joint angles, often known as measured trajectories (solid lines). Note that the desired trajectories and associated velocities were generated using the cubic polynomial approach (Craig, 2005). Intermediate plots of Figure 4.2 show the error as a function of time

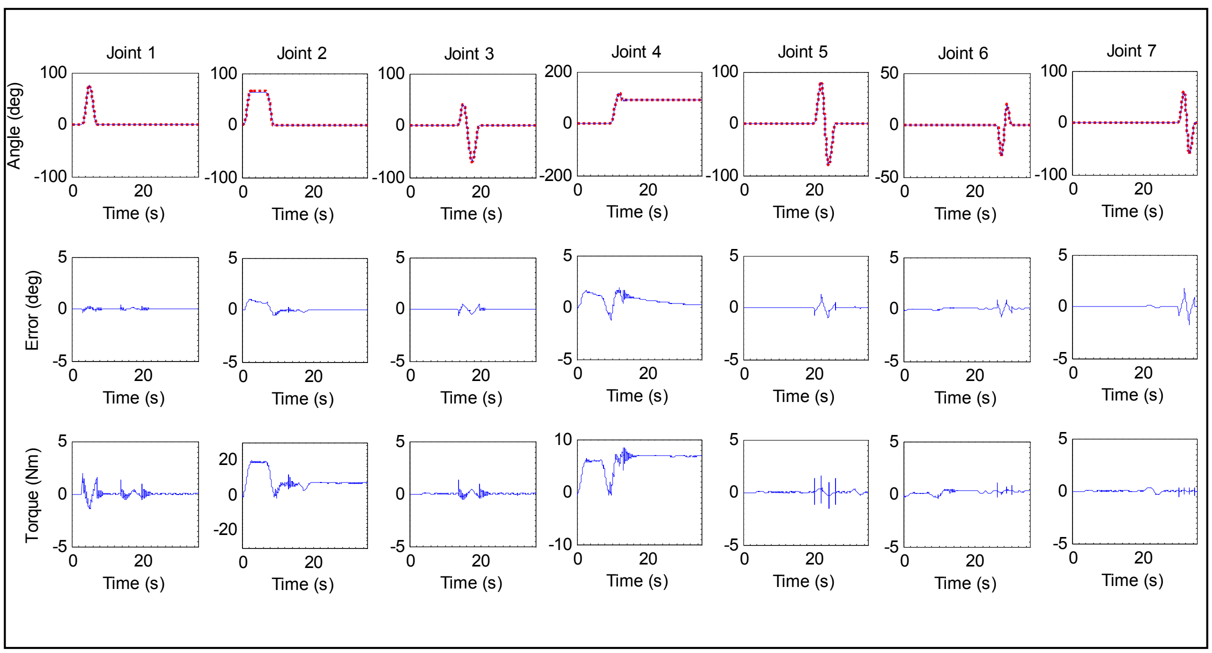


Figure 4.2 Simulated results with PID controller showing trajectory tracking for individual joint movement

(i.e., deviation between desired and measured trajectories). It is obvious from these plots that the controller's performance is excellent, as maximum tracking errors are found to be less than 2°. Generated joint torque corresponding to the trajectory are plotted in the bottom row.

Note that the control gains used for the simulation were found by trial and error, and are as follows:

$K_P = diag[175 \quad 1000 \quad 175 \quad 200 \quad 250 \quad 175 \quad 175]$,

$K_V = diag[0.5 \quad 0.5 \quad 0.5 \quad 0.5 \quad 0.5 \quad 0.5 \quad 0.5]$, and

$K_I = diag[2 \quad 100 \quad 2 \quad 15 \quad 2 \quad 2 \quad 2]$.

## 4.2 Compliance Control with Gravity Compensation

The gravity model of a manipulator is often added to the control law to realize the simple model based control (Craig, 2005) as well as to minimize the static position error. One of the existing techniques of gravity compensation is the addition of a gravity model with a control law, such as with a PID control law as found in (Craig, 2005; Yang *et al.*, 2011). De Luca *et al.* (2005) proposed a similar technique for the gravity compensation but with the PD control law. Both approaches mentioned above work on the stiff position control which is sometimes the cause of an end-effector being jammed or damaged when it interacts with the environment. As a solution to this problem, Salisbury (1980), proposed an active stiffness control technique where the position gain ($K_p$) of a joint based control system was modified to provide some stiffness to the end-effector along the Cartesian degree of freedom (Craig, 2005; Salisbury, 1980). Later, Craig (2005) implemented this concept with a PD control law, where the position gain of the controller was modified as proposed by Salisbury (1980). However, in this thesis, we propose a modified version of compliance control technique that combines the concept of softening position gains (Salisbury, 1980) and the gravity weight compensation (Craig, 2005). Therefore, the gravity model of the *ETS-MARSE* was included in the control law. The general layout of the compliance control technique is depicted in Figure 4.3. Unlike the compliance technique suggested by Salisbury (1980) and Craig

(2005), we have added an integral term to obtain a better tracking performance as well as to minimize the steady state error.

In this control scheme, the position gain ($K_p$) of the Equation (4.3), is modified to provide some stiffness to the end-effector along the Cartesian degree of freedom (Craig, 2005; Salisbury, 1980). We know that the stiffness characteristics of a spring can be expressed by the following equation.

$$F = K_{px}\Delta x \tag{4.5}$$

where $\Delta x \in \mathbb{R}^{6\times1}$ is the generalized displacement vector (consists of three $\mathbb{R}^{3\times1}$ orthogonal translation vector and three infinitesimal rotations $\mathbb{R}^{3\times1}$ about the orthogonal axis (Salisbury, 1980)), $F = [f_x \quad f_y \quad f_z \quad \tau_{xy} \quad \tau_{yz} \quad \tau_{zx}]^T \in \mathbb{R}^{6\times1}$ is the force and torque vector, and $K_{px} \in \mathbb{R}^{6\times6}$ is the positive definite diagonal matrix known as spring constant having three linear stiffnesses in X, Y, and Z directions followed by three rotational stiffnesses in XY, YZ and ZX planes.

Using the definition of Jacobian (Schilling, 1990) we may write:

$$dx = J(\theta)d\theta \tag{4.6}$$

where $J(\theta) \in \mathbb{R}^{6\times n}$ is the manipulator Jacobian matrix, and $dx$, $d\theta$ represents the infinitesimal displacement of tool and joints, respectively.

Now, if the tool (end-effector) deflection, $\Delta x$, and corresponding joint deflection $\Delta\theta$ are small enough, i.e., approaching infinitesimal, then we can equate $\Delta x$ with $dx$, and $\Delta\theta$ with $d\theta$ (Schilling, 1990), and thus equation (4.6) can be re-written as:

$$\Delta x = J(\theta)\Delta\theta \tag{4.7}$$

Combining relations (4.5) and (4.7), we have

$$F = K_{px} J(\theta) \Delta\theta \tag{4.8}$$

Therefore, considering a static force $F$ applied to the end-effector, the joint torques can be computed easily by:

$$\tau = J(\theta)^T F = \overbrace{J(\theta)^T K_{px} J(\theta)}^{K_s} \Delta\theta \tag{4.9}$$

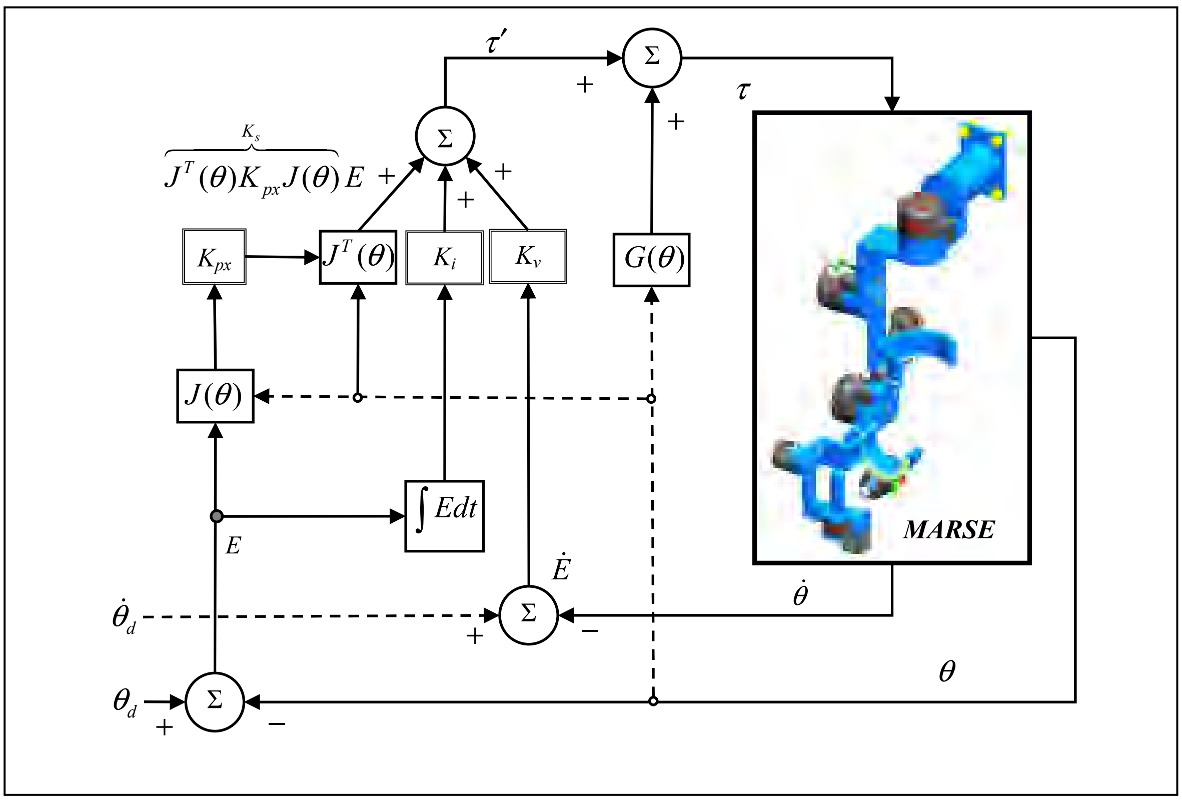


Figure 4.3 Schematic diagram of compliance control with gravity compensation

where $K_s$ is the joint space stiffness matrix. Note that the Jacobian is written here in the end-effector frame which transforms the Cartesian stiffness to the joint space stiffness. Therefore, equation (4.9) represents the required joint torques ($\tau$) that should be applied due to a change of joint angles ($\Delta\theta$) so that the end-effector behaves as a Cartesian spring (in 6 DoFs), of which the spring constant is denoted as $K_{px} \in \mathbb{R}^{6\times 6}$ (Salisbury, 1980).

The control law as seen from the schematic (Figure 4.3) can be expressed by the following relation:

$$\tau = \overbrace{J(\theta)^T K_{px} J(\theta)}^{K_s} E + K_v \dot{E} + K_i \int E\, dt + G(\theta) \tag{4.10}$$

where $G(\theta) = \left(\partial P_g(\theta)/\partial\theta\right)^T$ is the $.n \times 1$ gravitational vector, and $P_g(\theta)$ is the potential energy due to gravity (Craig, 2005).

Comparing equations (4.3) and (4.10), it is evident that control law for the developed compliance control technique is quite similar to the joint based position controller, except for the position gain ($K_p$, of equation (4.3)) which is modified to provide some stiffness to the end-effector so that it exhibits some spring characteristics along the Cartesian degree of freedom (Craig, 2005; Salisbury, 1980).

Note that the control gains $K_P$, $K_V$, $K_I$ of PID control and $K_{px}$, $K_v$, $K_i$ of compliance control are positive definite matrices. A proper choice of these matrices ensures the stability of the system (Alvarez-Ramirez, Cervantes and Kelly, 2000; Rocco, 1996).

## 4.3 Computed Torque Control (CTC)

To realize better tracking performance of the *ETS-MARSE,* the dynamic model of the *MARSE* (as well as dynamic model of the human upper limb) needs to be included in the control law. Next, we therefore implemented a nonlinear computed torque control (CTC) technique. Its control law includes both the human arm and *MARSE's* dynamic model. Note that human arm was modeled as purely viso-elastic (i.e., elastic/viscous behavior of arm was ignored).

The dynamic behavior of the *ETS-MARSE* can be expressed by the well-known rigid body dynamic equation as:

$$M(\theta)\ddot{\theta} + V(\theta,\dot{\theta}) + G(\theta) + F(\theta,\dot{\theta}) = \tau \tag{4.11}$$

where $\theta \in \mathbb{R}^7$ is the joint variables vector, $\tau$ is the generalized torque vector, $M(\theta) \in \mathbb{R}^{7\times7}$ is the inertia matrix, $V(\theta,\dot{\theta}) \in \mathbb{R}^7$ is the coriolis/centrifugal vector, $G(\theta) \in \mathbb{R}^7$ is the gravity vector, and $F(\theta,\dot{\theta}) \in \mathbb{R}^7$ is the friction vector. Note that the friction vector is modeled as a nonlinear coulomb friction, and can be expressed as:

$$\tau_{friction} = F(\theta,\dot{\theta}) = c.sgn(\dot{\theta}) \qquad (4.12)$$

where *c* is the coulomb-friction constant. Equation (4.11) can be written as:

$$\ddot{\theta} = -M^{-1}(\theta)\left[V(\theta,\dot{\theta}) + G(\theta) + F(\theta,\dot{\theta})\right] + M^{-1}(\theta)\tau \qquad (4.13)$$

$M^{-1}(\theta)$ always exists since $M(\theta)$ is symmetrical and positive definite.

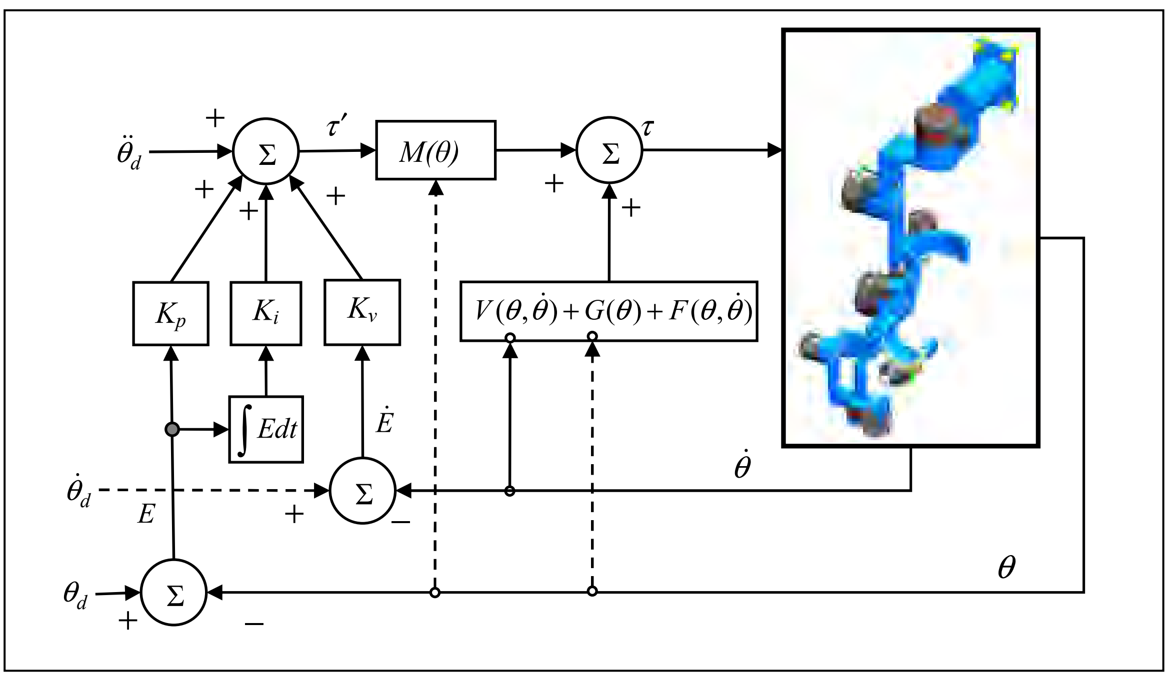


Figure 4.4 Schematic diagram of modified computed torque control

The layout of the modified computed torque control technique is depicted in Figure 4.4. Unlike the conventional computed torque control approach, here we have added an integral term to have a better tracking performance and to compensate the trajectory tracking error that usually occurs due to imperfect dynamic modeling, parameter estimation, and also for external disturbances. The control torque in Figure 4.4 can be written as:

$$\tau = M(\theta)\left[\ddot{\theta}_d + K_v(\dot{\theta}_d - \dot{\theta}) + K_p(\theta_d - \theta) + K_i \int (\theta_d - \theta)\, dt\right] + V(\theta, \dot{\theta}) + G(\theta) + F(\theta, \dot{\theta}) \tag{4.14}$$

From relations (4.11) and (4.14), we may write:

$$\ddot{\theta} = \ddot{\theta}_d + K_v(\dot{\theta}_d - \dot{\theta}) + K_p(\theta_d - \theta) + K_i \int (\theta_d - \theta)\, dt \tag{4.15}$$

where $\theta_d, \dot{\theta}_d,$ and $\ddot{\theta}_d$ are the desired position, velocity and acceleration, respectively, and $K_p$, $K_v$, and $K_i$ diagonal positive definite matrices. Let the error vector $E$ and its derivative be:

$$E = \theta_d - \theta;\ \dot{E} = \dot{\theta}_d - \dot{\theta}, \ddot{E} = \ddot{\theta}_d - \ddot{\theta} \tag{4.16}$$

Therefore, equation (4.15) can be rewritten in the following form:

$$\ddot{E} + K_v\dot{E} + K_pE + K_i \int E\, dt = 0 \tag{4.17}$$

where the control gains $K_p$, $K_v$, and $K_i$ are positive definite matrices. Therefore, a proper choice of these matrices ensures the stability of the system.

Simulation with CTC (Rahman *et al.*, 2011e):

To produce dynamic simulations, upper-limb parameters such as arm lengths (i.e., upper-arm, forearm, and hand), mass of different segments (e.g., forearm) and inertia parameters, were estimated according to the upper limb properties of a typical adult (Rahman *et al.*, 2011e; Winter, 1990).

Simulations were carried out to maneuver the *MARSE* to follow pre-programmed trajectories that correspond to recommended passive rehabilitation protocol (Mary and Mark, 2004; Physical Therapy Standards, 2011; *Stroke Rehab Exercises*, 2010).

Shoulder joint movements:

Figure 4.5 shows the simulation results of shoulder joint vertical flexion/extension motion (i.e., passive forward elevation) where the *MARSE* is supposed to lift the subject's arm (from the initial position, i.e., all joint angle at 0°) to a specific position over the head (e.g., in Figure 4.5a, the elevation was set at 115°), hold that position for a few seconds (e.g., in Figure 4.5a, 3s) and then slowly move the joint back to its initial position. The topmost plot of Figure 4.5 compares the desired joint angles (or reference trajectories, dotted line) to measured joint angles (or measured trajectories, solid line). The intermediate plot of Figure 4.5 shows the error as a function of time (i.e., deviation between desired and measured trajectories). It can be seen (Figure 4.5a) that the tracking error was quite small (<0.1°) and that the most noticeable one was the steady state error (i.e., when *MARSE* is maintaining the position at 115° against gravity) which lies below and/or near around 0.01°. The generated joint torque corresponding to the trajectory is plotted in the bottom row of Figure 4.5a.

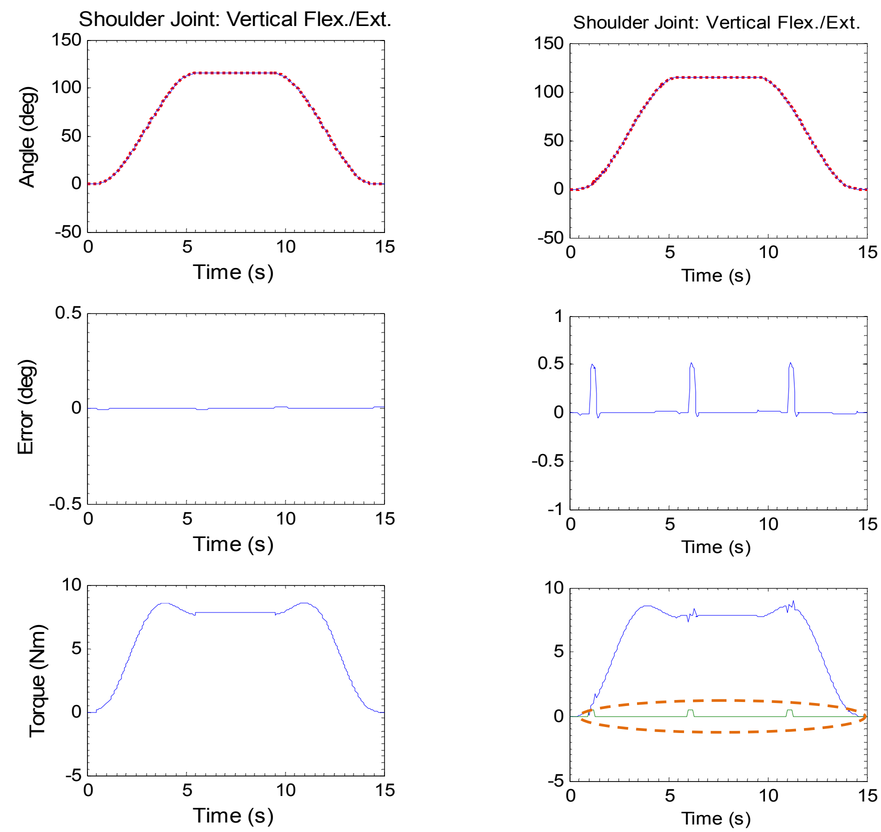


Figure 4.5 Passive rehabilitation exercise, shoulder joint vertical flexion/extension (a) Passive forward elevation considering perfect estimation of dynamic parameters (of human upper-limb) (b) Passive forward elevation of shoulder joint where some perturbations were added to disturb the system

Figure 4.5b shows the same exercise but some perturbations (10% of maximum joint torque as found in Figure 4.5a) were added, as apparent from three spikes (enclosed in orange dotted circle) from bottom row of Figure 4.5b. Adding sudden perturbation did not disturb the system, and the tracking performance of the controller was also very good, with tracking error less than 0.5°. Further, the system showed some amount of compliance, which is desirable for this kind of robot-assisted therapeutic system.

Figure 4.6 shows abduction/adduction motion (Figure 2.4) where a coordinated movement of shoulder horizontal and vertical flexion/extension motion were performed. Again, the tracking performance of the controller was excellent, with tracking error less than 0.5° and the steady state position error below $0.01^0$. Note that also in this case, the perturbation to the system (in the form of noise) was set at 10% of maximum joint torque.

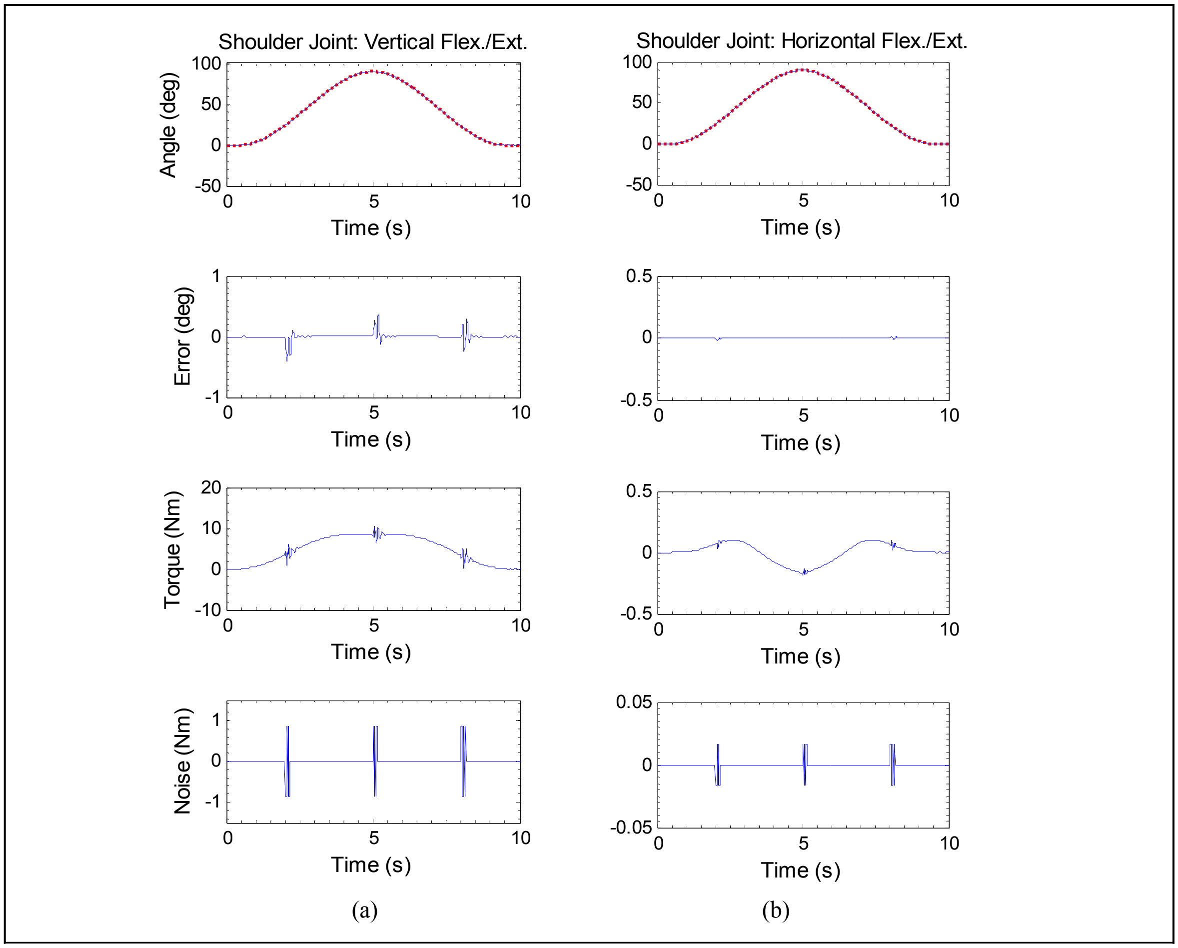


Figure 4.6 Shoulder joint abduction/adduction
(a) Shoulder joint vertical flexion/extension (0°-90°) (b) Shoulder joint horizontal flexion/extension (0°-90°)

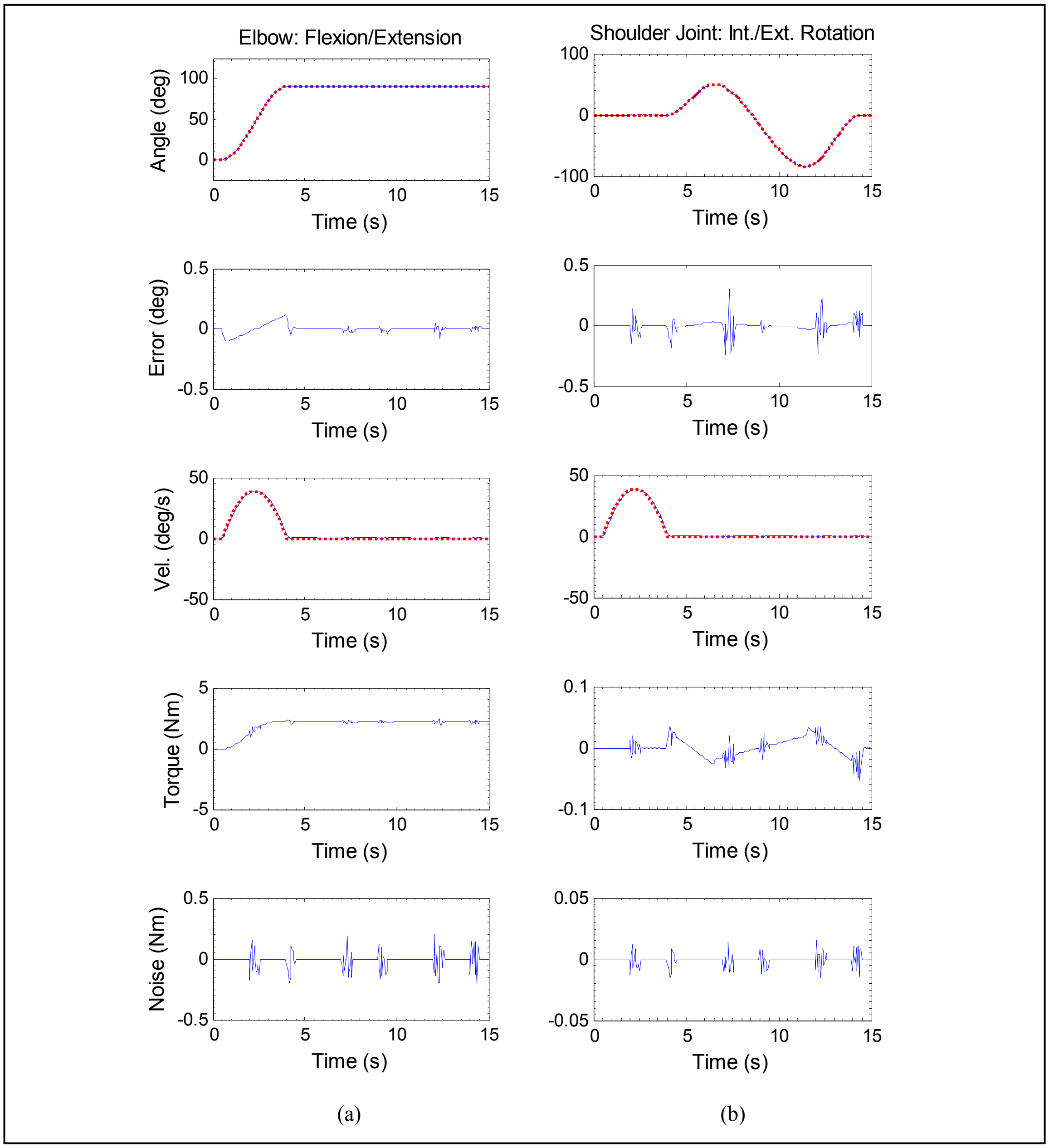


Figure 4.7 Cooperative movement of elbow and shoulder joint
(a) Elbow joint`s movement where *MARSE* is supposed to flex from its initial position up to an angle 90°, and finally maintain that position against gravity
(b) Shoulder joint internal/external rotation

A coordinated movement of the elbow (flexion/extension) and shoulder joint internal/external rotation is depicted in Figure 4.7. The exercise began with elbow flexion, followed by shoulder joint internal/external rotation (Figure 2.3) while maintaining the elbow at 90°. As for previous tracking simulations, Figure 4.7 also demonstrates the good performance of the controller, with error limited to less than 0.25°. The 3rd row of the plots displays velocity tracking, where it can be seen that the measured velocity (solid line) overlaps with the desired velocity (dotted line), thus demonstrating the excellent performance of the controller with respect to both position and velocity tracking.

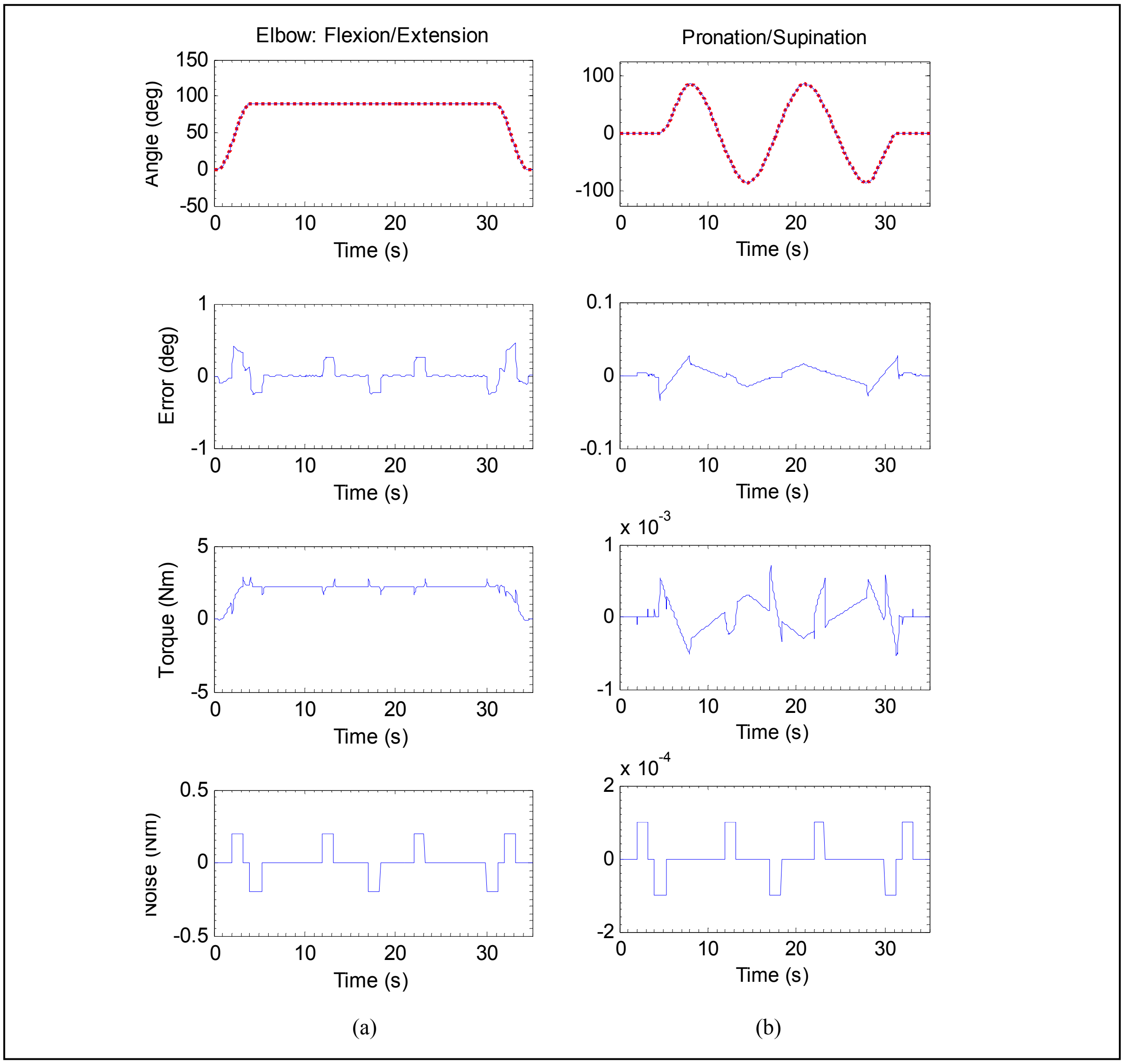


Figure 4.8 Passive arm therapy, a co-operative movement of forearm and elbow joint motion
(a) Elbow joint, flexion/extension (the exercise began with elbow flexion, then repetitive pronation/supination was performed (Figure 4.8b))
(b) Repetitive movement of forearm (pronation/supination)

Elbow and forearm movements:

Figure 4.8 shows a cooperative movement of both the elbow and the forearm. As shown in Figure 4.8a, the exercise began with elbow flexion, then repetitive pronation/supination was performed (Figure 4.8b); finally the exercise ends with the extension of the elbow to 0° (Figure 4.8a). Figure 4.8 also demonstrates the good performance of the controller, where measured trajectories overlapped with the reference trajectories, with the error in tracking limited to less than 1°.

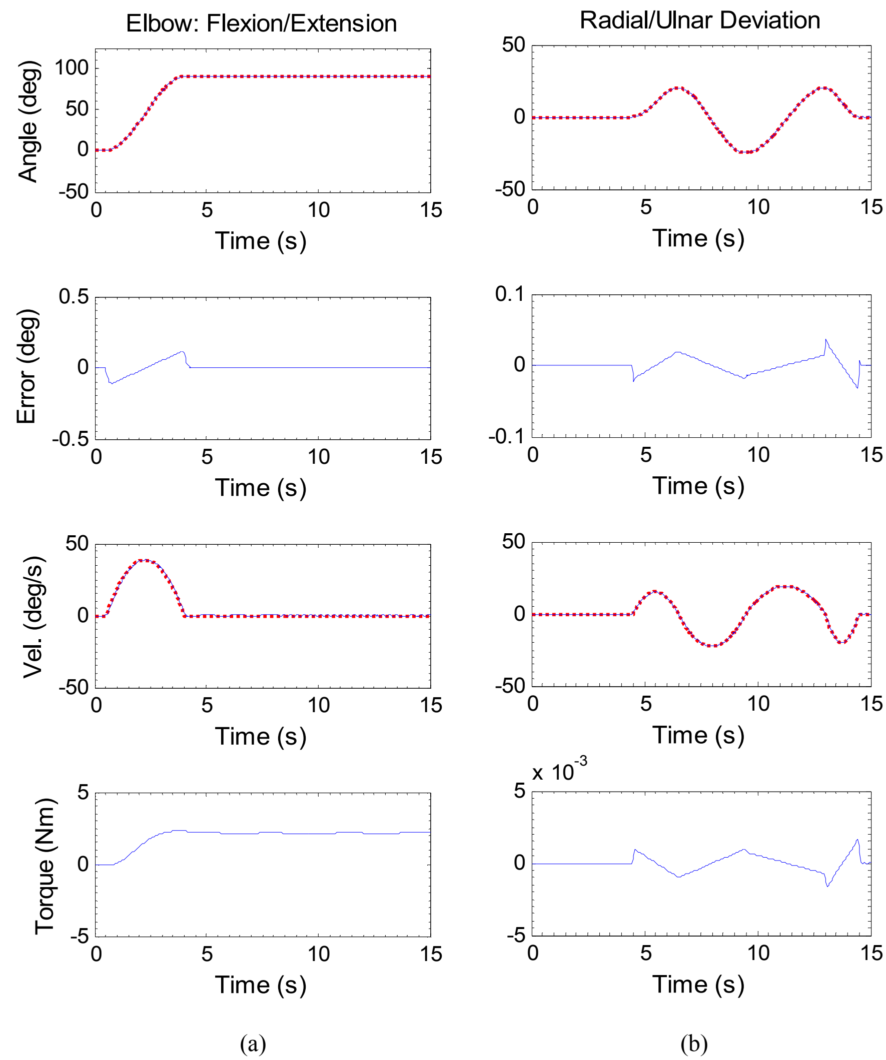


Figure 4.9 Repetitive movement of wrist joint (radial/ulnar deviation) while elbow maintaining steady position at 90°
(a) Elbow flexion at 90° (b) Radial/ulnar deviation

Wrist joint movements:

A simulation of recommended passive rehabilitation exercises involving movements of the wrist joint (Physical Therapy Standards, 2011) are depicted in Figure 4.9 and Figure 4.10. The objective of these exercises is to provide radial/ulnar movement (Figure 4.9) and flexion/extension motion of the wrist joint (Figure 4.10), while maintaining the elbow at 90°. It is also obvious from these plots that the tracking error was quite small since it lies below and/or near 0.25° and the steady state error was even less than 0.1°.

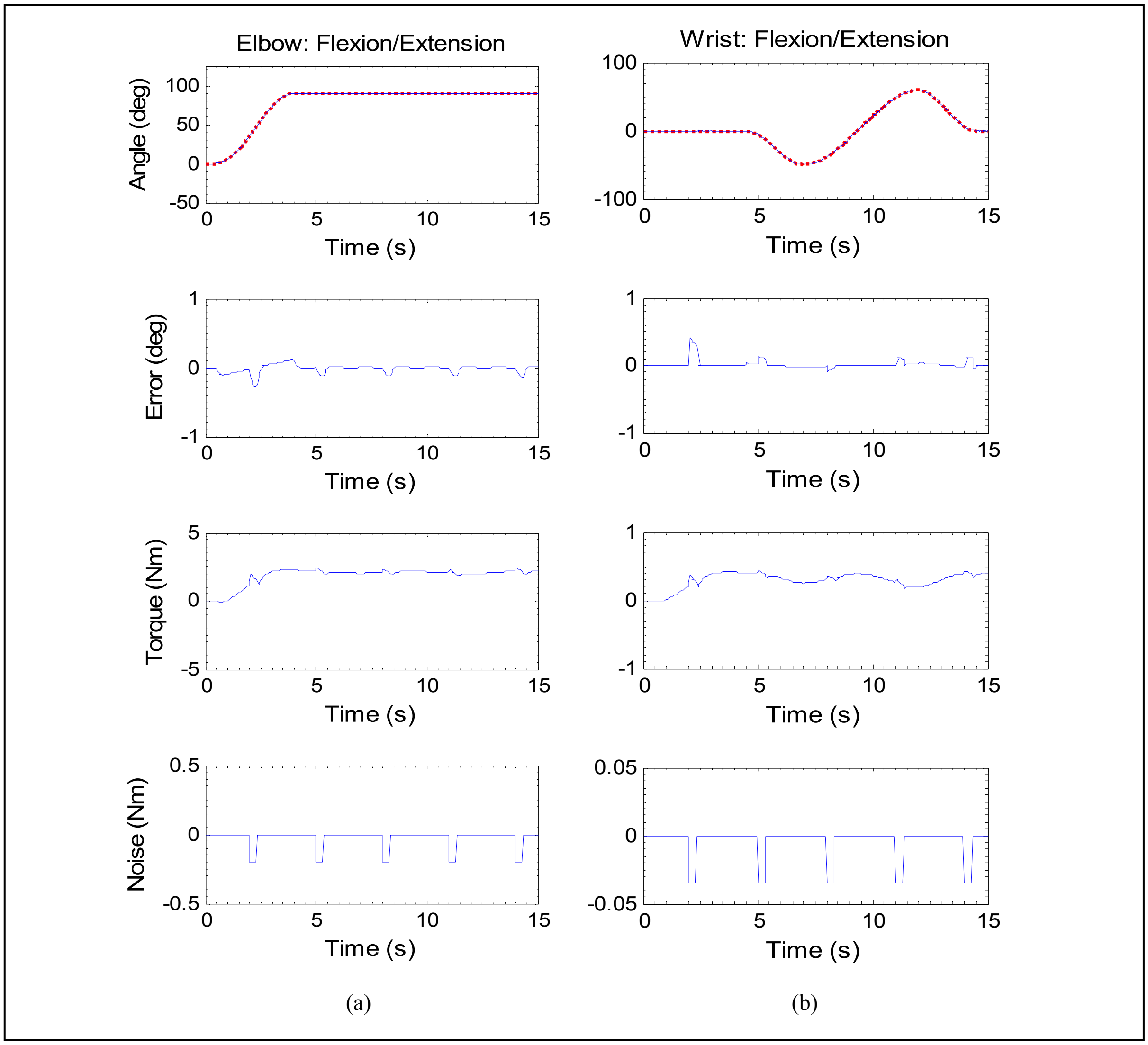


Figure 4.10 Repetitive movement of wrist joint (flexion/extension) while elbow maintaining steady position at 90°
(a) Elbow flexion at 90° (b) Wrist joint flexion/extension

For all tasks shown in Figure 4.5 through Figure 4.10, the maximum tracking deviation was below 1°, and for all cases the steady state error was always less than 0.1°. Simulation results thus validate the developed model and also evaluate the performance of the computed torque control technique with respect to trajectory tracking. Note that the control gains used for this control are as follows:

$K_P = diag[10 \quad 10 \quad 10 \quad 10 \quad 10 \quad 10 \quad 10]$, and
$K_V = diag[5 \quad 5 \quad 5 \quad 5 \quad 5 \quad 5 \quad 5]$.

### 4.4 Modified Sliding Mode with Exponential Reaching Law (*mSMERL*)

In this section, the theoretical structure of the *mSMERL* is presented for the dynamic trajectory tracking of the *ETS-MARSE*. We first define the control algorithm by conventional

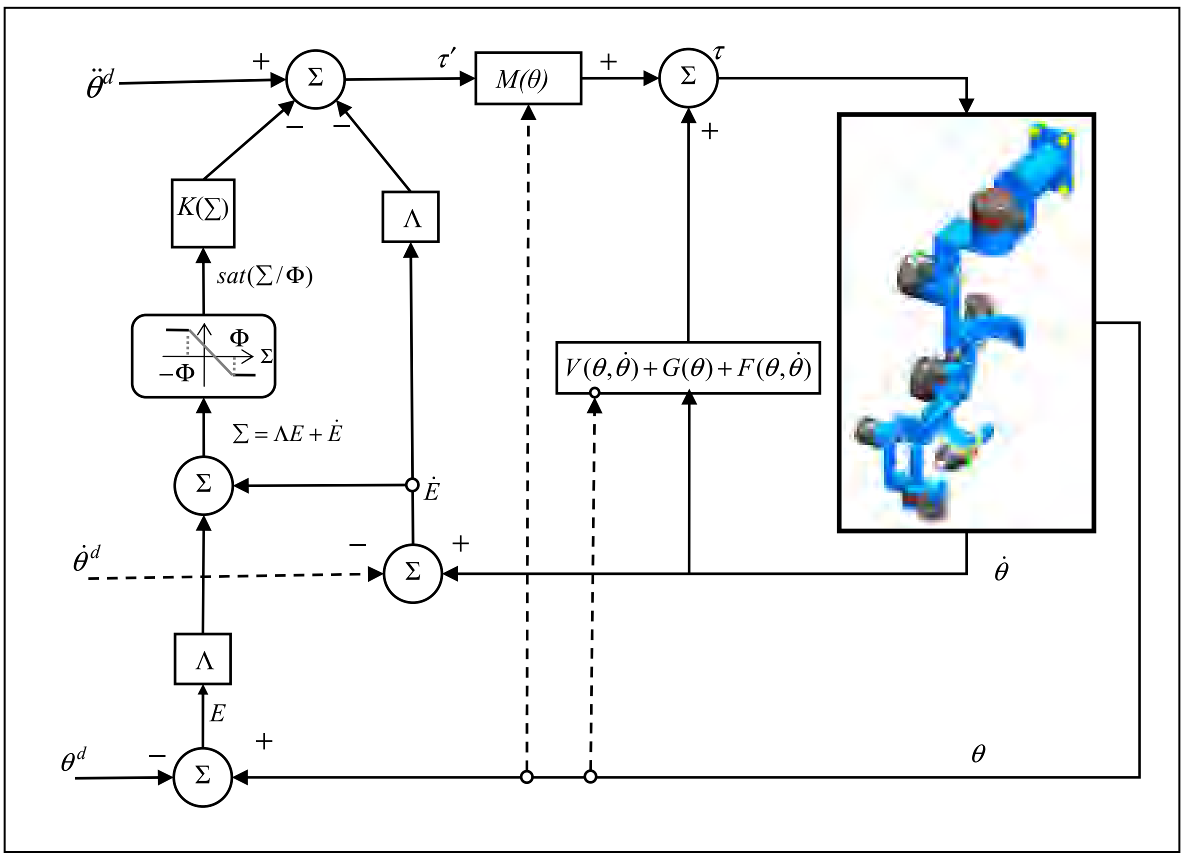


Figure 4.11 Schematic diagram of sliding mode ERL in combination with boundary layer neighboring to the sliding surface

sliding modes, and then modify the algorithm by exponential reaching law and adding boundary layer neighboring to the sliding surface. The general layout corresponding to the *mSMERL* is depicted in Figure 4.11.

The first step in the sliding mode control is to choose the sliding (or switching) surface $S$ in terms of the tracking error. Let the tracking error for each joint is defined as:

$$e_i = \theta_i - \theta_i^d \qquad \cdots \qquad (i = 1, \cdots, m) \tag{4.18}$$

and the sliding surface as:

$$S_i = \lambda_i e_i + \dot{e}_i \qquad \cdots \qquad (i = 1, \cdots, m) \tag{4.19}$$

where $\theta_i^d$ is the desired trajectory for joint $i$ , and $S_i$ is the sliding surface of each DoF.

Let $\Sigma = [S_1 \quad S_2 \quad \cdots \quad S_m]^T$ be the sliding surface for the *ETS-MARSE*. Therefore, we have:

$$\Sigma = \begin{bmatrix} \lambda_1 e_1 + \dot{e}_1 \\ \vdots \\ \lambda_m e_m + \dot{e}_m \end{bmatrix} \tag{4.20}$$

Equation (4.20) is a first order differential equation, which implies that if the sliding surface is reached, the tracking error will converge to zero as long as the error vector stays on the surface. The convergence rate is in direct relation with the value of $\lambda$. Figure 4.12 shows how this mechanism takes place in the phase plane; where it can be seen that there are two modes in sliding mode approach. The first mode, named reaching mode, is the step in which the error vector $(e, \dot{e})$ is attracted to the switching/sliding surface $\Sigma = 0$. In the second mode, also known as sliding mode, the error vector slides on the surface until it reaches the equilibrium point (0,0) .

Considering the following Lyapunov function candidate:

$$V = \frac{1}{2}\Sigma^T\Sigma \tag{4.21}$$

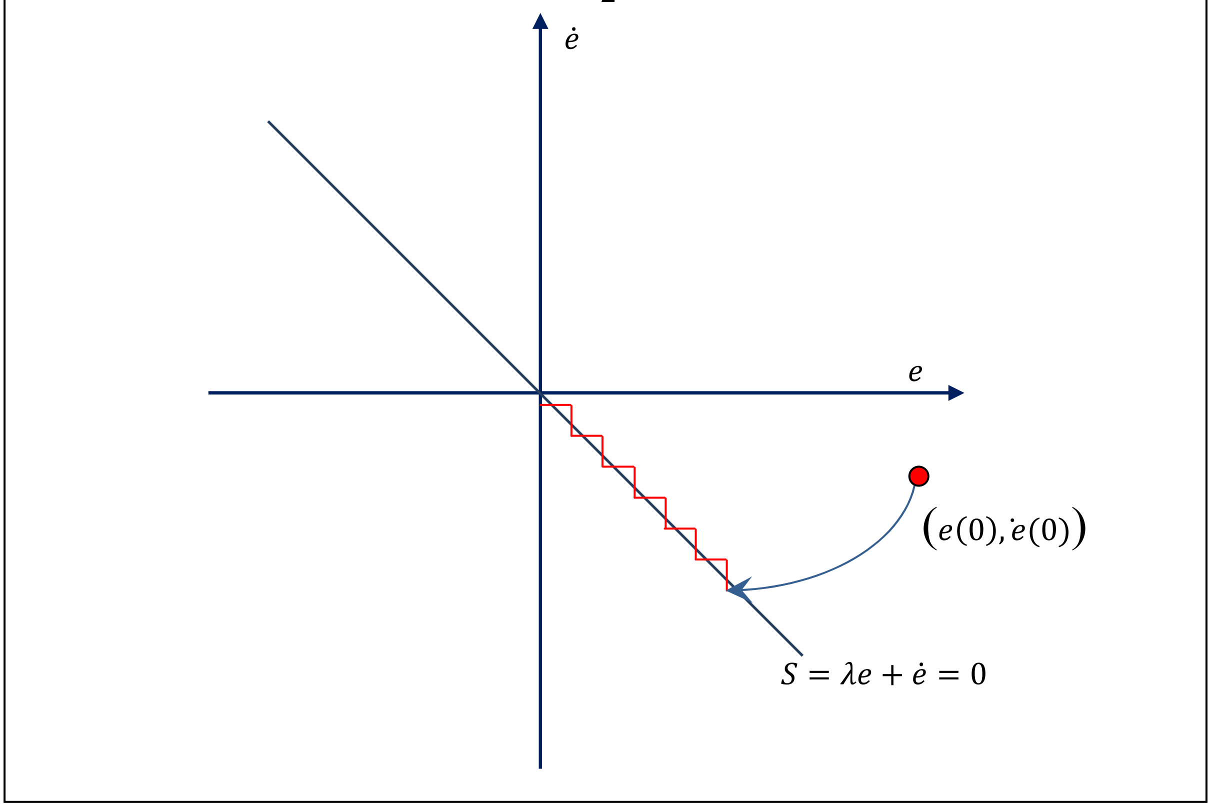


Figure 4.12 Sliding mode mechanism in phase plane

which is continuous and nonnegative. The derivative of $V$ yields:

$$\dot{V} = \Sigma^T\dot{\Sigma} \tag{4.22}$$

$$\dot{\Sigma} = -K.sign(\Sigma)\,,\ \forall t, K > 0 \ \Rightarrow \ \dot{V} < 0 \tag{4.23}$$

By choosing $\dot{\Sigma}$ as given in equation (4.23), relation (4.22) is ensured to be decreasing.

where, $sign(\Sigma) = [sign(\Sigma_1) \quad \dots \quad sign(\Sigma_n)]^T$, and $for\ (i \in \{1, \dots, n\})$:

$$sign(\Sigma_i) = \begin{cases} 1\ for\ \Sigma_i > 0 \\ 0\ for\ \Sigma_i = 0 \\ -1\ for\ \Sigma_i < 0 \end{cases} \tag{4.24}$$

Expression (4.23) is known as the reaching law. It is to be noted that the discontinuous term $K.sign(\Sigma)$ in Equation (4.23) often leads to a high control activity, known as chattering. In most systems, the chattering phenomenon is undesirable, because it can excite high frequency dynamics which could be the cause of severe damage. One of the most known approaches found in literature is to smoothen the discontinuous term in the control input with the continuous term $K.sat(\Sigma/\phi)$ (Slotine and Li, 1991).

where, $sat(\Sigma/\phi) = [sat(\Sigma_1/\phi_1) \quad \dots \quad sat(\Sigma_n/\phi_n)]^T$, and $for\ (i \in \{1, \dots, n\})$:

$$sat(\Sigma_i/\phi_i) = \begin{cases} 1 \text{ for } \Sigma_i \geq \phi_i \\ \Sigma_i/\phi_i \text{ for} -\phi_i \leq \Sigma_i \leq \phi_i \\ -1\ for\ \Sigma_i \leq \phi_i \end{cases} \quad \forall t, 0 < \phi_i \ll 1 \tag{4.25}$$

Using equation (4.25), the reaching law therefore becomes:

$$\dot{\Sigma} = -K.sat(\Sigma/\phi)\,,\ \forall t, K > 0 \tag{4.26}$$

However, by performing this substitution, the convergence of the system stays within a boundary layer neighborhood of the switching surface. The size of the neighborhood is directly affected by the choice of Φ. Therefore, with this technique, the chattering level is controlled, but the tracking performance of the system is negatively affected. However, the reaching law proposed by (Fallaha *et al.*, 2011), considers the above limitations and is designed based upon the choice of an exponential term that adapts with the variations of the switching function which is able to deal with the chattering/ tracking performance dilemma. The exponential reaching law (Fallaha *et al.*, 2011) can be expressed as:

$$\dot{\Sigma} = -K(\Sigma)\,.sign(\Sigma)\,,\ \forall t, K > 0 \tag{4.27}$$

where $0 < \delta_{0i} \leq 1;\ \alpha_i > 0, \text{and}, p_i > 0.$

where

$$K(\Sigma) = diag\left(\frac{k_i}{N_i\,(S_i)}\right) \quad \ldots \quad (i = 1, \ldots, m), \text{ and} \tag{4.28}$$

$$N_i(S_i) = \delta_{0i} + (1 - \delta_{0i})e^{-\alpha_i|S_i|^{p_i}} \tag{4.29}$$

The values of $\delta_{0i}$, $\alpha_i$, and $P_i$ can be fixed as proposed in (Fallaha *et al.*, 2011).

If $\delta_{0i}$ is selected as 1, the equation (4.27) becomes as equation (4.23). Therefore, it can be said that conventional SMC is a subset of exponential SMC. Fallaha et al.'s. (2011) findings for ERL are as follows (Fallaha *et al.*, 2011):

"In equation (4.27) with increasing $|S|$, $N(S)$ tend to $\delta_{0i}$ and consequently $k/N(S)$ converges to $k_i/\delta_{0i}$, which is greater than $k_i$. This means that $k/N(S)$ increases in the reaching phase, and accordingly the attraction of the sliding surface will be faster. On the other side, with decreasing $|S|$ , $N(S)$ tends to 1 and then $k/N(S)$ converges to $k$. This means

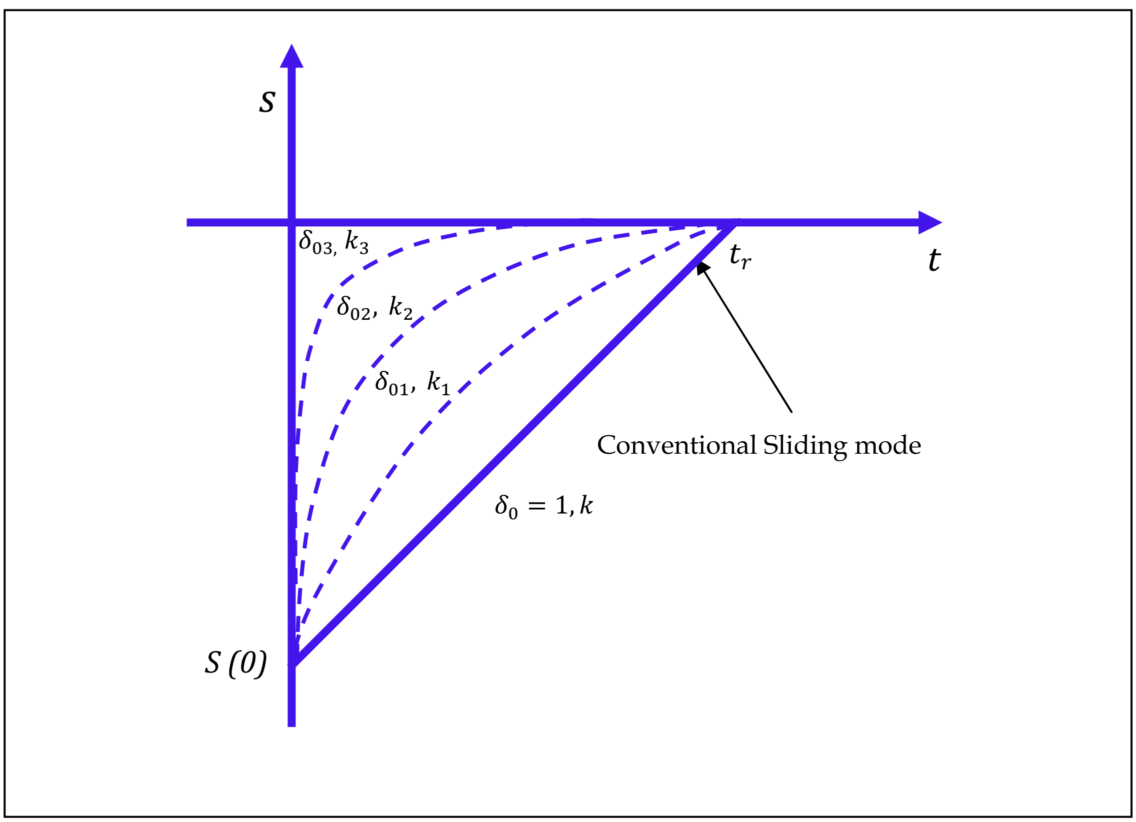


Figure 4.13 Switching function with ERL for different values of $k$ and $\delta_0$
Adapted from Fallaha et al. (2011)

that when the system approaches the sliding surface $k/N(S)$ gradually decreases and consequently reduces the chattering. The exponential sliding mode thus adapts to the variations of the switching function by letting $k/N(S)$ vary between $k$ and $k/\delta_0$. Figure 4.13 shows the switching function with the exponential sliding control for different values of $k$ and $\delta_0$. As can be seen in this figure, if we select $\delta_{0i} = 1$, the exponential sliding control will be the same as the conventional sliding mode control".

Note that though the chattering level is significantly reduced using ERL, still the controller shows high control activity during the transient. To deal with this problem, we propose a new reaching law, that combines the concept of ERL (Fallaha *et al.*, 2011) and that of the boundary layer (Slotine and Li, 1991) and can be written as follows:

$$\dot{\Sigma} = -K(\Sigma)\,.\,sat(\Sigma/\phi)\,,\ \forall t, K > 0 \tag{4.30}$$

Therefore and considering: $\ddot{\theta}^d = \left[\ddot{\theta}_1^d \quad \ddot{\theta}_2^d \quad \ldots \quad \ddot{\theta}_m^d\right]^T$,

$\dot{E} = [\dot{e}_1 \quad \dot{e}_2 \quad \cdots \quad \dot{e}_m]^T$, and

$$\Lambda = \begin{bmatrix} \lambda_i & 0 & 0 \\ 0 & \ddots & 0 \\ 0 & 0 & \lambda_m \end{bmatrix}.$$

$$\Sigma = \Lambda E + \dot{E} \quad \Rightarrow \quad \dot{\Sigma} = \Lambda \dot{E} + \ddot{E} \tag{4.31}$$

where $\ddot{E} = \ddot{\theta} - \ddot{\theta}^d$.Therefore, relation (4.31) can be written as:

$$\dot{\Sigma} = \Lambda \dot{E} + \ddot{\theta} - \ddot{\theta}^d \tag{4.32}$$

Substituting the value of $\ddot{\theta}$ from equation (4.13) in equation (4.32), we obtain:

$$\dot{\Sigma} = \Lambda \dot{E} - \ddot{\theta}^d - M^{-1}(\theta)\left[V\left(\theta,\dot{\theta}\right) + G(\theta) + F\left(\theta,\dot{\theta}\right)\right] + M^{-1}(\theta)\tau \tag{4.33}$$

Replacing $\dot{\Sigma}$ by its value given in equation (4.30)

$$-K(\Sigma).sat(\Sigma/\phi) = \Lambda\dot{E} - \ddot{\theta}^d - M^{-1}(\theta)\left[V(\theta,\dot{\theta}) + G(\theta) + F(\theta,\dot{\theta}) - \tau\right] \tag{4.34}$$

The torque $\tau$ can be isolated and thus give:

$$\tau = -M(\theta)\left(\Lambda\dot{E} - \ddot{\theta}^d + K(\Sigma).sat(\Sigma/\phi)\right) + \left[V(\theta,\dot{\theta}) + G(\theta) + F(\theta,\dot{\theta})\right] \tag{4.35}$$

where $K$ and $\Lambda$ are diagonal positive definite matrices, therefore the control law given in relation (4.35) ensures that the control system is stable. Details of the stability analysis can be found in (Fallaha *et al.*, 2011).

### 4.4.1 Simulated results with SMC (Rahman et al., 2010c):

A very commonly used rehabilitation exercise involving co-operative motion of the elbow and forearm (Physical Therapy Standards, 2011) is depicted in Figure 4.14. The objective of

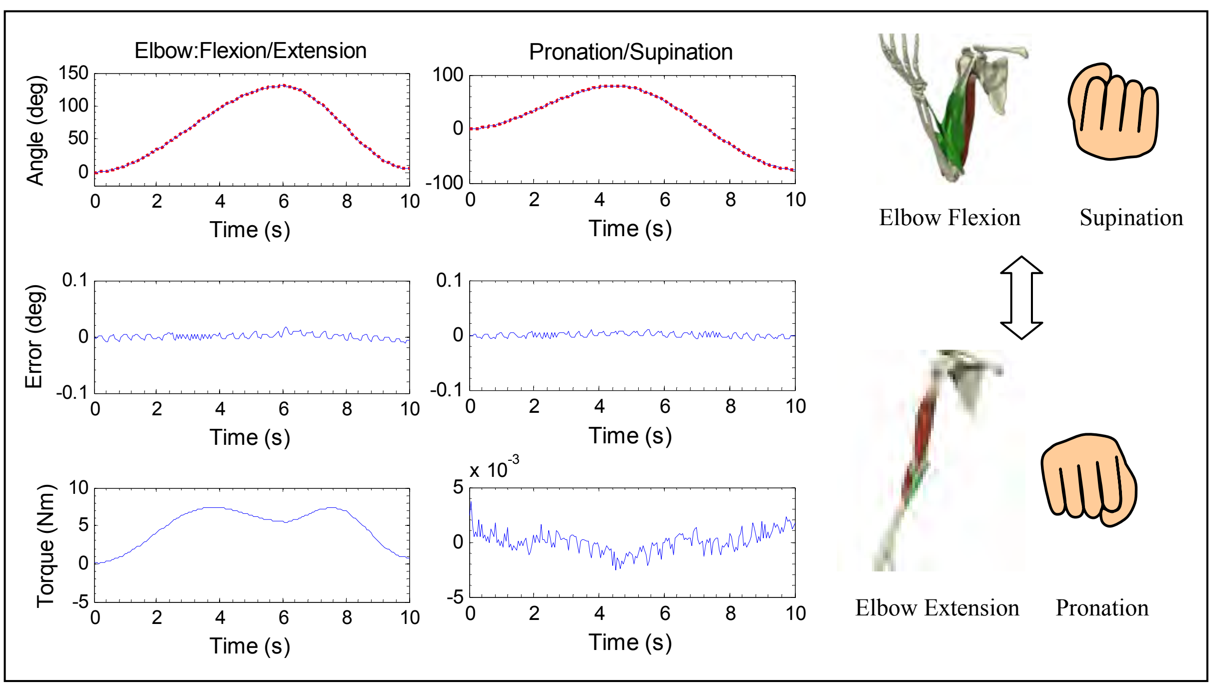


Figure 4.14 Cooperative movement of elbow and forearm

this task is to supinate the forearm from the initial position to the fully supinated position (Figure 2.6), while simultaneously flexing the elbow from complete extension to complete flexion (Figure 2.5) and next, to inversely move the forearm from full supination to full pronation (Figure 4.14), while the elbow simultaneously goes from complete flexion to extension. The top most plots of Figure 4.14 compare the desired trajectories to measured trajectories. Controller tracking performance is certainly obvious from this figure since the desired and measured trajectories also overlapped in this case and the deviation was well below 0.01°.

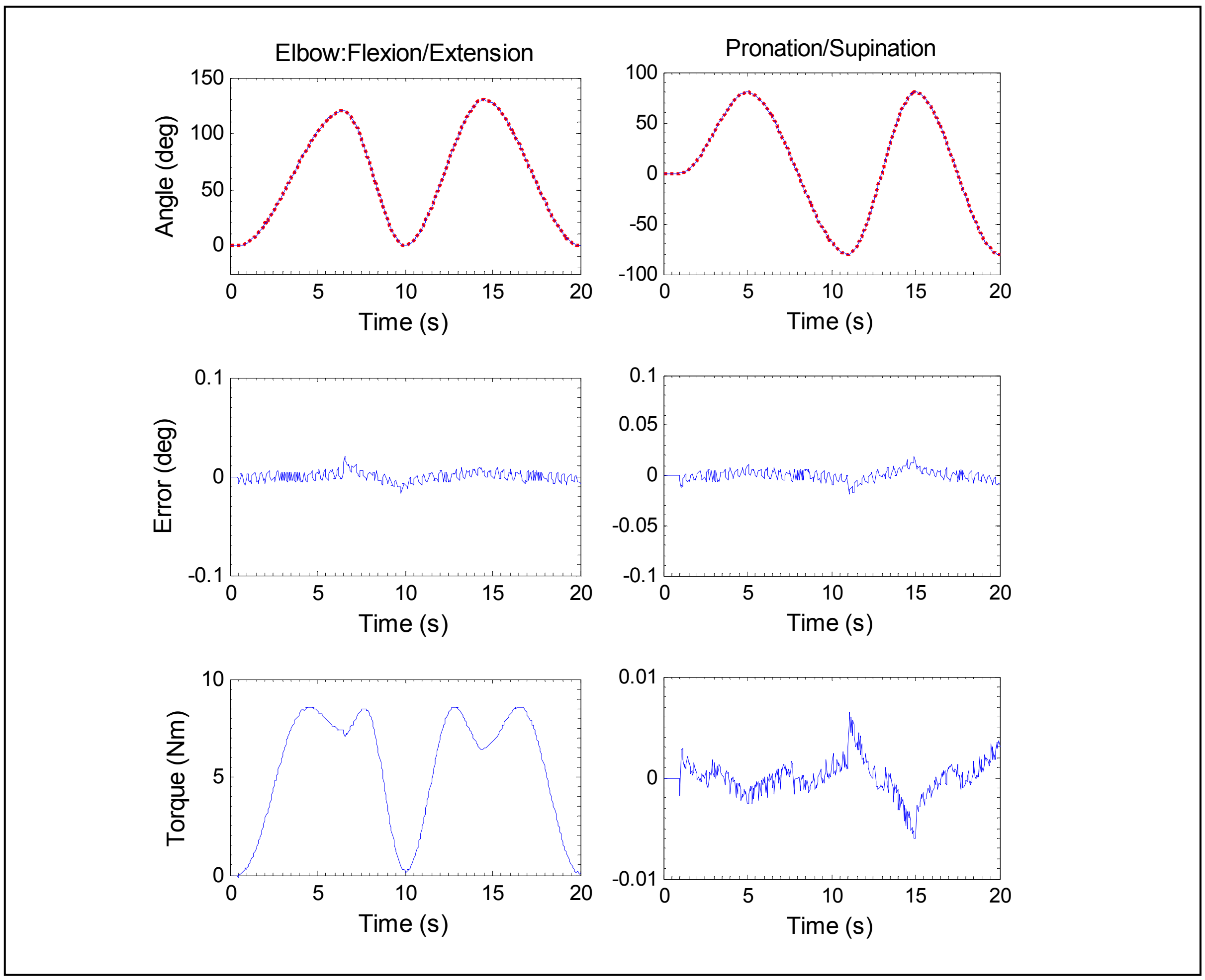


Figure 4.15 Cooperative movement of elbow and forearm, grabbing extra 0.5 kg mass

Figure 4.15 and Figure 4.16 show a similar type of rehabilitation exercises as Figure 4.14 except a weight of 0.5 kg mass is added to the user's wrist for the exercise of Figure 4.15 and a weight of 1.0 kg mass is added for the exercise depicted in Figure 4.16. These are a kind of typical occupational therapy, grabbing a weight of 0.5 kg to1.0 kg and lifting it up to elbow flexion of 120°.

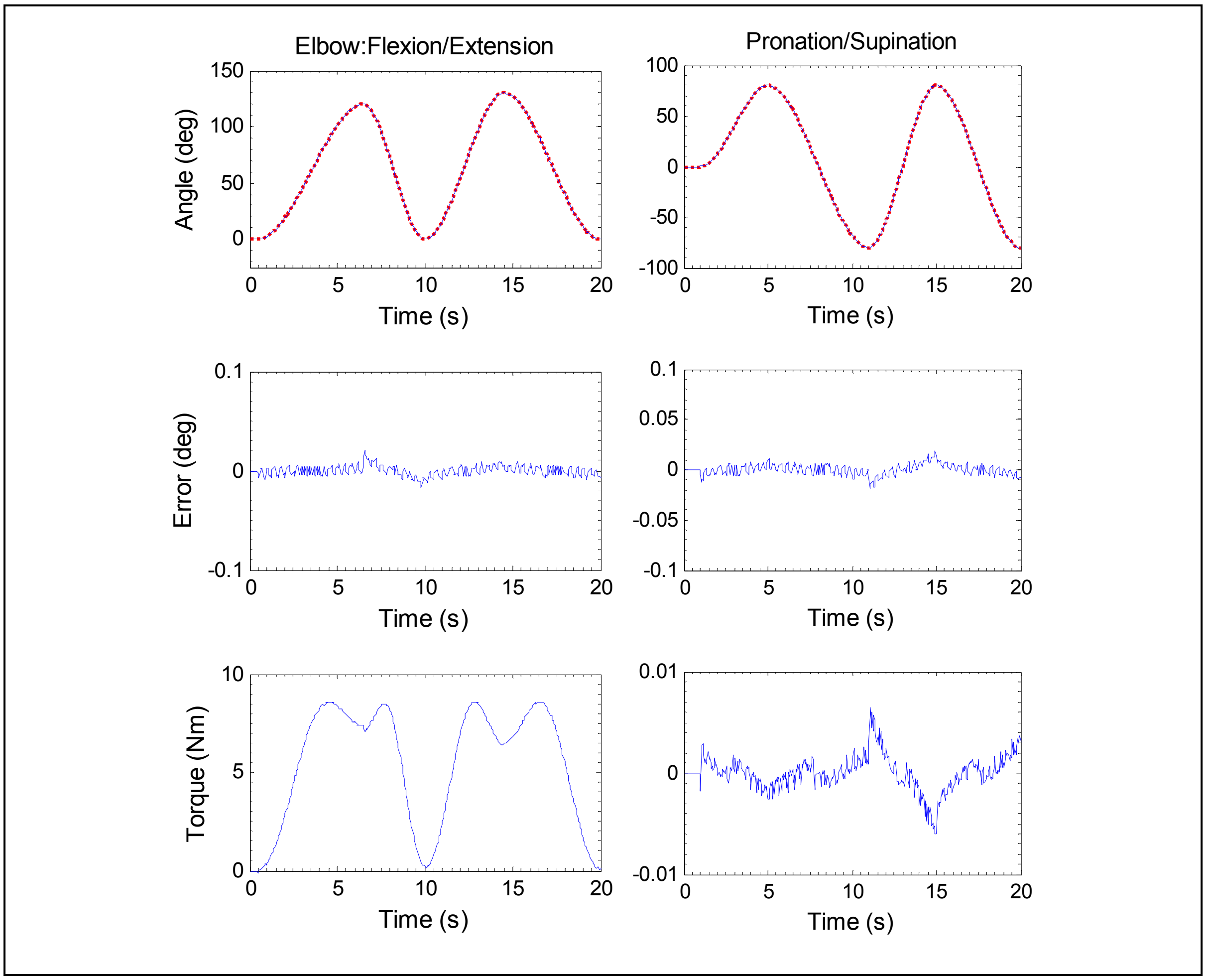


Figure 4.16 Cooperative movement of elbow and forearm, grabbing extra 1 kg mass

Like previous tracking simulations, Figure 4.15 and Figure 4.16 also demonstrate the good performance of the controller, with error limited to less than 0.01°.

As depicted in Figure 4.14 to Figure 4.16, the maximum tracking deviation is observed at the level of elbow flexion/extension which was below 0.01° (i.e., tracking error is 0.007% of the total range). Simulated results thus validate the developed model and also evaluate the performance of the control techniques in regard to trajectory tracking.

### 4.4.2 Simulated results with conventional SMERL

Reaching movement which is fundamental to many activities of daily life is depicted in Figure 4.17, where the subject is supposed to move his or her hand gently in a diagonal direction. This movement involves simultaneous and repetitive motion at the elbow and shoulder joints. The topmost plots of Figure 4.17 depict the measured trajectories (dotted line) and the desired trajectories (dotted line) where it can be found that both are matched together. It can also be seen from the error plots (intermediate plots) that the tracking errors

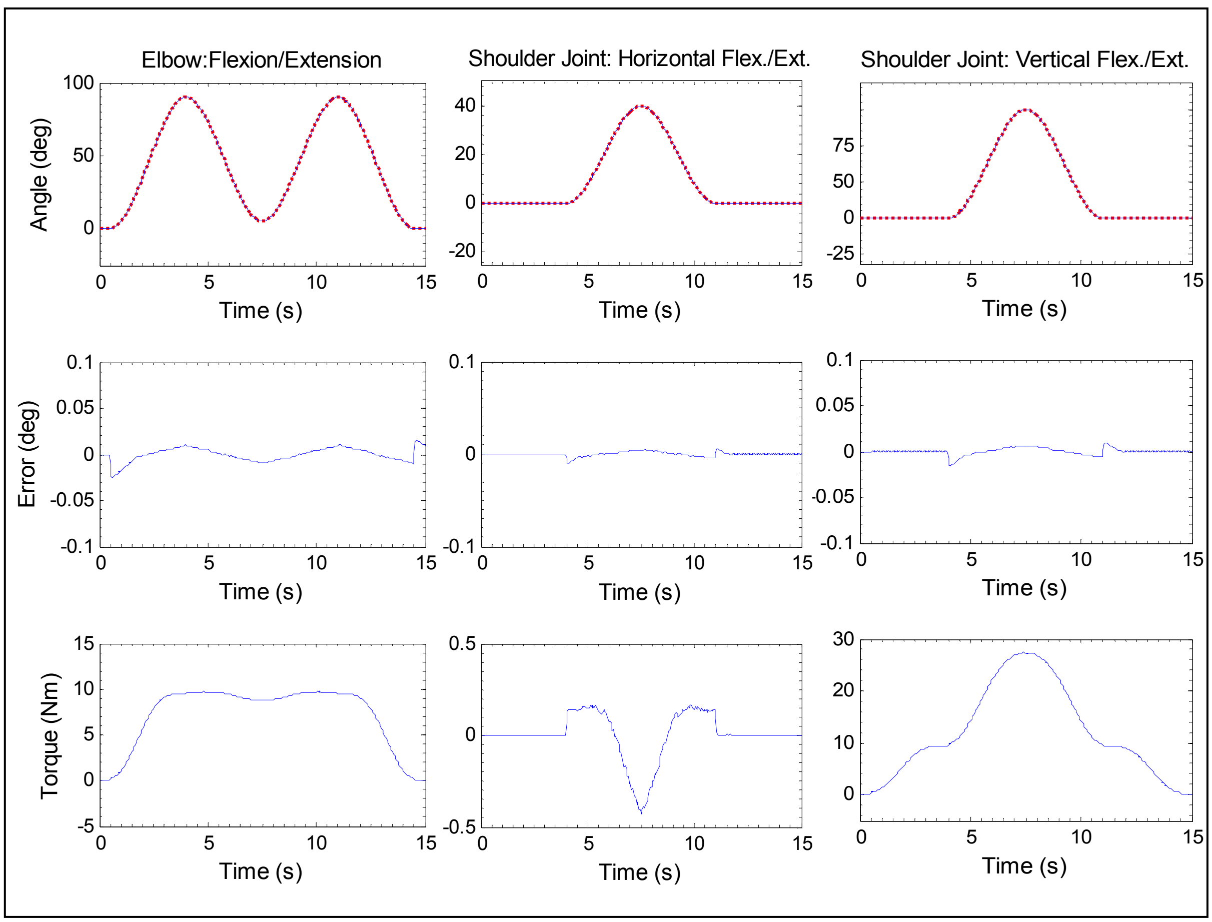


Figure 4.17 Simulated results with SMERL, diagonal reaching movement

are less than 0.1° and thus demonstrate the good performance of the controller.

Note that the control gains used for this simulation were found by trial and error, and are as follows:

For *SMC*

$\Lambda = diag[40 \quad 40 \quad 40 \quad 40 \quad 40 \quad 14 \quad 40]$, and

$K = diag[0.1 \quad 0.1 \quad 0.1 \quad 0.1 \quad 0.1 \quad 0.1 \quad 0.1]$.

For *SMERL*

$\delta_{0i} = 0.1, \alpha_i = 3, \ P_i = 1$ ,

$\Lambda = diag[40 \quad 40 \quad 40 \quad 40 \quad 40 \quad 14 \quad 40]$, and

$K = diag[0.01 \quad 0.01 \quad 0.01 \quad 0.01 \quad 0.01 \quad 0.01 \quad 0.01]$.

The next chapter focuses on experiments. Note that the experiments were conducted on subjects in a seated position. Since the *ETS-MARSE* is mounted on a rigid base structure on the floor, wearing the *ETS-MARSE* arm will not impinge any load to the subjects. Further, the control algorithm is designed to compensate gravity loads efficiently and smoothly (mass of the *MARSE* arm and that of the upper limb).

## 4.5 Cartesian Trajectory Tracking with Joint based Control

The general layout of the control architecture for 'Cartesian trajectory tracking with joint based control' is given in Figure 4.18 where $\theta_d$, $\dot{\theta}_d$ , $\ddot{\theta}_d$ represent desired joint position, velocity and acceleration respectively and those for Cartesian co-ordinates are represented by $v_d$, $\dot{v}_d$ , $\ddot{v}_d$ respectively.

The left dotted box (Figure 4.18) indicates the Cartesian to joint space trajectory conversion process. Given an end-effector position and orientation ($v_d$), desired Cartesian velocities

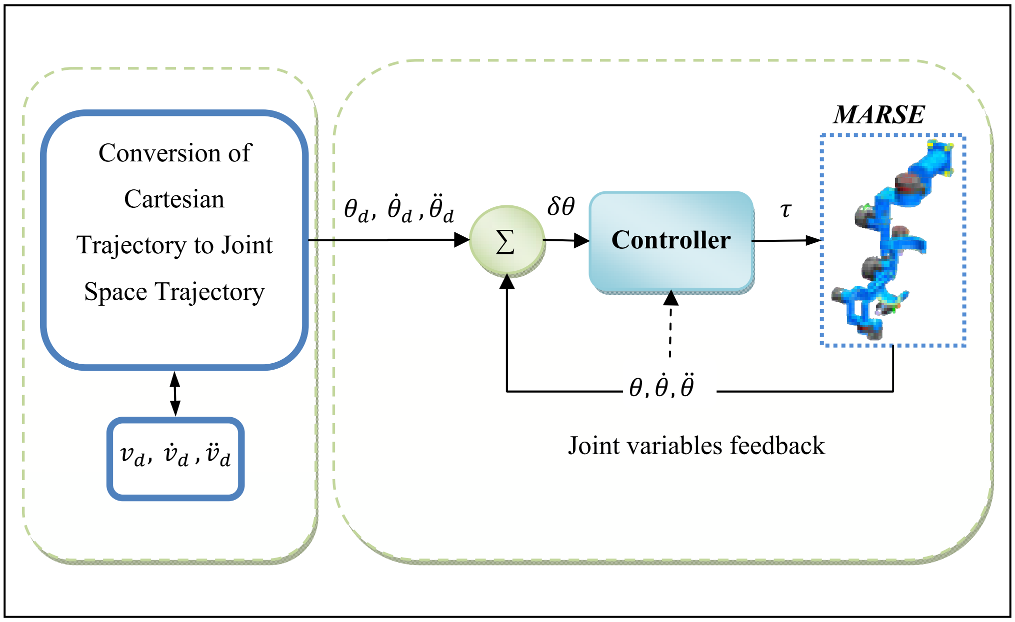


Figure 4.18 Cartesian trajectory tracking with joint based control

($\dot{v}_d$) and accelerations ($\ddot{v}_d$) can be found using cubic polynomial method (Craig, 2005). Once Cartesian velocities are found, it is quite simple to find joint space variables ($\theta_d$, $\dot{\theta}_d$, $\ddot{\theta}_d$) using Equation (3.7). It can also be seen from Figure 4.18 (the right dotted square box) that once desired joint variables are found the control scheme followed the principal of joint based control approach (Craig, 2005). As seen from Figure 4.18 the inputs to the controllers are joint errors ($\delta\theta$) and output is the torque command ($\tau$) to the *ETS-MARSE*.

# CHAPTER 5

# EXPERIMENTS AND RESULTS

The first section of this chapter briefly describes the experimental setup and the implementation of the control techniques. In the mid sections of the chapter, experimental results with different control techniques (e.g., PID, CTC, *mSMERL*) are presented. In experiments, we introduced two options for providing passive therapy. In the first option, the *MARSE* was maneuvered to follow a pre-programmed trajectory (Physical Therapy Standards, 2011) that corresponds to the recommended passive rehabilitation protocol. For the second option, users have the flexibility to maneuver the *ETS-MARSE* with the developed master exoskeleton arm (*mExoArm)*. Note that in all cases a quantitative measure of trajectory tracking that represents passive arm movement therapy is evaluated by measuring tracking errors as a function of time (i.e., deviation between desired and measured trajectories). The chapter ends with a brief discussion on the experimental results.

## 5.1 Experimental Setup and Control Implementation

Experimental set-up for the *ETS-MARSE* system is depicted in Figure 5.1. Potentiometers, which are incorporated with each joint of the *MARSE,* are sampled at 1 ms. The signals are then filtered prior to being sent to the controller. Filtering is important to eliminate high

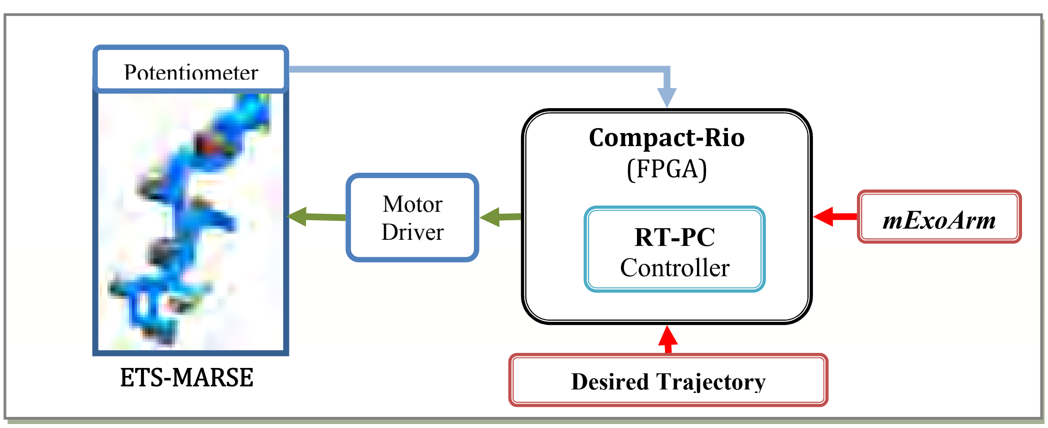


Figure 5.1 Experimental setup

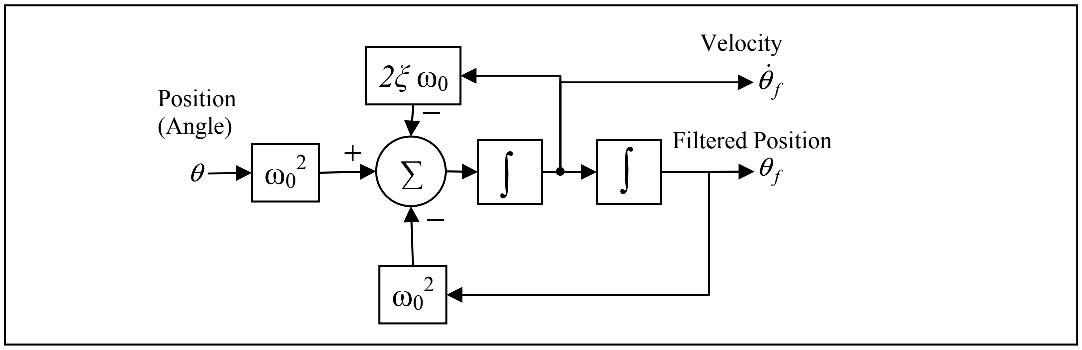


Figure 5.2 Schematic diagram of 2nd order filtering

frequency or noisy data from the desired signals. As depicted in Figure 5.2, the velocity of joints is found easily from the output vector of second order filtering. The parameters of the filter were set by trial and error to $\omega_0 = 30$ rad/s, and $\zeta = 0.9$.

Control architecture for the *ETS-MARSE* system is depicted in Figure 5.3. The joints' torque commands are the output of the controller. However, the torque commands are converted to motor currents and finally to reference voltage as voltage value is the drive command for the motor drivers. Note that the controller (PID/CTC/ mSMERL) updates the torque commands every 1.25 ms and is executed in RT-PC (left dotted circle, Figure 5.3). Furthermore, to realize the real time control of the *MARSE,* and also to ensure the right control torque

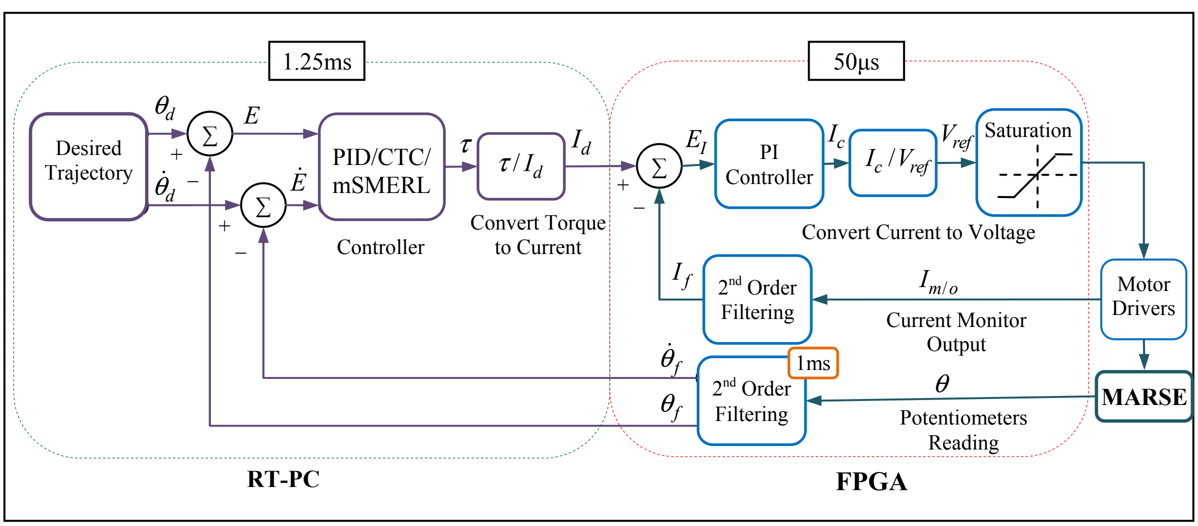


Figure 5.3 Control architecture

commands were sent to the joints (as well as the reference voltage commands for the drivers), we have also added a PI controller (right dotted circle, Figure 5.3) to minimize the differences between desired and measured currents (i.e., the error command to PI controller). The PI controller runs 25 times faster than the torque control loop and is executed in FPGA. The current signals measured from the current monitor output of motor drivers are sampled at 0.1 ms, and are then filtered with a $2^{nd}$ order filter with a damping factor $\zeta$=0.90 and natural frequency $\omega_0$=3000 rad/s prior to being sent to the PI controller.

## 5.2 Passive Rehabilitation Using Pre-determined Exercises

The intent of this protocol was to provide rehabilitation from a library of passive rehabilitation exercises, which was already formed (Chapter 4, subsections 4.3.1, and 4.4.1) according to recommended passive therapy (Physical Therapy Standards, 2011).

Experiments were carried out with healthy male human subjects (age: 24-34 years; height: 162-177cm; weight: 58-118 kg; number of subjects: 2) to provide a passive rehab therapy. This includes passive exercises for shoulder joint movement, elbow and forearm movement, and wrist joint movement.

### 5.2.1 Experimental Results with PID Control (Rahman *et al.*, 2011d; 2012d)

Shoulder joint movements:
Figure 5.4 shows the experimental results of shoulder joint vertical flexion/extension motion where the *MARSE* raises the subject's arm (from the initial position, i.e., all joints are at 0°) to a specific position over the head (e.g., in Figure 5.4a, the elevation was set to 130°), holds that position for a few seconds (e.g., in Figure 5.4a, 4sec) and then slowly moves the joint back to its initial position. The topmost plot of Figure 5.4 compares the desired joint angles (or reference trajectories, dotted line) to measured joint angles (or measured trajectories, solid line). It is obvious from the figure that the controller's performance was excellent since measured trajectories overlapped with the desired trajectories. The intermediate plot of

Figure 5.4 shows the error as a function of time (i.e., deviation between desired and measured trajectories). It can be seen that the tracking error was quite small (<2.5°) and that the most noticeable one was the steady state error (i.e., when *MARSE* is maintaining the position at 130° against gravity) which lies below and/or near around 0.1°. Note the two spikes as apparent in the error plots; these are due to static friction that has a large value during the initiation of the upward (where error was around 3°, Figure 5.4a) and the downward movement (e.g., in Figure 5.4a, downward movement starts from 130°, where deviation was around 4°). The generated joint torque corresponding to the trajectory is

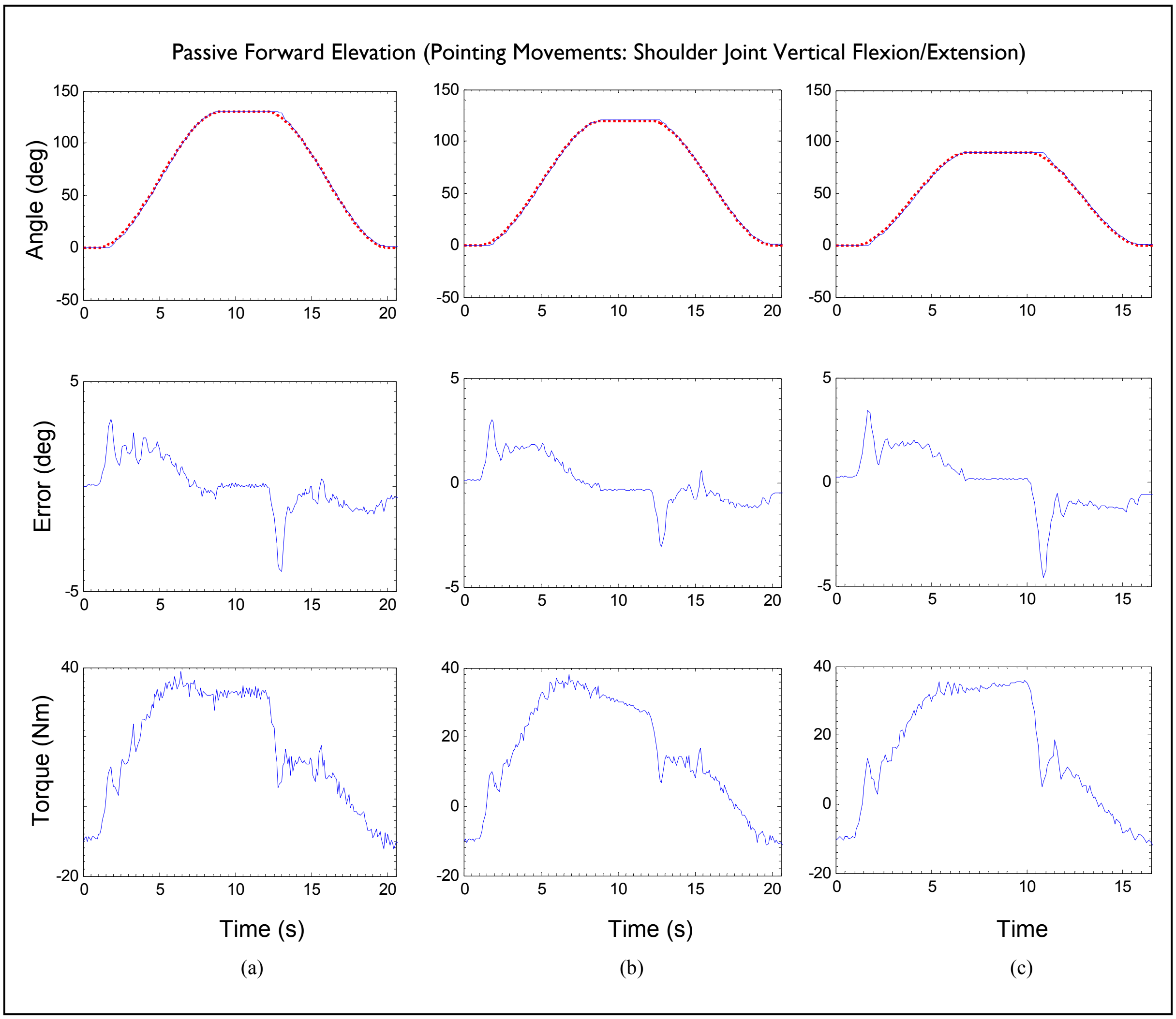


Figure 5.4 Shoulder joint vertical flexion/extension motion
(a) Passive forward elevation up to 130° (b) Passive forward elevation up to 120°
(c) Passive forward elevation up to 90°, showing fast movement compared to other exercises

plotted in the bottom row of Figure 5.4. Passive forward elevations at different joint angles are depicted in Figure 5.4b and Figure 5.4c. These exercises are also known as pointing movements, with the goal of gradually increasing the passive range of movement (ROM).

Figure 5.5 shows a passive horizontal flexion/extension motion of the shoulder joint, where passive forward elevation (i.e. vertical flexion of shoulder joint) is maintained at 90°. Again,

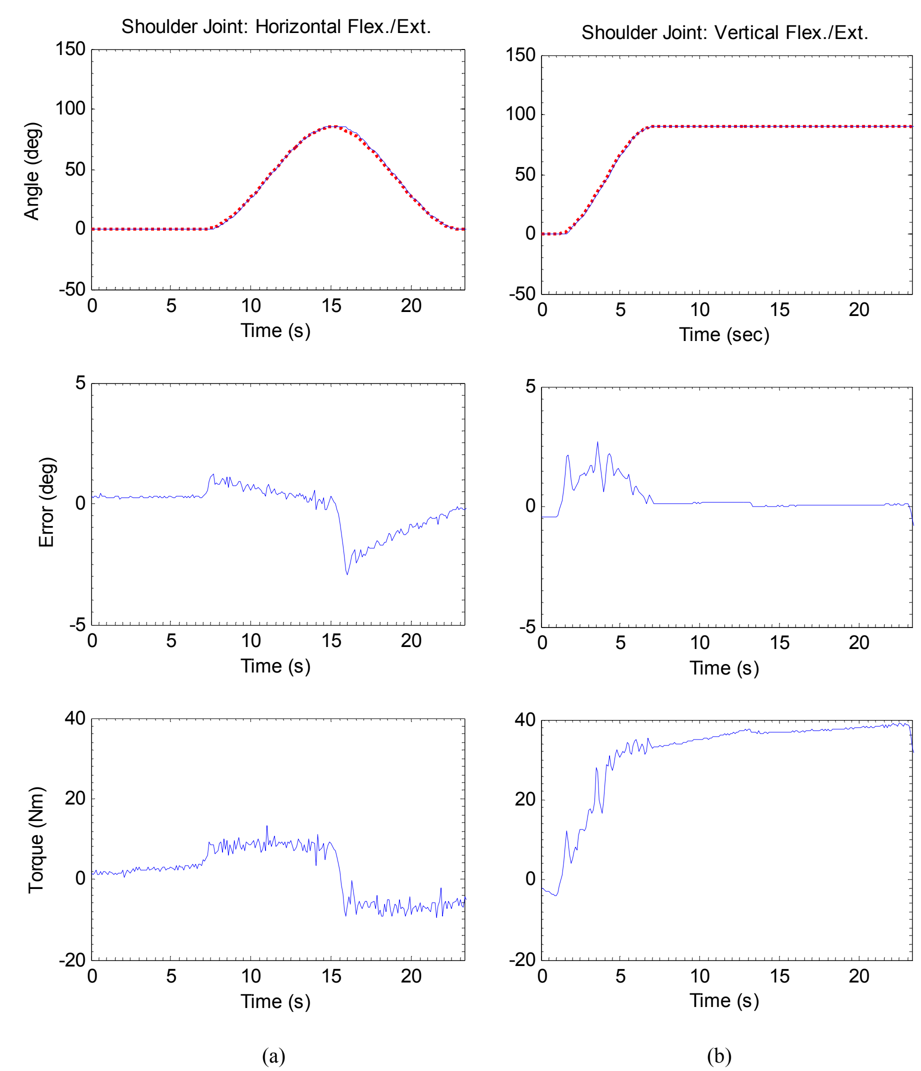


Figure 5.5 Passive arm movement along transverse plane
(a) Shoulder joint horizontal flexion/extension (b) Shoulder joint vertical flexion motion, up to 90° and maintaining that position while performing horizontal flexion/extension motion

the tracking performance of the controller was excellent, with tracking error less than 2° and the steady state position error below 0.05°.

Figure 5.6 demonstrates a co-operative movement of the elbow (flexion/extension) and shoulder joint (internal/external rotation). The objective of this exercise is to provide repetitive movement at the level of the shoulder joint while maintaining the elbow at 90°. As shown in Figure 5.6a, the exercise begins with elbow flexion, then repetitive internal/external

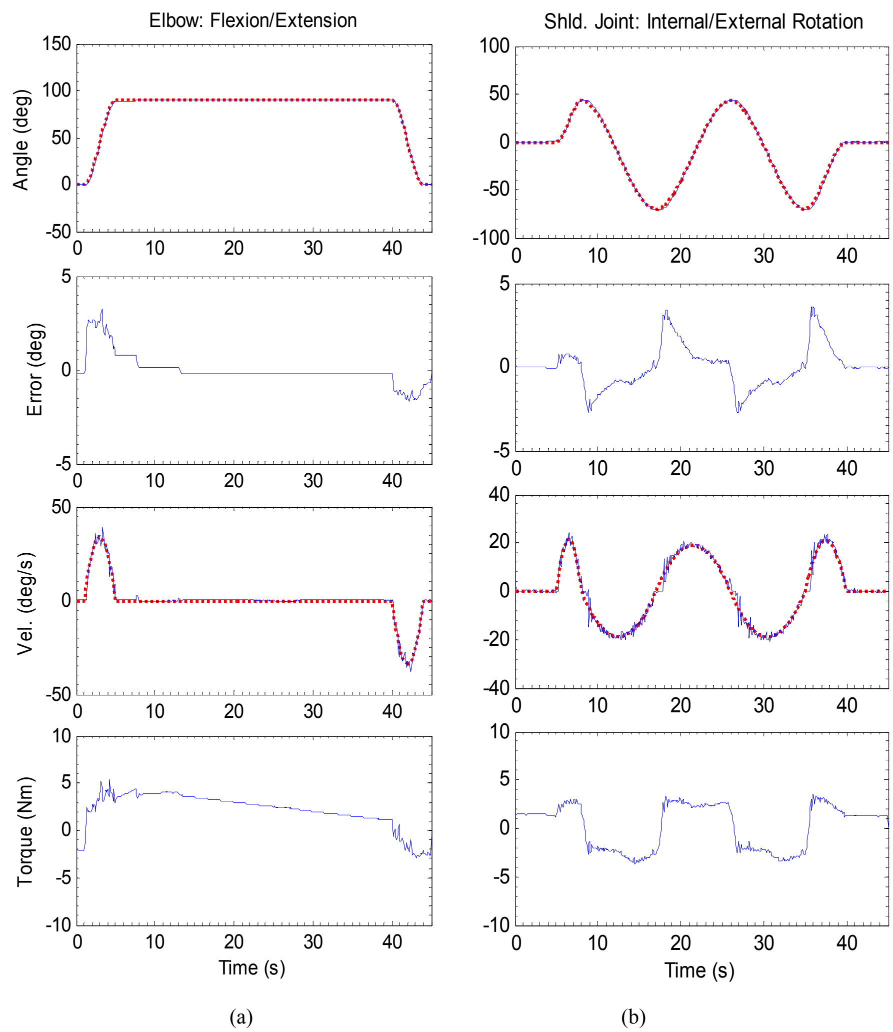


Figure 5.6 Passive arm therapy; a cooperative movement of shoulder and elbow joint motion
(a) Elbow joint flexion/extension
(b) Repetitive movement of shoulder joint internal/external rotation

rotation is performed (Figure 5.6b); the exercise ends with the extension of the elbow to 0° (Figure 5.6a). The 3rd row of the plots (from the top) displays velocity tracking (where dotted line indicates the desired velocity and the solid line indicates measured velocity). The results demonstrate good performance of the controller. The maximum tracking error was observed at the level of shoulder joint internal/external rotation which was around 2.75°. However, in this case as well, the steady state position error was found below 0.05°.

Elbow and forearm movements:

A typical rehabilitation exercise involving elbow joint flexion extension movement is depicted in Figure 5.7. The exercise began with the elbow joint at 90°. Also in this case, the

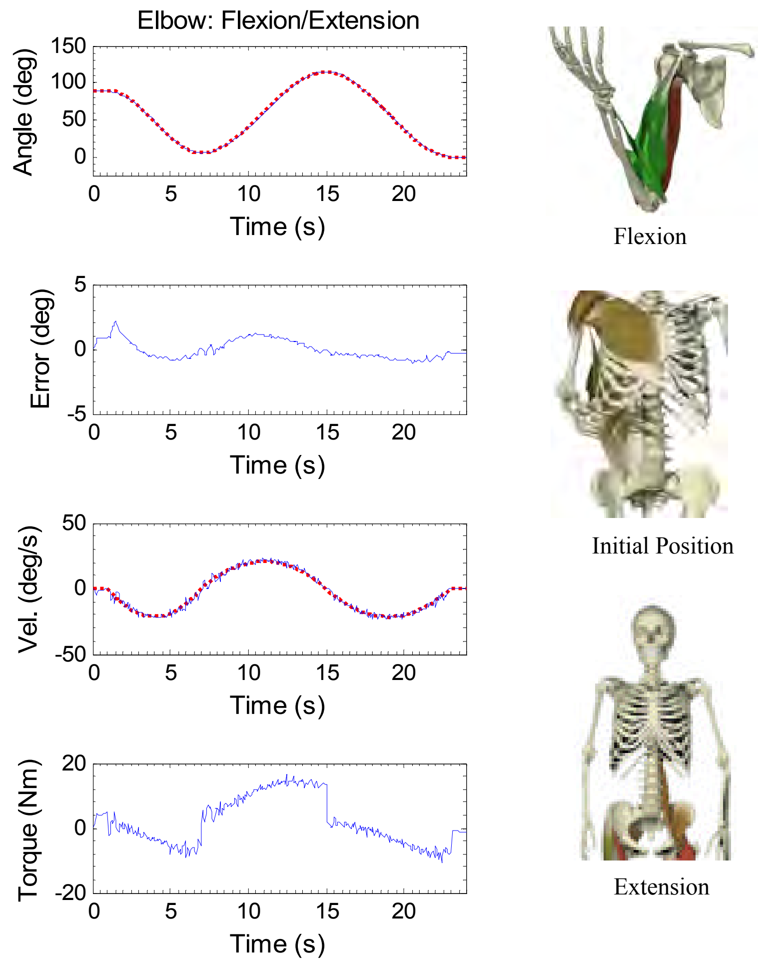


Figure 5.7 Elbow joint flexion/extension movement

tracking performance is obvious as the desired (dotted line) and measured trajectories (solid line) are overlapping and the tracking deviation is well below 1.5°.

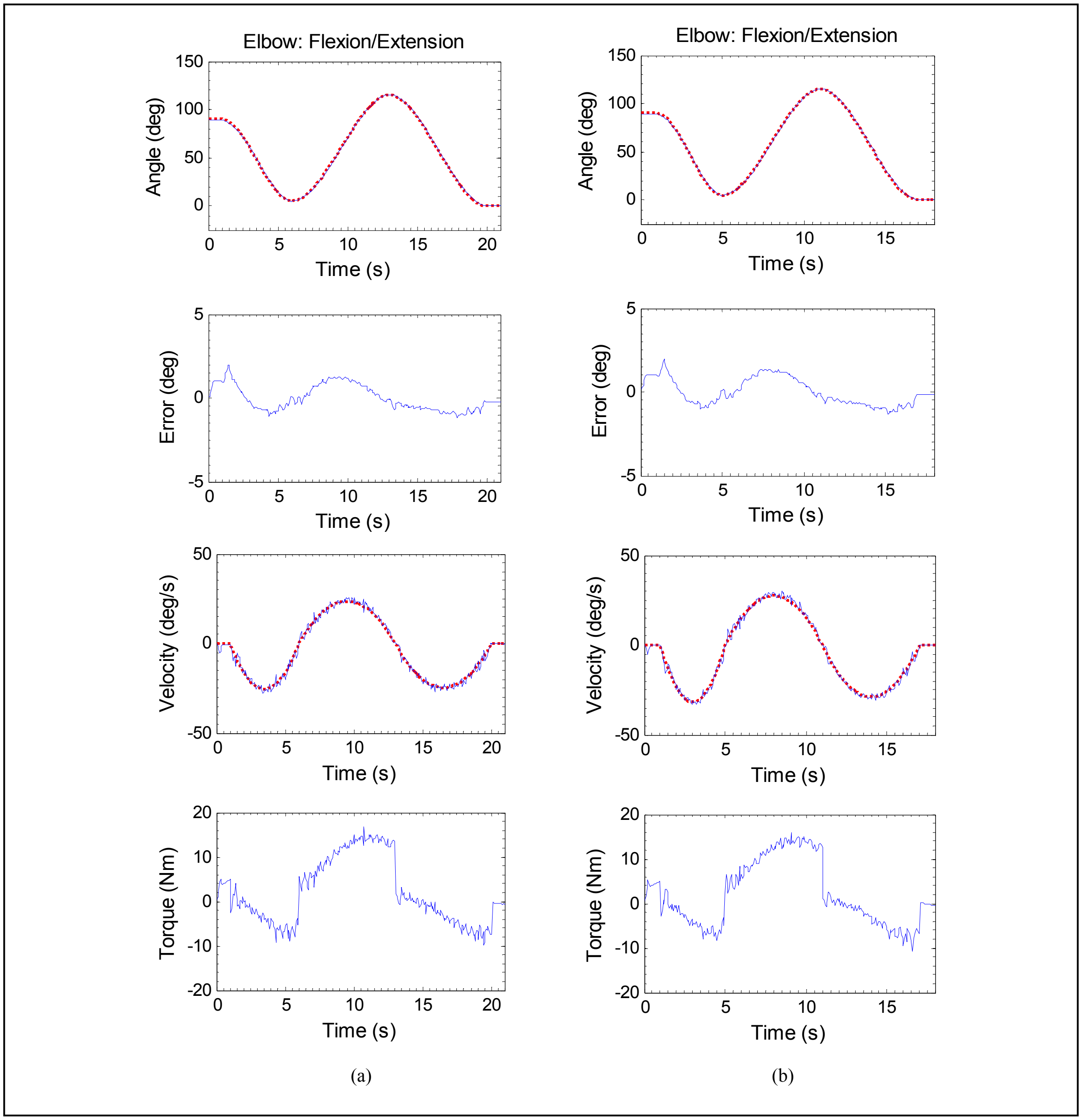


Figure 5.8 Elbow joint flexion/extension performed at different speeds
(a) Experiment duration 21s (b) Experiment duration 17s

Depending on the subject, it is often required to change the speed of such exercises. Figure 5.8 shows the similar exercises that were performed with different speeds of motion. The exercise as depicted in Figure 5.8(a) took 21s whereas the similar exercise as shown in Figure 5.8(b) took 17s to complete. Therefore, from Figure 5.7 and Figure 5.8, we may conclude that at a variety of speeds the controller shows excellent tracking performance with error limited to less than 1.5°.

Figure 5.9 shows the tracking performance of the controller during forearm pronation/supination. In this experiment, the full range of forearm movement was carried out from an initial position with the elbow joint at 90° and the forearm at 0°. Thereafter, as shown in Figure 5.9, the *MARSE* was directed to alternatively supinate and pronate the forearm , as it is often recommended to perform this movement repeatedly (Physical Therapy Standards, 2011). It can be seen that the tracking error was quite small (<2°).

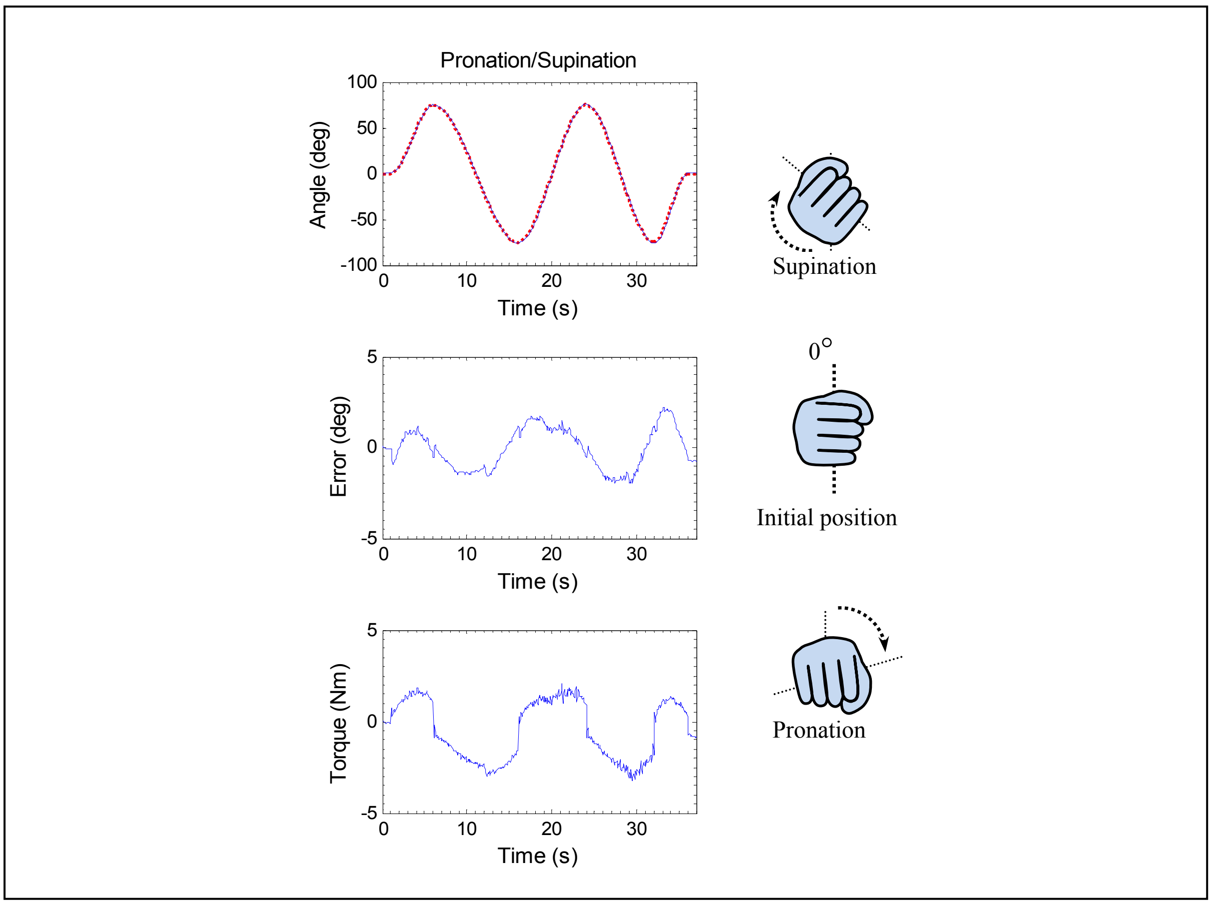


Figure 5.9 Repetitive movement of forearm pronation/supination

A very common rehabilitation exercise involving cooperative and simultaneous movements of the elbow and forearm is depicted in Figure 5.10. The objective of this task is to pronate the forearm from its initial position to the fully pronated position, while simultaneously flexing the elbow from its initial position (90°) to complete flexion and then to reverse the movement. Controller tracking performance is certainly obvious from these Figures since the desired and measured trajectories also completely overlapped in this case, with error smaller than 2.5°.

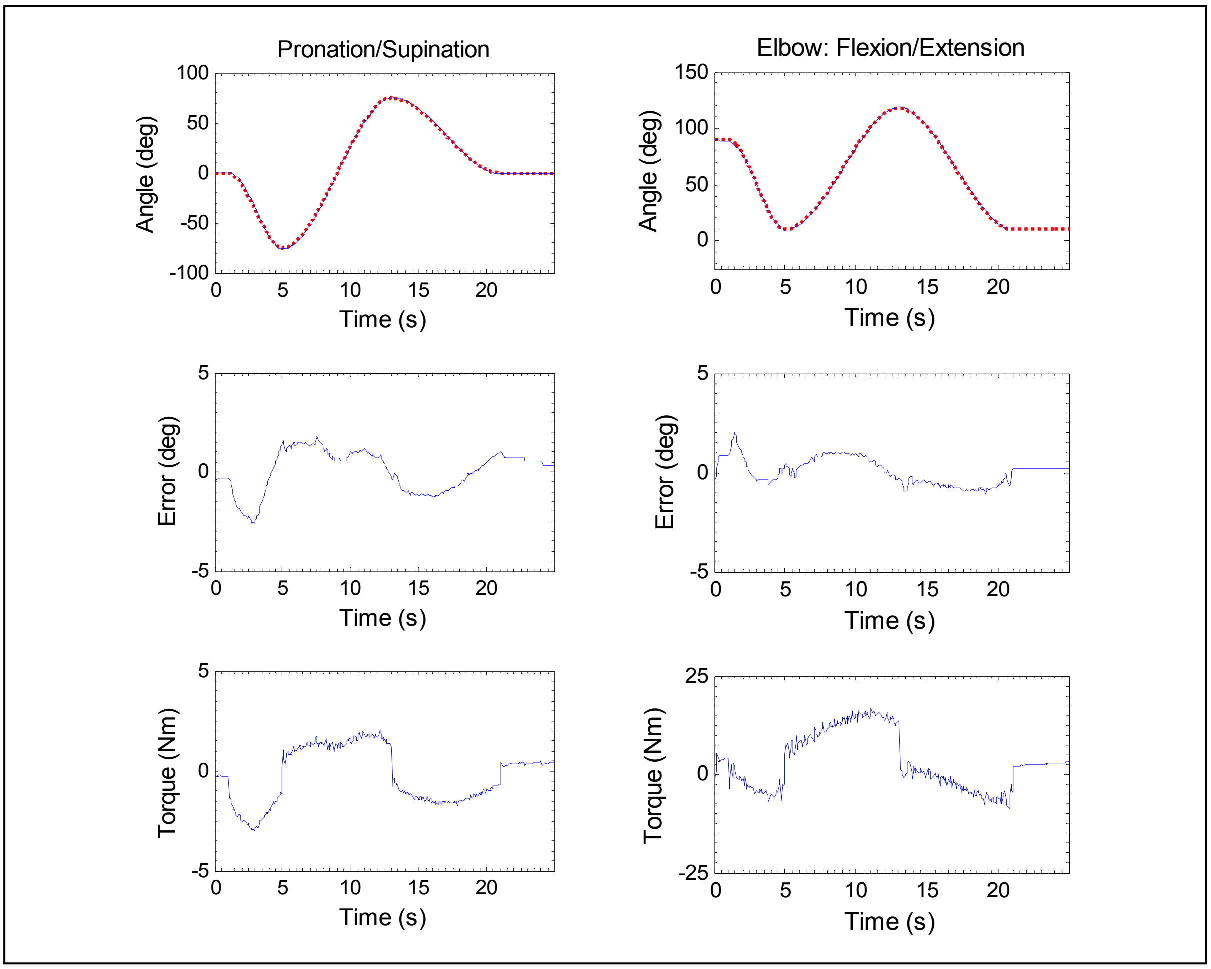


Figure 5.10 Cooperative and simultaneous motion of elbow and forearm movement

Wrist joint movements:

A typical rehabilitation exercise involving movements of wrist joint is depicted in Figure 5.11. The objective of these exercises is to provide radial/ulnar movement (Figure 5.11a) and flexion/extension motion of the wrist joint (Figure 5.11b). These exercises are typically carried out for a few minutes and involve repetitive movements of the wrist joint.

Note that because the physical limit of the developed wrist joint is +60° in flexion and -50° in extension, the trajectory tracking was performed within the range of +57° to -48°. These results show a similar tracking performance of the controller as for the other experiments.

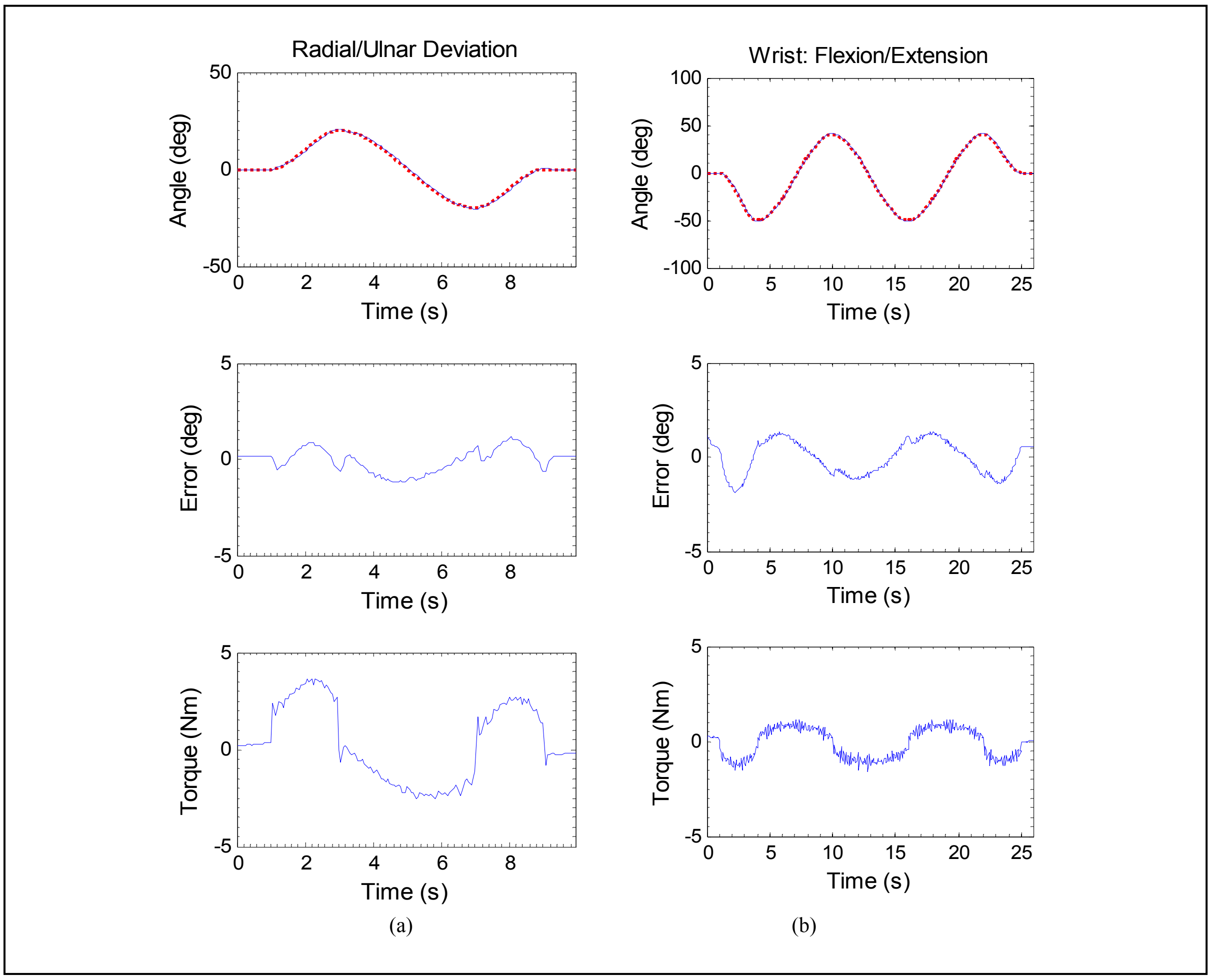


Figure 5.11 Wrist joint movements (a) Radial/ulnar deviation (b) Flexion/extension

Reaching movements:

Reaching movements are widely used and recommended for multi joint movement exercises. A repetitive diagonal reaching movement is depicted in Figure 5.12, where the subject is supposed to move his or her hand diagonally (with the elbow initially at 90°). Typically this exercise is repeated approximately 10 times (Physical Therapy Standards, 2011), therefore a few repetitions are depicted in Figure 5.12. It is obvious from these figures that the controller's performance was excellent since measured trajectories in this case also overlapped with the desired trajectories with error in tracking less than 2.5°.

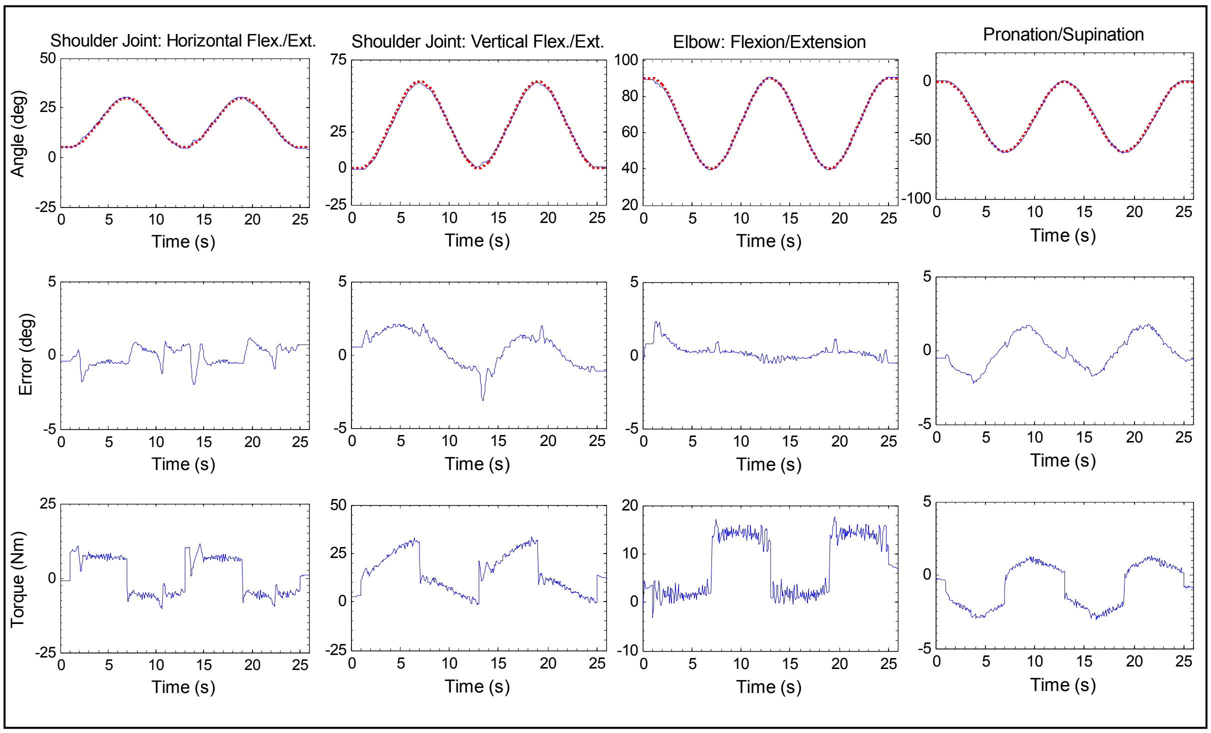


Figure 5.12 Diagonal reaching movements

All joints' simultaneous movements:

To further evaluate the performance of the controller with regard to multi joint movements, an experiment was performed that involves simultaneous movements of all joints; i.e., shoulder, elbow, forearm and wrist joint movements together (7DoFs). The results of this experiment are depicted in Figure 5.13. It can be seen from the plots that the controller performance was impressive as again the tracking error was quite small (< 2.8°) .

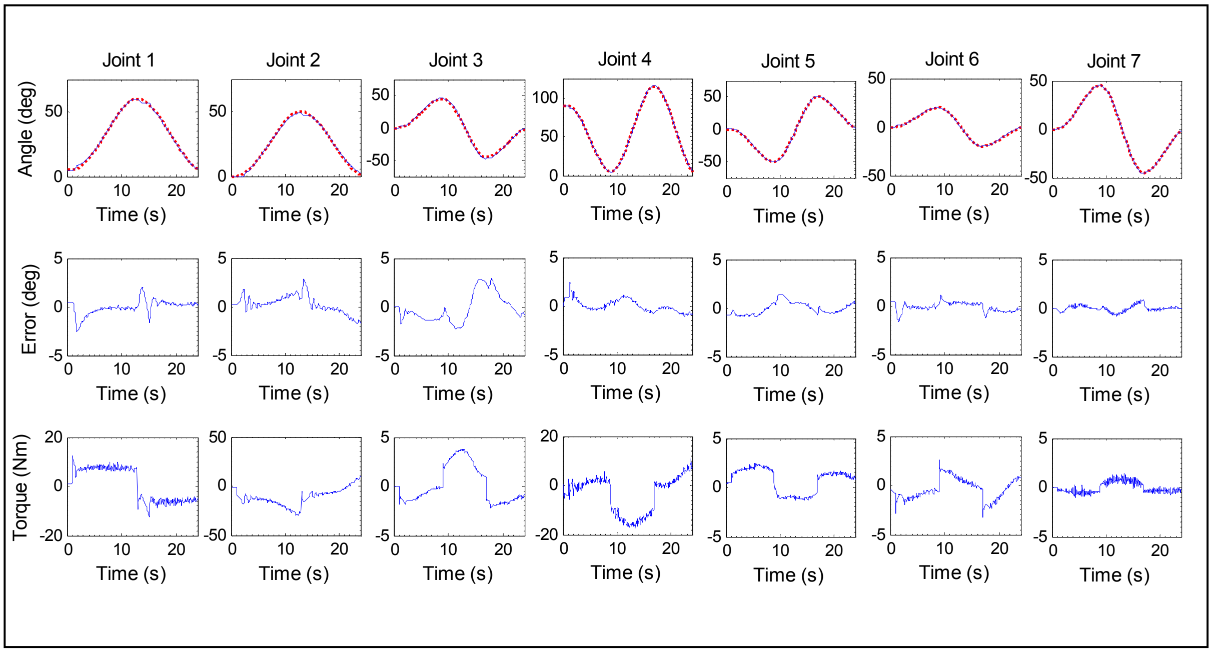


Figure 5.13 Simultaneous movements of *MARSE* arm in7DoFs

As depicted from Figure 5.4 to Figure 5.13, the maximum tracking deviation was observed to be around 2.8°, (at the level of shoulder joint internal/external rotation in case of all joints' simultaneous movement, Figure 5.13) with a maximum steady state position error of around 0.1°. Experimental results thus evaluate the performance of the *ETS-MARSE* and control technique (PID) in regard to trajectory tracking as well as to provide passive rehabilitation at the level of shoulder, elbow, and forearm and wrist joint movement.

Note that the control gains used for these experiments were found by trial and error, and are as follows:

$K_P = diag[110 \quad 250 \quad 75 \quad 175 \quad 75 \quad 50 \quad 20]$,

$K_V = diag[30 \quad 25 \quad 10 \quad 30 \quad 10 \quad 5 \quad 5]$,, and

$K_I = diag[30 \quad 100 \quad 25 \quad 100 \quad 25 \quad 50 \quad 10]$.

### 5.2.2 Experimental Results with Compliance Control (Rahman *et al.*, 2012d)

Figure 5.14 shows the results obtained with compliance control for elbow joint flexion/extension and shoulder joint internal/external rotation. It can be seen in Figure 5.14 that this control approach (compliance control with gravity compensation) gave better tracking performance compared to the PID control technique. Note that for the same passive exercises, the maximum tracking error was around 2.8° with the PID control technique, whereas with compliance control it was around 0.5° (compare Figure 5.14 with Figure 5.6b and Figure 5.7).

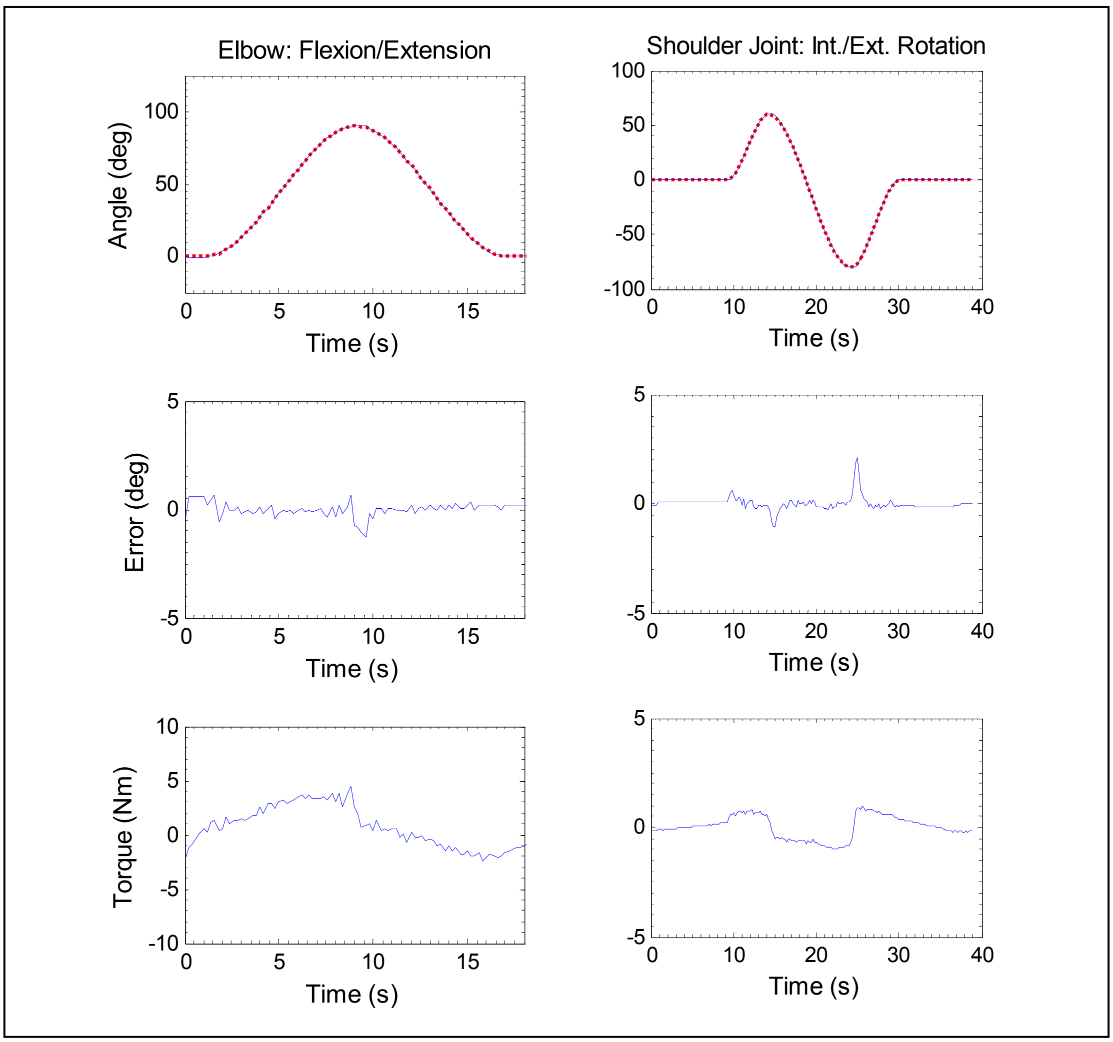


Figure 5.14 Trajectory tracking with compliance control

To further evaluate the performance of the compliance control technique and also to show some compliance nature of the controller, an experiment was carried out where the subject is directed to push the wrist handle (i.e., X, Y, and Z directions with respect base frame) while the *MARSE* is at the steady state position, maintaining the elbow joint angle at 90° against gravity (see topmost plot of Figure 5.15). The 2$^{nd}$ row of Figure 5.15 compares the desired positions of the wrist joint (dotted line) to the measured position (solid line) of wrist joint in Cartesian space. It is obvious from the figure that the end-effector exhibits some spring characteristics along the Cartesian degree of freedom (Figure 5.15, last two rows).

Experimental results thus evaluated the performance of the compliance control with regard to trajectory tracking. Note that these experiments were conducted with a 4DoFs *MARSE* (Rahman *et al.*, 2012d) that involves shoulder (3DoFs) and elbow joint (1DoF). The control

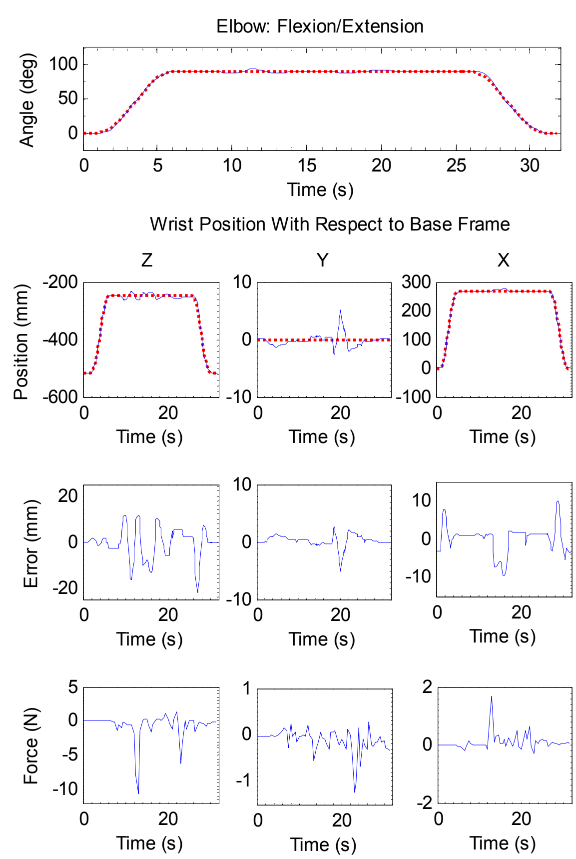


Figure 5.15 Stiffness characteristics of the end-effector

gains used for this control were found by trial and error, and are as follows:

$$K_{Px} = diag[20 \quad 20 \quad 20 \quad 60 \quad 60 \quad 60], K_v = diag[10 \quad 50 \quad 10 \quad 60], \text{ and}$$

$$K_i = diag[10 \quad 150 \quad 10 \quad 200].$$

### 5.2.3 Experimental Results with Computed Torque Control (Rahman *et al.*, 2011c)

Shoulder, elbow and forearm movements:

Passive rehabilitation exercises involving elbow joint movement are depicted in Figure 5.16,

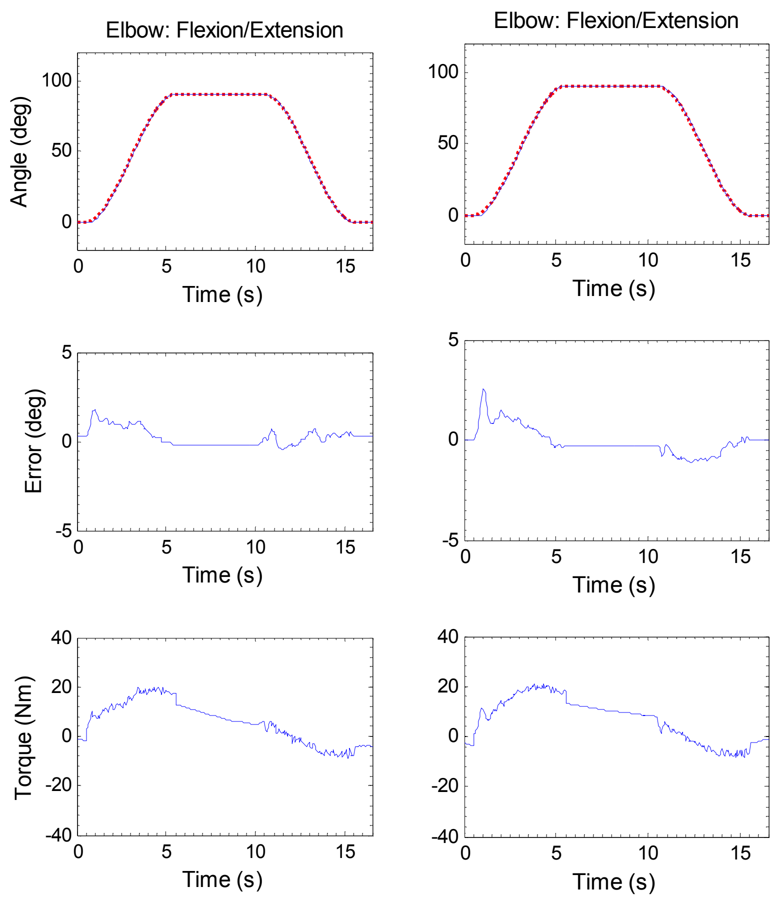


(a) (b)

Figure 5.16 Elbow joint flexion/extension
(a) Exercise was performed by subject-A having body weight of 63 kg, height 167cm
(b) Exercise was performed by subject-B having body weight of 100 kg, and height 180 cm

where the *ETS-MARSE* is supposed to flex from its initial position (0°), up to an angle of 90°, hold that position against gravity for few seconds, and then go back to the initial position, i.e., extension of the elbow to 0°. Note that all exercises presented in this thesis were performed with subject-A except this one which was performed with two participants (subjects-A & B). It is clear from the figure that the controller's performance was excellent since the measured trajectories (solid line) overlapped with the desired trajectories (dotted line). It can be seen that the tracking error was quite small (<2°) and that the most noticeable was the steady state error (i.e., when the *MARSE* is maintaining the position of 90° against gravity), which lies below 0.2°. It is important to perform passive repetitive movements to the elbow joint in order to increase mobility and muscle tone. A repetitive passive elbow flexion/extension (i.e., 0° to 120°) exercise is shown in Figure 5.17.

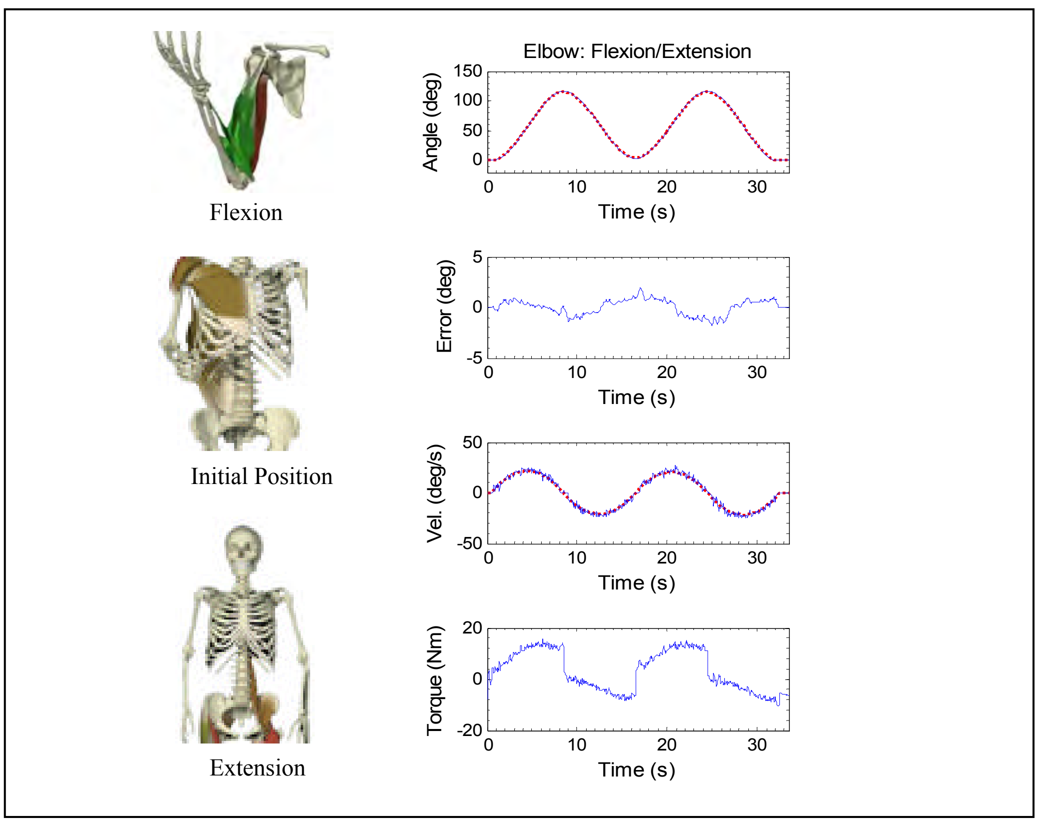


Figure 5.17 Repetitive elbow joint movement

Note that the control gains used for this control were found by trial and error, and are as follows:

$$K_P = diag[1000 \quad 700 \quad 115 \quad 800 \quad 1500 \quad 6000 \quad 750],$$
$$K_v = diag[100 \quad 120 \quad 15 \quad 110 \quad 100 \quad 300 \quad 110], \text{ and}$$
$$K_i = diag[100 \quad 800 \quad 300 \quad 800 \quad 1500 \quad 6000 \quad 1000].$$

A cooperative movement of the elbow (flexion/extension) and shoulder joint internal/external rotation are depicted in Figure 5.18. As shown in Figure 5.18, the exercise begins with elbow flexion, and then repetitive internal/external rotation is performed; finally, the exercise ends with the extension of the elbow to 0°. The 3rd row of the plots (from the top) displays velocity tracking (where the solid line indicates measured velocity and dotted line indicates

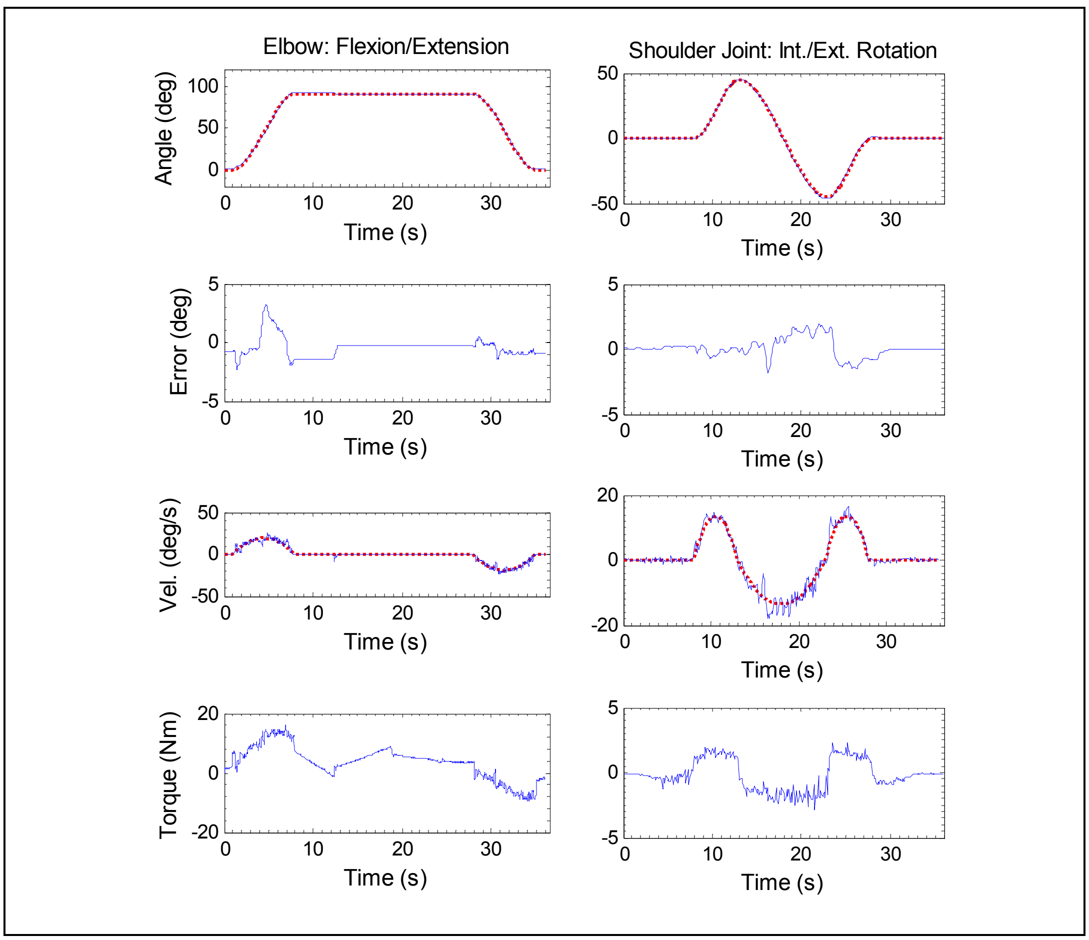


Figure 5.18 Cooperative movement of elbow and shoulder joint int./ext. rotation

desired velocity). It can be seen from the plots that the tracking error was quite small (<2.5°). Note that for the same passive exercises performed with the PID control technique, the maximum tracking error (at the level of shoulder joint internal/external rotation) was around 2.75° whereas with CTC it was around 1.5° (compare to Figure 5.18 with Figure 5.6b).

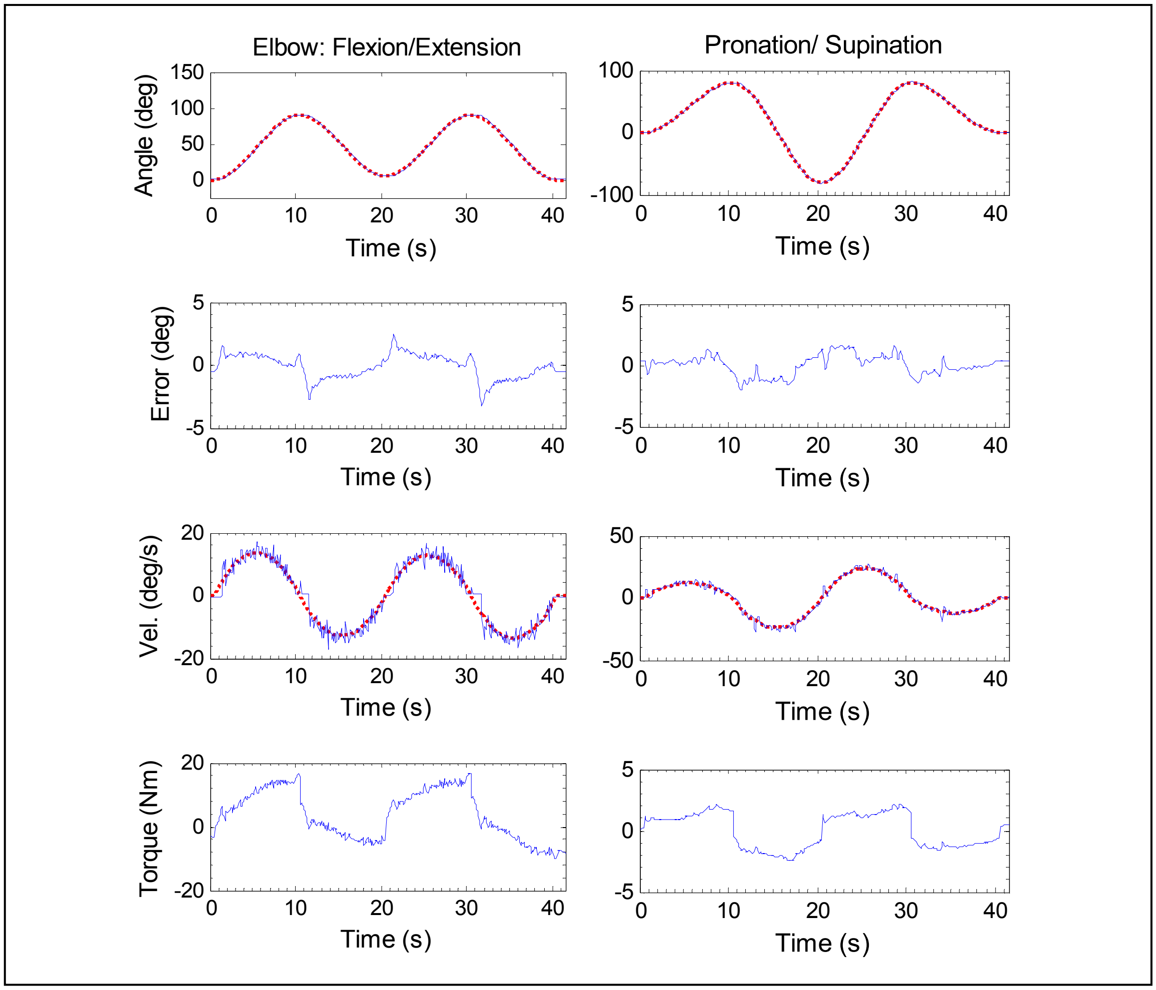


Figure 5.19 Cooperative and simultaneous motion of elbow and forearm

Figure 5.19 demonstrates a typical rehabilitation exercise involving simultaneous motions of the elbow and forearm. The objective of this task is to supinate the forearm from its initial position (0°) to the fully supinated position while simultaneously flexing the elbow from complete extension to complete flexion (120°) and next, inversely moving the forearm from full supination to a full pronation position (Figure 2.6), while the elbow simultaneously goes from complete flexion to extension (0°). Controller tracking performance is certainly obvious from these plots since the desired and measured trajectories overlapped again in this case with tracking error less than 2°.

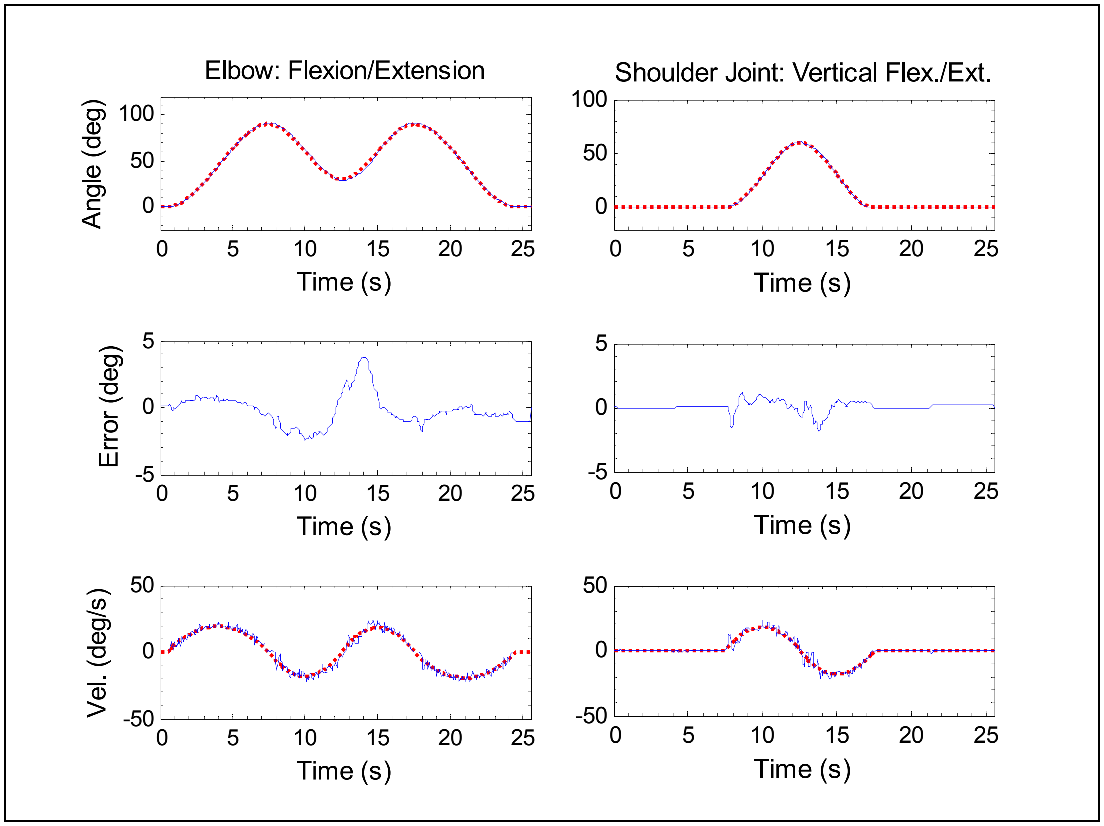


Figure 5.20 Reaching movement, straight ahead (cooperative and combined movement of shoulder and elbow joint)

Reaching movements are widely used and recommended for multi-joint movement exercises. A straight-ahead reaching movement is depicted in Figure 5.20, where the subject is supposed to slide his or her hand gently over the surface of a table, with the elbow initially at 90°. This movement is similar to dusting a table, which involves simultaneous and repetitive rotation at the elbow (extension) and shoulder joints. Typically this exercise is repeated approximately 10 times (Physical Therapy Standards, 2011), so a full cycle is depicted in Figure 5.20.

Wrist joint movements:

Figure 5.21 shows the motion of *ETS-MARSE* for radial/ulnar deviation. In these experiments, the elbow flexed to a 90° position, and thereafter, repetitive radial/ulnar movement is performed while maintaining the elbow at the same position. This is a type of typical occupational therapy, which gives the impression of dusting the surface of a table. It is sometimes recommended to keep the elbow at 90° while performing passive wrist movement (Physical Therapy Standards, 2011). However, it is certainly evident from these results that *MARSE* users can perform the same passive wrist movement in any elbow position, depending on the patient's physical condition. Moreover, these results also

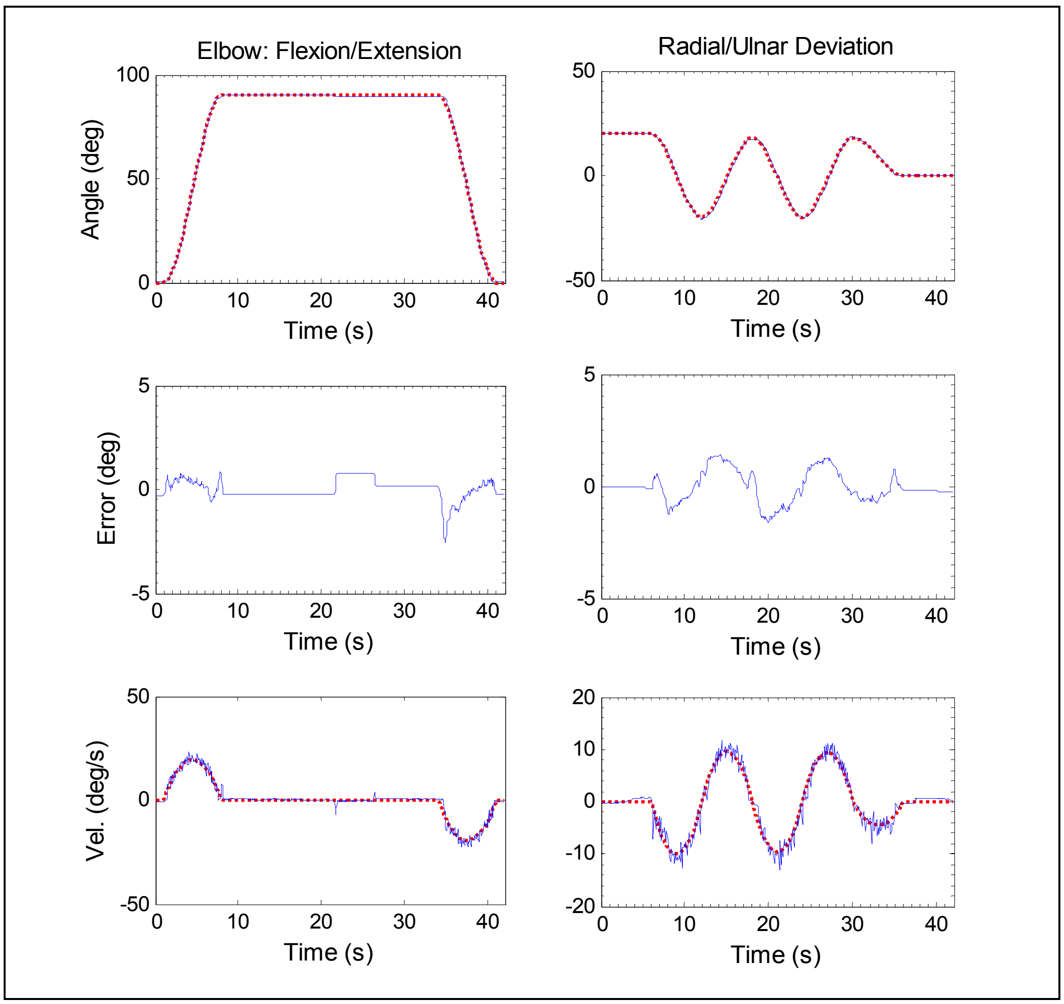


Figure 5.21 Repetitive movement of wrist joint (radial/ulnar deviation) while maintaining elbow at 90°

demonstrate that the *MARSE* is able to compensate for the gravity effect, which is very important for these types of robotic applications in addition to providing passive arm therapy.

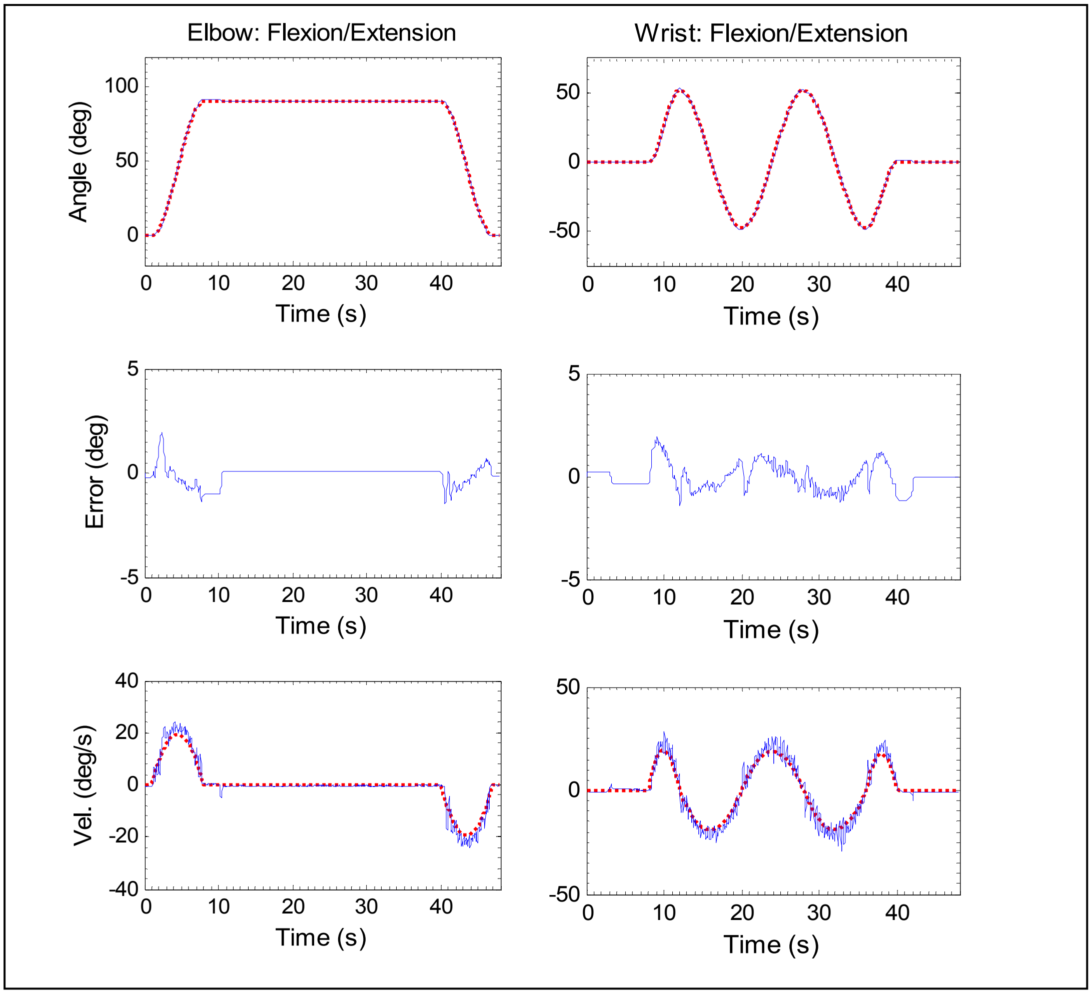


Figure 5.22 Repetitive movement of wrist joint (flexion/extension) while maintaining elbow at 90°

Figure 5.22 shows the passive flexion/extension motion of the wrist joint. Similar to the exercises depicted in Figure 5.18 and Figure 5.21, Figure 5.22 demonstrates the repetitive flexion/extension at the level of the wrist joint, where the elbow joint is supposed to be maintained at a 90° position while performing passive flexion/extension therapy. As shown in Figure 5.22, the tracking performance of the controller was excellent. Furthermore, the steady state position error was found to be quite small (<0.65°).

As depicted in Figure 5.16 to Figure 5.22, the maximum tracking deviation observed around was 2.5° and the maximum steady state position error around 0.65°. Experimental results thus evaluate the performance of the control technique with regard to trajectory tracking as well as to provide passive rehabilitation.

### 5.2.4 Evaluation of mSMERL Regard to Trajectory Tracking

In this section, the trajectory tracking performance of the *ETS-MARSE* was evaluated with the *mSMERL* (Equation (4.30)). Also, a comparison was made with the conventional SMC (Equation (4.26)) to further evaluate the *mSMERL's* performance with regard to chattering reduction. It is to be noted that, the 'conventional SMC' as mentioned in this thesis is the modified form of the basic SMC, where the discontinuous term $K.sign(\Sigma)$ of a basic SMC (Equation (4.23)) was smoothened with the continuous term $K.sat(\Sigma/\phi)$ (Equation (4.26)). The control gains used for the experiments were found by trial and error, and are as follows:

For conventional SMC:

$\Lambda = diag[10 \quad 10 \quad 10 \quad 10 \quad 10 \quad 10 \quad 10]$, and

$K = diag[200 \quad 100 \quad 230 \quad 400 \quad 2250 \quad 3500 \quad 500]$.

For mSMERL:

$\delta_{0i} = 0.5, \alpha_i = 2,\ P_i = 2$ ,

$\Lambda = diag[10 \quad 10 \quad 10 \quad 10 \quad 10 \quad 10 \quad 10]$, and

$K = diag[200 \quad 100 \quad 150 \quad 250 \quad 1500 \quad 3000 \quad 300]$.

Shoulder joint movements:

Figure 5.23 shows the experimental results of shoulder joint vertical flexion/extension motion. Note that in all our experiments (in this subsection and also shown in the next subsection) the *MARSE* initiated its motion with the elbow joint at 90°. Therefore, as shown in Figure 5.23 the experiment begins with the extension of elbow from its initial position

(90°) and thereafter the *MARSE* performs a shoulder joint vertical extension up to 90° and finally the trial ends with the flexion of the shoulder joint.

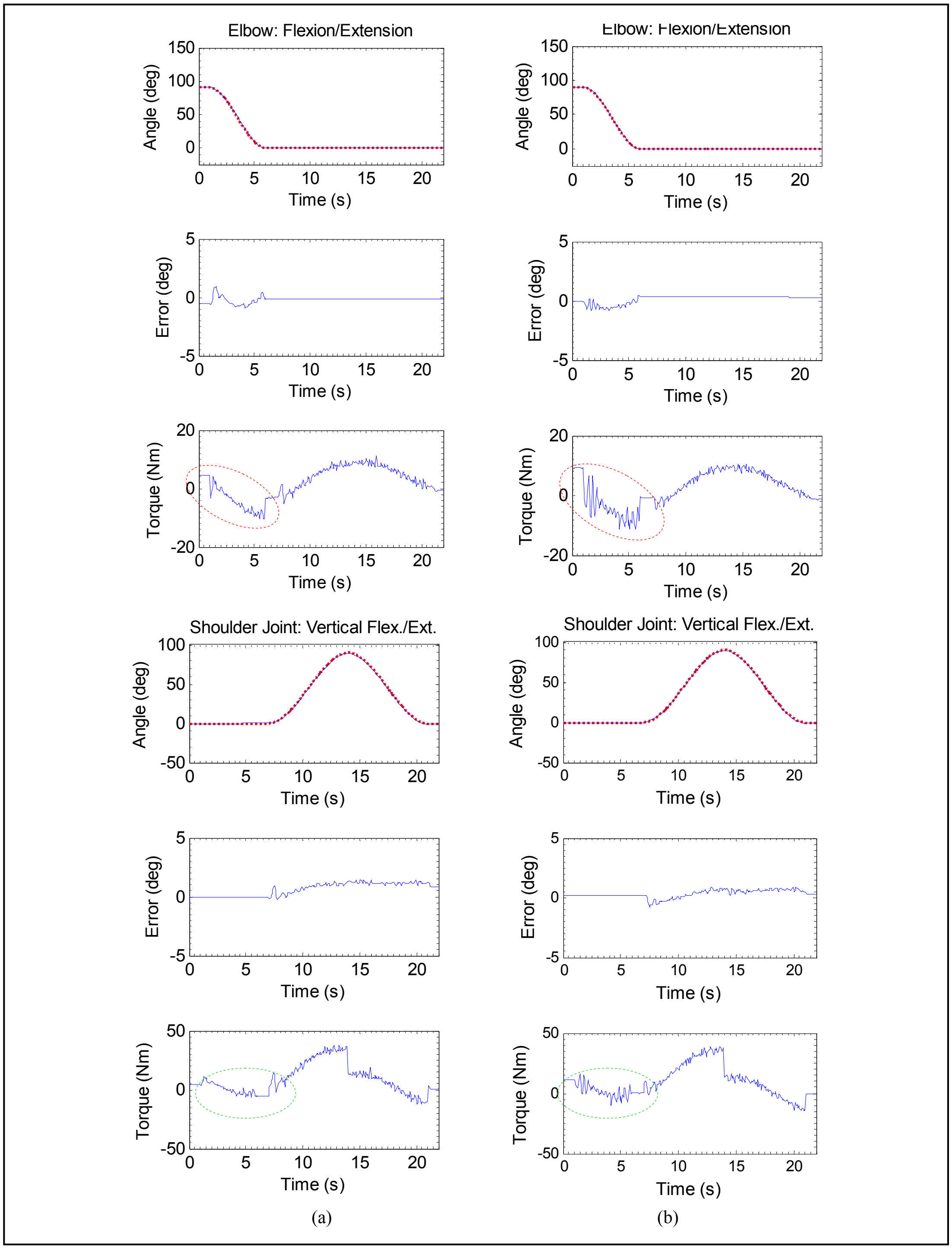


Figure 5.23 Shoulder joint vertical flexion/extension
(a) mSMERL (b) SMC with boundary layer

The 1st row of the plots of Figure 5.23 compares the desired joint angles (or reference trajectories, dotted line) to measured joint angles (or measured trajectories, solid line). It is clear from the Figure that both controllers' performance was excellent since measured trajectories overlapped with the desired trajectories.

The 2nd row of the plots shows the tracking error as a function of time i.e., the deviation between desired and measured trajectories. It can be seen that the tracking error was quite small (<1°) and that the most noticeable was the steady state error which lies below 0.1°. However, comparing the torque plots (3rd row of the plots), it seems that *mSMERL* gave smoother tracking (during the transient and steady state) and reduced chattering (dotted circle, 3rd row) compared to that of the conventional SMC technique.

To further evaluate the performance of the controllers, shoulder joint internal/external

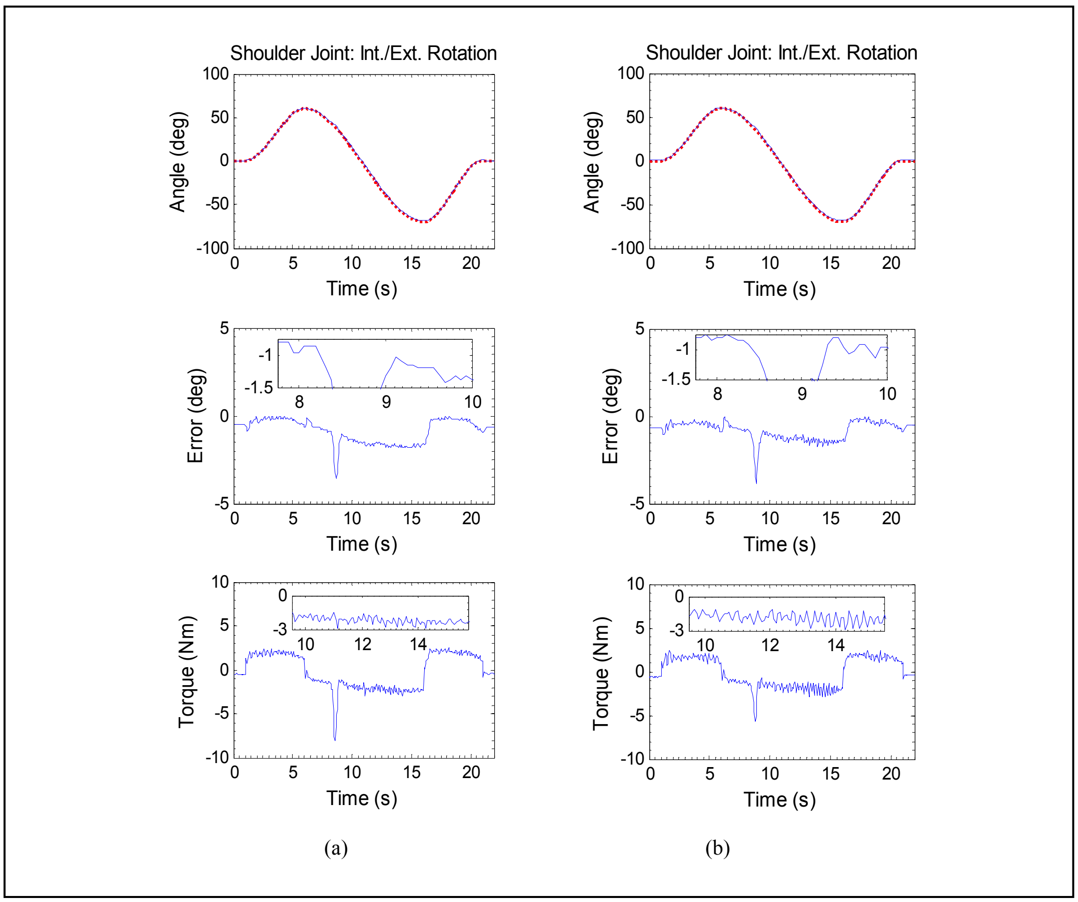


Figure 5.24 Shoulder joint internal/external rotation
(a) mSMERL (b) conventional SMC with boundary layer

movement was performed (keeping the elbow at its initial position i.e., 90°). Experimental results for these exercises are illustrated in Figure 5.24, where it can be found that the sudden perturbation (as apparent from the spike in the error/torque plots) was employed while following the trajectory. The results demonstrated that *mSMERL* responds faster than the conventional SMC to recover from a larger tracking error. Moreover, it gave smoother tracking as compared (see torque plots) to the conventional SMC.

Elbow and forearm movements:

Figure 5.25 demonstrates a cooperative movement of the elbow (flexion/extension) and forearm. The objective of this experiment was to demonstrate the tracking performance of the two controllers for forearm pronation/supination while maintaining the elbow steady at 90°. As shown in Figure 5.25, the exercise began with elbow extension followed by flexion up to 90°, thereafter maintaining that position while forearm pronation/supination was performed. Again, it was evident that tracking performance of the controllers was very good, with the steady state position error below 0.1°. In this case also, in this case modified ERL provided smoother tracking compared to SMC as evident from torque plots.

It is recommended to maintain shoulder joint vertical flexion at 90° while performing passive shoulder joint horizontal flexion/extension, and likewise, to maintain the elbow at 90° while performing internal/external rotation. However, it is evident from our results that *MARSE* users can do the same passive arm movements in any position of elbow and shoulder elevation, depending on the physical condition of patient. Moreover, these results demonstrate that the *ETS-MARSE* is able to compensate the gravity effect, which is very much important for this type of robotic applications, as well as to provide passive arm therapy.

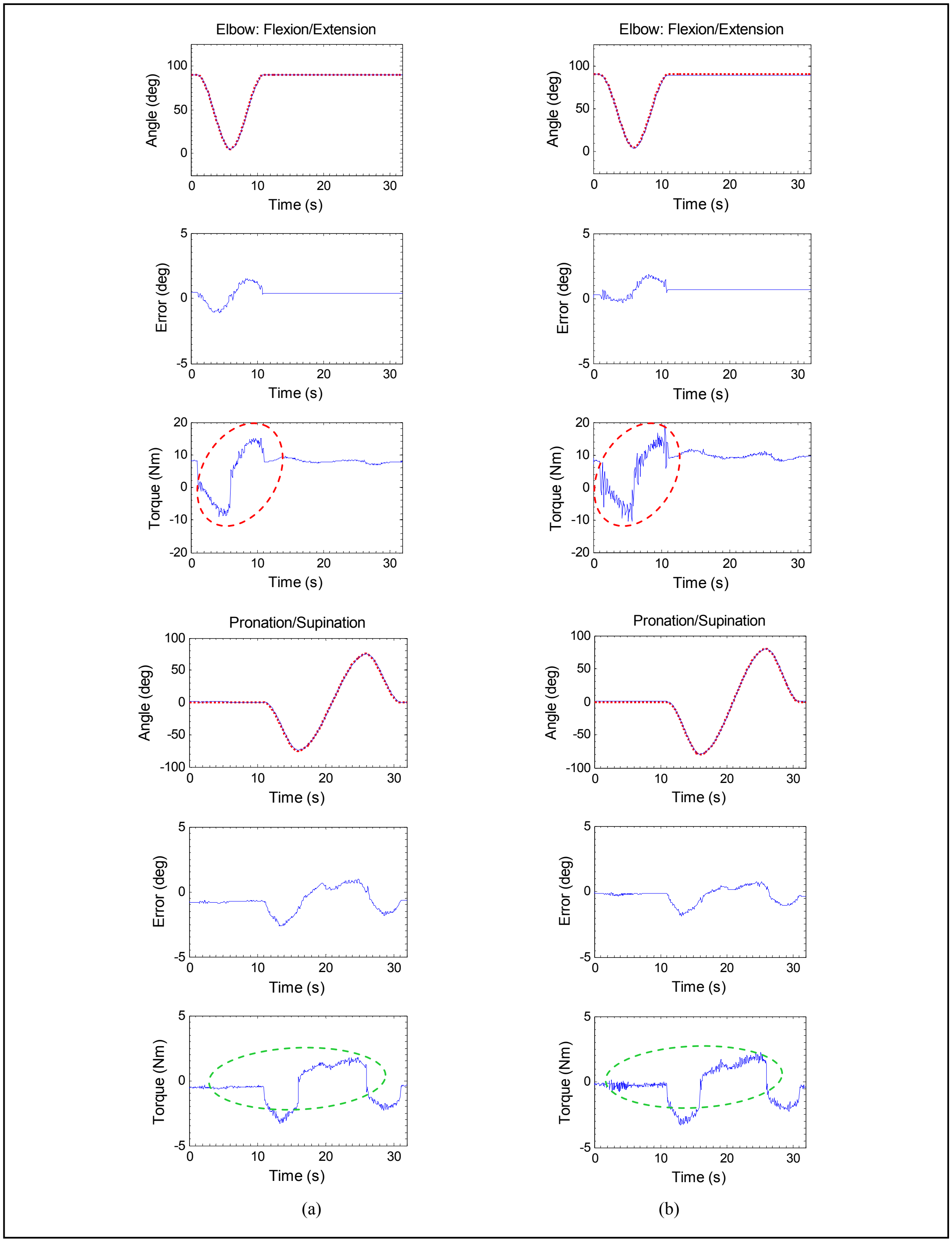


Figure 5.25 Cooperative movement of elbow and forearm
(a) mSMERL (b) Conventional SMC with boundary layer

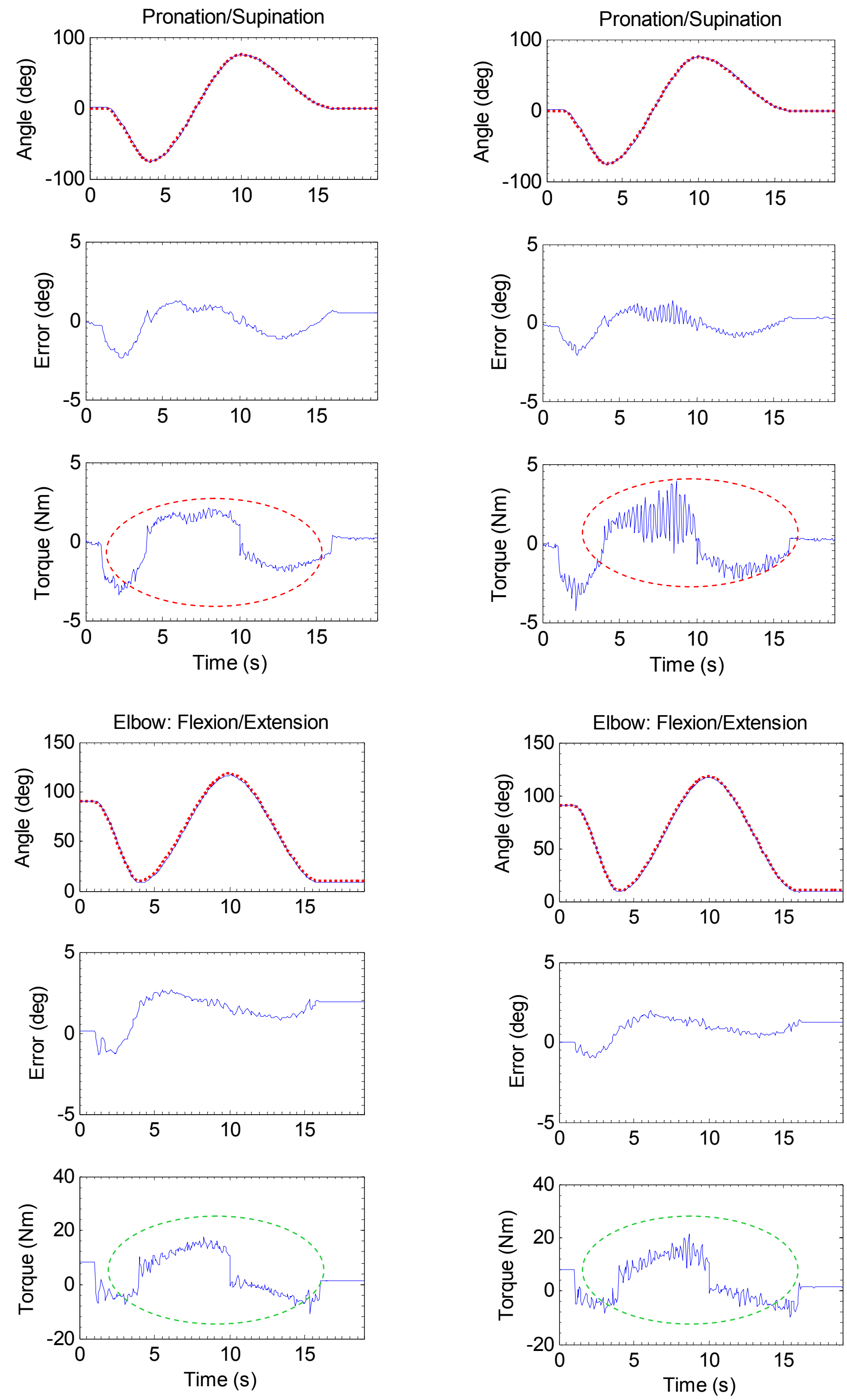


(b) (b)

Figure 5.26 Cooperative and simultaneous movement of elbow and forearm
(a) mSMERL (b) Conventional SMC with boundary layer

Figure 5.26 shows another experiment that involves a co-operative and simultaneous movement of both elbow and forearm. The objective of this task is to pronate the forearm from a neutral position, while simultaneously flexing the elbow from its initial position (90°) and then reversing the movement. The ability of the controller to track this movement is apparent from Figure 5.26, since the tracking errors are found to be quite small (<2.5°).

Wrist joint movements:

Figure 5.27 shows the trajectory tracking of the *MARSE* for wrist joint movements (radial/ulnar deviation and flexion/extension). The trial shows similar tracking performance of the *mSMERL*, where tracking error was found to be less than 1.5°.

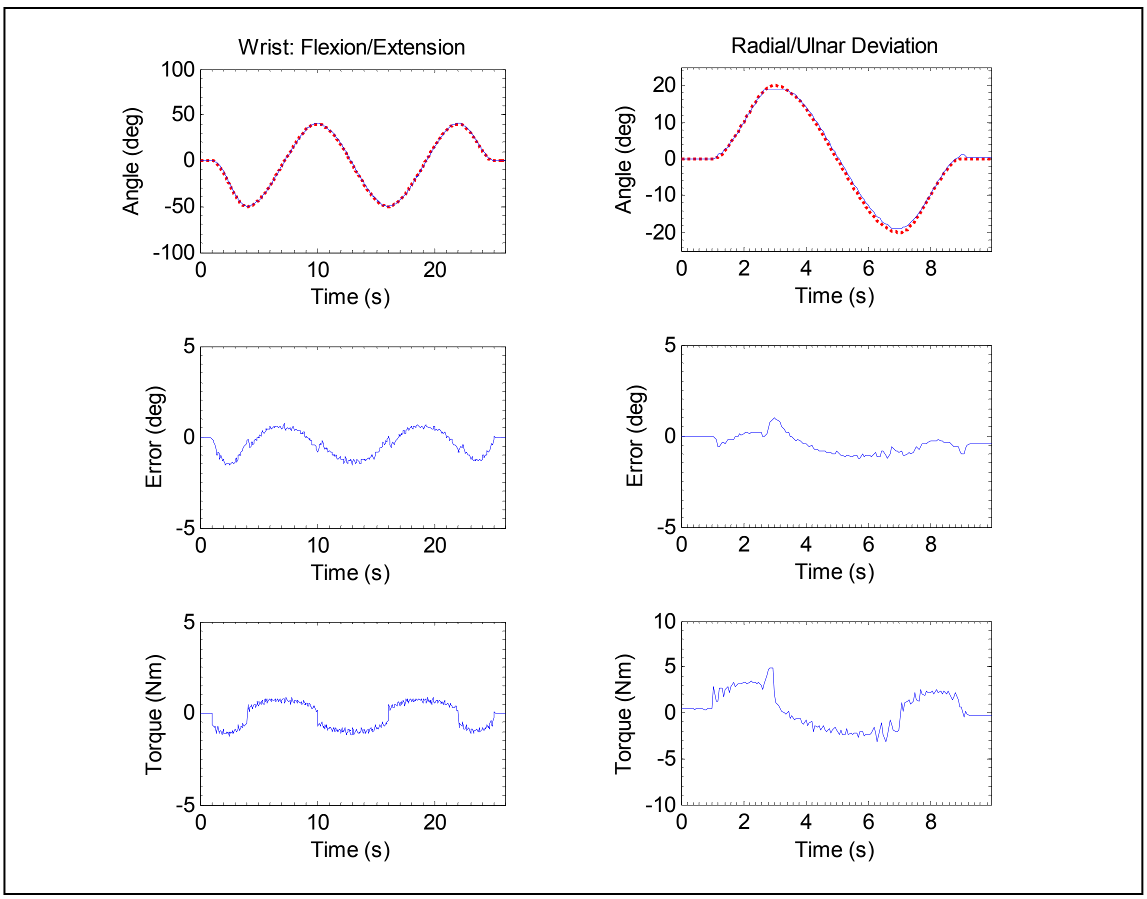


Figure 5.27 Wrist joint movements with *mSMERL*

Reaching movements:

Reaching movements in a diagonal direction, one of the popular multi-joint movement exercises, were performed, as depicted in Figure 5.28. The exercise involves simultaneous movements at the level of shoulder, elbow and forearm. These results also show the similar tracking performance of the modified *SMERL*, with error in tracking less than 1.5°.

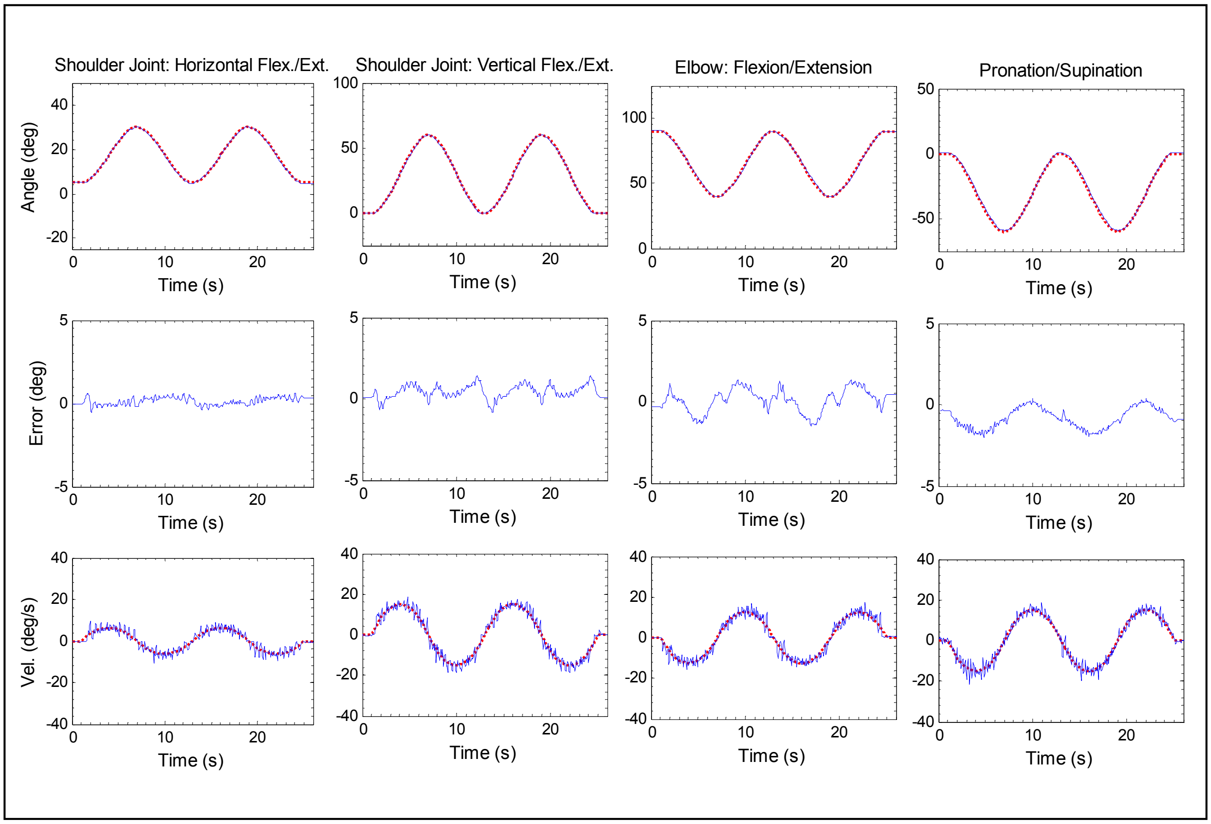


Figure 5.28 Diagonal reaching movement with *mSMERL*

All joints' simultaneous movements:

To further evaluate the performance of the *mSMERL* in regard to dynamic trajectory tracking, an experiment involving simultaneous movements of all joints; i.e., shoulder, elbow, forearm and wrist joint movements (7DoFs) was performed (Figure 5.29). It can be seen from the plots that the controller performance was excellent as again the tracking error was quite small (less than 1.5°), except for joints 2 to 4, where the maximum tracking error was observed at the level of shoulder joint internal rotation (due to the high static friction), which was around 5°.

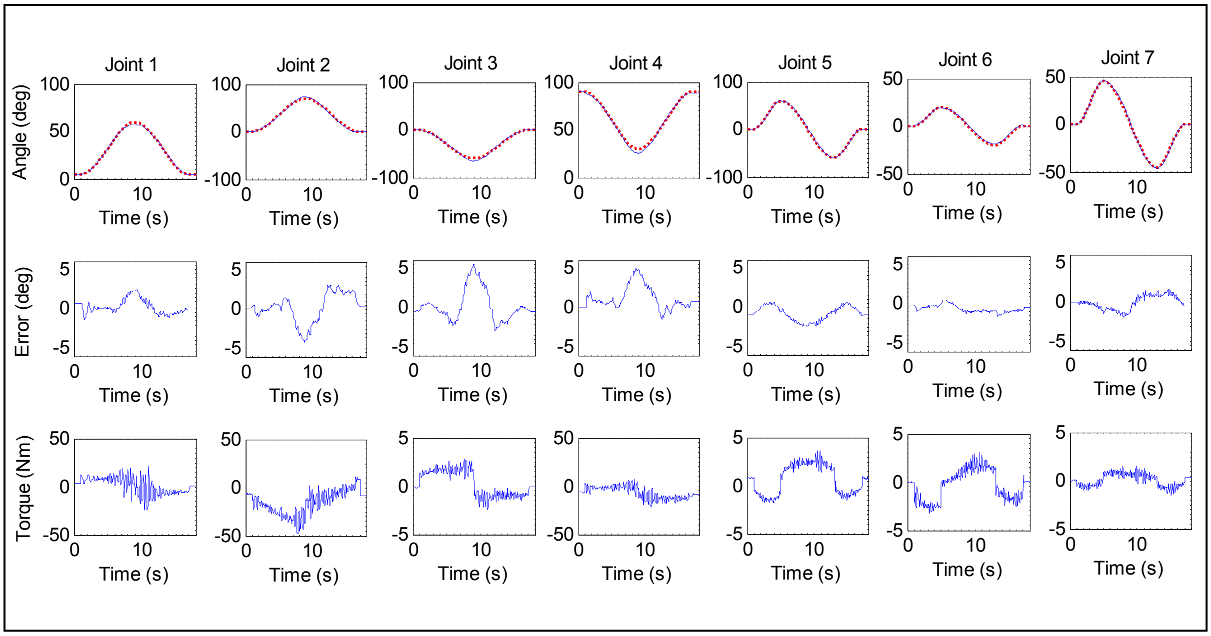


Figure 5.29 Simultaneous movements of shoulder, elbow, forearm and wrist

Experimental results thus demonstrated the efficient performance of the control techniques as well as the *ETS-MARSE* in regard to trajectory tracking. Moreover, it is apparent from these results that *mSMERL* reduced chattering (both during the transient and steady state) and gave better tracking compared to SMC. Note that these experiments are often used as an exercise to provide passive rehabilitation of the human upper limbs (Physical Therapy Standards, 2011) and therefore could be performed with the *ETS-MARSE* and *mSMERL*.

### 5.2.5 Trajectory Tracking Performance Evaluation of PID, CTC, and mSMERL

In this subsection we compare the dynamic trajectory tracking performance of the *ETS-MARSE* with the PID, CTC, and *mSMERL* controls. The exercises used for this comparison can be grouped under two categories; 'single joint movement' and 'multi joint movements'.

Single joint movement:

In this category, two experiments were conducted that show single joint movement. Among these, one joint movement was chosen so that its motion had relatively less influence on the system's dynamics, especially on the gravity terms. Therefore, a repetitive movement consisting in forearm pronation and supination was performed to compare the trajectory tracking performance of the PID, CTC, and mSMERL. A second joint was chosen so that its motion had significant effect on the dynamics of the system, especially on the gravity terms. Therefore, elbow joint flexion/extension motion was considered.

Figure 5.30 compares the trajectory tracking performance of the PID, CTC, and mSMERL

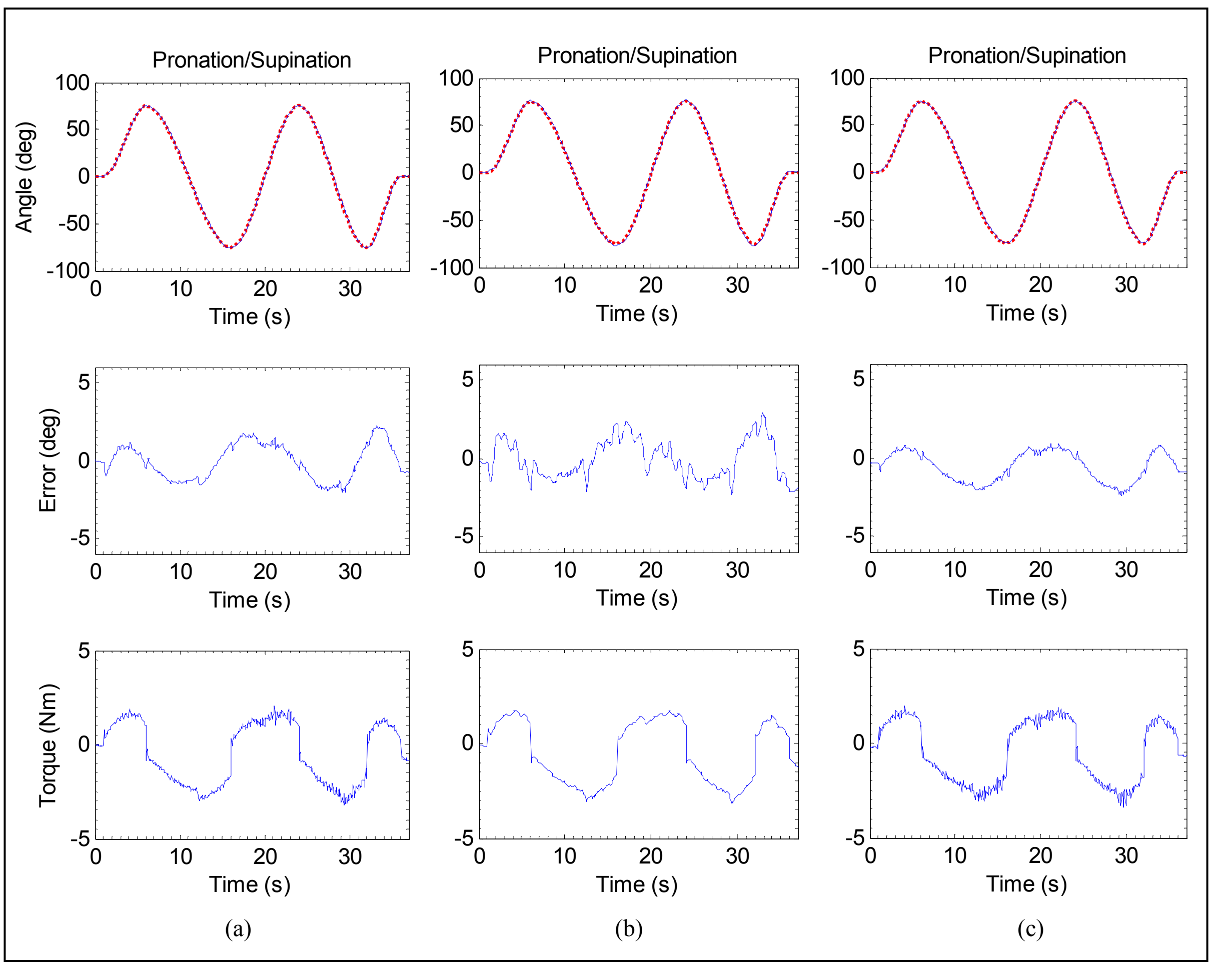


Figure 5.30 Forearm pronation/supination
(a) PID (b) CTC and (c) mSMERL

control for forearm pronation/supination movement. It can be seen from the error plots that the *mSMERL* gave the better tracking performance compared to PID and CTC; and CTC shows the poorer tracking.

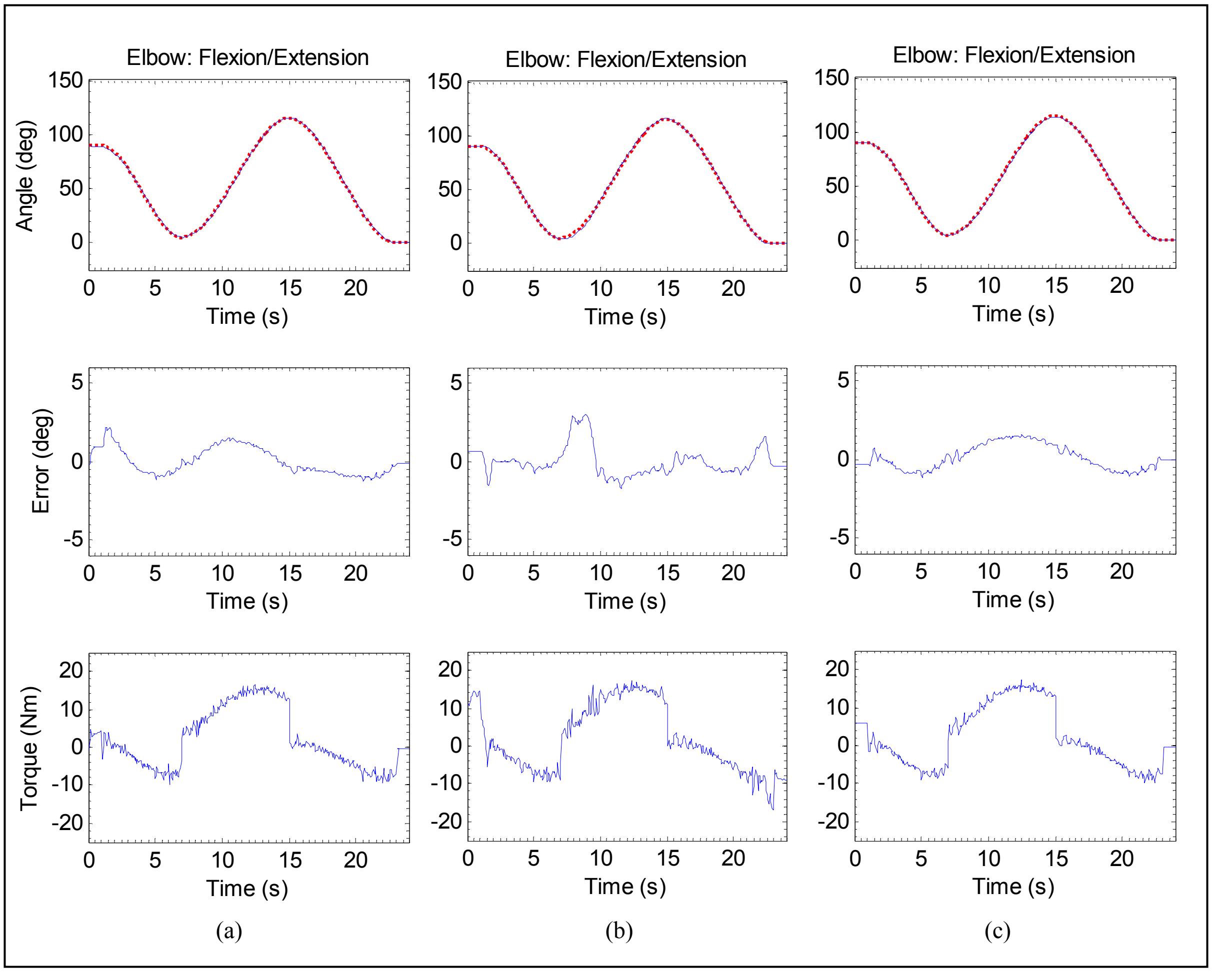


Figure 5.31 Elbow flexion/extension (maximum velocity 21.55 deg/s)
(a) PID (b) CTC and (c) mSMERL

Figure 5.31 to Figure 5.33 show elbow joint flexion/extension motion for tracking, conducted at three different speeds; 21.55 deg/s, 24.65 deg/s, and 28.75 deg/s respectively. As shown

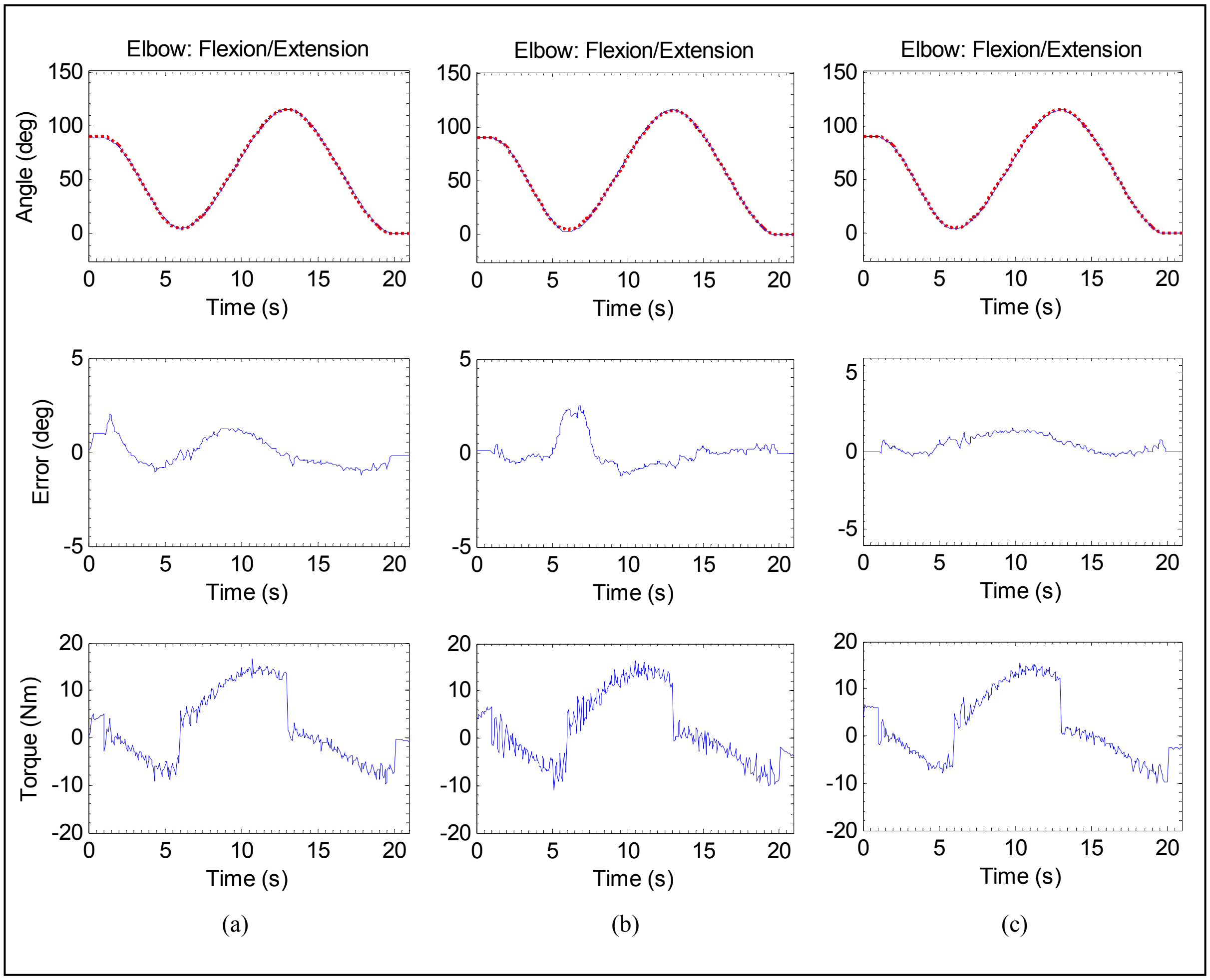


Figure 5.32 Elbow flexion/extension (maximum velocity 24.65 deg/s)
(a) PID (b) CTC (c) mSMERL

from Figure 5.31, the trial took 24 sec. to complete, whereas the experiment shown in Figure 5.32 took 21 sec., and the one depicted in Figure 5.33 took 18 sec. As for previous trials, *mSMERL* shows excellent tracking compared to PID and CTC; and also in this case CTC showed the poorest performance.

Note that passive arm movements and exercises are usually performed slowly (Physical Therapy Standards, 2011; *Stroke Rehab Exercises*, 2010) compared to the natural speed of arm movement; therefore all the exercises presented in this chapter were performed at a low to moderate speed, aiming to form a library of '*robot assisted passive rehabilitation protocol*'. However, to evaluate the tracking performance of the *ETS-MARSE* as well as the performance of the controllers at high speed, experiments involving multi joint movements were conducted. The next subsection describes two of these exercises.

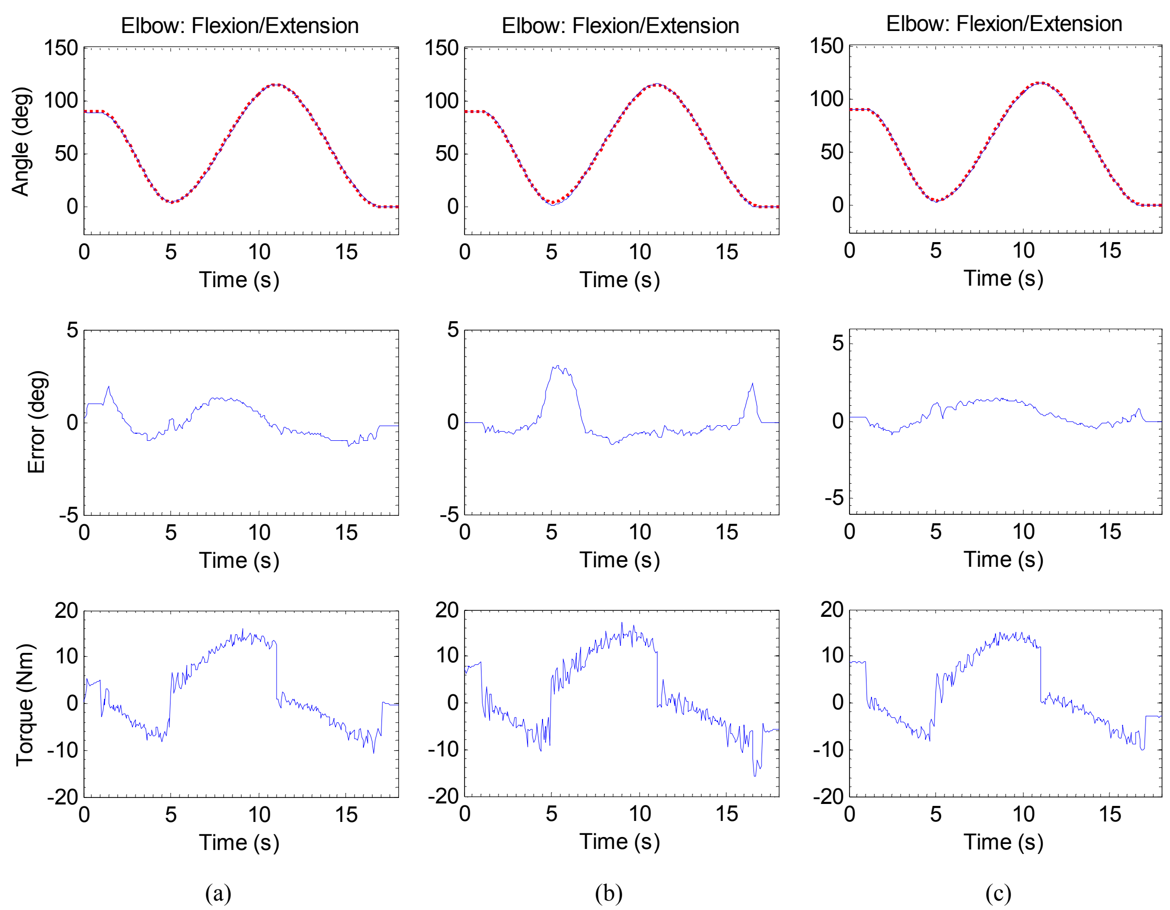


Figure 5.33 Elbow flexion/extension (maximum velocity 28.75 deg/s)
(a) PID (b) CTC and (c) mSMERL

Multi joint movements:

Figure 5.34 shows the cooperative and simultaneous movement of forearm pronation/supination and elbow flexion/extension which was performed at a relatively high speed. The maximum velocity observed at the level of elbow joint movement was 65.9 deg/s and that for the forearm movement was 58.5 deg/s. Figure 5.35 plotted the end-effector tracking for the same exercise. Also in this trial *mSMERL* showed better tracking compared to PID and CTC.

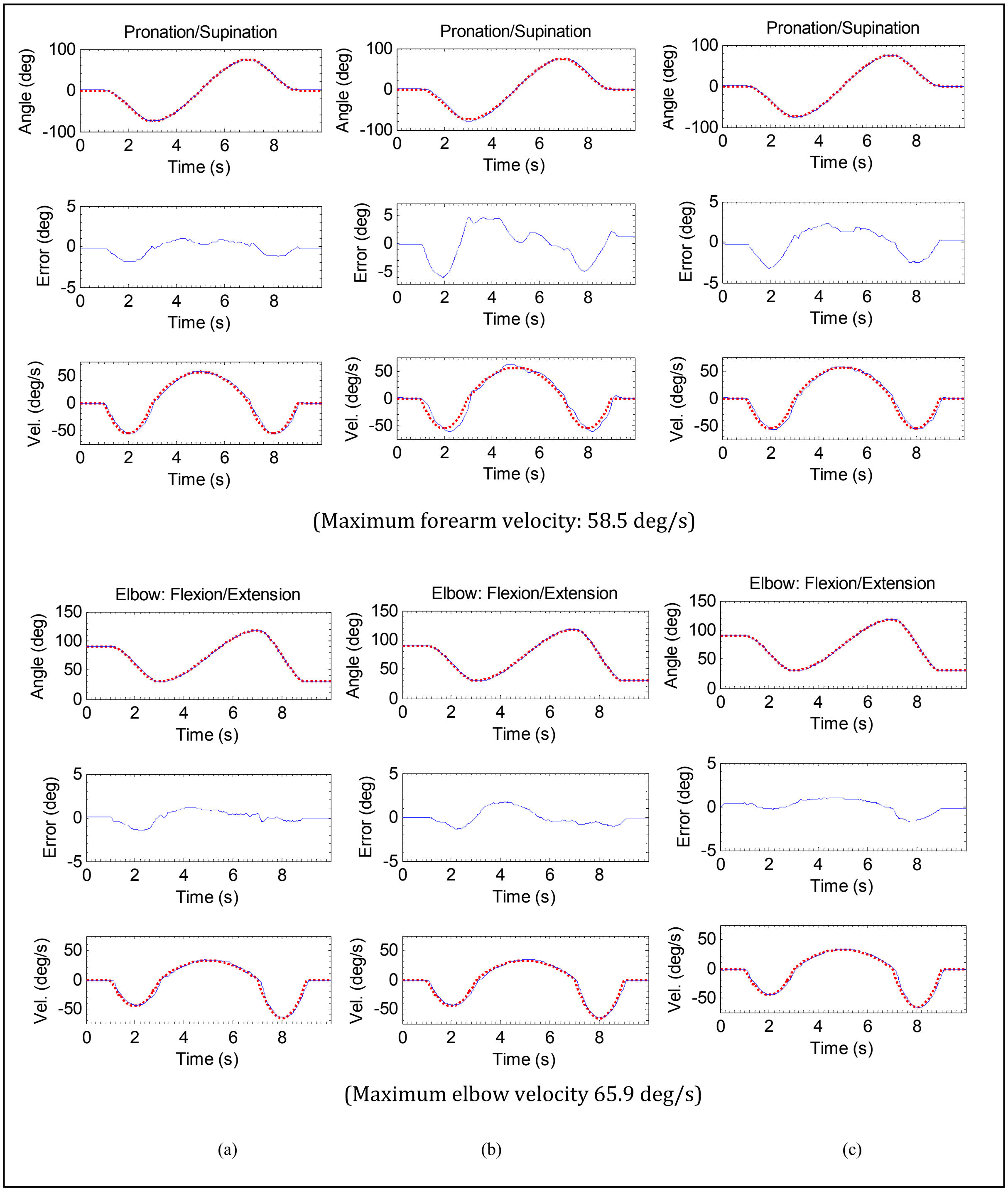


Figure 5.34 Simultaneous movement of elbow and forearm, exercise-1A
(a) mSMERL (b) CTC (c) PID

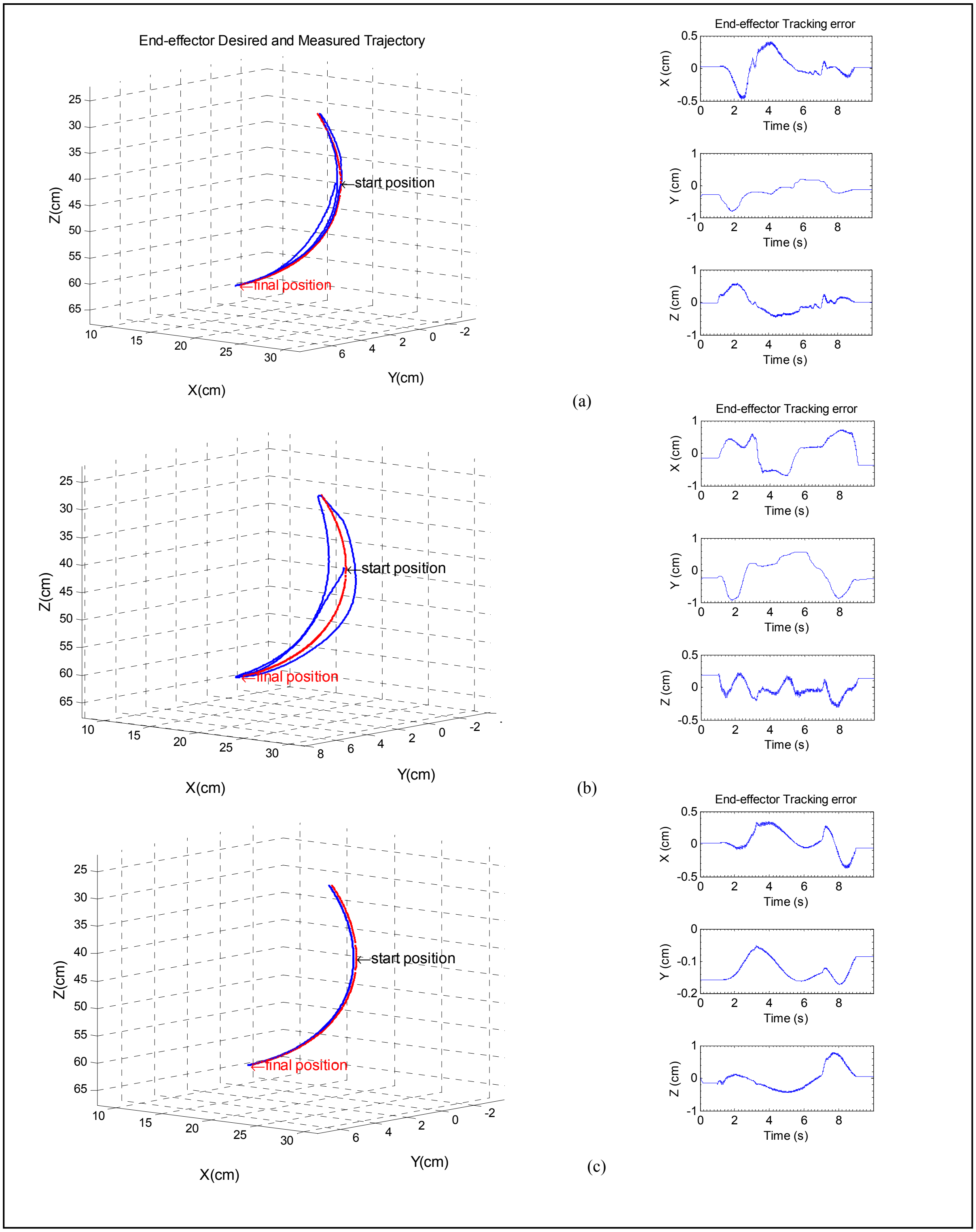


Figure 5.35 End-point tracking (simultaneous motion of elbow-forearm) exercise-1A
(a) mSMERL (b) CTC (c) PID

To further evaluate the performance of the controllers, the same exercise was performed (Figure 5.36) at higher speed. The maximum velocity observed in this case (Figure 5.36) was 88 deg/s at the level of elbow joint movement; and 90 deg/s for the forearm.

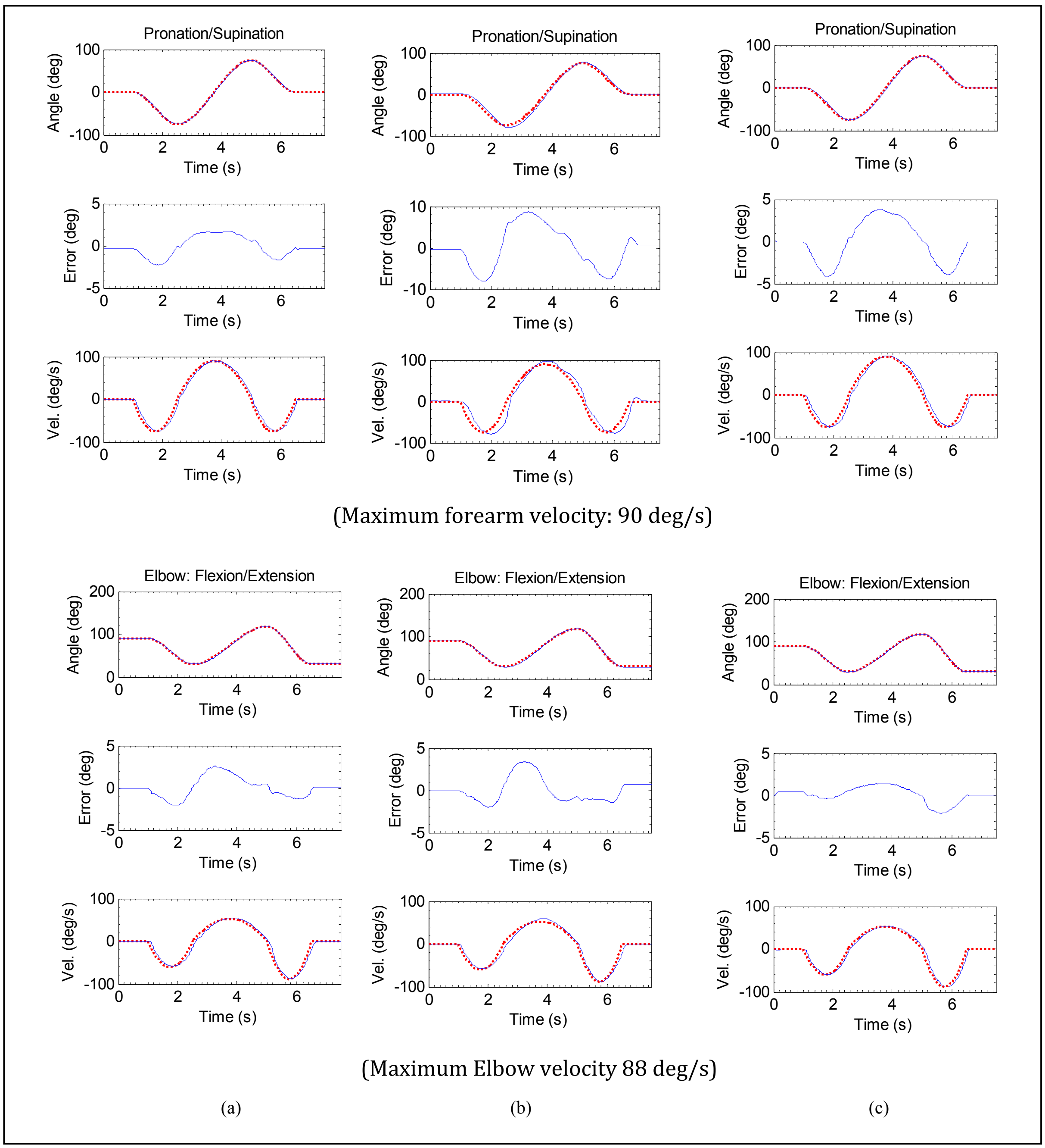


Figure 5.36 Simultaneous movement of elbow and forearm, exercise-1B
(a) mSMERL (b) CTC (c) PID

It can be seen from the Figure 5.36 that it took only 2 seconds to supinate the forearm from a fully pronated position, while simultaneously a flexion motion was performed from full extension of the elbow joint. Also, it was found from the Figure 5.36, that it took 1.5 sec for the extension motion to complete from a fully flexed position.

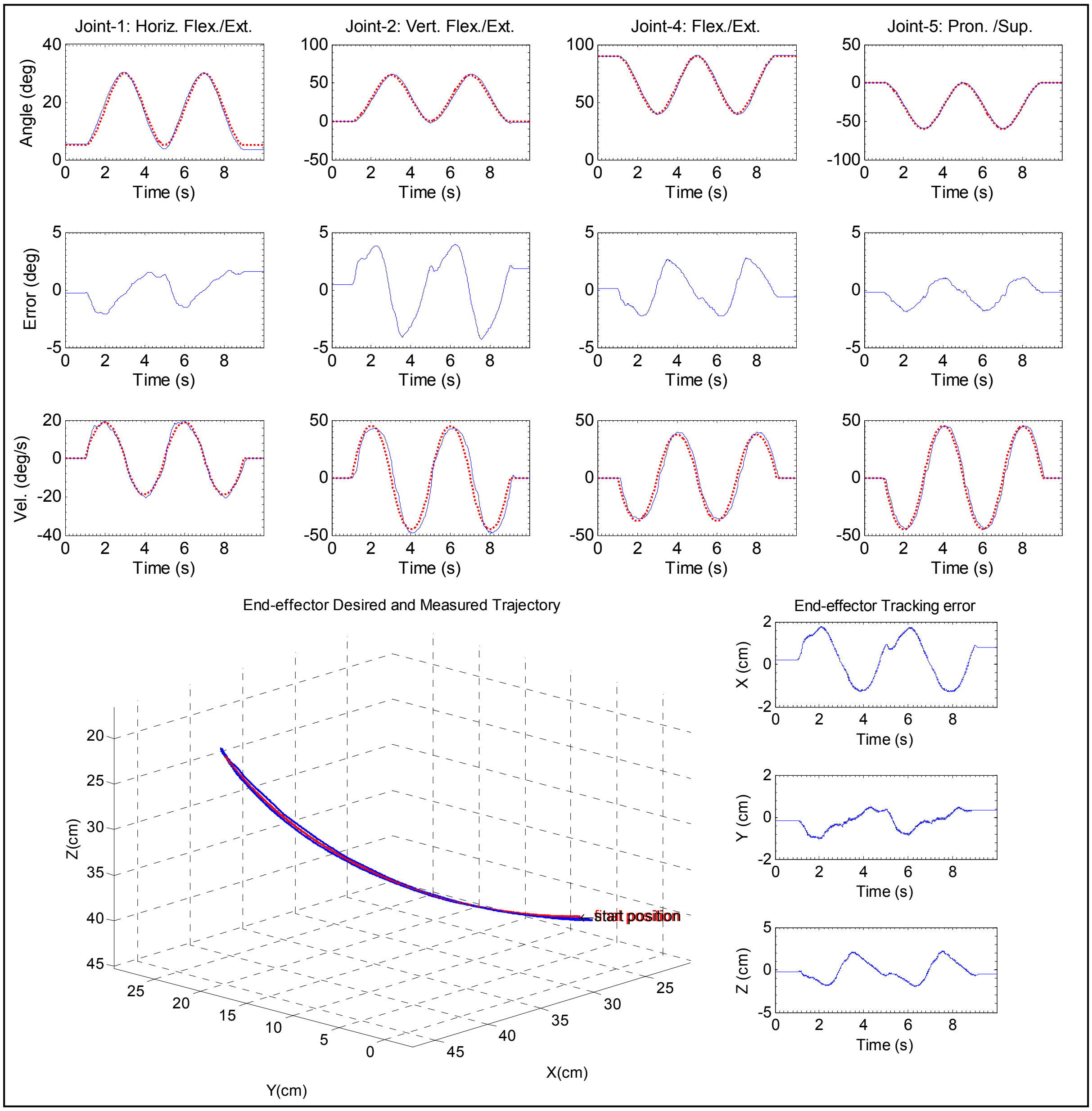


Figure 5.37 Diagonal reaching movements with mSMERL, exercise-2A
(time to reach a diagonal target: 2s.; Time to reach & back from a diagonal target: 4s.)

Figure 5.37 shows another multi-joint movement exercise, *'the diagonal reaching movements'*, which were performed relatively at a high speed with *mSMERL*. The exercise involves simultaneous movements in four joints, i.e., in 4DoFs (joint-1: shoulder joint horizontal flexion/extension, joint-2: shoulder joint vertical flexion/extension, joint-4: elbow

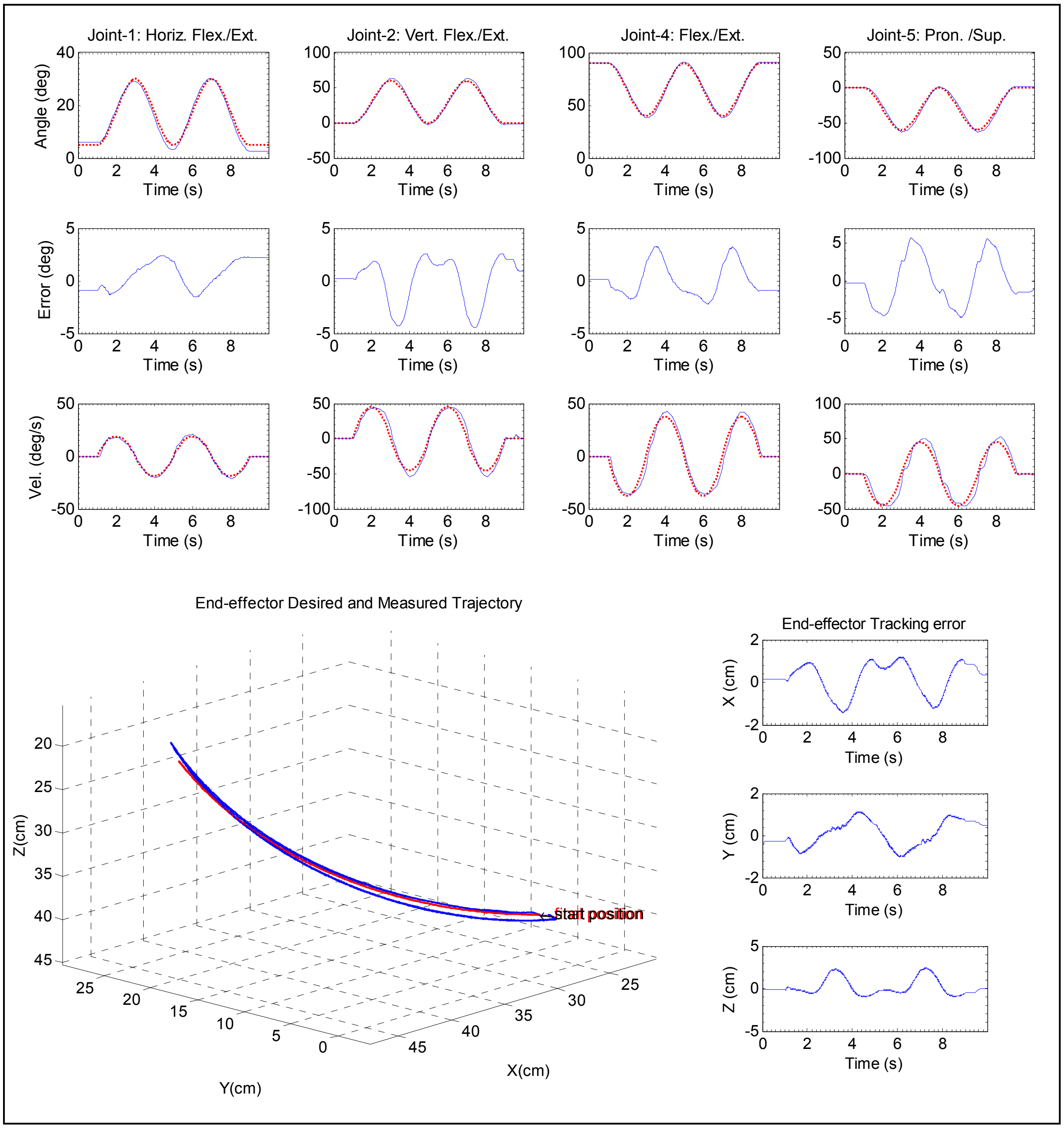


Figure 5.38 Diagonal reaching movements with CTC, exercise-2A
(time to reach a diagonal target: 2s.; time to reach & back from a diagonal target: 4s.)

flexion/extension, joint-5: pronation/supination). Figure 5.38 and Figure 5.39 show the same exercise performed with CTC and PID controls respectively. It can be seen from these figures that it took only 2 seconds to reach diagonal targets ahead, and the tracking error was

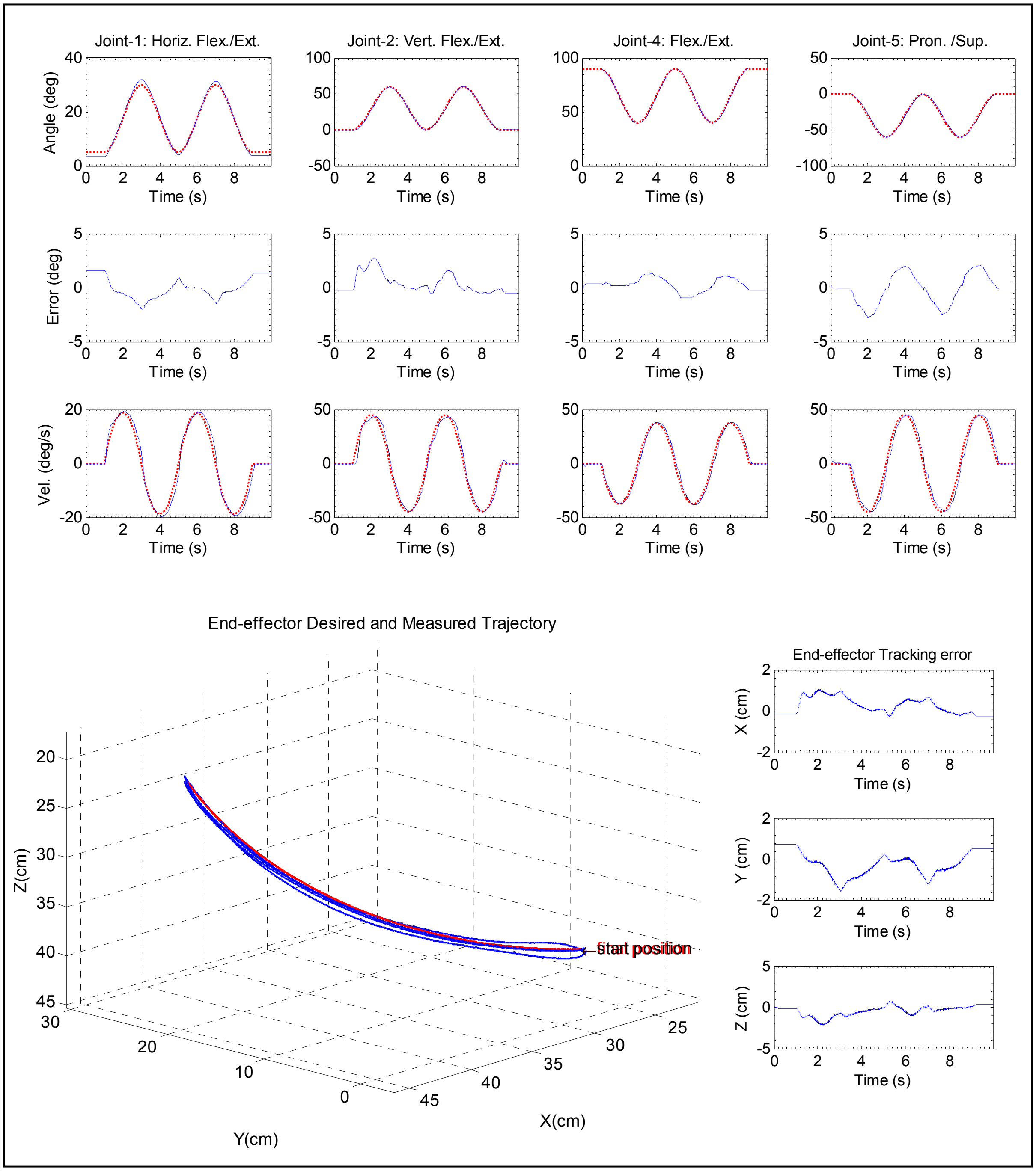


Figure 5.39 Diagonal reaching movements with PID, exercise-2A
(time to reach a diagonal target: 2s.; time to reach & back from a diagonal target: 4s.)

still found to be small in all cases (Figure 5.37 to Figure 5.39). The maximum end-point tracking error observed was 2.4 cm in the *Z* direction in CTC technique.

Figure 5.40 shows a similar diagonal reaching movement exercise but performed at much higher speed with a PID control technique. It can be seen from the plots that in this case the diagonal reaching to a target took only 1.4 seconds. The corresponding end-point tracking of the *ETS-MARSE* with *mSMERL,* CTC*,* and PID control techniques are depicted in Figure 5.41. Note that these exercises (Figure 5.34 to Figure 5.41) were performed only to show the performance of the *ETS-MARSE* at higher speed. The exercises are much faster than what is recommended for passive rehabilitation therapy, and therefore should not be used with the patient. However, it can be concluded from these experiments that the *ETS-MARSE* was able to perform trajectory tracking at a higher speed. The performance of the PID controller was noticeable even in the case of fast speed and gave better and smoother tracking compared to

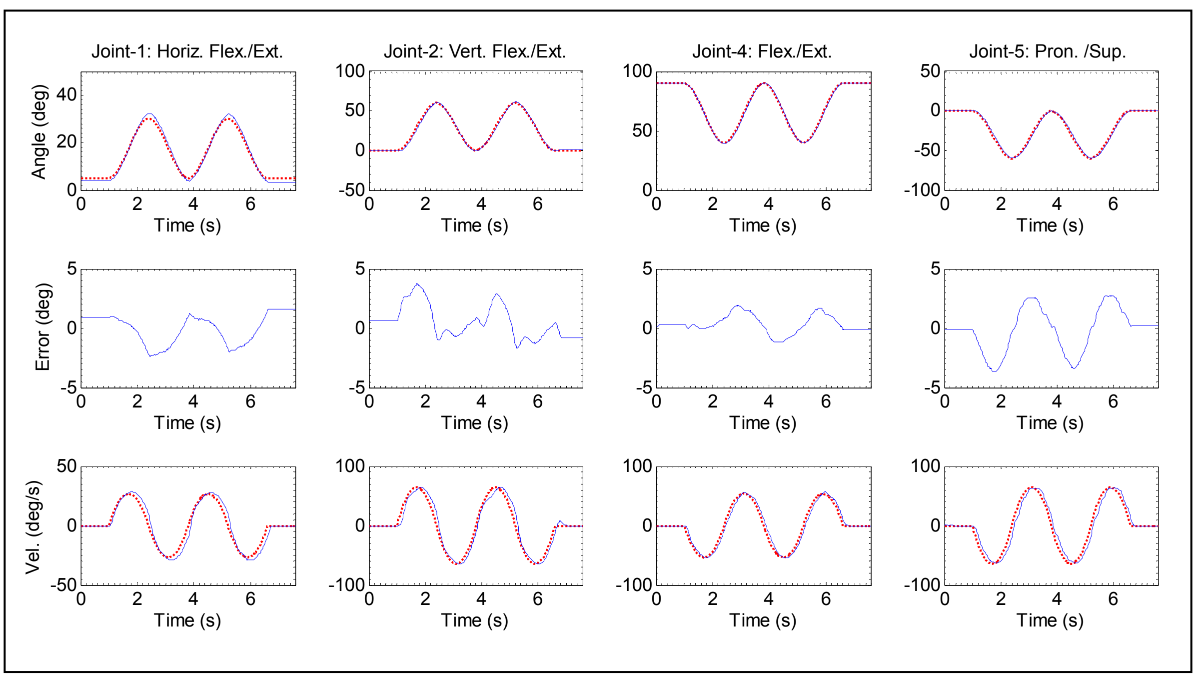


Figure 5.40 Diagonal reaching movements with PID, exercise-2B
(time to reach a diagonal target: 1.4s.; time to reach & back from a diagonal target: 2.8s.)

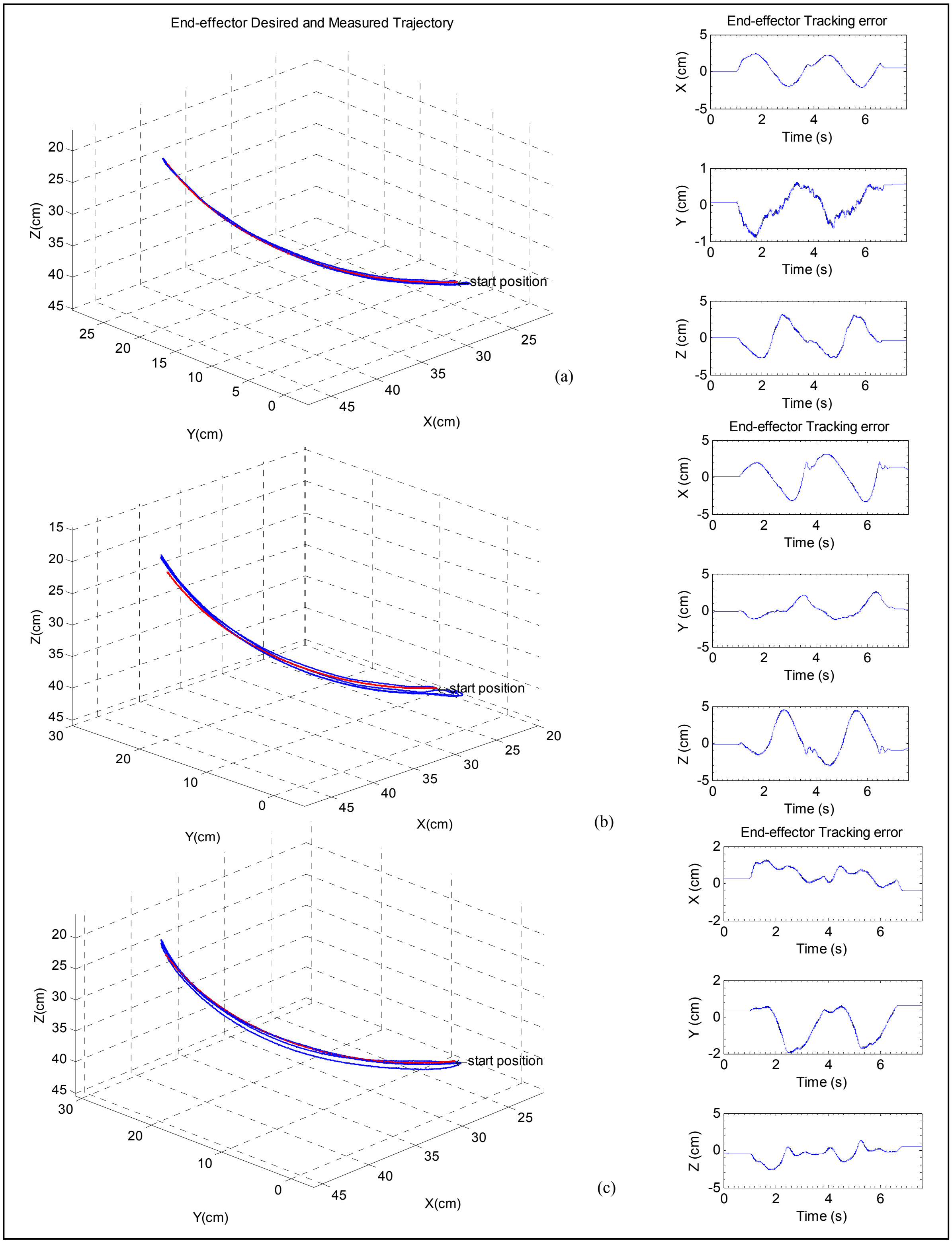


Figure 5.41 End-effector tracking (diagonal reaching) exercise-2B
(a) mSMERL (b) CTC (c) PID

*mSMERL* for elbow joint flexion/extension motion (as depicted in Figure 5.39). In the case of diagonal reaching movements, however, tracking error for the same motion was found to be larger for forearm pronation/supination when compared to *mSMERL*.

### 5.3 Cartesian Trajectory Tracking (Rahman *et al.*, 2012a)

The schematic diagram of the Cartesian trajectory tracking exercises is given in Figure 5.42. As shown in Figure 5.42a, the exercise began at point-A with elbow joint at 90° and then followed path **AB** to reach Target-1. While returning from Target-1, it followed path **CA** to reach point-C. The objective of this exercise is to reach different targets one after another which involve movement of the entire upper limb's joints. As shown in Figure 5.42a, to reach targets at three different locations (e.g., on a surface of a table), the exercise follows the path AB-BC-CD-DC-CEEC.

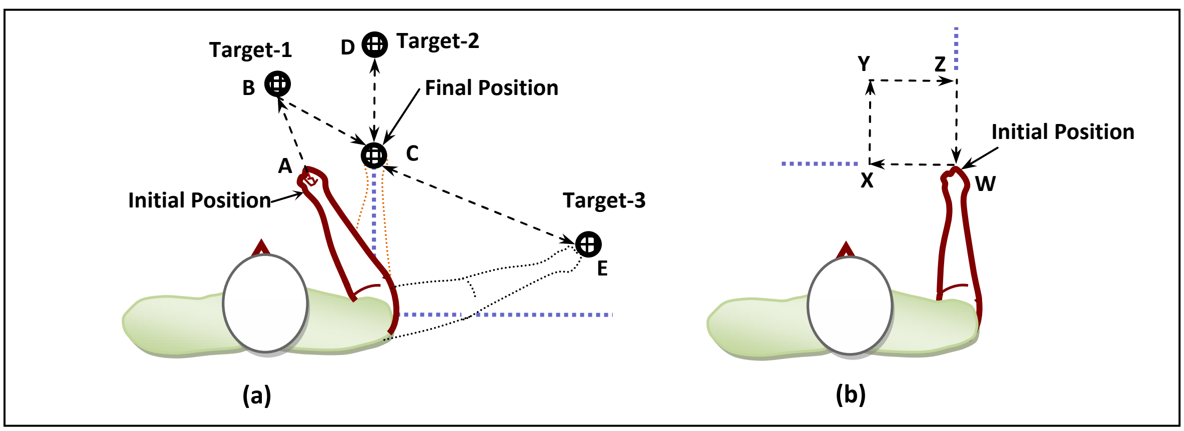


Figure 5.42 Schematic diagram of Cartesian trajectory tracking experiments
(a) Reaching movement at different targets in 2D plane
(b) Square shape trajectory tracking

Figure 5.43 and Figure 5.44 show the experimental results of reaching movement exercises performed with PID and SMERL controls respectively. It can be seen from the experimental results (in Figure 5.43 and Figure 5.44) that the measured (solid line) and desired (dotted line) trajectories overlapped each other with end-point tracking error less than 1.5cm, and thus showed good performance of the controllers in tracking Cartesian trajectories.

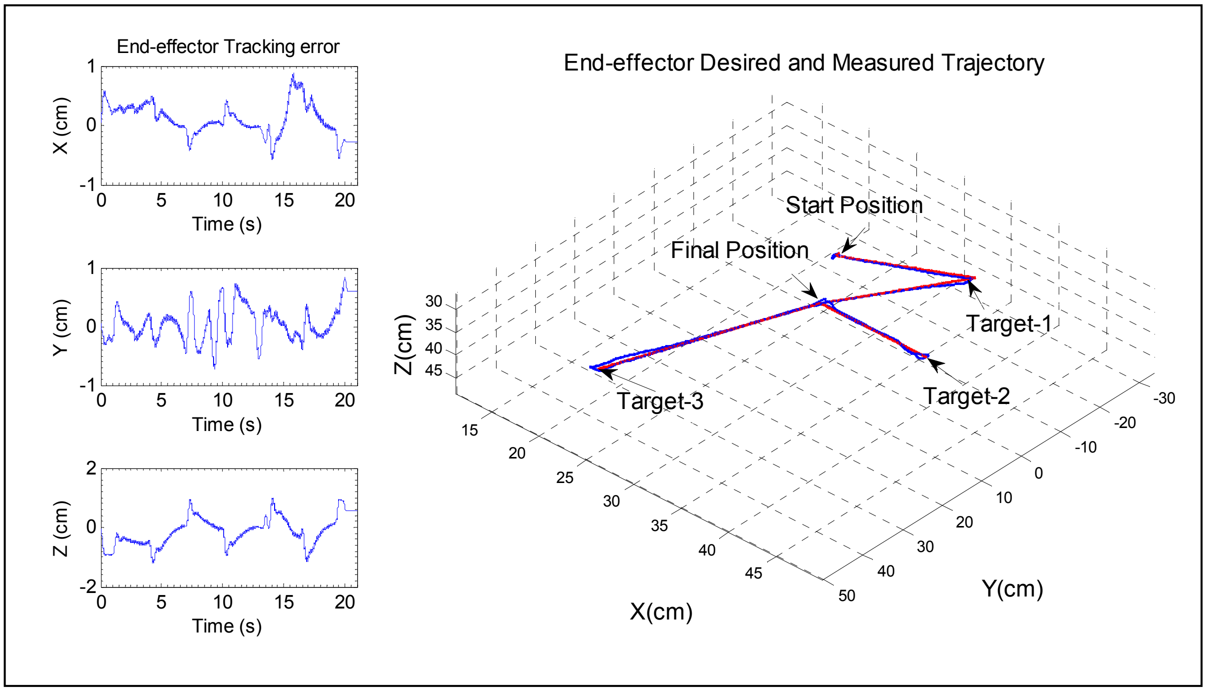


Figure 5.43 Reaching movement exercise with PID control


Figure 5.44 Reaching movement exercise with SMERL control

To further evaluate the performance of the *ETS-MARSE,* another exercise representing square shape trajectory (Figure 5.42b, path: WXYZ) tracking in a 2D plane was performed with both control techniques. The results of this trail are depicted in Figure 5.45, where it can be found that also in this case the errors are quite small. The maximum tracking error observed for the PID controller was less than 1.5cm and that for *SMERL* was less than 0.75cm.

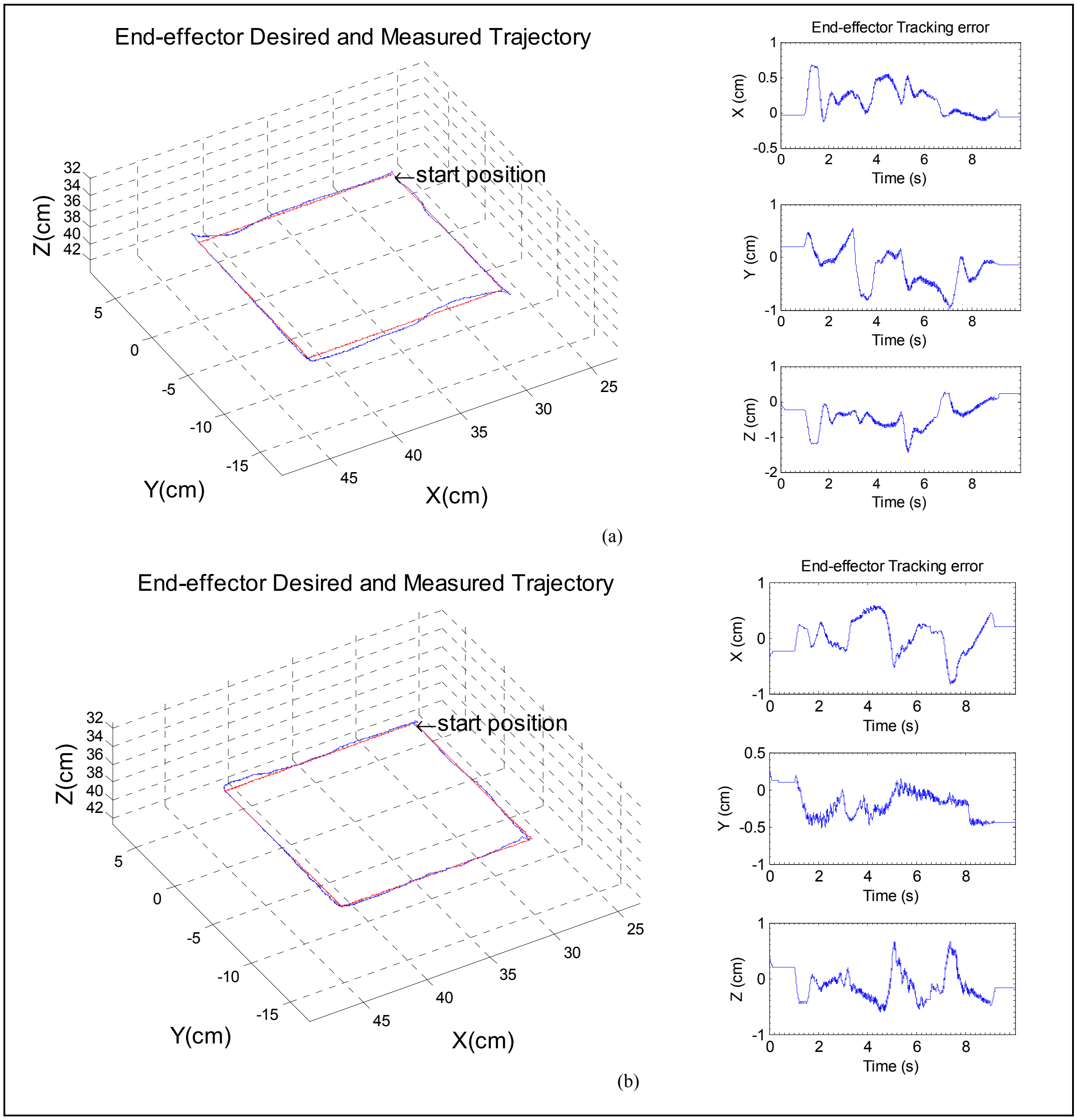


Figure 5.45 Square shape trajectory tracking on 2D plane
(a) PID control (b) SMERL control

Furthermore, to evaluate the performance of the *ETS-MARSE* for Cartesian trajectory tracking in a 3D plane, the same square shape trajectory tracking was performed in a 3D plane. The result of this experiment is show in Figure 5.46. Like previous trials, again the controller showed notable tracking performance with end-point tracking error below 1.5cm.

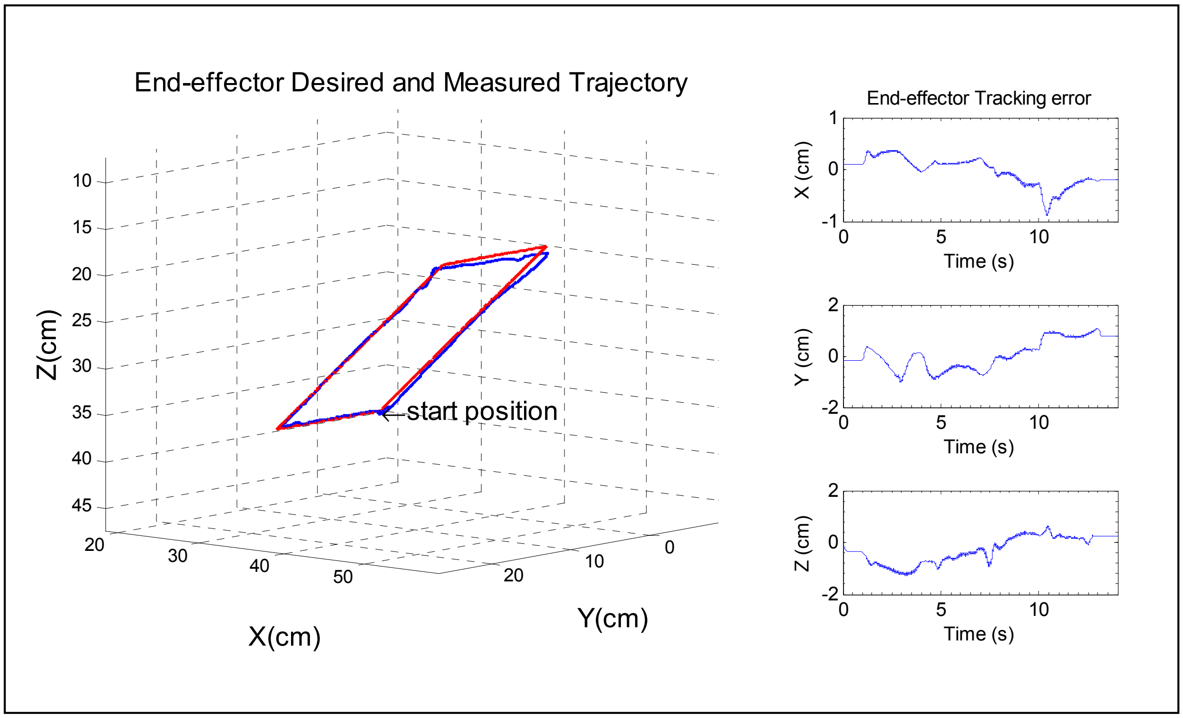


Figure 5.46 Square shape trajectory tracking in 3D plane (PID control)

From these experimental results it can be concluded that the *ETS-MARSE* is able to perform Cartesian trajectory tracking very efficiently.

## 5.4 Passive Rehab Therapy Using master Exoskeleton Arm (Rahman *et al.*, 2011g)

The 'master exoskeleton arm' (*mExoArm*) as shown in Figure 5.47 was developed to tele-operate the *ETS-MARSE* as well as to provide passive rehabilitation. It is assumed that users (patients) can operate the *mExoArm* with their good (functional) hand, or alternatively, that it can be operated by a family member or caretaker.

The entire *mExoArm* was constructed with ABS (acrylonitrile butadiene styrene) by rapid prototyping except the base, which was made in Aluminum (Figure 5.47c). As depicted in

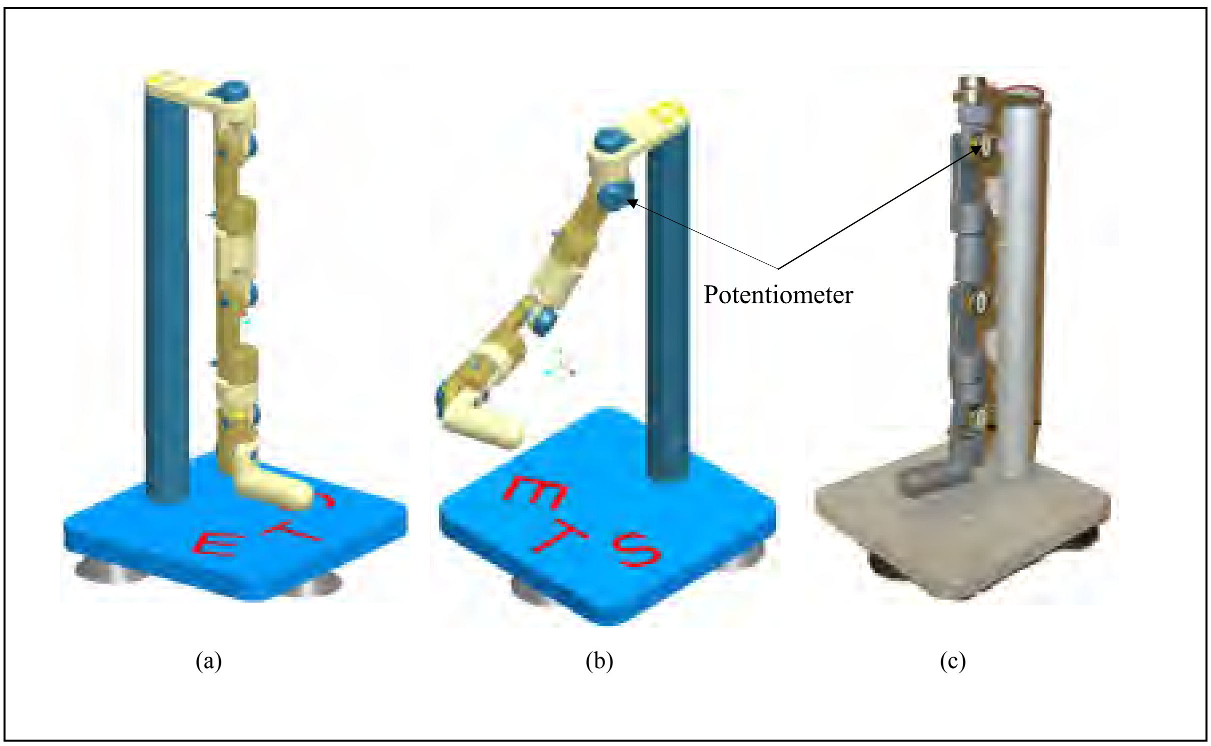


Figure 5.47 A 7DoFs upper-limb prototype *mExoArm*
(a) Left-front view (initial position) (b) Joints 1, 2 are rotated to 30°, joint 3 is to 60° and joint 4 is to70° (c) *mExoArm* after fabrication

Figure 5.47, a potentiometer was incorporated in each joint with the arm link to give the desired rotational movement of the joints as well as to measure the angle of rotation. For safety reasons, mechanical stoppers were added at each joint in the design of *mExoArm* to limit the joints' movement within the range of *MARSE's* joints' limits (see Table 2.4). Using *mExoArm* provides flexibility in choosing the range and speed of movements and as well as the ability to provide motion assistance.

### 5.4.1 Experimental Results with PID Control

The experimental results with the *mExoArm* for shoulder joint horizontal flexion/extension and internal/external rotation are depicted in Figure 5.48 and Figure 5.49, respectively. In those tasks, the subject (robot user) operates the *mExoArm* with his left hand to perform repetitive movements. It is seen from the top-most plots that the desired trajectories (solid line) overlapped with the measured ones (dotted line). The tracking error was once again found to be quite small (<4°).

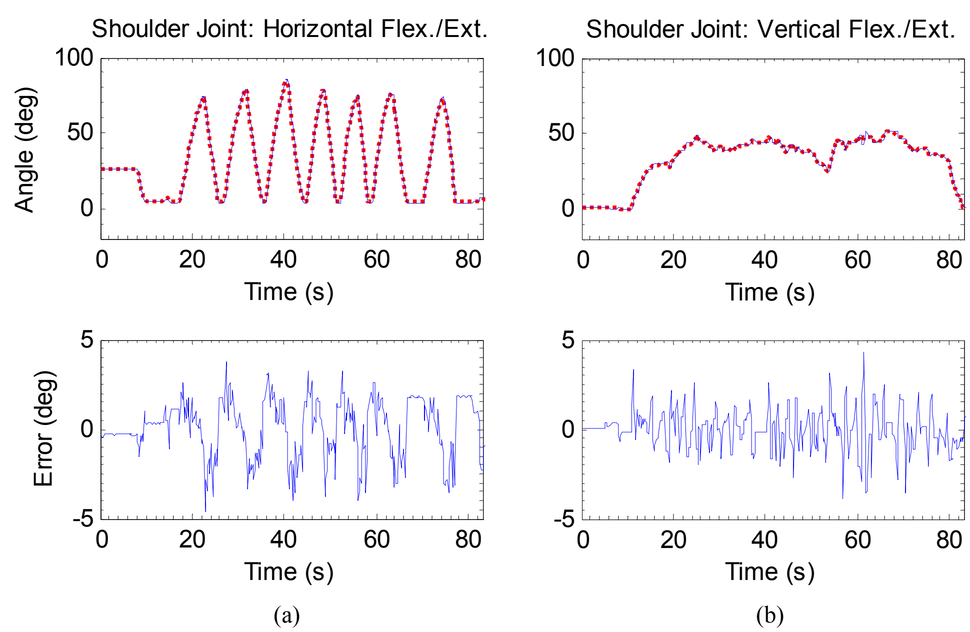


Figure 5.48 Shoulder joint movements by *mExoArm*
(a) Repetitive movement of shoulder joint horizontal flexion/extension
(b) Shoulder joint vertical flexion/extension

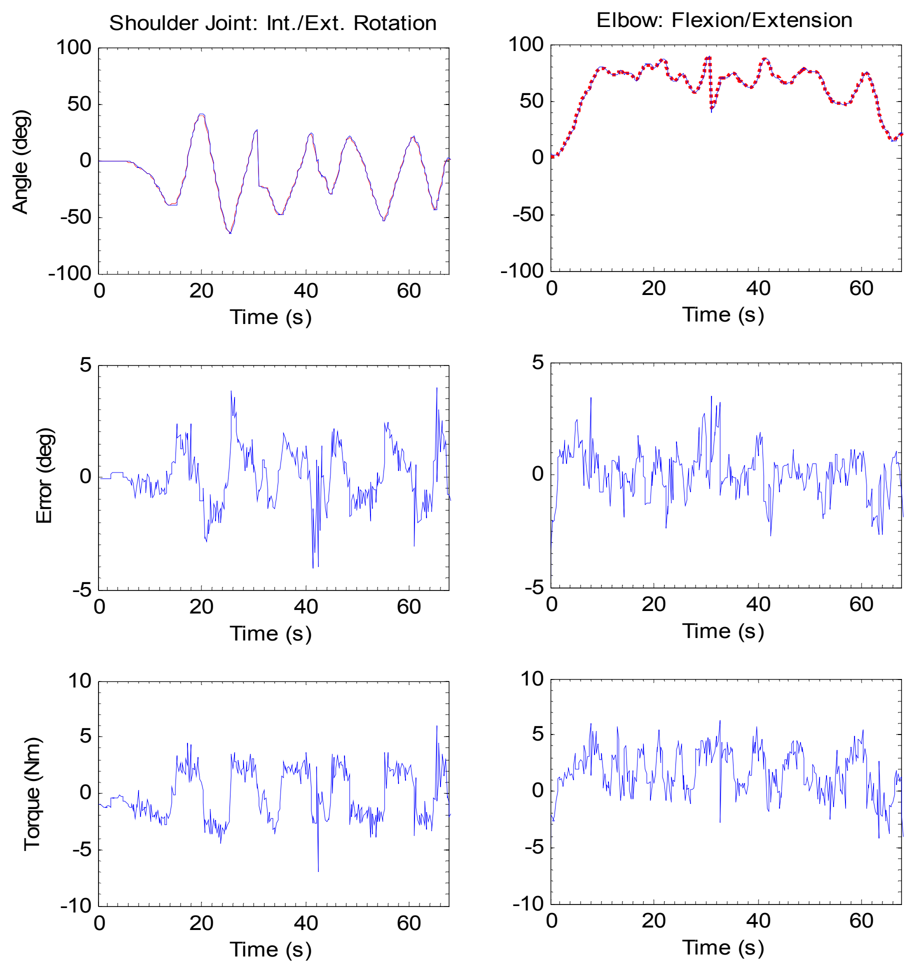


Figure 5.49 Passive rehabilitation by *mExoArm*, combined shoulder and elbow movement

To further evaluate the performance of the *mExoArm*, repetitive elbow flexion/extension movements were performed at various speeds. Experimental results for these exercises are illustrated in Figure 5.50. The results demonstrate excellent tracking performance of the controller even for the varying speed of movement. In this case, the maximum tracking error observed was around 5°.

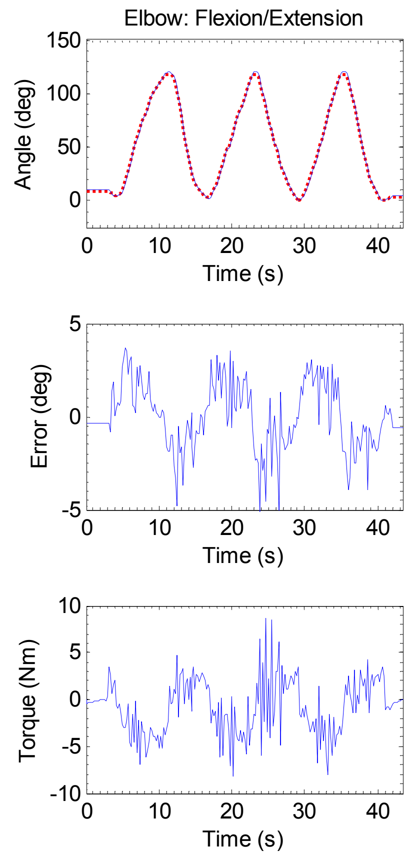


Figure 5.50 Repetitive elbow flexion/extension by *mExoArm*

To further evaluate the performance of the *mExoArm* to provide multi-joint movements exercises, a co-operative motion of elbow and shoulder movement was performed using the mExoArm, as shown in Figure 5.51. The results reveal that in all cases (Figure 5.51) the measured trajectory overlapped with the desired trajectory with tracking error less than 4°.

Finally, another co-operative exercise involving elbow and wrist joint flexion/extension movements is performed using the *mExoArm* (Figure 5.52). In these experiments, the elbow is supposed to flex at a 90° position, and thereafter, repetitive wrist joint (flexion/extension) movement is performed while maintaining the elbow at the same position. As shown in Figure 5.52, the exercise ends with a simultaneous movement of wrist and elbow joint. It is evident from this plots that the tracking errors are quite small (less than 3.8°) and thus demonstrate good performance of the controller in providing rehabilitation therapy using the *mExoArm*.

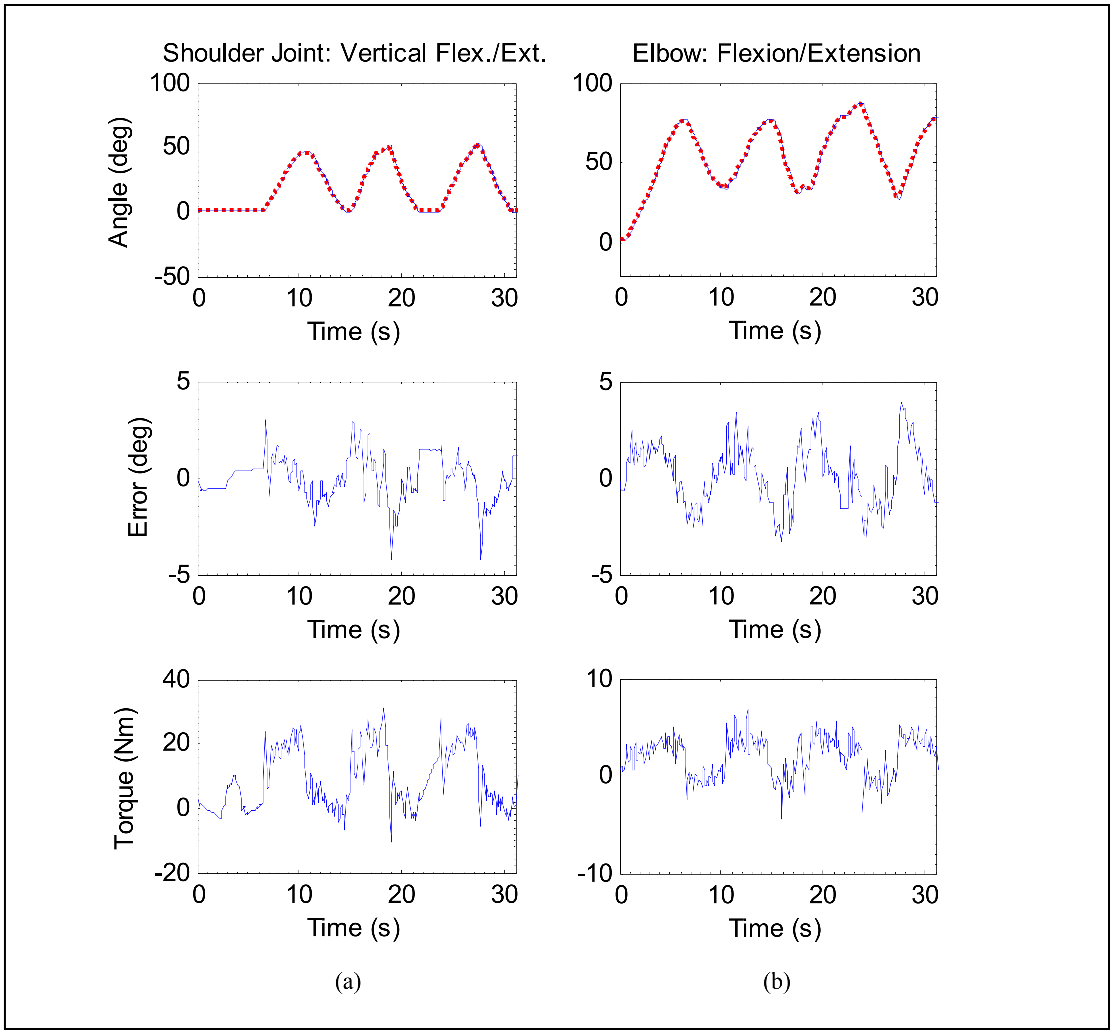


Figure 5.51 Reaching movement by *mExoArm*
(a) Shoulder joint vertical flexion/extension (b) Elbow flexion/extension

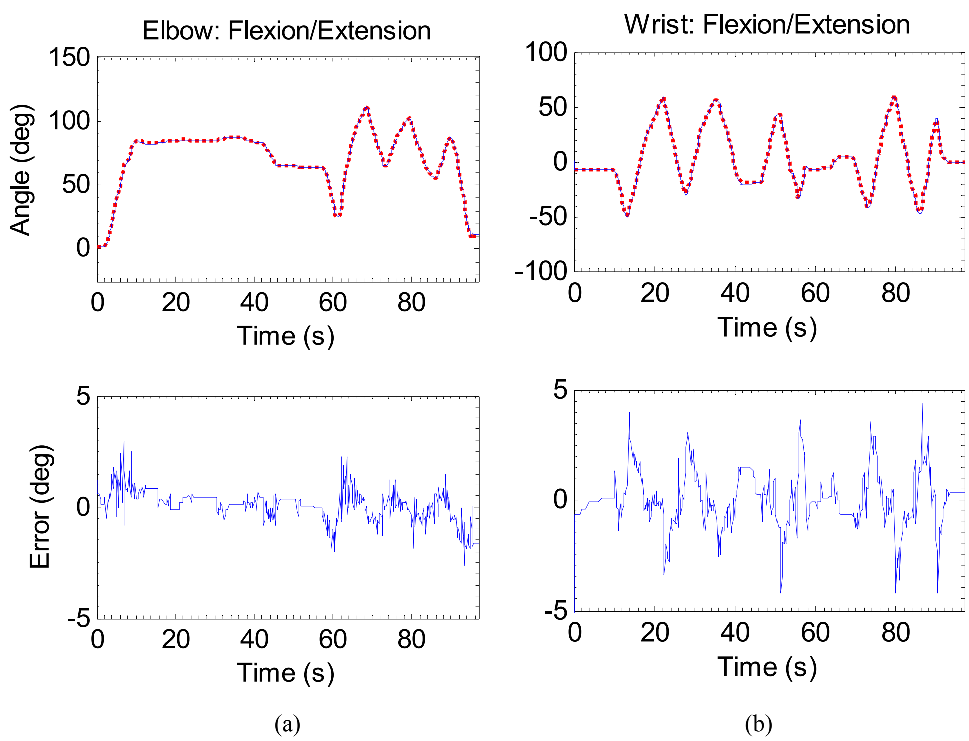


Figure 5.52 Cooperative motion of wrist and elbow joint using *mExoArm*
(a) Elbow flexion/extension (b) Repetitive movement of wrist joint flexion/extension

### 5.4.2 Experimental Results with CTC

The experimental results with the *mExoArm* for elbow flexion/extension are depicted in Figure 5.53. In these tasks, the subject (robot user) operates the *mExoArm* with his left hand to perform repetitive movement. As shown in the top-most plots, the desired trajectories (solid line) overlapped with the measured ones (dotted line). The tracking error was again was found to be quite small (<3°). Note that in the same experiment performed with PID control (Figure 5.50), the PID gave similar tracking performance as the CTC.

To further evaluate the performance of the *mExoArm*, repetitive forearm pronation/supination was performed at various speeds. Experimental results for these exercises are illustrated in

Figure 5.54. The results demonstrate excellent tracking performance of the controller even with varying speed of movement, where tracking error was found to be less than 2.5°.

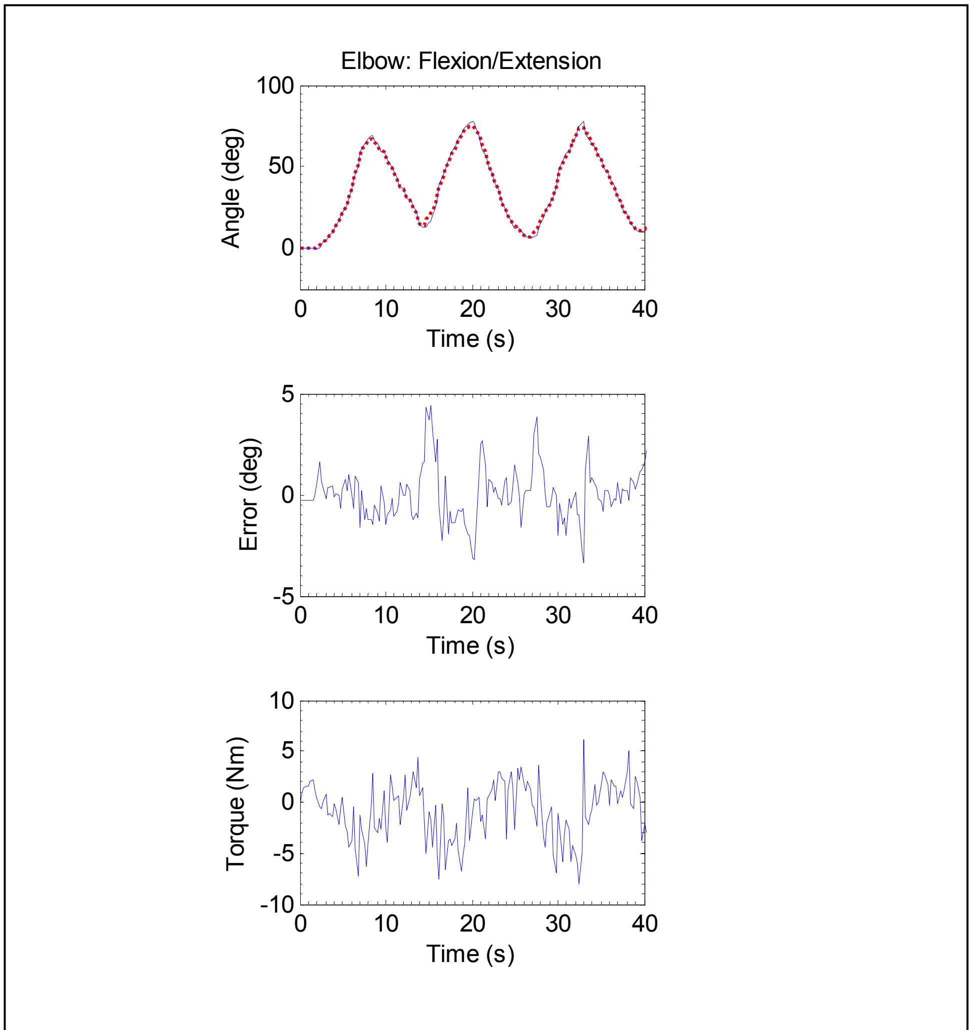


Figure 5.53 Repetitive movement of elbow joint using *mExoArm*

Finally, a cooperative motion of elbow and forearm movement using the *mExoArm* is shown in Figure 5.55. The results reveal that in all cases (Figure 5.55(a) and Figure 5.55(b)) the tracking errors are less than 3.5° and thus confirm the performance of effective passive rehabilitation using the *mExoArm*. Note that a few spikes are apparent in the error plots; these are due to static friction that has a large value in the transient and therefore shows a larger tracking error.

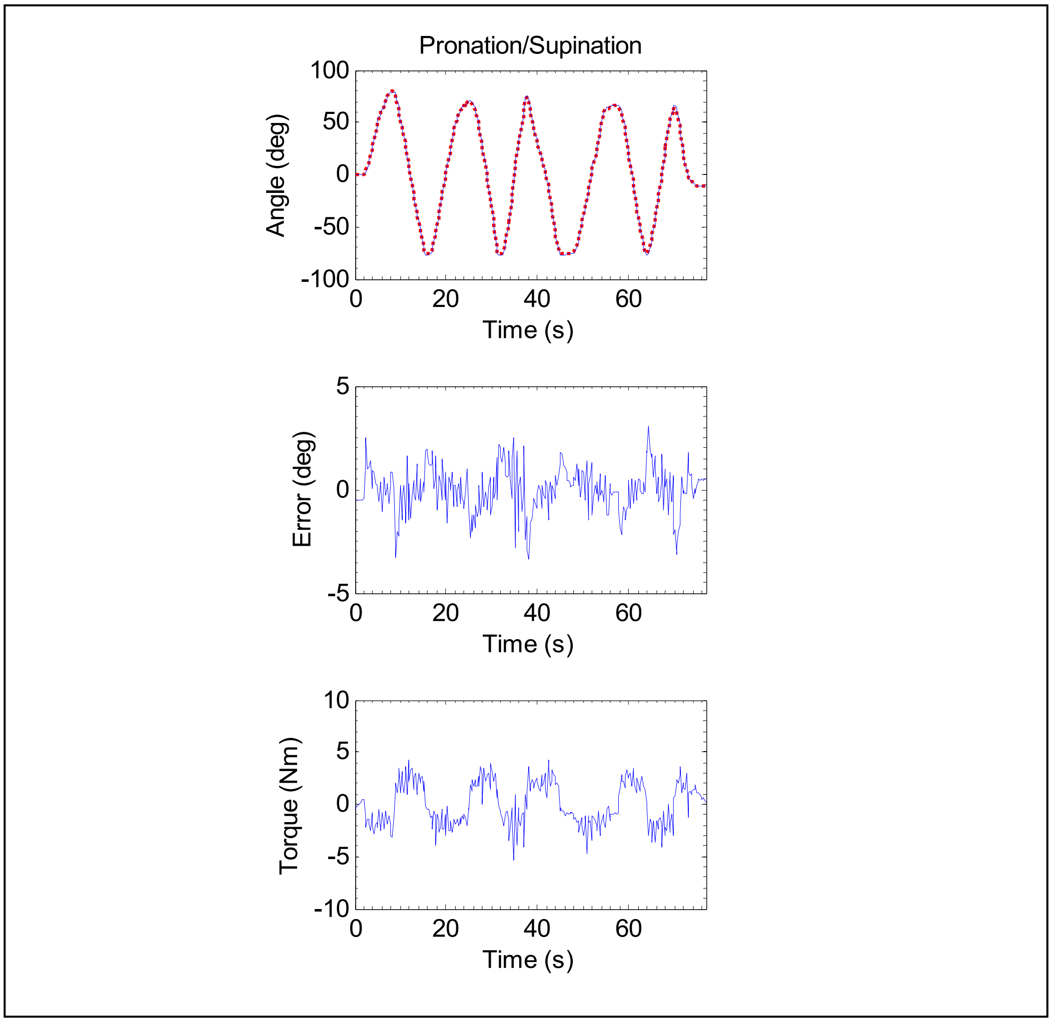


Figure 5.54 Repetitive movement of forearm using *mExoArm*

Using the *mExoArm* is an alternative way to provide passive therapy as well as to provide motion assistance. It gives therapists or caregivers the flexibility to replicate different rehabilitation trajectories promptly, according to subject's requirements, to maneuver the *ETS-MARSE.* Moreover, complex 3D joint space movement can be replicated easily by the *mExoArm* rather than using inverse kinematics, which might require a Jacobian matrix. Furthermore, the *mExoArm* could potentially be used to tele-operate the *MARSE*.

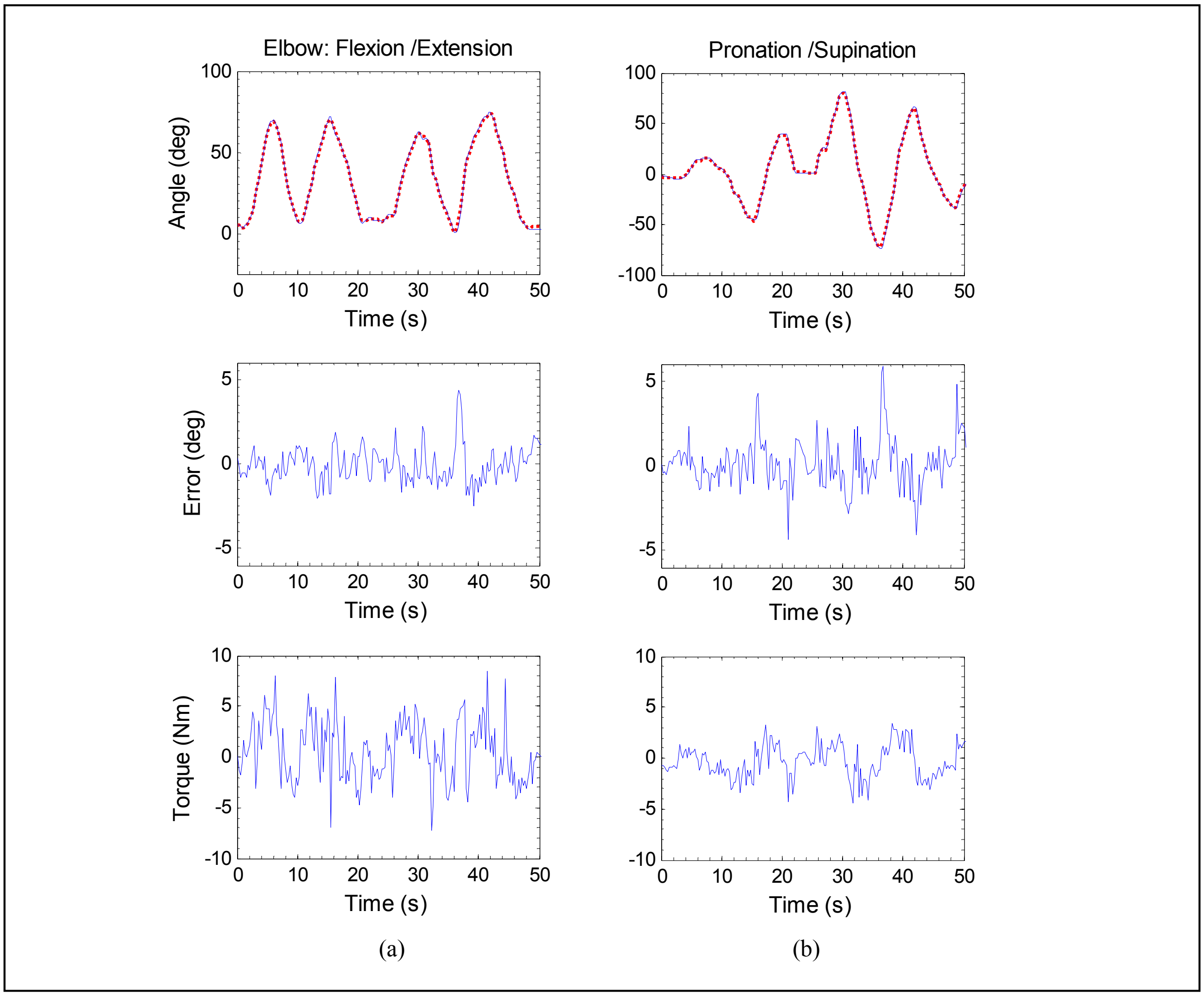


Figure 5.55 Passive rehabilitation by *mExoArm*
(simultaneous movement of elbow and forearm)

## 5.5 Discussion

The goal of this research was to design, build and control an exoskeleton robot to provide passive rehabilitation therapy. *ETS-MARSE,* a 7DoFs exoskeleton robot, was developed. As a control strategy to maneuver the *ETS-MARSE,* different control techniques were employed. Experimental results demonstrate that *mSMERL* and PID control techniques are the best choices to maneuver the *ETS-MARSE* to provide passive arm movement therapy. These control techniques are robust and simple to design. Theoretically, with perfect dynamic modeling, CTC should give better tracking performance compared to PID control when the *MARSE* is maneuvered at a high speeds. However, in practice it is difficult to estimate or find exact dynamic parameters. Moreover, it is challenging to model the nonlinear frictions terms. Therefore, while using a nonlinear control approach, it was often necessary to simplify the dynamic model. Indeed, we did so in the dynamic modeling of the *ETS-MARSE* using the following strategies:

- using only the diagonal elements (i.e., $I_{xx}$ , $I_{yy}$, and $I_{zz}$) of the inertial terms. The details of mass and inertia characteristics of each joint segment can be found in ANNEX I - ANNEX VII;

- assuming that the structure of the *MARSE* arm is symmetric. Therefore, the origin of the centre of gravity for each joint segment lies on the axis of symmetry. In our case, we have considered the axis of symmetry to be along the $Z_0$ axis (i.e., on $XZ_0$ plane);

- modeling of the viscous friction term was ignored, considering the exercises will be performed at a low speed (passive rehabilitation therapy exercises should be performed slowly because of the subject's arm impairment). However, viscous friction terms are relevant when the *MARSE* is maneuvered at high speeds. Therefore, a viscous friction model should be included in the control law when developing a control strategy to provide active motion assistance.

Note that this simplification in the modeling was done only to save computation time. However, comparing the natural variability of human arm movement (Buneo *et al.*, 1995; Hay *et al.*, 2005; Meyer *et al.*, 1988; Sanger, 2000; Sarlegna and Sainburg, 2007), with these results (Figure 5.4 - Figure 5.41) we may conclude that the *ETS-MARSE* can efficiently track the desired trajectories, and thus should be adequate for the purpose of performing passive arm movement therapy. Many individuals with arm impairment resulting from a surgery to the joints or following a stroke cannot perform their various activities of daily living independently. Thus, the development of the *ETS-MARSE* and the validation of the results were a very important first step for the use of *ETS-MARSE* in rehabilitation.

However, it should be noted that the *ETS-MARSE* with different control strategies could potentially be used as:

- a motion assistance device to help individuals with limited upper limb strength;
- a therapeutic device to provide different forms of rehabilitation therapy ranging from passive movements to assisted movements;
- a power assistance device, i.e.; as a human arm amplifier to scale down the load of interaction (Kazerooni, 1996);
- a master device for tele-operation (master/slave) of other robotic devices; and
- a haptic device.

# CONCLUSION

A 7DoFs robotic exoskeleton, *ETS-MARSE,* (*motion assistive robotic-exoskeleton for superior extremity*) corresponding to the human upper limb was developed to provide grounds for effective rehabilitation of people with disabilities at the level of shoulder, elbow, forearm and wrist joint movements. In this thesis we have presented the modeling, design (mechanical and electrical components), development, and control strategies of the *ETS-MARSE.*

To avoid the complex cable routing that can be found in many exoskeleton systems, an innovative power transmission mechanism (a combination of an open type bearing and a gear assembly) was introduced for assisting shoulder joint internal/external rotation and for forearm pronation/supination (Rahman *et al.*, 2012b).

The kinematic model of the *MARSE* was developed based on modified Denavit-Hartenberg notations, whereas in dynamic modeling the iterative Newton-Euler formulation was used. In experiments, typical rehabilitation exercises for single and multi joint movements (e.g., reaching) were performed with different control techniques such as PID, Compliance Control with Gravity Compensation, Computed Torque Control, and Sliding Mode Control with Exponential Reaching Law. Note that the control architecture was implemented on a field-programmable gate array (FPGA) in conjunction with a RT-PC.

To improve transient tracking performance and to reduce chattering in conventional sliding mode control, this thesis proposed the *mSMERL,* a novel nonlinear control strategy that combined the boundary layer technique and the exponential reaching law. Experiments were performed to compare the dynamic tracking performance of the conventional SMC and *mSMERL*, where it was demonstrated that *mSMERL* is able to reduce chattering (during the transient and steady state) and give better tracking performance.

Experiments were carried out with healthy human subjects where trajectories (i.e., pre-programmed trajectories recommended by a therapist/clinician) tracking in the form of passive rehabilitation exercises were carried out.

This thesis also focused on the development of a 7DoFs upper-limb prototype (lower scaled), *mExoArm*. Furthermore, experiments were carried out with the *mExoArm* where subjects (robot users) operated the *mExoArm* (like a joystick) to maneuver the *MARSE* to provide passive rehabilitation.

Experimental results show that the *ETS-MARSE* can effectively perform passive rehabilitation exercises for shoulder, elbow and wrist joint movements. Using *mExoArm* offers users some flexibility over the pre-programmed trajectory selection approach, especially in choosing the range of movement and the speed of motion. Moreover, the *mExoArm* could potentially be used to tele-operate the *MARSE* in providing rehabilitation exercises.

# RECOMMENDATIONS

To provide *‘active assistance rehabilitation,’* future projects may include developing a force sensor-based controller to control the *ETS-MARSE*. Future studies/works can also be expanded as follows:

- developing a lighter version of *ETS-MARSE* and introducing a shoulder joint centre of rotation mechanism (Rahman, 2005) to make the exoskeleton more realistic;
- considering many physically disabled individuals use wheel chairs, it is recommended to set up the system (*ETS-MARSE*) on a mobile wheel chair to increase the mobility of such individuals;
- to reflect the user’s intention of motion, an electromyogram (EMG) based control algorithm could be developed (Perry, Rosen and Burns, 2007; Rahman, 2005). This control technique could be used for motion assistance to perform daily upper-limb tasks, as well as to provide active and resistive rehabilitation;
- studies can be carried out to measure the effects of the use of the *ETS-MARSE* by analyzing the EMG signals during different experimental conditions;
- the assessment and evaluation of the *ETS-MARSE* used to perform therapy with upper limb-impaired individuals;
- development of a software to provide virtual reality based rehabilitation (Cardoso *et al.*, 2006; Carignan, Tang and Roderick, 2009; Filler, 1999; Frisoli *et al.*, 2009; Stewart *et al.*, 2006). This will help subjects to interact more with the *MASRE*;
- updating the library of existing passive rehabilitation exercises with more Cartesian trajectory based exercises, for example, to maneuver the *ETS-MARSE* to follow a circular trajectory. For this purpose, it is recommended to develop and use the analytic/geometric inverse kinematics solution of the *ETS-MARSE*;
- finally, it is recommended for the 2$^{nd}$ version of the *MARSE* to replace the existing actuators with another type that comes with an encoder.

## ANNEX I

## MASS CHARACTERISTICS OF UPPER LIMB

Table-A I-1 Mass characteristics of upper limb
Adapted from Winter (1990)

| Segments & Definition | Segment Length/ Stature | Segment Weight/ Body Weight | Centre of Mass / Segment length | | Radius of Gyration / Segment length | | |
|---|---|---|---|---|---|---|---|
| | | | *Proximal* | *Distal* | *C of G* | *Proximal* | *Distal* |
| Hand[a] | 0.108 | 0.006 | 0.506 | 0.494 | 0.297 | 0.587 | 0.577 |
| Forearm[b] | 0.146 | 0.016 | 0.430 | 0.570 | 0.303 | 0.526 | 0.647 |
| Upper arm[c] | 0.186 | 0.028 | 0.436 | 0.564 | 0.322 | 0.542 | 0.645 |
| F'arm and hand | 0.254 | 0.022 | 0.682 | 0.318 | 0.468 | 0.827 | 0.565 |
| Upper limb | 0.44 | 0.050 | 0.530 | 0.470 | 0.368 | 0.645 | 0.569 |

## ANNEX II

## REGRESSION COEFFICIENT FOR INERTIA CHARACTERISTICS OF UPPER LIMB

Table-A II-1 Regression coefficients for inertia characteristics of upper limb Adapted from Zatsiorsky and Seluyanov (1983)

| Limb Segment | Constant | Body Weight (kg) | Stature (cm) | R |
|---|---|---|---|---|
| Moment of Inertia around X axis[1] (kg.cm$^2$) | | | | |
| Upper arm | -250.70 | 1.56 | 1.512 | 0.62 |
| Forearm | -64.00 | 0.95 | 0.340 | 0.71 |
| Hand | -19.50 | 0.17 | 0.116 | 0.50 |
| Moment of Inertia around Y axis (kg.cm$^2$) | | | | |
| Upper arm | -232.00 | 1.525 | 1.343 | 0.62 |
| Forearm | -67.90 | 0.855 | 0.376 | 0.71 |
| Hand | -13.68 | 0.088 | 0.092 | 0.43 |
| Moment of Inertia around Z axis (kg.cm$^2$) | | | | |
| Upper arm | -16.90 | 0.6620 | 0.0435 | 0.44 |
| Forearm | 5.66 | 0.3060 | -0.0880 | 0.66 |
| Hand | -6.26 | 0.0762 | 0.0347 | 0.43 |

The origin of the coordinate system for each segment is the center of gravity of that segment. The X axis is defined as the frontal plane and +X is the direction from origin towards the front of the body. The Y axis is defined as the saggital plane and +Y is the direction from the origin towards the left of the body. The Z axis is defined as the transverse plane and +Z is the direction from the origin towards the head.

[1] Ex.: Moment of Inertia of hand around X axis (kg.cm$^2$) = -19.5 + 0.17×Body weight (kg) +0.116×Stature (cm)

# ANNEX III

## MASS AND INERTIA PROPERTIES OF ETS-MARSE (JOINT 1)

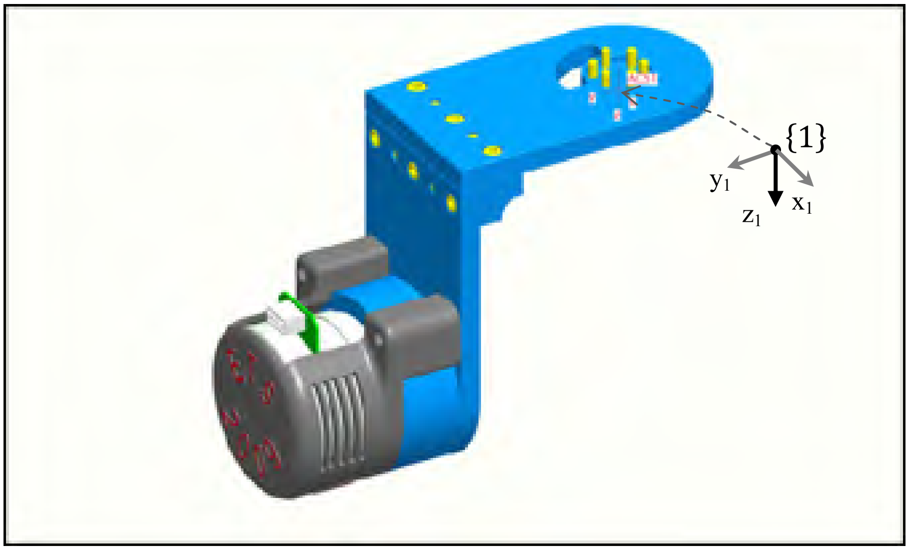


```
VOLUME =  1.1666059e+06  MM^3
SURFACE AREA =  2.6215932e+05  MM^2
AVERAGE DENSITY =  2.9789404e-06 KILOGRAM / MM^3
MASS =  3.4752495e+00 KILOGRAM

CENTER OF GRAVITY with respect to ACS1 coordinate frame:
X   Y   Z     7.1281479e-02  1.3820600e+02  9.8419371e+01  MM

INERTIA with respect to ACS1 coordinate frame:  (KILOGRAM * MM^2)

INERTIA TENSOR:
Ixx Ixy Ixz  1.2331398e+05  8.0547490e+00  1.7284770e+01
Iyx Iyy Iyz  8.0547490e+00  4.8503730e+04 -5.5872595e+04
Izx Izy Izz  1.7284770e+01 -5.5872595e+04  7.9265440e+04

INERTIA at CENTER OF GRAVITY with respect to ACS1 coordinate frame:  (KILOGRAM * MM^2)

INERTIA TENSOR:
Ixx Ixy Ixz  2.3271023e+04  4.2291269e+01  4.1665308e+01
Iyx Iyy Iyz  4.2291269e+01  1.4841151e+04 -8.6017360e+03
Izx Izy Izz  4.1665308e+01 -8.6017360e+03  1.2885029e+04

PRINCIPAL MOMENTS OF INERTIA:  (KILOGRAM * MM^2)
I1   I2   I3    5.2057331e+03  2.2520233e+04  2.3271236e+04

ROTATION MATRIX from ACS1 orientation to PRINCIPAL AXES:
      -0.00328       -0.00506       -0.99998
       0.66596        0.74596       -0.00596
       0.74598       -0.66597        0.00092

ROTATION ANGLES from ACS1 orientation to PRINCIPAL AXES (degrees):
angles about x  y  z  81.186        -89.654        122.943

RADII OF GYRATION with respect to PRINCIPAL AXES:
R1  R2  R3 3.8703296e+01  8.0499549e+01  8.1830787e+01  MM
---------------------------------------------
```

## ANNEX IV

## MASS AND INERTIA PROPERTIES OF MARSE (JOINT 3 TO 4)

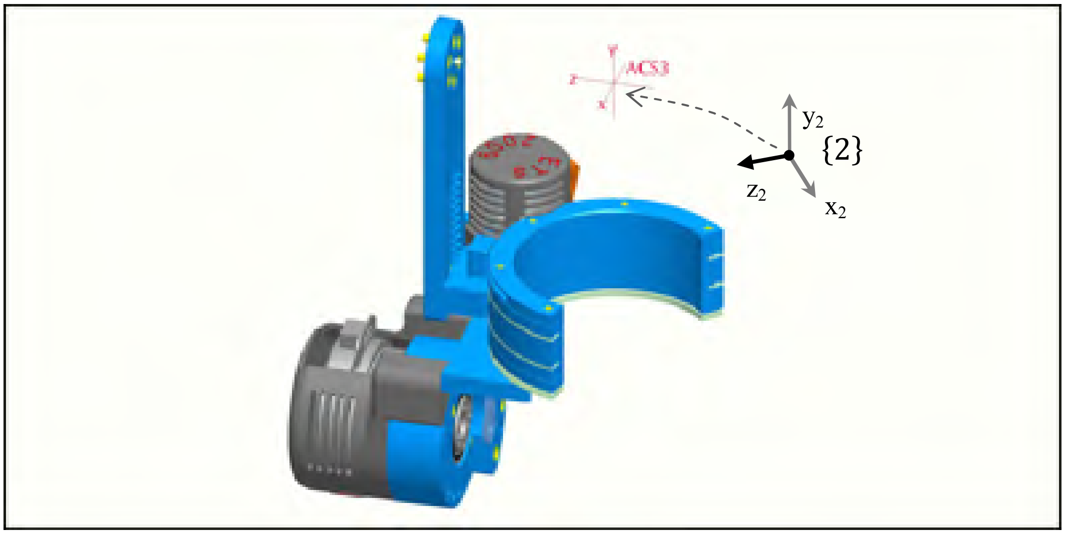


```
VOLUME =  1.2802069e+06  MM^3
SURFACE AREA =  4.0565661e+05  MM^2
AVERAGE DENSITY =  2.9192983e-06 KILOGRAM / MM^3
MASS =  3.7373057e+00 KILOGRAM

CENTER OF GRAVITY with respect to ACS3 coordinate frame:
X   Y   Z    -1.3132288e+01 -1.9564783e+02  9.7970448e+01  MM

INERTIA with respect to ACS3 coordinate frame:  (KILOGRAM * MM^2)

INERTIA TENSOR:
Ixx Ixy Ixz  2.0221063e+05 -7.6078882e+03  2.6231526e+03
Iyx Iyy Iyz -7.6078882e+03  4.9351145e+04  7.7300247e+04
Izx Izy Izz  2.6231526e+03  7.7300247e+04  1.6380061e+05

INERTIA at CENTER OF GRAVITY with respect to ACS3 coordinate frame:  (KILOGRAM * MM^2)

INERTIA TENSOR:
Ixx Ixy Ixz  2.3282321e+04  1.9943853e+03 -2.1851758e+03
Iyx Iyy Iyz  1.9943853e+03  1.2835181e+04  5.6646701e+03
Izx Izy Izz -2.1851758e+03  5.6646701e+03  2.0099222e+04

PRINCIPAL MOMENTS OF INERTIA:  (KILOGRAM * MM^2)
I1   I2   I3    9.1803237e+03  2.2523374e+04  2.4513026e+04

ROTATION MATRIX from ACS3 orientation to PRINCIPAL AXES:
      -0.19549        0.56925        0.79858
       0.85399        0.49916       -0.14676
      -0.48217        0.65329       -0.58372

ROTATION ANGLES from ACS3 orientation to PRINCIPAL AXES (degrees):
angles about x  y  z 165.887         52.995       -108.953

RADII OF GYRATION with respect to PRINCIPAL AXES:
R1  R2  R3 4.9562098e+01  7.7631399e+01  8.0987717e+01  MM
```

# ANNEX V

## MASS AND INERTIA PROPERTIES OF MARSE (JOINT 5 TO 6)

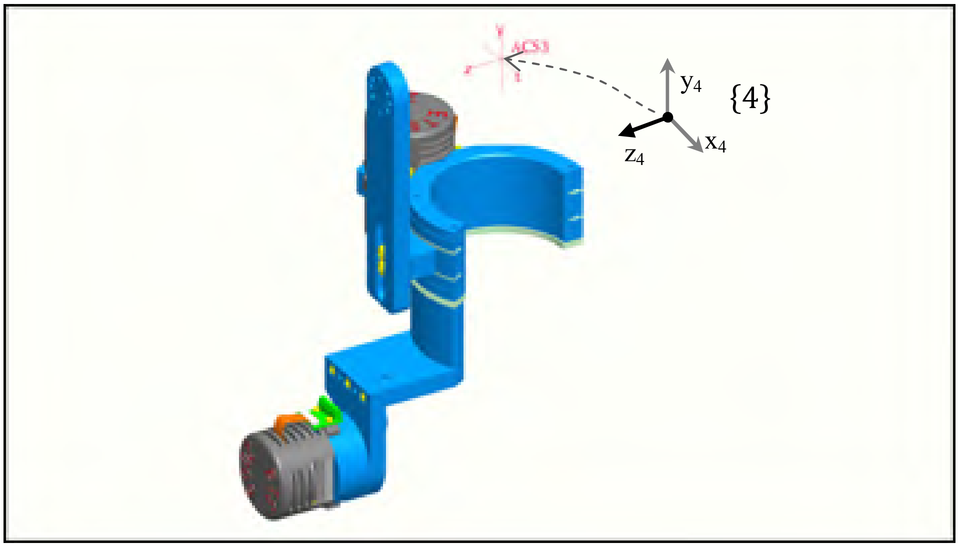


```
VOLUME =  7.1350560e+05  MM^3
SURFACE AREA =  2.8785468e+05  MM^2
AVERAGE DENSITY =  2.8968622e-06 KILOGRAM / MM^3
MASS =  2.0669274e+00 KILOGRAM

CENTER OF GRAVITY with respect to ACS3 coordinate frame:
X   Y   Z    -2.9383700e+01 -1.6327282e+02  5.8954981e+01  MM

INERTIA with respect to ACS3 coordinate frame:  (KILOGRAM * MM^2)

INERTIA TENSOR:
Ixx Ixy Ixz  7.8898450e+04 -7.7485550e+03  8.8775641e+02
Iyx Iyy Iyz -7.7485550e+03  1.9006818e+04  2.5121506e+04
Izx Izy Izz  8.8775641e+02  2.5121506e+04  6.9550487e+04

INERTIA at CENTER OF GRAVITY with respect to ACS3 coordinate frame:  (KILOGRAM * MM^2)

INERTIA TENSOR:
Ixx Ixy Ixz  1.6614270e+04  2.1676525e+03 -2.6928139e+03
Iyx Iyy Iyz  2.1676525e+03  1.0038230e+04  5.2257871e+03
Izx Izy Izz -2.6928139e+03  5.2257871e+03  1.2665717e+04

PRINCIPAL MOMENTS OF INERTIA:  (KILOGRAM * MM^2)
I1  I2  I3   4.9852696e+03  1.6297714e+04  1.8035234e+04

ROTATION MATRIX from ACS3 orientation to PRINCIPAL AXES:
      -0.27911        0.48242        0.83028
       0.74558        0.65377       -0.12922
      -0.60515        0.58298       -0.54215

ROTATION ANGLES from ACS3 orientation to PRINCIPAL AXES (degrees):
angles about x  y  z 166.593         56.128       -120.052

RADII OF GYRATION with respect to PRINCIPAL AXES:
R1  R2  R3 4.9111332e+01  8.8797499e+01  9.3411056e+01  MM
```

# ANNEX VI

## MASS AND INERTIA PROPERTIES OF MARSE JOINT (6 TO 7)

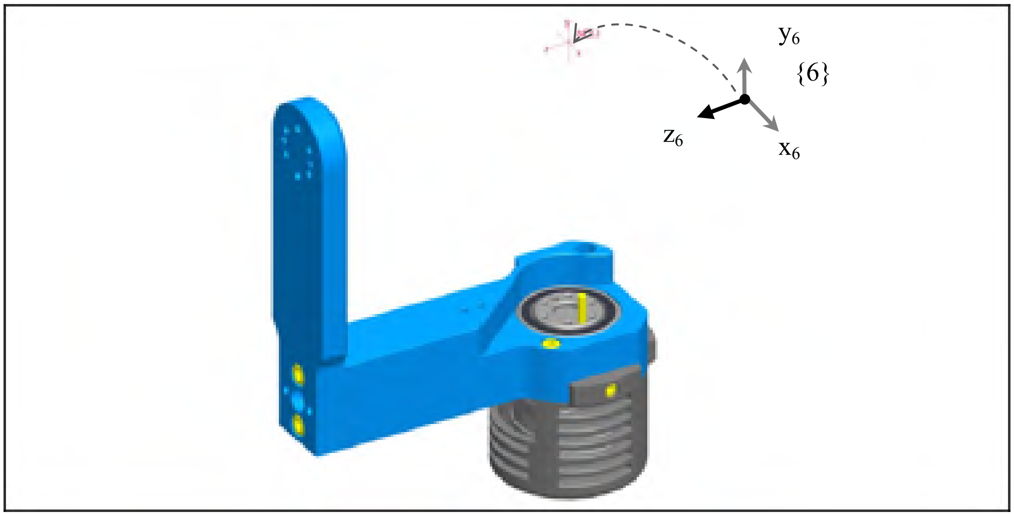


```
VOLUME =  2.8582113e+05  MM^3
SURFACE AREA =  8.5025779e+04  MM^2
AVERAGE DENSITY =  2.7274235e-06 KILOGRAM / MM^3
MASS =  7.7955526e-01 KILOGRAM

CENTER OF GRAVITY with respect to ACS3 coordinate frame:
X   Y   Z    -3.5105217e-01 -1.2182464e+02  4.1709658e+01  MM

INERTIA with respect to ACS3 coordinate frame:  (KILOGRAM * MM^2)

INERTIA TENSOR:
Ixx Ixy Ixz  1.5876690e+04 -3.2520218e+01 -5.5588749e+00
Iyx Iyy Iyz -3.2520218e+01  3.2997940e+03  2.9519696e+03
Izx Izy Izz -5.5588749e+00  2.9519696e+03  1.2791835e+04

INERTIA at CENTER OF GRAVITY with respect to ACS3 coordinate frame:  (KG * MM^2)

INERTIA TENSOR:
Ixx Ixy Ixz  2.9509324e+03  8.1886817e-01 -1.6973330e+01
Iyx Iyy Iyz  8.1886817e-01  1.9435091e+03 -1.0091564e+03
Izx Izy Izz -1.6973330e+01 -1.0091564e+03  1.2221701e+03

PRINCIPAL MOMENTS OF INERTIA:  (KILOGRAM * MM^2)
I1  I2  I3   5.1109475e+02  2.6541433e+03  2.9513736e+03

ROTATION MATRIX from ACS3 orientation to PRINCIPAL AXES:
       0.00549       -0.03516       -0.99937
       0.57593        0.81710       -0.02558
       0.81748       -0.57542        0.02474

ROTATION ANGLES from ACS3 orientation to PRINCIPAL AXES (degrees):
angles about x  y  z  45.960        -87.960         81.120

RADII OF GYRATION with respect to PRINCIPAL AXES:
R1  R2  R3 2.5605146e+01  5.8349714e+01  6.1530244e+01  MM
```

## ANNEX VII

## MASS AND INERTIA PROPERTIES OF ETS-MARSE (JOINT 7)

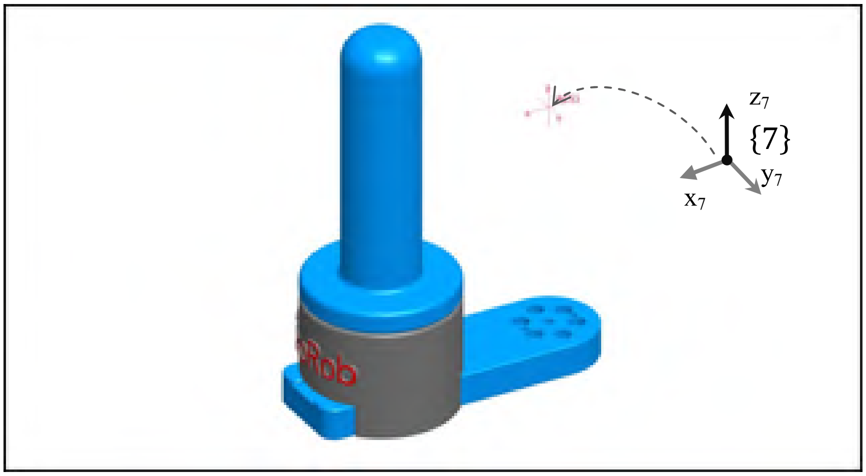


```
VOLUME =  2.2210442e+05  MM^3
SURFACE AREA =  5.6142600e+04  MM^2
AVERAGE DENSITY =  2.2358638e-06 KILOGRAM / MM^3
MASS =  4.9659523e-01 KILOGRAM

CENTER OF GRAVITY with respect to ACS5 coordinate frame:
X   Y   Z     6.2263936e+01 -3.2098638e-04 -5.0780305e+01  MM

INERTIA with respect to ACS5 coordinate frame:  (KILOGRAM * MM^2)

INERTIA TENSOR:
Ixx Ixy Ixz  2.3267685e+03  7.3359374e-02  1.3953111e+03
Iyx Iyy Iyz  7.3359374e-02  4.4618044e+03 -1.1194287e-02
Izx Izy Izz  1.3953111e+03 -1.1194287e-02  2.2712931e+03

INERTIA at CENTER OF GRAVITY with respect to ACS5 coordinate frame:  (KG * MM^2)

INERTIA TENSOR:
Ixx Ixy Ixz  1.0462285e+03  6.3434483e-02 -1.7481457e+02
Iyx Iyy Iyz  6.3434483e-02  1.2560652e+03 -3.0998907e-03
Izx Izy Izz -1.7481457e+02 -3.0998907e-03  3.4609385e+02

PRINCIPAL MOMENTS OF INERTIA:  (KILOGRAM * MM^2)
I1   I2   I3    3.0487194e+02  1.0874504e+03  1.2560652e+03

ROTATION MATRIX from ACS5 orientation to PRINCIPAL AXES:
       0.22951        0.97331        0.00036
      -0.00001       -0.00037        1.00000
       0.97331       -0.22951       -0.00007

ROTATION ANGLES from ACS5 orientation to PRINCIPAL AXES (degrees):
angles about x  y  z -90.004          0.000        -76.732

RADII OF GYRATION with respect to PRINCIPAL AXES:
R1   R2   R3 2.4777498e+01  4.6795432e+01  5.0292685e+01  MM
```

# ANNEX VIII

## FORCE SENSOR SPECIFICATIONS, NANO-17

**English Calibrations**

| SENSING RANGES | Calibrations | | |
|---|---|---|---|
| Axes | US-3-1 | US-6-2 | US-12-4 |
| Fx, Fy (±lbf) | 3 | 6 | 12 |
| Fz (±lbf) | 4.25 | 8.5 | 17 |
| Tx, Ty (±lbf-in) | 1 | 2 | 4 |
| Tz (±lbf-in) | 1 | 2 | 4 |

| RESOLUTION | System Type* | | | | | |
|---|---|---|---|---|---|---|
| Axes | CON | DAQ | CON | DAQ | CON | DAQ |
| Fx, Fy (lbf) | 1/640 | 1/5120 | 1/320 | 1/2560 | 1/160 | 1/1280 |
| Fz (lbf) | 1/640 | 1/5120 | 1/320 | 1/2560 | 1/160 | 1/1280 |
| Tx, Ty (lbf-in) | 1/4000 | 1/32000 | 1/2000 | 1/16000 | 1/1000 | 1/8000 |
| Tz (lbf-in) | 1/4000 | 1/32000 | 1/2000 | 1/16000 | 1/1000 | 1/8000 |

**Metric Calibrations**

| SENSING RANGES | Calibrations | | |
|---|---|---|---|
| Axes | SI-12-0.12 | SI-25-0.25 | SI-50-0.5 |
| Fx, Fy (±N) | 12 | 25 | 50 |
| Fz (±N) | 17 | 35 | 70 |
| Tx, Ty (±Nmm) | 120 | 250 | 500 |
| Tz (±Nmm) | 120 | 250 | 500 |

| RESOLUTION | System Type* | | | | | |
|---|---|---|---|---|---|---|
| Axes | CON | DAQ | CON | DAQ | CON | DAQ |
| Fx, Fy (N) | 1/160 | 1/1280 | 1/80 | 1/640 | 1/40 | 1/320 |
| Fz (N) | 1/160 | 1/1280 | 1/80 | 1/640 | 1/40 | 1/320 |
| Tx, Ty (Nmm) | 1/32 | 1/256 | 1/16 | 1/128 | 1/8 | 1/64 |
| Tz (Nmm) | 1/32 | 1/256 | 1/16 | 1/128 | 1/8 | 1/64 |

| Single-Axis Overload | English | Metric |
|---|---|---|
| Fxy | ±79 lbf | ±350 N |
| Fz | ±180 lbf | ±800 N |
| Txy | ±22 lbf-in | ±2.5 Nm |
| Tz | ±31 lbf-in | ±3.5 Nm |
| **Stiffness (Calculated)** | **English** | **Metric** |
| X-axis & Y-axis force (Kx, Ky) | 4.7x10⁴ lb/in | 8.2x10⁶ N/m |
| Z-axis force (Kz) | 6.5x10⁴ lb/in | 11x10⁶ N/m |
| X-axis & Y-axis torque (Ktx, Kty) | 2.1x10³ lbf-in/rad | 240 Nm/rad |
| Z-axis torque (Ktz) | 3.4x10³ lbf-in/rad | 380 Nm/rad |
| **Resonant Frequency (Measured)** | | |
| Fx, Fy, Tz | 7200 Hz | |
| Fz, Tx, Ty | 7200 Hz | |
| **Physical Specifications** | **English** | **Metric** |
| Weight* | 0.020 lb | 9.1 g |
| Diameter* | 0.669 in | 17 mm |
| Height* | 0.571 in | 14.5 mm |

*Specifications include standard interface plates.

# ANNEX IX

## MOTOR SPECIFICATIONS, MAXON EC-45

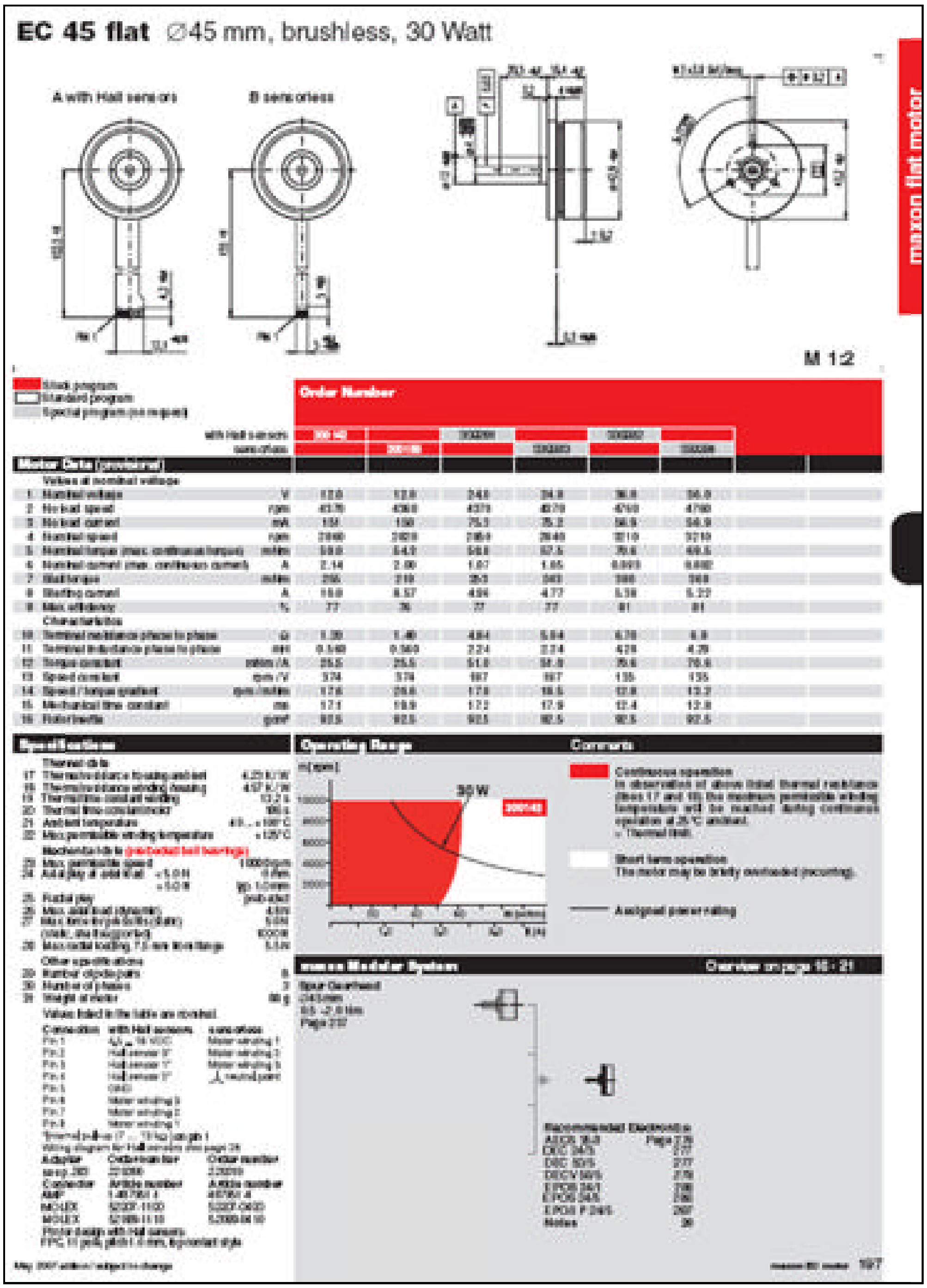

## ANNEX X

## MOTOR SPECIFICATIONS, MAXON EC-90

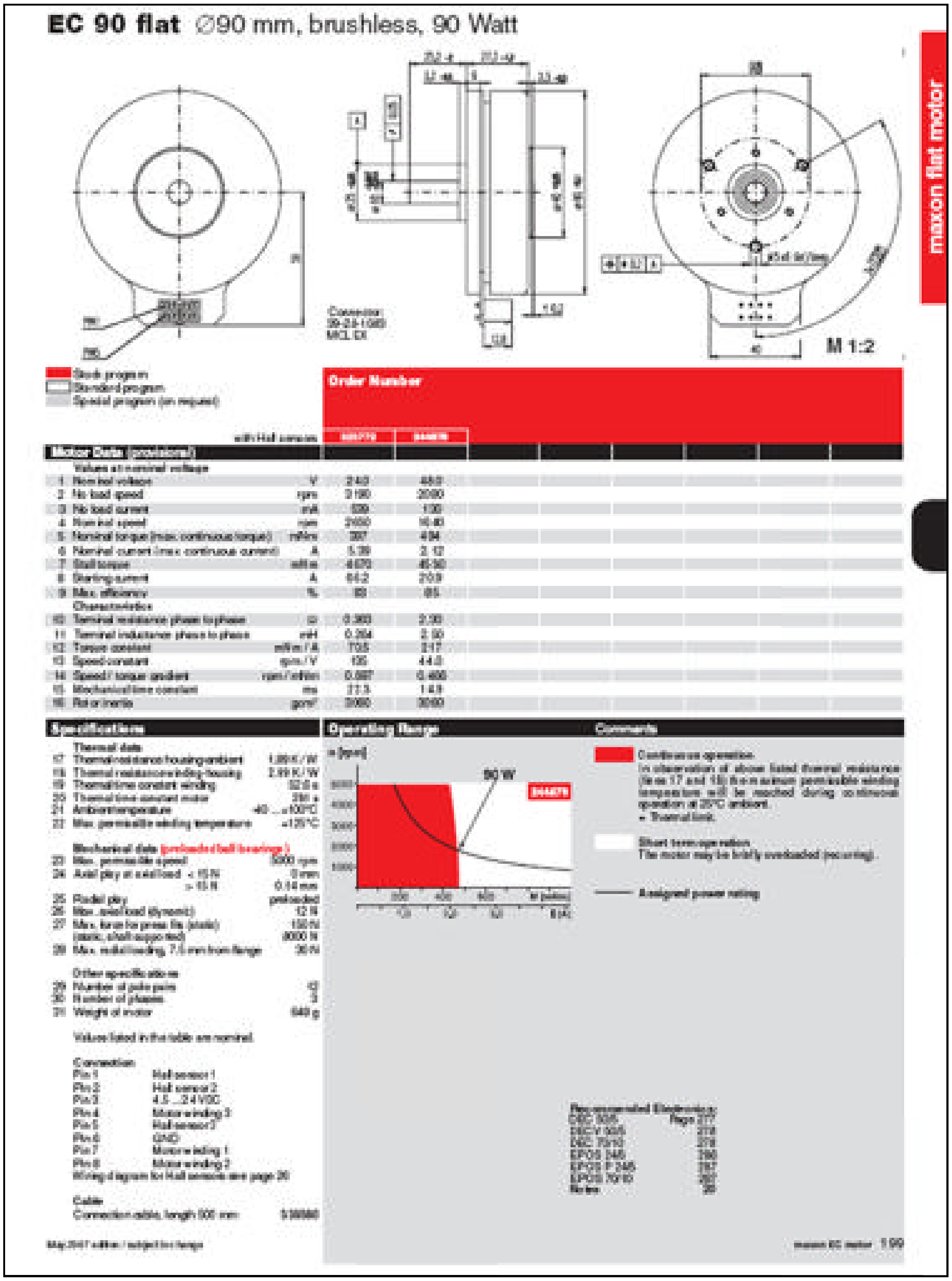

# ANNEX XI

# HARMONIC DRIVE (HD) SPECIFICATIONS

## CSF Rating Table

Table 1

| Size | Ratio | Rated Torque at 2000 $T_r$ r/min (Nm) | (in-lb) | Limit for Repeated Peak Torque Nm (Nm) | (in-lb) | Limit for Average Torque Nm (Nm) | (in-lb) | Limit for Momentary Peak Torque Nm (Nm) | (in-lb) | Maximum Input Speed r/min (Oil) | (Grease) | Limit for Average Input Speed r/min (Oil) | (Grease) | Moment of Inertia ($\times10^{-4}$kg m$^2$) | ($\times10^{-5}$kgf m s$^2$) |
|---|---|---|---|---|---|---|---|---|---|---|---|---|---|---|---|
| 8 | 30 | 3.0 | 8 | 1.8 | 16 | 1.4 | 12 | 3.2 | 28 | 14000 | 8500 | 6500 | 3500 | 0.003 | 0.0031 |
| | 50 | 1.8 | 16 | 3.3 | 29 | 2.3 | 20 | 6.6 | 58 | | | | | | |
| | 100 | 2.4 | 21 | 4.8 | 42 | 3.3 | 29 | 9.0 | 80 | | | | | | |
| 11 | 30 | 2.2 | 19 | 4.5 | 40 | 3.4 | 30 | 8.5 | 75 | 14000 | 8500 | 6500 | 3500 | 0.012 | 0.012 |
| | 50 | 3.5 | 31 | 8.3 | 73 | 5.5 | 49 | 17 | 150 | | | | | | |
| | 100 | 5.0 | 44 | 11 | 97 | 8.9 | 79 | 25 | 221 | | | | | | |
| 14 | 30 | 4.0 | 35 | 9.0 | 80 | 6.8 | 60 | 17 | 150 | 14000 | 8500 | 6500 | 3500 | 0.033 | 0.034 |
| | 50 | 5.4 | 48 | 18 | 159 | 6.9 | 61 | 35 | 310 | | | | | | |
| | 80 | 7.8 | 69 | 23 | 204 | 11 | 97 | 47 | 416 | | | | | | |
| | 100 | 7.8 | 69 | 28 | 248 | 11 | 97 | 54 | 478 | | | | | | |
| 17 | 30 | 8.8 | 78 | 16 | 142 | 12 | 106 | 30 | 266 | 10000 | 7300 | 6500 | 3500 | 0.079 | 0.081 |
| | 50 | 16 | 142 | 34 | 301 | 26 | 230 | 70 | 620 | | | | | | |
| | 80 | 22 | 195 | 43 | 381 | 27 | 239 | 87 | 770 | | | | | | |
| | 100 | 24 | 212 | 54 | 478 | 39 | 345 | 108 | 956 | | | | | | |
| | 120 | 24 | 212 | 54 | 478 | 39 | 345 | 86 | 761 | | | | | | |
| 20 | 30 | 15 | 133 | 27 | 239 | 20 | 177 | 50 | 443 | 10000 | 6500 | 6500 | 3500 | 0.193 | 0.197 |
| | 50 | 25 | 221 | 56 | 496 | 34 | 301 | 98 | 867 | | | | | | |
| | 80 | 34 | 301 | 74 | 655 | 47 | 416 | 127 | 1124 | | | | | | |
| | 100 | 40 | 354 | 82 | 726 | 49 | 434 | 147 | 1301 | | | | | | |
| | 120 | 40 | 354 | 87 | 770 | 49 | 434 | 147 | 1301 | | | | | | |
| | 160 | 40 | 354 | 92 | 814 | 49 | 434 | 147 | 1301 | | | | | | |
| 25 | 30 | 27 | 239 | 50 | 443 | 38 | 336 | 95 | 841 | 7500 | 5600 | 5600 | 3500 | 0.413 | 0.421 |
| | 50 | 39 | 345 | 98 | 868 | 55 | 487 | 186 | 1646 | | | | | | |
| | 80 | 63 | 558 | 137 | 1212 | 87 | 770 | 255 | 2257 | | | | | | |
| | 100 | 67 | 593 | 157 | 1390 | 108 | 956 | 284 | 2513 | | | | | | |
| | 120 | 67 | 593 | 167 | 1478 | 108 | 956 | 304 | 2690 | | | | | | |
| | 160 | 67 | 593 | 176 | 1558 | 108 | 956 | 314 | 2779 | | | | | | |
| 32 | 30 | 54 | 478 | 100 | 885 | 75 | 664 | 200 | 1770 | 7000 | 4800 | 4600 | 3500 | 1.69 | 1.72 |
| | 50 | 76 | 673 | 216 | 1912 | 108 | 956 | 382 | 3381 | | | | | | |
| | 80 | 118 | 1044 | 304 | 2690 | 167 | 1478 | 568 | 5027 | | | | | | |
| | 100 | 137 | 1213 | 333 | 2947 | 216 | 1912 | 647 | 5726 | | | | | | |
| | 120 | 137 | 1213 | 353 | 3124 | 216 | 1912 | 686 | 6071 | | | | | | |
| | 160 | 137 | 1213 | 372 | 3292 | 216 | 1912 | 686 | 6071 | | | | | | |
| 40 | 50 | 137 | 1213 | 402 | 3558 | 196 | 1735 | 686 | 6071 | 5600 | 4000 | 3600 | 3000 | 4.50 | 4.59 |
| | 80 | 206 | 1823 | 519 | 4593 | 284 | 2513 | 980 | 8673 | | | | | | |
| | 100 | 265 | 2345 | 568 | 5027 | 372 | 3292 | 1080 | 9558 | | | | | | |
| | 120 | 294 | 2602 | 617 | 5460 | 451 | 3991 | 1180 | 10443 | | | | | | |
| | 160 | 294 | 2602 | 647 | 5726 | 451 | 3991 | 1180 | 10443 | | | | | | |
| 45 | 50 | 176 | 1558 | 500 | 4425 | 265 | 2345 | 950 | 8408 | 5000 | 3800 | 3300 | 3000 | 8.68 | 8.86 |
| | 80 | 313 | 2770 | 706 | 6248 | 390 | 3452 | 1270 | 11240 | | | | | | |
| | 100 | 353 | 3124 | 755 | 6682 | 500 | 4425 | 1570 | 13895 | | | | | | |
| | 120 | 402 | 3558 | 823 | 7284 | 620 | 5487 | 1760 | 15576 | | | | | | |
| | 160 | 402 | 3558 | 882 | 7806 | 630 | 5576 | 1910 | 16904 | | | | | | |
| 50 | 50 | 245 | 2168 | 715 | 6328 | 350 | 3098 | 1430 | 12656 | 4500 | 3500 | 3000 | 2500 | 12.5 | 12.8 |
| | 80 | 372 | 3292 | 941 | 8328 | 519 | 4593 | 1860 | 16461 | | | | | | |
| | 100 | 470 | 4160 | 980 | 8673 | 666 | 5894 | 2060 | 18231 | | | | | | |
| | 120 | 529 | 4682 | 1080 | 9558 | 813 | 7195 | 2060 | 18231 | | | | | | |
| | 160 | 529 | 4682 | 1180 | 10443 | 843 | 7461 | 2450 | 21683 | | | | | | |
| 58 | 50 | 353 | 3124 | 1020 | 9027 | 520 | 4602 | 1960 | 17346 | 4000 | 3000 | 2700 | 2200 | 27.3 | 27.9 |
| | 80 | 549 | 4859 | 1480 | 13098 | 770 | 6815 | 2450 | 21683 | | | | | | |
| | 100 | 696 | 6160 | 1590 | 14072 | 1060 | 9381 | 3180 | 28143 | | | | | | |
| | 120 | 745 | 6593 | 1720 | 15222 | 1190 | 10532 | 3330 | 29471 | | | | | | |
| | 160 | 745 | 6593 | 1840 | 16284 | 1210 | 10709 | 3430 | 30356 | | | | | | |

## BIBLIOGRAPHY


Alexander, M. A., M. R. Nelson and A. Shah. 1992. « Orthotics, adapted seating and assistive device ». In *Pediatric Rehabilitation*, 2nd p. 186-187. Baltimore: MD: Williams and Wilkins.

Alvarez-Ramirez, J., I. Cervantes and R. Kelly. 2000. « PID regulation of robot manipulators: stability and performance ». *Systems & Control Letters,* vol. 41, n$^{o}$ 2, p. 73-83.

Arciero, R. A., and D. C. Taylor. 1998. « Primary anterior dislocation of the shoulder in young patients. A ten-year prospective study ». *J Bone Joint Surg Am,* vol. 80, n$^{o}$ 2 (Feb), p. 299-300.

Bartolini, G., A. Ferrara, E. Usai and V. I. Utkin. 2000. « On multi-input chattering-free second-order sliding mode control ». *IEEE Transactions on Automatic Control,* vol. 45, n$^{o}$ 9, p. 1711-1717.

Benjuya, N., and S. B. Kenney. 1990. « Hybrid Arm Orthosis ». *Journal of Prosthetics and Orthotics,* vol. 2, n$^{o}$ 2 (Win), p. 155-163.

Bergamasco, M., B. Allotta, L. Bosio, L. Ferretti, G. Parrini, G. M. Prisco, F. Salsedo and G. Sartini. 1994. « An Arm Exoskeleton System for Teleoperation and Virtual Environments Applications ». In *1994 IEEE International Conference on Robotics and Automation: Proceedings*. Vol. 1-4, p. 1449-1454.

Beyl, P., P. Cherelle, K. Knaepen and D. Lefeber. 2008. « A proof-of-concept exoskeleton for robot-assisted rehabilitation of gait ». In *4th European Conference of the International Federation for Medical and Biological Engineering, ECIFMBE 2008, November 23, 2008 - November 27, 2008*. Vol. 22, p. 1825-1829. Coll. « IFMBE Proceedings ». Antwerp, Belgium: Springer Verlag.

Brose, S. W., D. J. Weber, B. A. Salatin, G. G. Grindle, H. Wang, J. J. Vazquez and R. A. Cooper. 2010. « The role of assistive robotics in the lives of persons with disability ». *Am J Phys Med Rehabil,* vol. 89, n$^{o}$ 6 (Jun), p. 509-521.

Buneo, C. A., J. Boline, J. F. Soechting and R. E. Poppele. 1995. « On the form of the internal model for reaching ». *Experimental Brain Research,* vol. 104, n$^{o}$ 3, p. 467-479.

Burgar, C. G., P. S. Lum, P. C. Shor and H. F. Machiel Van der Loos. 2000. « Development of robots for rehabilitation therapy: The Palo Alto VA/Stanford experience ». *Journal of Rehabilitation Research and Development,* vol. 37, n$^{o}$ 6, p. 663-673.

Cardoso, L. S., R. M. E. M. da Costa, A. Piovesana, M. Costa, L. Penna, A. C. Crispin, J. Carvalho, H. Ferreira, M. L. Lopes, G. Brandao and R. Mouta. 2006. « Using virtual environments for stroke rehabilitation ». In *2006 International Workshop on Virtual Rehabilitation, 29-30 Aug. 2006*. p. 5 Piscataway, NJ, USA.

Carignan, C., J. Tang and S. Roderick. 2009. « Development of an exoskeleton haptic interface for virtual task training ». In *2009 IEEE/RSJ International Conference on Intelligent Robots and Systems, IROS 2009, October 11, 2009 - October 15, 2009*. p. 3697-3702. St. Louis, MO, USA.

CIA. 2011. « The World Factbook ». USA: Central Intelligence Agency, <https://www.cia.gov/library/publications/the-world-factbook/index.html>. [Accessed, April 2, 2012].

Colombo, R., F. Pisano, S. Micera, A. Mazzone, C. Delconte, M. C. Carrozza, P. Dario and G. Minuco. 2005. « Robotic techniques for upper limb evaluation and rehabilitation of stroke patients ». *IEEE Trans Neural Syst Rehabil Eng,* vol. 13, nº 3 (Sep), p. 311-324.

Craig, J. J. 2005. *Introduction to robotics : mechanics and control*, 3rd. Upper Saddle River, N.J.: Pearson/Prentice Hall, viii, 400 p.

Culmer, P. R., A. E. Jackson, S. Makower, R. Richardson, J. A. Cozens, M. C. Levesley and B. B. Bhakta. 2010. « A control strategy for upper limb robotic rehabilitation with a dual robot system ». *IEEE/ASME Transactions on Mechatronics,* vol. 15, nº 4, p. 575-585.

Defoort, M., T. Floquet, A. Kokosy and W. Perruquetti. 2008. « Sliding-Mode Formation Control for Cooperative Autonomous Mobile Robots ». *IEEE Transactions on Industrial Electronics,* vol. 55, nº 11 (Nov), p. 3944-3953.

Denavit, J., and R. S. Hartenberg. 1955. « A Kinematic Notation for Lower-Pair Mechanisms Based on Matrices ». *Trans ASME J. Appl. Mech.,* vol. 23, p. 215-221.

Dobkin, B. H. 2004. « Strategies for stroke rehabilitation ». *Lancet Neurol,* vol. 3, nº 9 (Sep), p. 528-536.

Erbatur, K., and O. Kaynak. 2001. « Use of adaptive fuzzy systems in parameter tuning of sliding-mode controllers ». *IEEE/ASME Transactions on Mechatronics,* vol. 6, nº 4 (Dec), p. 474-482.

Fallaha, C. J., M. Saad, H. Y. Kanaan and K. Al-Haddad. 2011. « Sliding-Mode Robot Control With Exponential Reaching Law ». *IEEE Transactions on Industrial Electronics,* vol. 58, nº 2, p. 600-610.

Fazekas, G., M. Horvath and A. Toth. 2006. « A novel robot training system designed to supplement upper limb physiotherapy of patients with spastic hemiparesis ». *International Journal of Rehabilitation Research,* vol. 29, n° 3, p. 251-254.

Filler, R. 1999. « Healthcare in the 21st century: "virtual" hospitals, tele-homecare and robots ». *Hosp Q,* vol. 3, n° 1 (Fall), p. 68-70.

Foo, G., and M. F. Rahman. 2010. « Sensorless Sliding-Mode MTPA Control of an IPM Synchronous Motor Drive Using a Sliding-Mode Observer and HF Signal Injection ». *IEEE Transactions on Industrial Electronics,* vol. 57, n° 4 (Apr), p. 1270-1278.

Frisoli, A., F. Salsedo, M. Bergamasco, B. Rossi and M. C. Carboncini. 2009. « A force-feedback exoskeleton for upper-limb rehabilitation in virtual reality ». *Applied Bionics and Biomechanics,* vol. 6, n° 2, p. 115-126.

Gao, W. B., and J. C. Hung. 1993. « Variable Structure Control of Nonlinear-Systems - a New Approach ». *IEEE Transactions on Industrial Electronics,* vol. 40, n° 1 (Feb), p. 45-55.

Garrec, P., J. P. Friconneau, Y. Measson and Y. Perrot. 2008. « ABLE, an innovative transparent exoskeleton for the upper-limb ». In *2008 IEEE/RSJ International Conference on Intelligent Robots and Systems, 22-26 Sept. 2008*. p. 1483-1488. Piscataway, NJ, USA: IEEE.

Glinka, T., and A. Polak. 2001. « Efficiency of brushless DC motor drives excited with permanent magnets ». *Maszyny Elektryczne*, n° 63, p. 57-63.

Gomes, M. A., G. L. M. Silveira and A. A. G. Siqueira. 2009. « Gait-Pattern Adaptation Algorithms based on Neural Network for Lower Limbs Active Orthoses ». *2009 IEEE-Rsj International Conference on Intelligent Robots and Systems*, p. 4475-4480.

Gopal, M. 2002. *Control systems: principles and design*, 2nd. New-Delhi, India: Tata McGraw-Hill, 951 p.

Gopura, R. A. R. C., K. Kiguchi and Li Yang. 2009. « SUEFUL-7: a 7DOF upper-limb exoskeleton robot with muscle-model-oriented EMG-based control ». In *2009 IEEE/RSJ International Conference on Intelligent Robots and Systems (IROS 2009), 11-15 Oct. 2009*. p. 1126-1131. Piscataway, NJ, USA.

Gordon, N. F., M. Gulanick, F. Costa, G. Fletcher, B. A. Franklin, E. J. Roth and T. Shephard. 2004. « Physical activity and exercise recommendations for stroke survivors: an American Heart Association scientific statement from the Council on Clinical Cardiology, Subcommittee on Exercise, Cardiac Rehabilitation, and Prevention; the Council on Cardiovascular Nursing; the Council on Nutrition, Physical Activity, and Metabolism; and the Stroke Council ». *Stroke,* vol. 35, n° 5 (May), p. 1230-1240.

Gray, H. , and C. D. Clemente. 1985. *Anatomy of the human body*, 30th American. Philadelphia: Lea & Febiger, xvii, 1,676 p.

Gresham, G. E., D. Alexander, D. S. Bishop, C. Giuliani, G. Goldberg, A. Holland, M. Kelly-Hayes, R. T. Linn, E. J. Roth, W. B. Stason and C. A. Trombly. 1997. « American Heart Association Prevention Conference. IV. Prevention and Rehabilitation of Stroke. Rehabilitation ». *Stroke,* vol. 28, n° 7 (Jul), p. 1522-1526.

Gupta, A., and M. K. O'Malley. 2006. « Design of a haptic arm exoskeleton for training and rehabilitation ». *IEEE/ASME Transactions on Mechatronics,* vol. 11, n° 3, p. 280-289.

Hallaceli, H., M. Manisali and I. Gunal. 2004. « Does scapular elevation accompany glenohumeral abduction in healthy subjects? ». *Archives of Orthopaedic and Trauma Surgery,* vol. 124, n° 6, p. 378-381.

Hamilton, N., W. Weimar and K. Luttgens. 2008. *Kinesiology : scientific basis of human motion*, 11th. Boston: McGraw-Hill Higher Education, xv, 627 p.

Hartenberg, R. S., and J. Denavit. 1964. *Kinematic Synthesis of Linkages*. New York: McGraw-Hill, 435 p.

Hay, L., C. Bard, C. Ferrel, I. Olivier and M. Fleury. 2005. « Role of proprioceptive information in movement programming and control in 5 to 11-year old children ». *Hum Mov Sci,* vol. 24, n° 2 (Apr), p. 139-154.

Hillman, S. K. 2003. *Interactive Functional Anatomy-DVD*. Primal Pictures Ltd., London

Holzbaur, K. R. S., W. M. Murray and S. L. Delp. 2005. « A model of the upper extremity for simulating musculoskeletal surgery and analyzing neuromuscular control ». *Annals of Biomedical Engineering,* vol. 33, n° 6, p. 829-840.

Homma, K., and T. Arai. 1995. « Design of an upper limb motion assist system with parallel mechanism ». In *Proceedings of the 1995 IEEE International Conference on Robotics and Automation. Part 1 (of 3), May 21, 1995 - May 27, 1995*. Vol. 2, p. 1302-1307. Nagoya, Japan.

Islam, S., and X. P. P. Liu. 2011. « Robust Sliding Mode Control for Robot Manipulators ». *IEEE Transactions on Industrial Electronics,* vol. 58, n° 6 (Jun), p. 2444-2453.

Johnson, G. R., and M. A. Buckley. 1997. « Development of a new motorised upper limb orthotic system (MULOS) ». In *Proceedings of RESNA '97. Lets Tango - Partnering People and Technologies, 20-24 June 1997*. p. 399-401. Arlington, VA, USA.

Kawamura, A., H. Ito and K. Sakamoto. 1992. « Chattering reduction of disturbance observer based sliding mode control ». In *Industry Applications Society Annual Meeting, 1992., Conference Record of the 1992 IEEE* (4-9 Oct 1992). Vol. 1, p. 490-495.

Kazerooni, H. 1996. « The human power amplifier technology at the University of California, Berkeley ». *Rob Auton Syst,* vol. 19, p. 179-87.

Kiguchi, K., K. Iwami, M. Yasuda, K. Watanabe and T. Fukuda. 2003. « An exoskeletal robot for human shoulder joint motion assist ». *IEEE/ASME Transactions on Mechatronics,* vol. 8, n° 1, p. 125-135.

Kothari, D. P. , and I. J. Nagrath. 2004. *Electric machines*, 3rd. New Delhi, India: Tata McGraw-Hill, 758 p.

Krebs, H. I., B. T. Volpe, M. L. Aisen and N. Hogan. 2000. « Increasing productivity and quality of care: Robot-aided neuro-rehabilitation ». *Journal of Rehabilitation Research and Development,* vol. 37, n° 6 (Nov-Dec), p. 639-652.

Kwakkel, G., B. J. Kollen and H. I. Krebs. 2008. « Effects of robot-assisted therapy on upper limb recovery after stroke: a systematic review ». *Neurorehabil Neural Repair,* vol. 22, n° 2 (Mar-Apr), p. 111-121.

Kyoungchul, K., and M. Tomizuka. 2009. « Control of exoskeletons inspired by fictitious gain in human model ». *IEEE/ASME Transactions on Mechatronics,* vol. 14, n° 6, p. 689-698.

Lo, A. C., P. D. Guarino, L. G. Richards, J. K. Haselkorn, G. F. Wittenberg, D. G. Federman, R. J. Ringer, T. H. Wagner, H. I. Krebs, B. T. Volpe, C. T. Bever, Jr., D. M. Bravata, P. W. Duncan, B. H. Corn, A. D. Maffucci, S. E. Nadeau, S. S. Conroy, J. M. Powell, G. D. Huang and P. Peduzzi. 2010. « Robot-assisted therapy for long-term upper-limb impairment after stroke ». *N Engl J Med,* vol. 362, n° 19 (May 13), p. 1772-1783.

Loureiro, R., F. Amirabdollahian, M. Topping, B. Driessen and W. Harwin. 2003. « Upper limb robot mediated stroke therapy - GENTLE/s approach ». *Autonomous Robots,* vol. 15, n° 1 (Jul), p. 35-51.

Luh, J. Y. S., M. W. Walker and R. P. C. Paul. 1980. « On-line computational scheme for mechanical manipulators ». *ASME J. of Dynamic Systems, Measurement, and Control,* vol. 102, n° 2, p. 69-76.

Lum, P. S., C. G. Burgar and P. C. Shor. 2004. « Evidence for improved muscle activation patterns after retraining of reaching movements with the MIME robotic system in subjects with post-stroke hemiparesis ». *IEEE Transactions on Neural Systems and Rehabilitation Engineering,* vol. 12, n° 2, p. 186-194.

Lum, P. S., C. G. Burgar, P. C. Shor, M. Majmundar and M. Van der Loos. 2002. « Robot-assisted movement training compared with conventional therapy techniques for the rehabilitation of upper-limb motor function after stroke ». *Archives of Physical Medicine and Rehabilitation,* vol. 83, n° 7, p. 952-959.

Mackay, J., and G. Mensah. 2004. *Atlas of Heart Disease and Stroke*. Brighton, UK: World Health Organization, Nonserial Publication.

Mary, E. M., and A. J. Mark. 2004. « Clinical evaluation, diagnosis and passive management of the shoulder complex ». *NZ Journal of Physiotherapy,* vol. 32, n° 2, p. 55-65.

Masia, L., H. I. Krebs, P. Cappa and N. Hogan. 2007. « Design and characterization of hand module for whole-arm rehabilitation following stroke ». *IEEE/ASME Transactions on Mechatronics,* vol. 12, n° 4, p. 399-407.

Masiero, S., A. Celia, G. Rosati and M. Armani. 2007. « Robotic-assisted rehabilitation of the upper limb after acute stroke ». *Arch Phys Med Rehabil,* vol. 88, n° 2 (Feb), p. 142-149.

Maza, J. I. , and A Ollero. 2001. « Hemero: A MATLAB-simulink toolbox for robotics ». In *1st Workshop on Robotics Education and Training*. Weingarten, Germany.

Mehta, J. A., and G. I. Bain. 2004. « Elbow dislocations in adults and children ». *Clin Sports Med.,* vol. 23, n° 4, p. 609-627.

Meng, Q. , and M. H. Lee. 2006. « Design issues for assistive robotics for the elderly ». *Advanced Engineering Informatics,* vol. 20, n° 2, p. 171-186.

Meyer, D. E., R. A. Abrams, S. Kornblum, C. E. Wright and J. E. Smith. 1988. « Optimality in human motor performance: ideal control of rapid aimed movements ». *Psychol Rev,* vol. 95, n° 3 (Jul), p. 340-370.

Ming-Kun, C., and Y. Tsan-Hsiu. 2009. « Experimental implementations of adaptive self-organizing fuzzy sliding mode control to 3-DOF rehabilitation robot ». *International Journal of Innovative Computing, Information & Control,* vol. 5, n° 10(B), p. 3391-3404.

Nagai, K., I. Nakanishi, H. Hanafusa, S. Kawamura, M. Makikawa and N. Tejima. 1998. « Development of an 8 DOF robotic orthosis for assisting human upper limb motion ». In *1998 IEEE International Conference on Robotics and Automation*. p. 3486-3491. Leuven, Belgium.

Nef, T., M. Guidali, V. Klamroth-Marganska and R. Riener. 2009. « ARMin - Exoskeleton Robot for Stroke Rehabilitation ». In *11th International Congress of the IUPESM.*

*Medical Physics and Biomedical Engineering. World Congress 2009. Neuroengineering, Neural Systems, Rehabilitation and Prosthetics, 7-12 Sept. 2009*. p. 127-130. Berlin, Germany.

Nef, T., M. Guidali and R. Riener. 2009. « ARMin III - arm therapy exoskeleton with an ergonomic shoulder actuation ». *Applied Bionics and Biomechanics,* vol. 6, n$^{o}$ 2, p. 127-142.

Nef, T., M. Mihelj and R. Riener. 2007. « ARMin: a robot for patient-cooperative arm therapy ». *Medical & Biological Engineering & Computing,* vol. 45, n$^{o}$ 9 (Sep), p. 887-900.

*Nonoperative Treatment: Physical Therapy*. 2011. Spine Centre, University of Virginia Health System. <http://www.uvaspine.com/physical-therapy.php>. [Accessed, April 2, 2012].

Noritsugu, T., and T. Tanaka. 1997. « Application of rubber artificial muscle manipulator as a rehabilitation robot ». *IEEE/ASME Transactions on Mechatronics,* vol. 2, n$^{o}$ 4, p. 259-267.

Parker, V. M., D. T. Wade and H. R. Langton. 1986. « Loss of arm function after stroke: measurement, frequency, and recovery ». *Int. Rehabilitation Medicine,* vol. 8, n$^{o}$ 2, p. 69-73.

Perry, J. C., J. Rosen and S. Burns. 2007. « Upper-limb powered exoskeleton design ». *IEEE/ASME Transactions on Mechatronics,* vol. 12, n$^{o}$ 4, p. 408-417.

*Physical Therapy Standards*. 2011. Department of Rehabilitation Services, Brigham and Women's Hospital <http://www.brighamandwomens.org/Patients_Visitors/pcs/rehabilitationservices/StandardsofCare.aspx>. [Accessed, April 2, 2012].

*Post-Stroke Rehabilitation Fact Sheet*. 2011. Bethesda, MD 20892, USA National Institute of Neurological Disorders and Stroke, National Institutes of Health. <http://www.ninds.nih.gov/disorders/stroke/poststrokerehab.htm>. [Accessed, April 2, 2012].

Rahman, M. H. 2005. « Development of a 3DOF Mobile Exoskeleton Robot for Human Upper-Limb Motion Assist ». Masters Thesis, Saga, Saga University, 115 p.

Rahman, M. H., O. L. Cristobal, M. Saad, J. P. Kenne and P. S. Archambault. 2012a. « Cartesian Trajectory Tracking of an Upper Limb Exoskeleton Robot ». In *IECON 2012*, Montreal, (Accepted)

Rahman, M. H., K. Kiguchi, M. M. Rahman and M. Sasaki. 2006. « Robotic exoskeleton for rehabilitation and motion assist ». In *1st International Conference on Industrial and Information Systems, ICIIS 2006, August 8, 2006 - August 11, 2006*. p. 241-246. Peradeniya, Sri lanka.

Rahman, M. H., T. Kittel-Ouimet, M. Saad, J. P. Kenne and P. S. Archambault. 2011a. « Dynamic modeling and evaluation of a robotic exoskeleton for upper-limb rehabilitation ». *International Journal of Information Acquisition,* vol. 8, n$^o$ 1, p. 82-102.

Rahman, M. H., M. Saad, J. P. Kenne and P.S. Archambault. 2011b. « Robot assisted rehabilitation for elbow and forearm movements ». *Int. J. Biomechatronics and Biomedical Robotics,* vol. 1, n$^o$ 4, p. 206-218.

Rahman, M. H., T. K. Ouimet, M. Saad, J. P. Kenne and P. S. Archambault. 2010a. « Development and control of a wearable robot for rehabilitation of elbow and shoulder joint movements ». In *IECON 2010 - 36th Annual Conference of IEEE Industrial Electronics, 7-10 Nov. 2010*. p. 1506-1511. Piscataway, NJ, USA.

Rahman, M. H., T. K. Ouimet, M. Saad, J. P. Kenne and P. S. Archambault. 2011c. « A 7DOFs Robotic Exoskeleton for Passive Rehabilitation: Design, Development and Control ». *IEEE/ ASME Trans. Mechatronics,* (Submitted).

Rahman, M. H., T. K. Ouimet, M. Saad, J. P. Kenne and P. S. Archambault. 2011d. « Control of a Powered Exoskeleton for Elbow, Forearm and Wrist Joint Movements ». In *IEEE International Conference on Robotics and Biomimetics*. p. 1561-1566. Phuket, Thailand.

Rahman, M. H., T. K. Ouimet, M. Saad, J. P. Kenne and P. S. Archambault. 2011e. « Dynamic Modeling and Evaluation of a Robotic Exoskeleton for Upper-Limb Rehabilitation ». *International Journal of Information Acquisition,* vol. 8, n$^o$ 1, p. 83-102.

Rahman, M. H., T. K. Ouimet, M. Saad, J. P. Kenne and P. S. Archambault. 2011f. « Nonlinear Control of an Upper-Limb Exoskelton Robot ». In *IEEE International Conference on Electronics, Circuits, and Systems (ICECS)* p. 772-775. Beirut, Lebanon.

Rahman, M. H., T. K. Ouimet, M. Saad, J. P. Kenne and P. S. Archambault. 2011g. « Tele-operation of a Robotic Exoskeleton for Rehabilitation and Passive Arm movement Assistance ». In *2011 IEEE International Conference on Robotics and Biomimetics*. p. 443-448. Phuket, Thailand.

Rahman, M. H., T. K. Ouimet, M. Saad, J. P. Kenne and P. S. Archambault. 2012b. « Development and Control of a Robotic Exoskeleton for Shoulder, Elbow and Forearm Movement Assistance ». *Applied Bionics and Biomechanics,* (in press).

Rahman, M. H., T. K. Ouimet, M. Saad, J. P. Kenne and P. S. Archambault. 2012c. « Development and Control of an Exoskeleton Robot Arm with Sliding Mode Exponential Reaching Law ». *International Journal of Control, Automation and Systems,* (Submitted).

Rahman, M. H., T. K. Ouimet, M. Saad, J. P. Kenne and P. S. Archambault. 2012d. « Development of a 4DoFs Exoskeleton Robot for Passive Arm Movement Assistance ». *Int. J. Mechatronics and Automation,* vol. 2, n° 1, p. 34-50.

Rahman, M. H., M. Saad, J. P. Kenne and P. S. Archambault. 2009. « Modeling and control of a 7DOF exoskeleton robot for arm movements ». In *2009 IEEE International Conference on Robotics and Biomimetics (ROBIO 2009), 19-23 Dec. 2009*. p. 245-250. Guilin, China.

Rahman, M. H., M. Saad, J. P. Kenne and P. S. Archambault. 2010b. « Modeling and Development of an Exoskeleton Robot for Rehabilitation of Wrist Movements ». In *2010 IEEE/ASME International Conference on Advanced Intelligent Mechatronics (AIM 2010), 6-9 July 2010*. p. 25-30. Montreal, Canada.

Rahman, M. H., M. Saad, J. P. Kenne and P. S. Archambault. 2011h. « Robot Aided Arm Rehabilitation: State of the Arts ». *IJIA,* (Prepared for Submission).

Rahman, M. H., M. Saad, J. P. Kenne and P.S. Archambault. 2010c. « Exoskeleton robot for rehabilitation of elbow and forearm movements ». In *2010 18th Mediterranean Conference on Control & Automation (MED 2010)* (23-25 June 2010). p. 1567-1572. Marrakech, Morocco.

Rahman, T., W. Sample, R. Seliktar, M. Alexander and M. Scavina. 2000. « A body-powered functional upper limb orthosis ». *Journal of Rehabilitation Research and Development,* vol. 37, n° 6, p. 675-680.

Reid, D. C. 1992. *Sports Injury Assessment and Rehabilitation*. New York, NY: Churchill Livingstone.

Rocco, P. 1996. « Stability of PID control for industrial robot arms ». *IEEE Transactions on Robotics and Automation,* vol. 12, n° 4, p. 606-614.

Rosen, J., J. C. Perry, N. Manning, S. Burns and B. Hannaford. 2005. « The human arm kinematics and dynamics during daily activities - toward a 7 DOF upper limb powered exoskeleton ». In *Advanced Robotics, 2005. ICAR '05. Proceedings., 12th International Conference on* (18-20 July 2005). p. 532-539.

Sabanovic, A. 2011. « Variable Structure Systems With Sliding Modes in Motion Control-A Survey ». *IEEE Transactions on Industrial Informatics,* vol. 7, n° 2 (May), p. 212-223.

Salisbury, J. K. 1980. « Active Stiffness Control of a Manipulator in Cartesian Coordinates ». In *19th IEEE Conference on Decision and Control*. p. 95-100.

Sanchez, R. J., Jr., E. Wolbrecht, R. Smith, J. Liu, S. Rao, S. Cramer, T. Rahman, J. E. Bobrow and D. J. Reinkensmeyer. 2005. « A pneumatic robot for re-training arm movement after stroke: rationale and mechanical design ». In *2005 IEEE 9th International Conference on Rehabilitation Robotics, 28 June-1 July 2005*. p. 500-4. Coll. « 2005 IEEE 9th International Conference on Rehabilitation Robotics (IEEE Cat. No. 05EX1028) ». Piscataway, NJ, USA: IEEE.

Sanger, T. D. 2000. « Human arm movements described by a low-dimensional superposition of principal components ». *Journal of Neuroscience,* vol. 20, n° 3 (Feb 1), p. 1066-1072.

Sarlegna, F. R., and R. L. Sainburg. 2007. « The effect of target modality on visual and proprioceptive contributions to the control of movement distance ». *Experimental Brain Research,* vol. 176, n° 2 (Jan), p. 267-280.

Sasaki, D., T. Noritsugu and M. Takaiwa. 2005. « Development of active support splint driven by pneumatic soft actuator (ASSIST) ». In *2005 IEEE International Conference on Robotics and Automation (ICRA)*. Vol. 1-4, p. 520-525. Barcelona, Spain.

Schilling, R. J. 1990. *Fundamental of Robotics: Analysis and Control*. Englewood Cliffs, NJ: Prentice Hall.

Sheps, D. M., K. A. Hildebrand and R. S. Boorman. 2004. « Simple dislocations of the elbow: evaluation and treatment ». *Hand Clin,* vol. 20, n° 4 (Nov), p. 389-404.

Siciliano, B., L. Sciavicco and L. Villani. 2009. *Robotics: Modelling, Planning and Control* 2nd. London: Springer, 666 p.

Slotine, J. J. E., and W. Li. 1991. *Applied nonlinear control*. Englewood Cliffs, N.J.: Prentice-Hall, xv, 459 p.

Stewart, J. C., S-C. Yeh, Y. Jung, H. Yoon, M. Whitford, S-Y. Chen, L. Li, M. McLaughlin, A. Rizzo and C. J. Winstein. 2006. « Pilot trial results from a virtual reality system designed to enhance recovery of skilled arm and hand movements after stroke ». In *5th International Workshop on Virtual Rehabilitation, IWVR 2006, August 29, 2006 - August 30, 2006*. p. 11-17. New York, NY, USA.

*Stroke Rehab Exercises*. 2010. Stroke-Rehab.com. <http://www.stroke-rehab.com/stroke-rehab-exercises.html>. [Accessed, April 2, 2012].

Takahashi, C. D., L. Der-Yeghiaian, V. Le, R. R. Motiwala and S. C. Cramer. 2008. « Robot-based hand motor therapy after stroke ». *Brain,* vol. 131, n$^{o}$ Pt 2 (Feb), p. 425-437.

*Tracking Heart Disease and Stroke in Canada*. 2009. Public Health Agency of Canada. <http://www.phac-aspc.gc.ca/publicat/2009/cvd-avc/pdf/cvd-avs-2009-eng.pdf>. [Accessed, April 2, 2012].

Tsagarakis, N. G., and D. G. Caldwell. 2003. « Development and control of a 'soft-actuated' exoskeleton for use in physiotherapy and training ». *Autonomous Robots,* vol. 15, n$^{o}$ 1 (Jul), p. 21-33.

Tsao, C. C., and M. M. Mirbagheri. 2007. « Upper limb impairments associated with spasticity in neurological disorders ». *J Neuroeng Rehabil,* vol. 4, p. 1-15.

Turcotte, M., and G. Schellenberg. 2007. « A Portrait of Seniors in Canada ». n$^{o}$ Catalogue no. 89-519-XIE. <http://www.statcan.gc.ca/pub/89-519-x/89-519-x2006001-eng.pdf>. [Accessed, April 2, 2012].

Wang, D. 2011. « Physical Therapy Exercises for a Stroke Patient's Arm ». (March 28, 2011). <http://www.livestrong.com/article/312280-physical-therapy-exercises-for-a-stroke-patients-arm/>. [Accessed, April 2, 2012].

Westin, C. D., E. A. Gill, M. E. Noyes and M. Hubbard. 1995. « Anterior shoulder dislocation. A simple and rapid method for reduction ». *Am J Sports Med,* vol. 23, n$^{o}$ 3 (May-Jun), p. 369-371.

Winstein, C. J., A. S. Merians and K. J. Sullivan. 1999. « Motor learning after unilateral brain damage ». *Neuropsychologia,* vol. 37, n$^{o}$ 8 (Jul), p. 975-987.

Winstein, C. J., J. P. Miller, S. Blanton, E. Taub, G. Uswatte, D. Morris, D. Nichols and S. Wolf. 2003. « Methods for a multisite randomized trial to investigate the effect of constraint-induced movement therapy in improving upper extremity function among adults recovering from a cerebrovascular stroke ». *Neurorehabil Neural Repair,* vol. 17, n$^{o}$ 3 (Sep), p. 137-152.

Winter, D. A. 1990. *Biomechanics and motor control of human movement*, 2nd ed. New York: J. Wiley, xvi, 277 p.

Xinghuo, Y., and O. Kaynak. 2009. « Sliding-Mode Control With Soft Computing: A Survey ». *IEEE Transactions on Industrial Electronics,* vol. 56, n$^{o}$ 9, p. 3275-3285.

Xu, G. H., Z. H. Xiao, Y. Guo and X. B. Xiang. 2007. « Trajectory tracking for underwater manipulator using sliding mode control ». In *2007 IEEE International Conference on Robotics and Biomimetics*. Vol. 1-5, p. 2127-2132.

Yang, C., J. Han, O. O. Peter and Q. Huang. 2011. « PID control with gravity compensation for hydraulic 6-DOF parallel manipulator ». In *PID Control, Implementation and Tuning*, sous la dir. de Mansour, Tamer. InTech. <http://www.intechopen.com/articles/show/title/pid-control-with-gravity-compensation-for-hydraulic-6-dof-parallel-manipulator>. [Accessed, April 2, 2012].

Yang, Y., C. J. Yang, K. M. Lee and H. Yu. 2009. « Model-based Fuzzy Adaptation for Control of a Lower Extremity Rehabilitation Exoskeleton ». In *2009 IEEE/ASME International Conference on Advanced Intelligent Mechatronics*. Vol. 1-3, p. 350-355.

Yu, W., and J. Rosen. 2010. « A novel linear PID controller for an upper limb exoskeleton ». In *2010 49th IEEE Conference on Decision and Control, CDC 2010, December 15, 2010 - December 17, 2010*. p. 3548-3553. Atlanta, GA, USA.

Yupeng, R., P. Hyung-Soon and Z. Li-Qun. 2009. « Developing a whole-arm exoskeleton robot with hand opening and closing mechanism for upper limb stroke rehabilitation ». In *2009 IEEE International Conference on Rehabilitation Robotics: Reaching Users & the Community (ICORR), 23-26 June 2009*. p. 761-765. Coll. « 2009 IEEE International Conference on Rehabilitation Robotics: Reaching Users the Community (ICORR) ». Piscataway, NJ, USA: IEEE.

Zatsiorsky, V. M., and V. N. Seluyanov. 1983. « Mass and inertia characteristics of the main segments of the human body ». In *Biomechanics 8-B, Proceedings of the 8th International Congress of Biomechanics*. Vol. 4B, p. 1152-1159. Nagoya, Japan.